7-28-1977

DETERMINATION OF SIZE DISTRIBUTIONS IN HETERODISPERSE SYSTEMS OF HOMOGENEOUS, NON-ABSORBING SPHERES FROM ANGULAR LIGHT SCATTERING EXTREMA

Werner Bergman
Wayne State University

DETERMINATION OF SIZE DISTRIBUTIONS IN HETERODISPERSE SYSTEMS OF HOMOGENEOUS, NON-ABSORBING SPHERES FROM ANGULAR LIGHT SCATTERING EXTREMA

by

Werner Bergman

A DISSERTATION

Submitted to the Office for Graduate Studies,
Graduate Division of Wayne State University,
Detroit, Michigan
in partial fulfillment of the requirements
for the degree of

DOCTOR OF PHILOSOPHY

1977

MAJOR: CHEMISTRY (PHYSICAL)

APPROVED BY:

W. Heller 7/28/77

Advisor Date

ACKNOWLEDGMENT

I am deeply indebted to Professor Wilfried Heller for the many hours of advice and guidance that were generously given throughout the course of this study.

I want to thank Professor Milton D. Glick of the Chemistry Department for his help in obtaining the computer money that made this study possible, Professor Harry H. Denman of the Physics Department for helpful discussions on numerical methods, Professor K. C. Kapur of the Engineering Department for providing information on the Fibonacci Search algorithm, the Computer Department of Ford Motor Company for providing the EXFIND program, and Dr. Jack P. Witeczek of Clairol Company for providing experimental light scattering data. I would also like to thank Mr. H. Wade Patterson, Dr. Thomas R. Crites and Mr. Richard V. Griffith of the Hazards Control Department at the Lawrence Livermore Laboratory for providing me the time to write this manuscript.

I am especially grateful to my wife, Barbara, for providing my financial support and for making personal sacrifices that allowed me to complete this study.

TABLE OF CONTENTS

LIST OF TABLES

LIST OF FIGURES

I. Introduction

The measurement of particle size distributions is important in many fields of science and engineering. Much of the current emphasis on air pollution control is concerned with reducing particulate emissions from industrial sources. Particle size distributions determine not only what control strategy will be used but also the potential adverse health effects from the respirable fraction. The polymer, pharmaceutical and cosmetic industries rely heavily on particle size measurements to manufacture their products with the desired properties. Medical research is devoting a considerable effort to measuring biological particles ranging from blood cells to possible cancer viruses in hopes of understanding and preventing disease. These few examples illustrate the widespread interest in measuring particle size distributions.

The methods used to measure particle size distributions are as diverse as the fields in which they are used. These methods include centrifugation, cascade impaction, electrostatic contact charge transfer, acoustical techniques, gas adsorption, flame photometry and optical techniques just to name a few.[1,2] The optical techniques in turn consist of several dozen different methods which may be classified as scattering from single particles or scattering from a collection of particles.

The many different single particle techniques use the intensity of light scattered or the degree of light extinction to size individual particles. A multichannel analyzer then assembles particle size statistics from a large number of such counts. After a short time, (e.g. 1 sec) the instrument has counted and sized thousands of particles, thus providing a histogram of the number size distribution. To insure that only one particle is counted at a time, these techniques require a very dilute system of particles. Moreover, all of the single particle techniques require taking a small sample of the

particle stream and passing it through the detector.

In contrast, the techniques based on scattering from a collection of particles must unfold the size distribution from the integrated scattering of many particles. This is a very difficult task and is generally performed by a computer matching of theoretical and experimental data. Kerker[3] has reviewed a large number of different methods using scattering from a collection of particles. A few of the more widely used methods include angular maxima and minima in the scattered intensity, angular variation of scattered intensity at a fixed wavelength and spectral variation of turbidity or scattered light at a fixed angle. The potential advantages of these techniques compared to the single particle techniques include a smaller detectable size, remote measurements, and representative measurements of the complete distribution. Since scattering from the complete distribution is measured rather than from individual particles, the time required for measuring the scattering is reduced by a factor equal to the number of individual particles counted.

Although many different theoretical and experimental techniques based on scattering from a collection of particles have been developed, the full potential of these methods have not been reached. Experimentally, the problems with excessive particle concentration and detector solid angle have required a series of measurements at decreasing concentration and solid angle with subsequent extrapolation. This greatly increased the experimental time. However, modern laser optical systems can significantly reduce and possibly eliminate these experimental problems. The greater intensity of the laser allows much lower concentration of particles and smaller solid angle. In addition the interpretation of the experimental data to obtain particle size distributions has been very time consuming.

The purpose of this investigation is to further develop the method based on angular maxima and minima in the scattered intensity. Compared to the other scattering methods from a collection of particles, this techique has the potential for faster size determination and is less prone to the experimental problems of particle concentration and detector solid angle. In view of these advantages, a large number of investigations have been made using scattering extrema. However these prior investigations have considered only limited cases. The present study performs a systematic investigation of the scattering extrema and provides a foundation for developing specific techniques. Several promising techniques have emerged from this study.

II. Prior Investigations of Angular Light Scattering Maxima and Minima

The earliest application of light scattering extrema to determine particle sizes was developed in La Mer's[4-6] laboratory, where the angular positions of the red and green bands in the scattered light, called higher order Tyndall spectra, were measured using incident white light. The colors in the scattered light arise because the scattered intensities at any given angle and particle size are different for each wavelength. Particle sizes are then determined by matching the angular position of the red and green bands with theoretical calculations. Although this technique has been investigated and improved by other researchers[7], the method is best applied to atmospheric or cosmic[8] particles where the incident radiation is a continuous spectrum.

Using monochromatic incident light greatly simplifies the angular extema method. Dandliker[9] was the first to demonstrate this simplification by measuring the location of the first minimum intensity encountered in the forward direction. The particle size is then determined using equation 1 based on the Rayleigh-Gans-Debye, (RGD), theory.[3]

$$\alpha \sin(\theta/2) = k \qquad (1)$$

where α is the relative particle size D/λ

D is the particle diameter in μm

λ is the wavelength of light in μm

θ is the angle of observation from the forward direction in degrees

k is an empirical constant

Nakagaki and Heller[10] extended the method by showing the systematic behavior of the angular scattering maxima and minima using the RGD theory. An empirical equation was developed that gave the approximate location of the

scattering maxima and minima based on discrepancies between the RGD data and the Mie[3] data at one refractive index. Their equation, rewritten in a form similar to equation 1, is

$$\alpha \sin(\theta/2) = \frac{k_{RGD}}{.40 + .61\ M} \qquad (2)$$

where k_{RGD} is a constant from the RGD theory

M is the refractive index of the particle divided by the refractive index of the medium.

This equation shows the decrease in $\alpha \sin(\theta/2)$ with an increase in M. In a later study Heller and Nakagaki[11] improved the accuracy of equation 2 by replacing the denominator with a more complicated function of M. The resultant equation correctly predicted the angular location of the extrema to within 1^{o} for the general size range of interest in colloid chemistry. This same equation was also shown to predict extrema obtained from varying the wavelength of the incident radiation at a fixed angle.

Dezelic and Kratohvil[12] were able to show good agreement between experimental light scattering measurements using the angular extrema method and electron microscopy. They measured the angular location of each of the accessible maxima and minima of the scattered intensity for several monodisperse polystyrene latexes. The particle sizes were then obtained by comparing the experimental extrema angles to theoretical calculations until a match was obtained. An important experimental observation of their study indicated that the method based on the location of the extrema is less affected by multiple scattering than other scattering methods.

Maron and his co-workers[13, 14] conducted a series of experimental and theoretical investigations that generalized Dandliker's method. They had observed, as Nakagaki and Heller[10] had shown earlier that the constant k

in equation 1 decreases as the relative refractive index, M, increases. The empirical equation developed from these studies is shown in equation 3.

$$\alpha \sin(\theta_i/2) = k_{1i} - k_{2i}M \qquad (3)$$

where k_{1i} and k_{2i} are empirical constants

i is the order (number) of the extremum minimum or maximum counting from the forward direction

These studies also indicated that unpolarized light could also be used to size particles by using different constants in equation 3. Subsequent investigations by Maron et al[15, 16] showed that equation 3 could also be used to find particle sizes from experiments using angular variation of the polarization ratio or higher order Tyndall spectra. The polarization ratio is defined as the ratio of the intensities of the two orthogonal components of light scattered by a sphere from incident unpolarized light.

Kerker et al[17] have tested the range of validity of equation 3 using extensive computer calculations of the angular intensity extrema. Very accurate determinations of the extrema locations were possible because intensity data were calculated at every 1^o over a wide range of M and α values. Previous researchers had to interpolate angular extrema data from tables of Pangonis and Heller[18] or of Lowan[19] where the intensity data were spaced every 5^o or 10^o respectively. Kerker et al[17] found that equation 3 is a good approximation for the angular extrema provided that neither M nor α is too large.

A large number of empirical equations describing the angular extrema location were recently derived by Patitsas[20-23] using extensive Mie calculations at intervals of 0.4^o. He showed that the constant in equation 1 decreases with particle size in addition to the refractive index. The rate

at which the constant decreases with particle size also increases as the refractive index increases. Patitsas also found that using $\theta/2$ in place of $\sin(\theta/2)$ results in a more systematic behavior of the extrema. One of his most interesting observations was that the extrema in the backward direction for particles with large refractive indexes and large diameters obey equation 4.[22]

$$\alpha \sin[(180-\theta_i)/2] = k_i \qquad (4)$$

Unfortunately he does not discuss the implication of this observation and treats this as another one of the many empirical equations found in his papers.

The investigations described so far have been concerned with measuring monodisperse particle size distributions using primarily polarized monochromatic light with the electric vector vibrating perpendicular to the plane of observation. Maron et al[13, 14] had previously tried to relate the difference in particle sizes obtained at two different wavelengths to the degree of heterodispersion but was not successful. Prior to the present investigation, the only way heterodisperse distributions could be obtained from extrema measurements was to use a technique developed by Wallace and Kratohvil[24]. This technique consisted of first finding the modal size of the distribution by matching the extrema minima in the forward direction with the theoretical extrema from monodisperse particle sizes. They found that the location of the extrema minima in the forward direction were independent of the degree of heterodispersion for a constant modal size. The degree of heterodispersion was then found from the ratio of the intensity maximum to the intensity minimum for a given extrema pair. As the heterodispersion increased, this ratio would decrease monotonically to the limiting value of 1 where the extrema pair is washed out.

Wallace et al have examined this technique using vertically polarized[24], unpolarized and horizontally polarized[26] scattered light and the polarization ratio[25]. They found that the most sensitive measurements were made using vertical polarization and the least sensitive using horizontal polarization. However all of these methods greatly overestimate the experimentally determined heterodispersion compared to electron microscope data.

The preceeding investigations have been concerned with developing techniques to measure particle sizes using either empirical equations or graphical comparisons. They have not been concerned with investigating and interpreting the scattering patterns themselves. The earliest attempt at understanding the complex pattern of the scattered intensity as a function of particle size and angle of observation was made by Van DeHulst[27,28]. He devised an altitude chart using the phase shift parameter $2\alpha(M-1)$ as the ordinate and the diffraction parameter $\alpha\theta$ as the abscissa. Contours of constant scattering amplitude were then drawn on the graph. This representation allowed one to view diffraction minima or maxima as an oscillating curve meandering about a constant $\alpha\theta$. Very small values of $2\alpha(M-1)$ correspond to the RGD theory where the extrema show constant values of $2\alpha \sin(\theta/2)$. Large values of $2\alpha(M-1)$ on the other hand correspond to Fraunhoffer diffraction where $\alpha \sin\theta$ describes the extrema.

Penndorf[29] modified the altitude chart by using the diffraction parameter $\alpha \sin\theta$ instead of $\alpha\theta$. This change showed that the intensity minima in the forward direction meandered about the classical diffraction minima at $\alpha \sin\theta = 3.83$, 7.02 and 10.17. He argued that the extrema in the forward direction can be described as diffractive extrema. Penndorf[30,31] also observed that the contour plots of the angular intensity extrema could be

divided into two regions. One region was defined by the extrema that migrate in the forward direction with increasing size α. The other region consists of extrema that migrate in the backward direction with increasing size α. Rowell[32] had also observed this behavior.

Penndorf[30,31] reasoned that if the extrema migrating in the forward direction were described as diffractive extrema then the extrema migrating in the backward direction could be described as reflective extrema. If the diffractive extrema show a constant value of $\alpha \sin \theta$ then the reflective extrema will have a constant value of $\alpha \sin(\pi-\theta)$. Penndorf[33] then constructed a new altitude chart which was equally divided into diffraction and reflection regions. The extrema in the diffraction regions were plotted as α versus $\alpha \sin \theta$ with the resulting contours wandering about constant $\alpha \sin \theta$ values. Similarly, the extrema in the reflective region, when plotted as α versus $\alpha \sin(\pi-\theta)$, were seen as curves oscillating about constant $\alpha \sin(\pi-\theta)$ values. Although Penndorf correctly assessed the extrema that migrate in the backward direction as originating from a reflection phenomena, he used the wrong function to describe the behavior. The term $\alpha \sin(\pi-\theta)$ would only apply for very large particles where Fresnel's equations could be used. Similarly, plotting the diffractive extrema against $\alpha \sin \theta$ applies for very large particles where the Fraunhoff diffraction theory holds.

III Calculation of Angular Light Scattering Maxima and Minima

A. Survey of Problem and Initial Calculations

The initial and most time consuming phase of the present investigation was concerned with developing computer programs to calculate angular light scattering extrema. Previous investigators had obtained the angular extrema in one of two ways. One method involved graphical interpolation of angular intensity data previously tabulated [10, 11, 13-16, 29-31, 33]. However, graphical interpolation is very time consuming and is only feasible for analyzing a limited number of data. For more extensive extrema analysis, previous investigators chose the other method which required a computer to perform a point by point comparison of closely spaced data despite the greater number of data points required. [17, 20-26, 32]

The accuracy of these previous methods, as well as the method used in the present study, is strongly dependent on the angular spacing of the calculated scattering data. Thus the extrema angles obtained from graphical interpolation of scattering data spaced at 5^{o} intervals would be accurate to within 1^{o}. The accuracy of the technique based on a comparison of consecutive angular scattering data is equal to the angular spacing of the data. The most accurate of these previous investigations determined the extrema for monodisperse distributions to within 0.4^{o} using a comparison of consecutive data spaced at 0.4^{o} intervals [21-23]. Preliminary calculations in the present study indicated that the location of the angular extrema had to occasionally be known to within 0.1^{o} to resolve certain particle size distributions. Using either of the previous methods was out of the question for the proposed comprehensive study because of the enormous computational and graphical time requirements. A method had, therefore, to be devised which could determine the angular scattering extrema with the required high precision without excessive computer time and cost.

A number of different approaches to determine the angular extrema were investigated. The initial response to finding the scattering extrema was to take derivatives of the Mie[3] functions as is done for elementary functions. However, setting the resultant derivative to zero and solving for the angular roots appeared to be far too complicated and subject to very large errors in the extrema locations. A closely related method in which the derivative of the Mie functions are used in the Newton-Raphson method[34] seemed to be feasible. The major drawback of this method was the development and testing of an entirely new computer code. The code for determining the scattering intensities from heterodisperse distributions had taken over two years to develop.[35] Rather than spend a considerable amount of time to develop a new code it was decided to modify the available Mie intensity code* for the present investigation and apply numerical methods to find the extrema.

The Fibonacci method[37] was selected to determine the extrema of the scattered intensities. This is the most widely used single variable search technique constrained to search within a given interval. The procedure is based on reducing the interval in which an extremum is located by systematically eliminating a portion of the original interval using positive integers known as the Fibonacci numbers. The Fibonacci numbers are used to locate two points within the interval for function evaluation. The function values at these two points determine the portion of the interval that should be eliminated. This process is continued by repeatedly determining function values within the reduced interval and making the appropriate interval reduction.

The computer code listed in the book by Kuester and Mize[37] was modified to reduce the number of function evaluations. As written, the code would re-evaluate

*The Mie intensity code was previously written to generate tables of light scattering intensities.[36]

one of the two points used to reduce the search interval for each iteration. Minor changes in their program to eliminate this re-evaluation reduced the number of required function evaluations by about half.

An important aspect of all the numerical methods used in the present study to locate extrema is the initial detection of an extremum. It is a waste of computer time to perform a detailed extremum search in an angular region that does not contain an extremum. Therefore, an initial search of the extrema was made using intensity data spaced at sufficiently small intervals to allow detection of the extrema yet large enough to minimize the number of data points. The initial search method used for all of the numerical techniques in the present investigation is described later in this chapter.

Despite the significant improvement over the methods used by previous investigators, the computer code using the Fibonacci algorithm combined with the modified light scattering code was far too time consuming for the proposed investigation. It was estimated that the computation time would have to be reduced by two orders of magnitude to allow the calculations to be run in the neighborhood of 10 hours central processor time for the IBM-360-65 computer. To accomplish this reduction an extensive investigation was made on optimizing the light scattering code and developing improved extrema search algorithms.

B. Optimization Of The Light Scattering Code

The light scattering code developed by Yajnik et al[35] calculated the angular scattering intensity for heterodisperse distributions by integrating ther scattering intensity from a weighted average of monodisperse particles. The code for determining the scattering from monodisperse particles was very similar to the one developed by Denman et al.[38] A comparison of monodisperse calculations in the present investigation with

Denman's results generally indicated agreement to five decimal places with occasional differences of one unit in the fifth place. Although attempts to improve the efficiency of Denman's code were unsuccessful, a significant reduction in computation costs were obtained by optimizing the integration method.

1. Numerical Integration Over a Particle Size Distribution Using Simpson's Rule

The size distribution function used to calculate the integrated intensity function for heterodisperse systems is defined[39] by

$$f(r,r_o,s) = (r-r_o)\exp\left\{-[(r-r_o)/s]^3\right\}, \quad r > r_o$$
$$= 0 \qquad\qquad r \leq r_o \tag{5}$$

where r is the particle radius in μm

r_o is the particle radius of the smallest particle present in μm

s is a parameter proportional to the width of the distribution in μm.

The modal radius (radius at the peak of the distribution curve), r_M, is defined by

$$r_M = r_o + s/\sqrt[3]{3} \tag{6}$$

The distribution is shown in Figure 1 where the characteristic features of a sharp cut off in small particle sizes and the positive skew at large particle sizes are seen. The modal radius is also indicated. Such a distribution was found to describe particle size distributions found in many different systems.[39]

Since the light scattering process depends on the relative size of the particles compared to the wavelength of light and not on the absolute size, the common practice is to use the relative sizes. Therefore, instead of

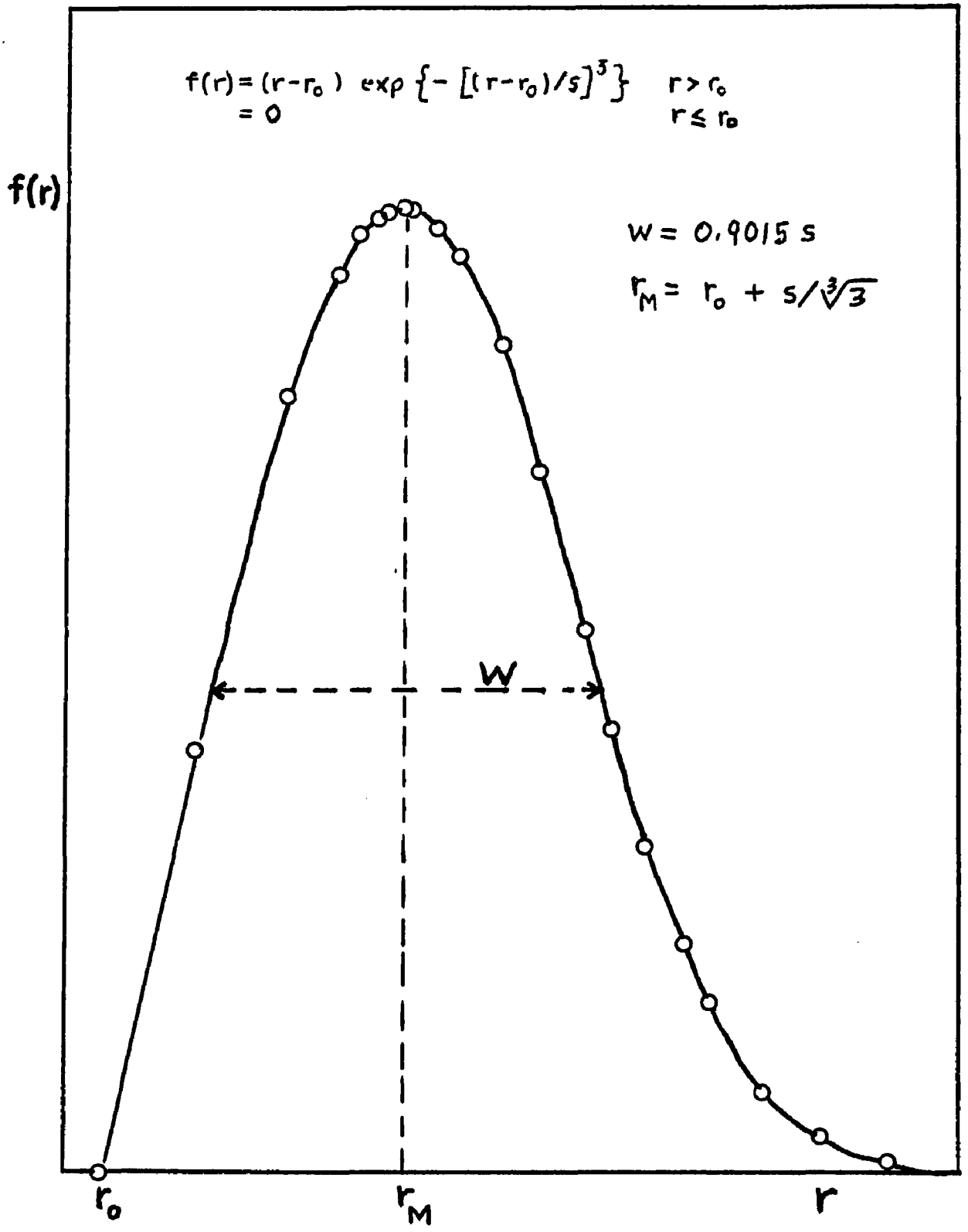

Fig. 1. The Exponential Distribution Function used in This Investigation

using the absolute terms r, r_o, r_m, and s one uses the relative terms α, ρ, α_M and q respectively. These terms are defined[39] below.

$$\alpha = 2\pi r/\lambda \tag{7}$$

$$\rho = 2\pi r_o/\lambda \tag{8}$$

$$\alpha_M = 2\pi r_M/\lambda \tag{9}$$

$$q = 2\pi s/\lambda \tag{10}$$

Using these relative terms, one can calculate the integrated scattering intensity from the heterodisperse distribution given by equation 5.

$$I(\rho, q, \theta) = \int_{\rho}^{\alpha_L} f(\alpha, \rho, q)\ i(\alpha,\theta)d\alpha \tag{11}$$

where $I(\rho, q, \theta)$ is the intensity scattered at angle θ from a heterodispersion characterized by ρ and q

θ is the scattering angle measured from the forward direction

$i(\alpha,\theta)$ is the Mie scattering intensity[38] at angle θ for a particle of size α

α_L is the largest particle size of the distribution that contributes to the integrated scattering.

Since a computer performs the integration a summation is used instead of equation 11.

$$I(\rho, q, \theta) = \sum_{j=1}^{j=n} f(\alpha_j, \rho, q)\ i(\alpha_j, \theta)\ W(\alpha_j) \tag{12}$$

where j is an integer representing the jth argument of the integration

n is the number of arguments used in the integration and depends on the integration method

$W(\alpha_j)$ is a weighting function that depends on the integration technique

Although the available code written by Yajnik et al[35] used Simpson's rule to perform the integration, a fresh look at all of the possible integration methods was considered important to reduce the computational costs. It is well known that Gaussian quadrature techniques are more accurate than integration techniques using equally spaced arguments.[34,40] However the Gaussian techniques dictate the location of the arguments to be used in the integration. The location and intervals between these arguments are such that different size distributions have a different set of arguments even if the two distributions overlap significantly.

In contrast, the integration techniques based on equally spaced arguments would allow different distributions to use the same arguments that occur in overlapping size distributions with a tremendous saving in computer time. The integration method used by Yajnik et al[35] thus proved to be the best choice for the present application. He used Simpson's rule, which has equally spaced arguments and better approximates sinusoidal type of functions than other methods like the trapezoidal rule.[34]

2. Selecting the Integration Limits and Integrand Intervals Based on Error Analysis

Having decided on Simpson's rule, the choices for the integration limits and the size of the integrand intervals had to be made. Normally the decision for the size of the interval is not required because computer codes using Simpson's rule reduce the interval size by half after every integration until two consecutive integrations differ by less than the desired accuracy.

This approach was not satisfactory for the present investigation because half of the integrand points are then used as an accuracy check on the integration. If the number of integration arguments required for the desired accuracy were known for a given integration, then the convergence test can be eliminated and thereby reduce the integration arguments by half.

In most cases the saving in the number of integration agruments does not warrant the additional programming time required to determine the number of arguments needed for a desired accuracy. It is generally more efficient, considering the programmer's time and the computional time, to let the computer determine the integration accuracy for each case. However, the potential saving in the present investigation was substantial, thus making the additional accuracy checks worthwhile.

The number of integration arguments required to accurately determine the integrated scattering intensity from equation 12 is determined for the integrand, $f(\alpha_j, \rho, q)\, i(\alpha_j, \theta)$, which is the product of the size distribution function of equation 5 and the Mie intensity function. The parameters ρ, q, and θ will determine the number of integrand points that are needed to accurately determine the integration. Figures 2-4 show plots of the integrand versus the relative size α for different parameter values. These graphs show the expected result that as the heterodispersion increases from $q = 0.2$ in Figure 2 to $q = 5.0$ in Figure 4 the integrand covers a larger α range and becomes more oscillatory. Note that Figure 2 has an expanded α scale compared to Figures 3 and 4. To maintain the same accuracy for integrating these curves will require a greater number of α_j arguments for the larger q values.

The effect of the parameter ρ on the integrand is seen in Figure 3 where

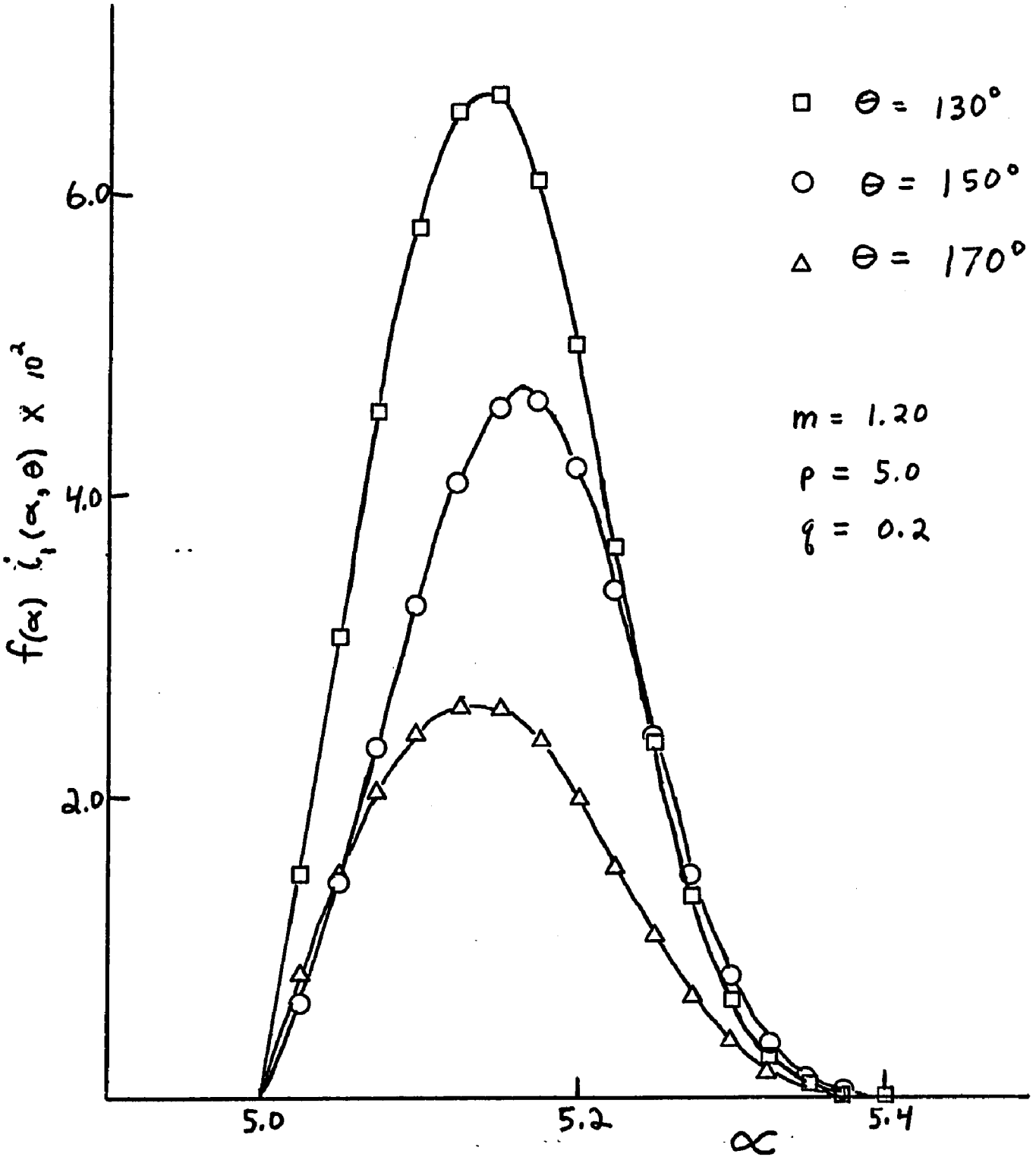

Fig. 2. Integrand Values Versus Relative Particle Size α for m=1.20, p=5.0, q=0.2 and I_1

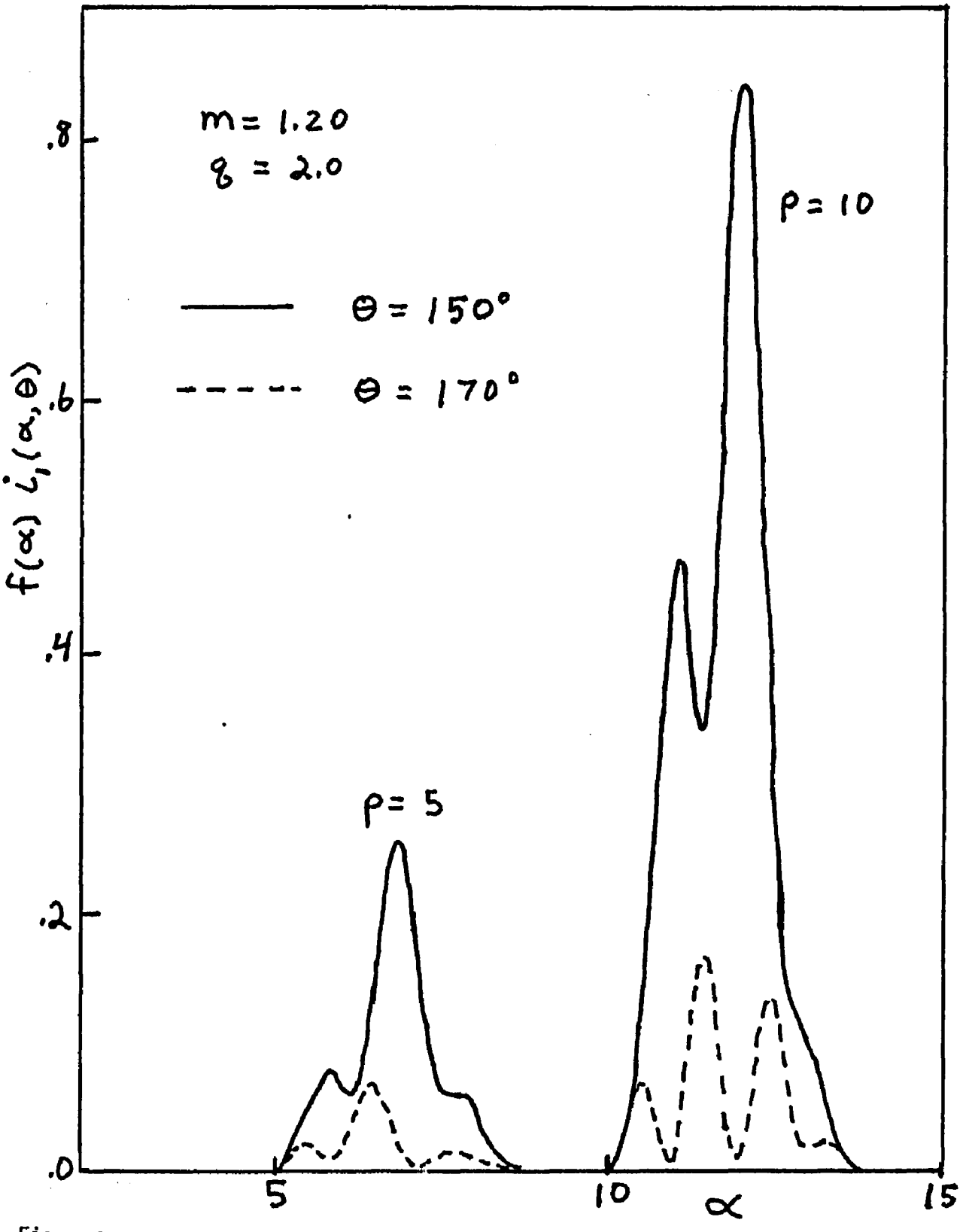

Fig. 3. Integrand Values Versus Relative Particle Size α for m=1.20, p=5.0 and 10.0, q=2.0 and I_1

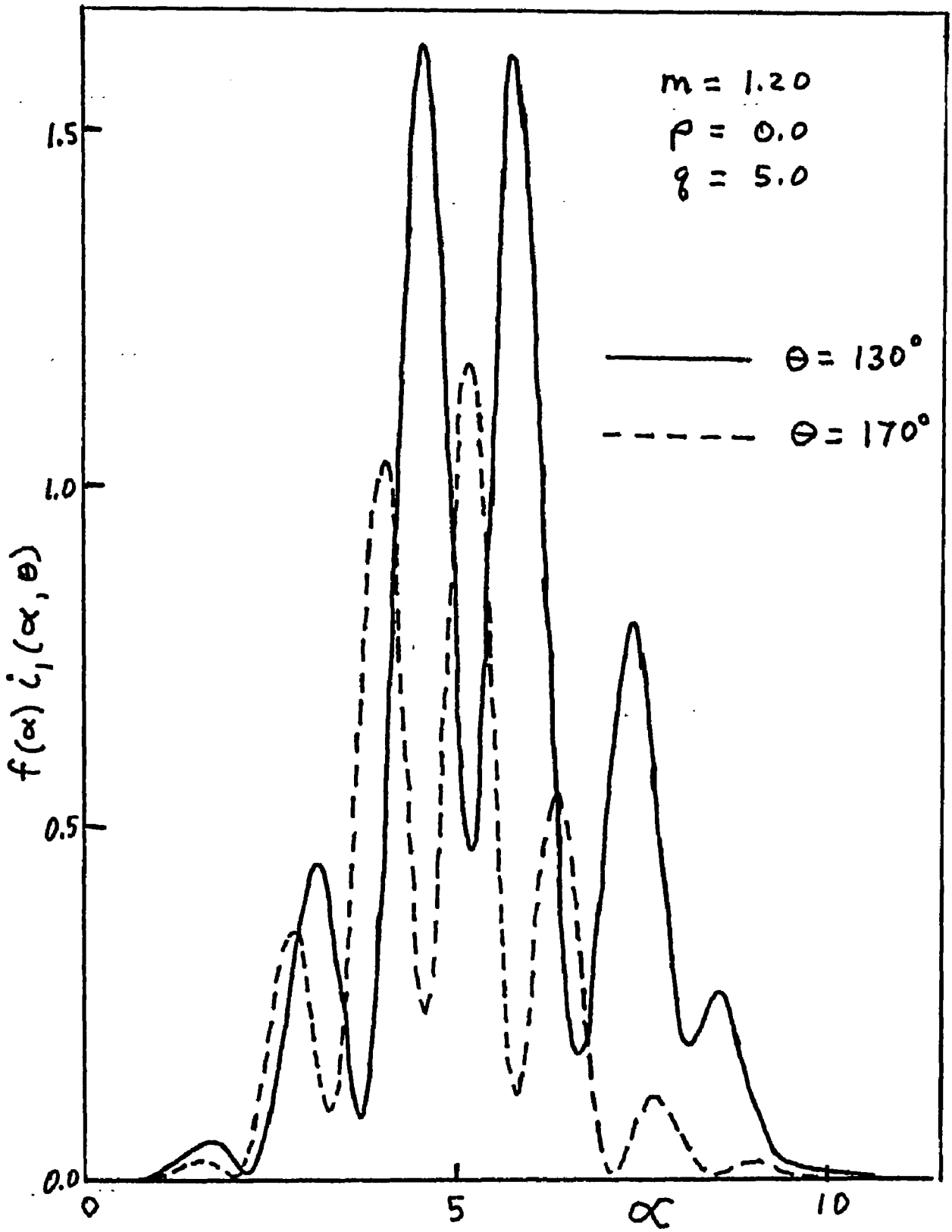

Fig. 4. Integrand Values Versus Relative Particle Size α for m=1.20, p=0.0, q=5.0 and I_1

integrands for $\rho = 5$ and $\rho = 10$ are plotted. Increasing the ρ value generally increases the magnitude of the integrand but not the basic oscillatory pattern. This follows from the approximately periodic oscillations in the scattering functions with increasing α shown in the study by Heller and Nakagaki.[41] The number of arguments required to obtain a given integration accuracy depends on the oscillation pattern of the integrand. ρ is therefore expected to have little effect on the accuracy of integration for a given number of arguments.

Figure 3 also shows that increasing the angle θ from 150° to 170° results in a greater number of oscillations, thus requiring more α_j arguments to maintain a constant integration accuracy. Conversely, at a fixed number of arguments, the integration at 170° will be less accurate than the integration at 150°.

A systematic study was then made to quantitatively assess the error due to the number of arguments used in the integration. The parameters used in this study were $q = 0.2, 1.0, 2.0$; $\rho = 0(5)15$; $\theta = 30^{\circ}(30^{\circ})\ 150^{\circ}, 170^{\circ}$; $m = 1.20$; and vertical polarization. Each combination of parameters represents a particular integrand similar to the ones drawn in Figures 2 and 3. The error analysis consisted of integrating a particular integrand curve five different times using a larger number of arguments for each integration. Twenty arguments were used for the initial integration with each subsequent integration using twenty additional points until 100 points were used to evaluate the final integration.

The results for all of the parameters having $\rho = 5$ are shown in Figure 5 where the relative error is plotted against the heterodispersion parameter q.

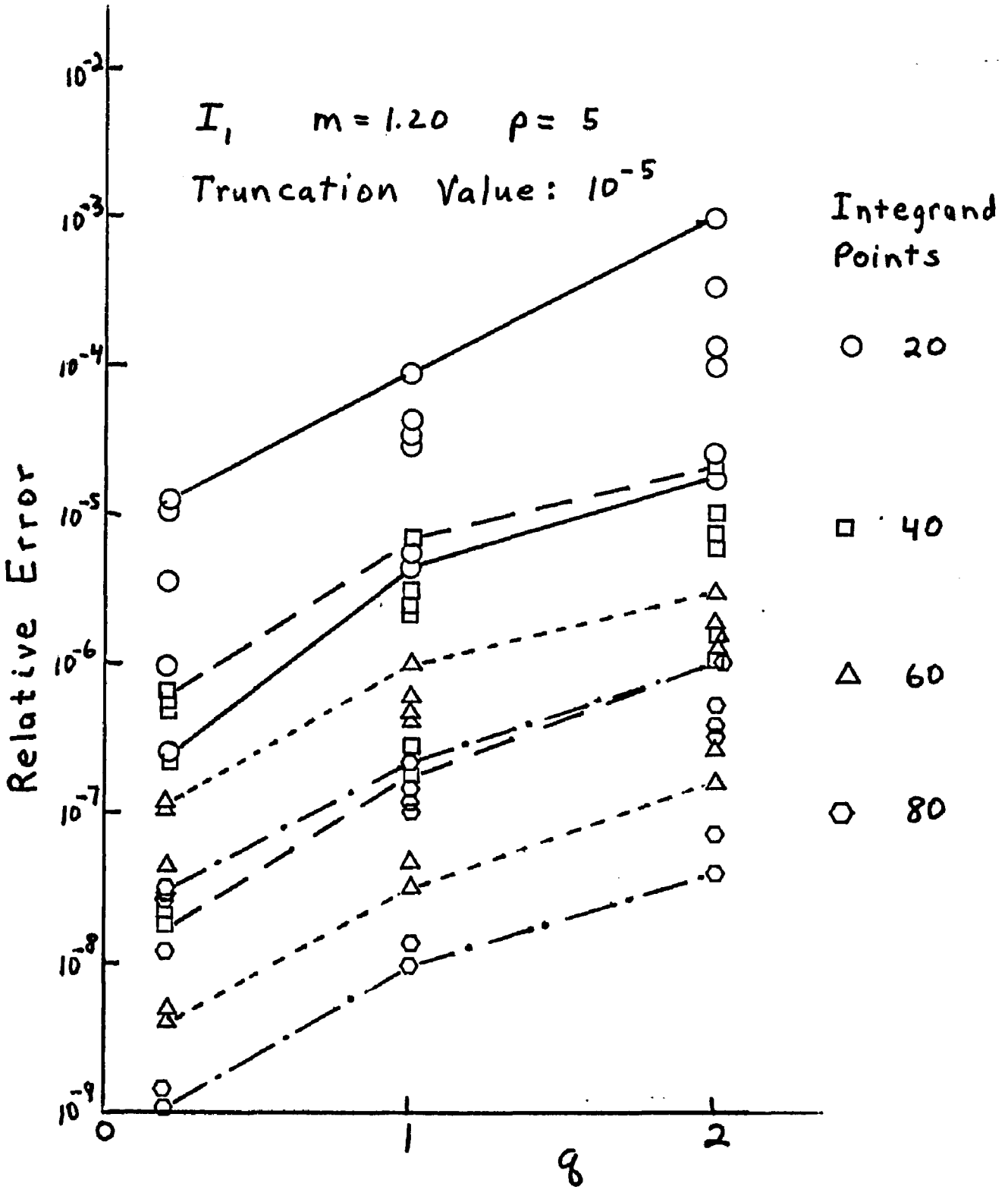

Fig. 5. Relative Error of the I_1 Integrated Intensity Versus q Using Different Numbers of Integrand Points. The Distribution Functions Have p=5.0 and Are Truncated When Its Value Is Less Than 10^{-5}

The relative error is defined as $(I_n - I_{100})/I_{100}$, where I represents the integrated intensity and the subscripts represent the number of arguments used in the integration. Line segments separate the regions where a different number of arguments were used to evaluate the integral. The points shown on the graph correspond to the individual angles used in this study. Note the large variation in the relative error at a given q value and constant number of integrand points. This variation is due to the significant changes that occur in the integrand curves for different angles. The accuracy of the integrated intensity is in general much better in the forward scattering direction than in other directions because the integrand curve has progressively fewer oscillations as the angle θ is reduced to 0^o. Deviations from this trend occur whenever the integrand curve at a given angle shows a less complicated curve than the corresponding integrands at smaller angles.

Figure 5 also shows the expected increase in the relative error with an increase in q while maintaining the same number of integrand points. Note that the increase in the relative error from $q = 0.2$ to $q = 2.0$ for the angular range as a whole is approximately equal to the variation in relative error within the angular range at a constant q. Moreover, the relative error does not increase uniformly for all angles as the heterodispersion is increased. This non-uniformity results in a periodic rearrangement of the general pattern where smaller angles exhibit smaller relative errors.

The most important feature in Figure 5 for the present investigation is the decrease in the relative error of the scattered intensity with an increase in the number of integrand points used in the integration. To obtain the desired accuracy for the integrated intensity the number of integrand points

is adjusted for the different variables using the relative error information in Figure 5. Ideally the number of integrand points should be minimized as a function of the heterodispersion q and the angle θ while maintaining a constant accuracy. Although minimizing the number of integrand points to provide a uniform accuracy for all angles will save a few points for individual angles, doing this will actually result in a tremendous increase in the total number of points required for all the angles. By using a different number of integrand points for each angle, the integrated intensity from different angles could not reuse the points from previous angles.

The problem is compounded since overlapping size distributions would not have any integrand points in common. Recall that Simpson's rule was chosen for the integration method rather than the more efficient Gaussian quadrature because of the tremendous savings that result in reusing the integrand points. Similarly the immediate savings realized by minimizing the number of arguments for each angle is insignificant compared to the added number required for all the angles.

The number of points in the integrand for a given size distribution characterized by ρ and q were therefore selected on the basis that the relative error for all angles was equal to the greatest error. In addition, similar results for $\rho = 0$, 10 and 15 indicated that except for $\rho = 0$, the relative error was approximately independent of ρ. The data for $\rho = 0$ showed a smaller error as expected because the integrand has not yet developed the oscillations seen at higher ρ values.[41]

Thus, for a given number, j, of α_j points, q is the only remaining variable in the integrand, $f(\alpha_j, \rho, q)\ i(\alpha_j, \theta)$, of equation 12 that affects the relative

error of the integrated intensity, $I(\rho, q, \theta)$. This relationship allows one to calculate the number of integrand points required to obtain a desired accuracy for a given q value. The accuracy of the integrated scattering intensity to five decimal places was considered sufficient for the present study. The number of integrand points were then determined from Figure 5 so that the relative error would be less than 10^{-5} for every q value considered. An additional restriction was placed on the number of integrand points because the size distribution parameters were changed in increments of 0.2. To enable overlapping size distributions to use all of the integrand points in common, the size increment between points had to be a fraction or multiple of 0.2.

Strictly speaking the integrand points, $f(\alpha_j, \rho, q)\ i(\alpha_j, \theta)$, at different α_j arguments can not be reused for overlapping size distributions or different angles having the same size distribution. This follows because $f(\alpha_j, \rho, q)$ changes with different size distributions and $i(\alpha_j, \theta)$ changes with different angles. The integrand points were said to be reusable for different size distributions and different angles because the most time consuming portion of the integrand points can be reused. The Mie intensity function is given by the following equation[38]:

$$i(\alpha,\theta) = \left| \sum_{n=1}^{\infty} A_n(\alpha)\,\pi_n(\theta) + B_n(\alpha)\,\tau_n(\theta) \right|^2 \qquad (13)$$

where $A_n(\alpha)$ and $B_n(\alpha)$ are the Mie coefficients

$\pi_n(\theta)$ and $\tau_n(\theta)$ are angular functions

The Mie coefficients $A_n(\alpha)$ and $B_n(\alpha)$ are very complicated functions of Bessel functions and are responsible for most of the computational time in calculating Mie intensity functions. These Mie coefficients are saved and reused in over-

lapping size distributions and different angles. In addition, the size distribution function $f(\alpha, \rho, q)$ is reused when scattering intensities for the same distribution but different angles are calculated.

Table I shows the number of integrand points required for different q values when both the relative error of the integration and the restriction on the size increment $\Delta\alpha$ are taken into account. The α range for the integration and the size increment between the points are also shown. The upper size limit for the integration α range shown in Table I represents the point at which the size distribution was truncated. The truncation value of the size distribution shown in equation 5 was 10^{-6} for the present study. All of the scattering intensities calculated in the present investigation used the number of integrand points shown in Table I for different q values. Since the analysis was not extended to higher q values, the size increment was maintained at 0.1 for those occasional calculations.

A very important feature in Table I is the dependence of the size increment $\Delta\alpha$ on q. To maintain a given accuracy in the calculated scattering intensity, the size increment $\Delta\alpha$ must be greatly reduced as the particle size distribution becomes more monodisperse (lower q values). The increased error at small q values observed in the tabulations by Yajnik et al[36] resulted from using a larger size increment $\Delta\alpha$ than recommended in the present study.

Dave[42] investigated the effect of using different size increments ranging from 0.1 to 2.0 to integrate scattering functions and concluded that size increments of 0.1 must be used to obtain accurate results. His study used only two very heterodisperse size distributions and consequently failed to observe the dependence of the integration accuracy on the heterodispersion

TABLE I

Number of Integrand Points Required for Different q Values to Make the Integration Relative Error Less than 10^{-5}

q	α Range	$\Delta\alpha$	No. Points
.2	0.5	.0125	40
.4	1.0	.025	40
.6	1.5	.025	60
.8	2.0	.05	40
1.0	2.5	.05	50
1.2	3.0	.05	60
1.4	3.5	.05	70
1.6	4.0	.1	40
1.8	4.5	.1	45
2.0	5.0	.1	50

and scattering angle.

The preceding analysis allowed the number of integrand points required for evaluating integrated light scattering intensities to be reduced by approximately half when compared to the conventional application of Simpson's rule. In the conventional method the number of integrand points are doubled after each integration until two consecutive integrations agree to within the desired accuracy. Additional computer savings were obtained by computing the integrand points for only one size distribution at a time and storing only that fraction that overlapped the next size distribution. Storing all of the integrand points as done previously[36] until the desired computations were completed results in high computer memory costs.

The effect of the integration limits on the accuracy of the integrated scattering intensity was also investigated. The size distribution function used in the present study (equation 5) has a sharp cut off for small particles and therefore does not contribute to any error. However, the upper limit of the distribution function shows an exponential decay which continues to infinity. The error in the calculated intensity will increase as the exponential tail is truncated at smaller particle sizes or, equivalently, at larger values of the distribution function.

A series of intensity calculations were made to quantitatively measure the error due to truncating the size distribution at different values. The parameters used in this study were q = 0.2, 1.0, 2.0; ρ= 0(5)15; θ = 60°, 120°, 170°; m = 1.20; and vertical polarization. Each set of parameters represents one particular integrand. The relative error resulting from the truncated distribution is defined by $(I_n - I_{-7}) / I_{-7}$, where I represents the integrated

intensity and the subscripts represent the base 10 logarithms of the distribution function at the truncation point. Thus I_{-7} represents the integrated scattering intensity from a size distribution that was truncated when its value dropped to 10^{-7}.

Figure 6 shows the relative error of the scattered intensity for $\rho = 5$ at different angles and degree of heterodispersions plotted against the truncated value of the distribution function. The expected decrease in the relative error for smaller truncation values is readily seen. In addition there is a trend, although not consistent, toward larger relative errors with larger q values. The behavior for the different angles is not clear.

Corresponding data for $\rho = 10$ and 15 show approximately the same values as seen in Figure 6 for $\rho = 5$. However, the data for $\rho = 0$ shows a higher relative error than the larger P values. This observation is expected because the scattering intensity increases very rapidly from the Rayleigh region at $\rho = 0$ and therefore magnifies any changes in the tail section of the distribution. Based on these results the truncation value of the distribution was set at 10^{-6} for the scattering calculations in the present study.

The investigations on the relative error due to the number of integrand points and the truncation of the distribution function were based on calculations using $m = 1.20$ and incident light polarized perpendicular to the plane of observation. The optimum number of integrand points and the truncation values from these studies were then used on m values ranging from 1.05 to 1.333 and incident light that was unpolarized and polarized parallel and perpendicular to the plane of observation. Based on the discussion earlier in this chapter, the relative error for the integrated intensities will increase

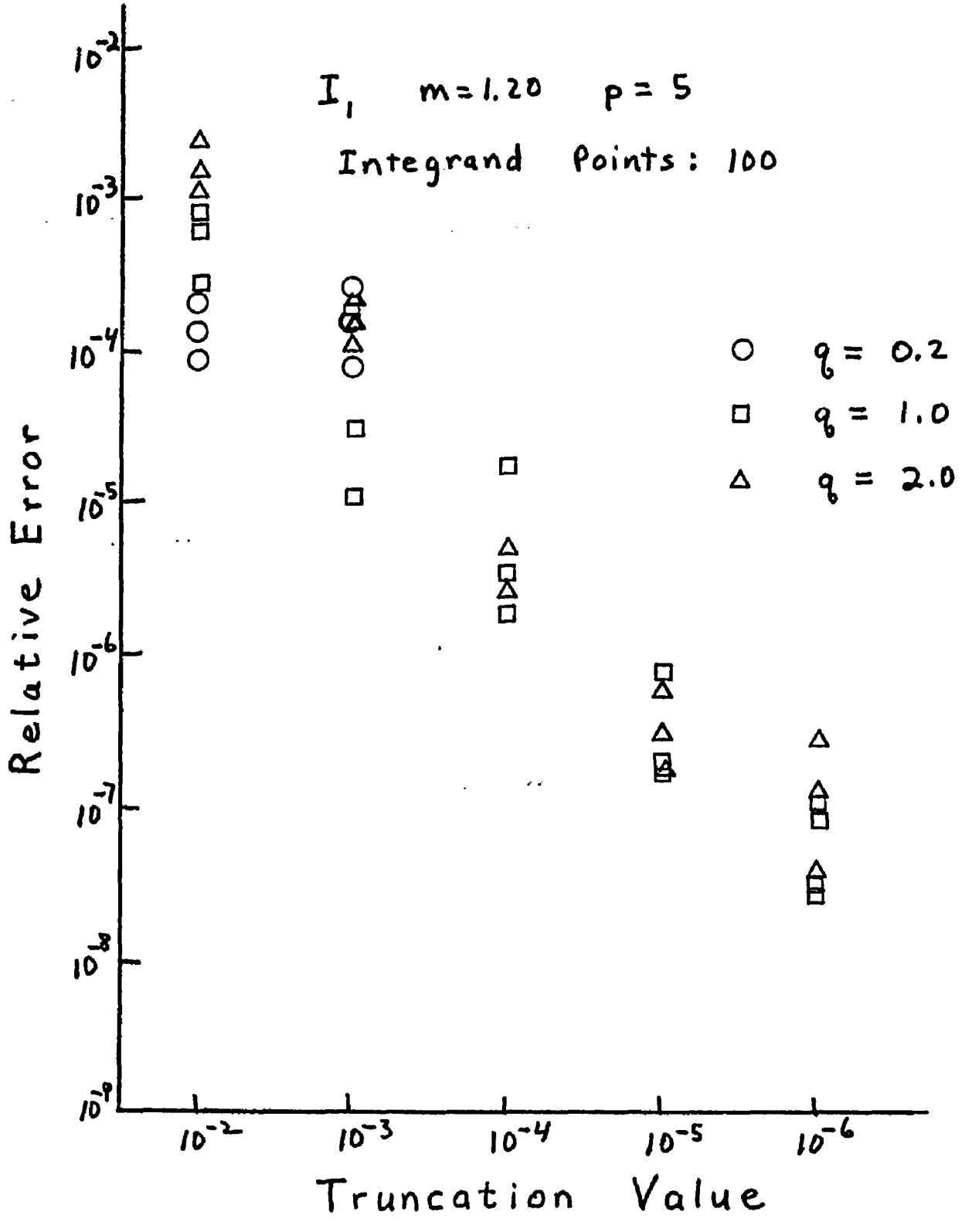

Fig. 6. Relative Error of the I_1 Integrated Intensity Versus the Distribution Truncation Value Using 100 Integrand Points. The Distribution Functions Have p=5.0 and the Stated q Values

as m increases from 1.20 to 1.333 and decrease as m decreases from 1.20 to 1.05. The primary factor that controls the relative error is the oscillation of the integrand which increases slightly with larger m values.

The relative error due to truncating the size distribution should remain approximately constant with changes in m. This error depends on the relative scattering intensity for particle sizes at the tail of the distribution compared to the scattering intensity from the rest of the size distribution. As the refractive index increases the two regions will change proportionately.

Changing the polarization of the incident light is expected to have a minimal effect on the relative error of the integrated scattering intensity. Since the scattering from unpolarized light is very similar to that for perpendicular polarized light, the expected relative error would be similar. The monodisperse scattering from horizontally polarized light is generally less oscillatory than from vertically polarized light and should therefore also have lower relative errors for the integrated scattering.

C. Development And Evaluation Of Extrema Search Algorithms

The first algorithm used to determine the maxima and minima of angular light scattering intensities was the Fibonacci algorithm[37] described earlier in this chapter. However, the number of intensity functions required to determine an extremum was far too great for this method to be considered. An extensive study was then made of the numerical methods for obtaining light scattering extrema. These methods were restricted to those algorithms that do not require function derivatives.

1. Interval Halving

The next method investigated was an interval halving algorithm called

EXFIND obtained from the Ford Motor Company.[43] This algorithm determines extrema in the following manner. Function values y(x), y(x+h) and y(x+2h) were calculated at three equispaced points, x, x+h and x+2h starting from an initial point x and the slopes of the two connecting line segments determined. If the slopes did not differ in sign then a new function value y(x+3h) was calculated at a point x+3h determined by adding the increment h to the last point. The slope from the new segment is then compared to the previous segment. If the slopes do not differ in sign again the preceding steps are repeated. However, if the slopes of the last two line segments differ in sign, then a new increment h_1 is obtained by halving the previous increment and reversing its sign.

Now that an extremum has been detected a detailed search is undertaken using the same instructions from the initial search but a new increment h_1. Three new function values y(x), $y(x+h_1)$ and $y(x+2h_1)$ are then calculated at the three equidistant points x, $x+h_1$ and $x+2h_1$*. The slopes for the line segments are then determined and the above procedure repeated. Note that this iteration search moves in the opposite direction using half the increment size compared to the initial search. When consecutive slopes in this first iteration differ in sign, a new increment h_2 is obtained by halving the previous increment h_1 and reversing its sign. Thus the extrema search in the second iteration is in the same direction as the original search but with the search increment reduced by $(1/2)^2$. Higher iterations will search for the extremum first in one direction and then the other, using smaller increments each time.

*Although the EXFIND code recalculated the points y(x) and $y(x+2h_1)$, over 50% savings can be obtained by storing these previous calculations.

After n iterations the interval in which the extremum is located will be reduced by $(1/2)^n$.

2. Generalized Interval Reduction

The concept of the interval halving method was then generalized to any reduction factor r. However using interval reduction factors much smaller than 0.5 presents the problem of where to begin the new search. Starting from the end point of the previous interval, as done in the interval halving method, would be very inefficient for most of the extrema determinations. The exception would be those extrema that occur near the endpoint. However in the majority of cases the extrema lie in the central portion of the three point interval.

A number of different approaches could be used to locate the initial search area. The generalized interval reduction method uses points already calculated by initially having the middle point of the larger interval be the first point of the reduced interval. Other approaches would use the points from the larger interval only to estimate the location of the extremum. The reduced interval would then be centered on this estimate. A possible method for estimating the extremum location would be to fit a parabola to the initial three points and determine the parabola extremum. This approach will be discussed as the next extremum search method.

The generalized interval reduction method uses the same initial search technique as in the interval halving method to initially locate an extremum. Once the extremum is located within a three point region the increment h is reduced by the factor r and the middle point x_m from the larger interval is used as the middle point x_m in the reduced interval. Since it is possible that the extremum will not lie within the interval $x_m \pm h_1$, only one of the

new end points will be calculated for a preliminary test. This new end point is calculated at x_m+h_1 in the direction of the steepest slope. The steepest slope refers to the largest slope of the two line segments containing the previous three points. The other end point is retained from the line segment having the steepest slope.

A preliminary test is then made to see if the extremum is contained within the region by comparing the sign of the two slopes corresponding to the line segments in this new region. If the two slopes have the same sign then the new end point has undershot the extremum. When this happens a new point is calculated at $x_m + 2h_1$ and the slopes of the two line segments in the interval x_m to $x_m + 2\ h_1$ compared to see if the extremum has now been enclosed. If not, additional points are calculated in the same direction at increments of h_1 until the extremum has been enclosed.

However if the two slopes in the preliminary test have opposite signs then the new end point has correctly overshot the extremum. The other end point is then calculated at $x_m - h_1$ and the sign of the two slopes of the line segments from $x_m - h_1$ to $x_m + h_1$ compared. If the slopes do not differ in sign then the extremum is not contained within the region and a new point is calculated at $x_m - 2h_1$. Additional points as needed are calculated in the same direction at increments of h_1 until the extremum is enclosed within the interval.

After the extremum has been enclosed within the interval a check is made to see if the interval were reduced to the desired level. If not, then the increment h_1 is reduced by the factor r and the preceding sequence of steps

repeated a second time. After n iterations the increment is reduced by $(r)^n$.

3. Parabola Fitting

Another method for determining where to begin searching for an extremum already enclosed within an interval uses the extremum of a parabola fitted to the three points. In contrast, the interval halving method begins at the endpoint while the generalized interval reduction begins at the midpoint. Once the points are found that enclose the extremum, a parabola is fitted, to these points. The extremum from the parabola will then serve as the midpoint x_m in the search of a reduced interval using smaller increments h. Except for this change in determining the middle point x_m in the reduced interval, the parabola fitting and the interval reduction methods are identical.

4. Comparison of Extrema Search Algorithms

The preceding numerical methods for determining extrema locations were then tested on the light scattering curves shown in Figure 7. This figure shows the scattered intensity plotted against the angle of observation for the four different monodisperse particle size distributions characterized by $p = 3$, 5, 7 and 15 and $q = 0$. The relative refractive index for the system is 1.20, and the incident light is polarized perpendicular to the plane of observation. The extrema from these scattering curves are typical of the ones encountered in the present investigation and will therefore be a realistic test of the relative performance of the numerical methods.

All of the numerical methods used the same initial search technique described earlier to locate the general region of each extremum. The initial search would scan one curve at a time using intensity data spaced every 5^o and

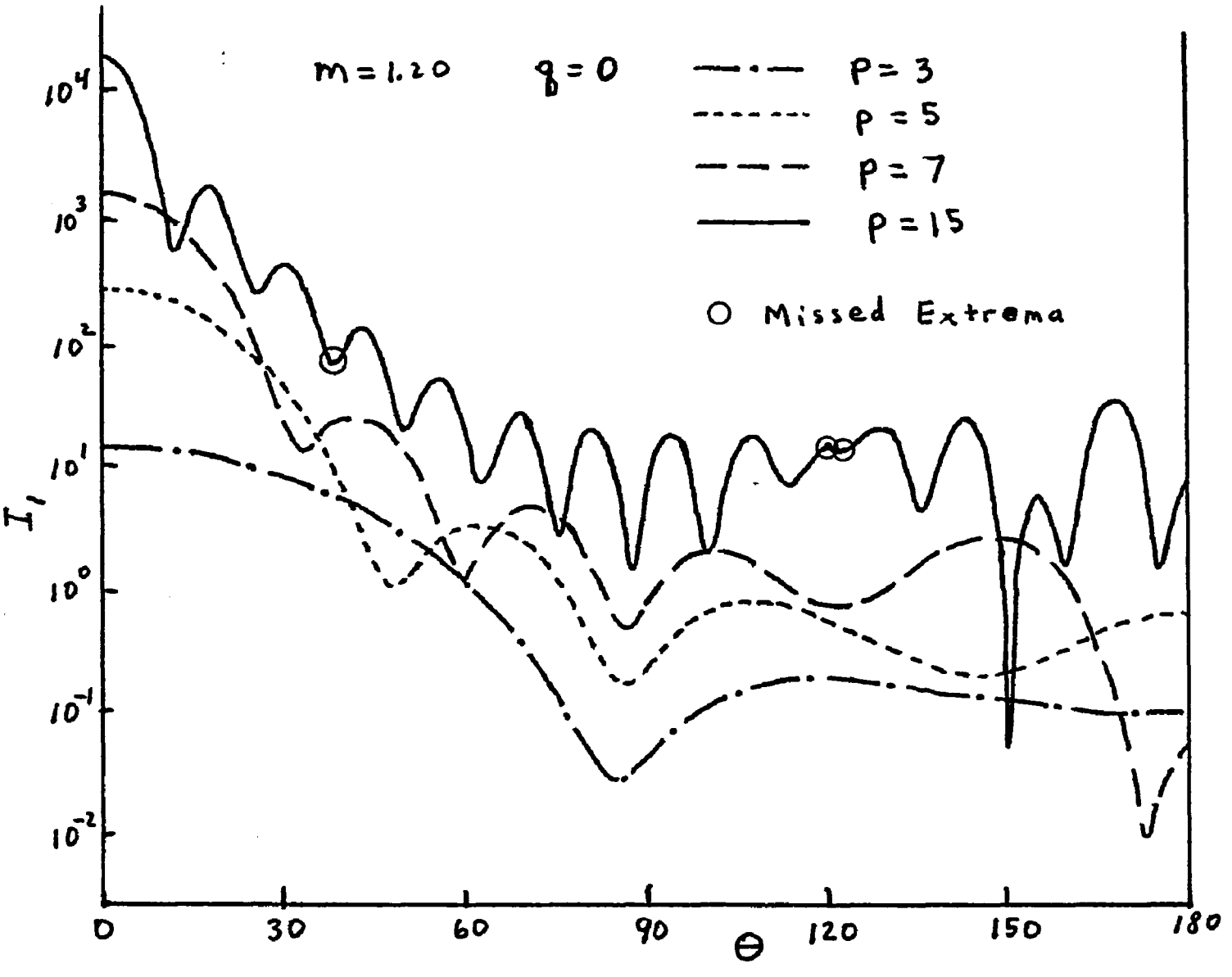

Fig. 7. Scattered Intensity I_1 Versus Angle θ from Particle Size Distributions Having p=3, 5, 7 and 15 and q=0.0

locate the extrema within a three point interval. Once the extrema were located within an interval of $\pm 5^{\circ}$ the numerical methods would resolve the extrema locations to $\pm 0.005^{\circ}$. The total number of points required to determine all of the extrema from the curves in Figure 7 to an accuracy of $\pm .005^{\circ}$ was then determined for each numerical method. The initial points spaced every 5° were not counted in the total. Several repetitions of the extrema searches were required for the parabola fitting and interval reduction methods to compare different reduction factors.

Although there are 43 extrema in Figure 7, three of the extrema were missed by the initial search at 5° intervals. These extrema are indicated in the curve for $\rho = 15$. The two shallow extrema at 120.5° and 123.0° were missed because the 5° spacing was too large. However, the minimum at 37.7° was missed even though the initial search technique indicated the presence of an extremum. All of the different numerical methods calculated the adjacent maximum at 42.7° instead. This behavior occurs periodically when no restrictions are placed on the region of the detailed search.

The results of using the different numerical methods to find the extrema of the graphs in Figure 7 are shown in Figure 8. This figure shows the total number of points needed to determine the extrema locations from an initial uncertainty of $\pm 5^{\circ}$ to a final uncertainty of $\pm 0.005^{\circ}$ plotted as a function of the interval reduction factor. The Fibonacci search algorithm has only one point because the interval in which an extremum is located is reduced by a constant factor for each iteration. This factor is controlled by the Fibonacci numbers. Similarly, the interval halving method, by definition, has a constant interval reduction factor of 0.5. Note that the Fibonacci

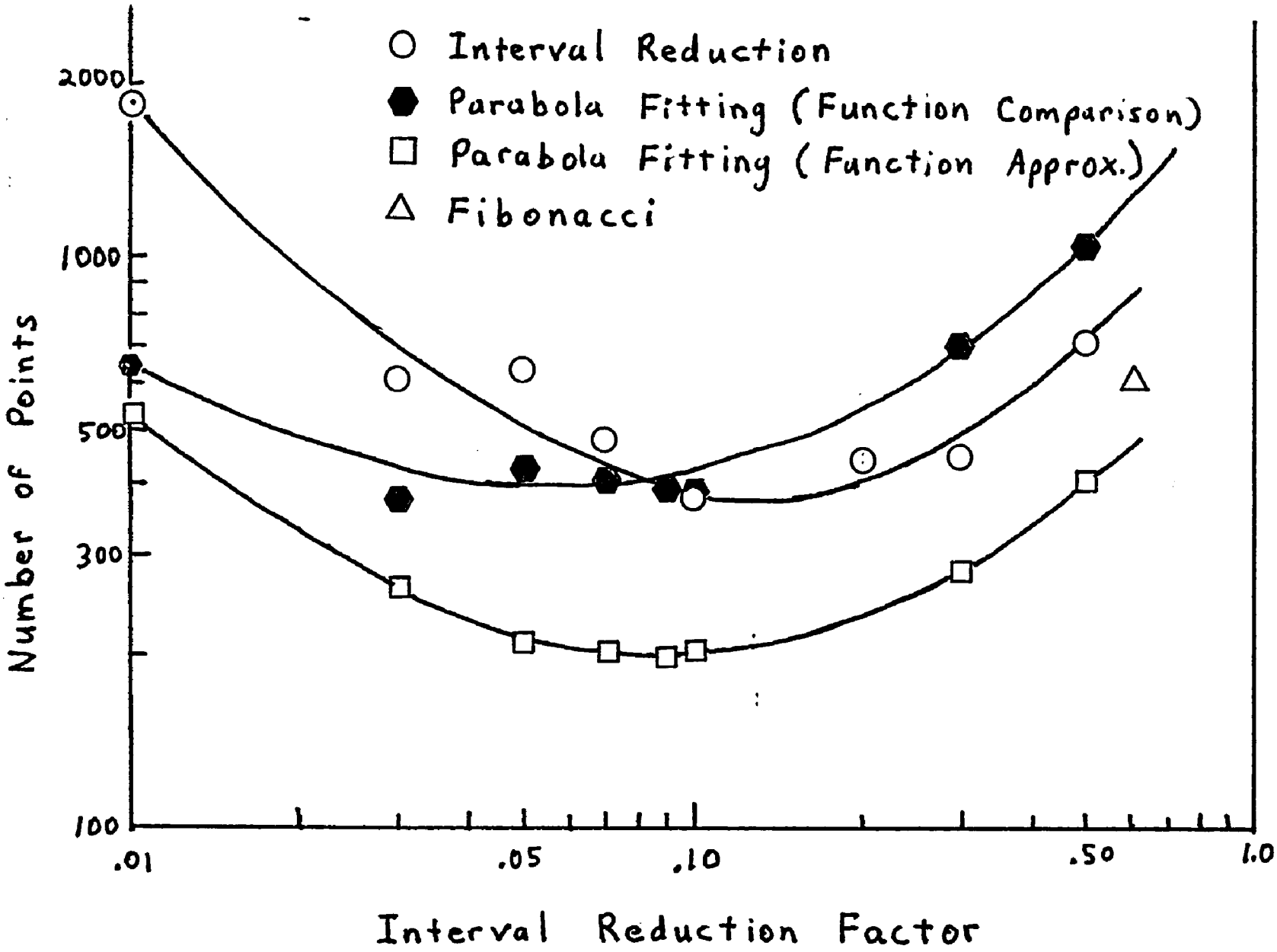

Fig. 8. Total Number of Intensity Calculations Required to Determine the Angular Extrema Locations in Figure 7 from an Initial Uncertainty of $\pm 5.0^{o}$ to a Final Uncertainty of $\pm 0.005^{o}$. This Number Is Plotted Against the Interval Reduction Factor Used to Reduce the Angular Uncertainty for Each Iteration of the Different Numerical Methods

and interval halving algorithms require approximately the same number of points to locate the extrema in figure 7 to $\pm$ 0.005°. The generalized interval reduction algorithm was tested at a number of different reduction factors from 0.01 to 0.5. Although there is some scatter about the curve drawn through these different tests the curve shows a pronounced minimum for an interval reduction factor of about 0.1.

A minimum is expected from an analysis of the two opposing processes involved for reducing the initial interval in which an extremum is located to the desired interval. One process is dependent on the interval reduction factor r. The number of times n that the interval must be reduced to reach a final interval decreases with smaller reduction factors since the total reduction after n repetitions is r^n. Each repetition of the interval reduction requires a minimum number of points. For the generalized interval reduction algorithm the minimum is two points while for the parabola fitting algorithm the minimum is three points. The total number of points is then n times this minimum.

The other process depends on the number of points required to enclose the extremum within an interval. As the interval initially containing an extremum is reduced to a smaller size, the extremum will frequently lie outside of the reduced interval. Additional points must then be calculated until an interval is found that encloses the extremum.

The two processes show the opposite trends as the interval reduction factor is reduced, thus resulting in a minimum. In the first process, the number of points required to reduce the interval decreases with r because

fewer repetitions n will result in the same total reduction r^n. However, as the interval reduction factor decreases, the extremum will not lie within the new interval and a greater number of points will be required to search for the extremum.

The extremes of these two cases require an infinite number of points to locate the extremum. For an interval reduction factor of 1.0 (i.e., no reduction at all) the interval will not be reduced regardless of how many attempts are made. Similarly an infinitesimal interval reduction factor will require an infinite number of points to locate the extremum since the consecutive points in the search move only in infinitesimal increments.

The criterion used for determining when a given extremum has been located to within $\pm$ 0.005° can make a large difference in the number of points required. This criterion is based on the type of extremum search methods used. Murray[44] has classified the linear search methods into two categories, one based on function comparison and the other based on function approximation. The function comparison methods compare the values of the function at different points to reduce the interval in which an extremum has been located. The difference in the various algorithms is how the location of the functions are to be determined. The Fibonacci, interval halving and interval reduction algorithms all fit in this category. In addition, the parabola fitting algorithm can also be placed in this category if the extremum from the parabola is used to calculate a point for a comparison test.

In the function comparison category the parabola extremum is not assumed to be an approximation of the extremum to be determined. This

point is used only to compute a function value for the function comparison test. The true extremum in these function comparison methods can never be assigned to a single point but rather to some interval. Thus the number of points required to determine an extremum to an accuracy of $\pm$ 0.005° is equal to the number which will reduce the interval in which the extremum is located to $\pm$ 0.005°.

The category of linear search techniques based on function approximation[44] use a simple function to approximate the function whose extremum is to be found. The simple function is often a polynomial generated from a fixed number of points calculated from the primary function. The extremum of the simple function serves as an approximation of the true extremum. More accurate approximations are obtained by determining the function value at the approximate extremum and using it to generate an improved simple function. This process is continued until the approximate extrema from the last two consecutive simple functions agree within the desired accuracy. In contrast to the function comparison methods, the extremum in this approach may be very accurately determined with only a small reduction in the interval containing the extremum.

The parabola fitting algorithm can be interpreted as either a function comparison or a function approximation method. Since the two interpretations show a large difference in the number of points required to determine an extremum, the results for both interpretations are plotted in Figure 8. The interpretation of the parabola fitting algorithm as a function comparison method is shown as the dashed curve. Note that above the interval reduction factor of 0.09 the parabola fitting algorithm requires more points to deter-

mine the extremum than the interval reduction algorithm. The total number of points in this region of larger reduction factors is primarily due to the minimum number of points required to reduce the $\pm 5^{o}$ interval to $\pm 0.005^{o}$. Since the number of iterations are the same, the greater number of total points required for the parabola fitting algorithm is due to the minimum number of points for each iteration. The parabola fitting algorithm requires three while the interval reduction algorithm requires only two.

The opposite trend is seen in the region of smaller interval reduction factors where the parabola fitting algorithm requires fewer points to locate the extremum than the interval reduction algorithm. The number of points required to determine an extremum in this region of small reduction factors is dominated by the search for additional points to enclose the extremum. Since the parabola fitting algorithm allows the search to be conducted near the extremum fewer points are required compared to the interval reduction algorithm.

If the parabola fitting algorithm were interpreted as a function approximation then the number of points required to determine the extrema is shown as the lowest curve in Figure 8. Although both interpretations used the same data points, the one based on the function approximation shows a considerable decrease in the number of points required. This decrease results from the ability of the function approximation method to predict the extremum location. The extremum in this approach is determined when two consecutive predictions agree within $\pm 0.005^{o}$ even though the interval of the data points is $\pm 0.05^{o}$ or even $\pm 0.5^{o}$. In practical applications the parabola fitting algorithms would be interpreted as the more efficient approximation method.

5. Repeated Polynomial Fitting Algorithm

Despite the significant reduction in the number of data points required to accurately locate an extremum, the computer time requirements were still excessive. A more thorough investigation of the function approximation methods was then made. The parabola fitting algorithm calculated three new points for every iteration to generate an improved parabola.* However an improved parabola can be obtained by only calculating the function value at the extremum of the parabola and using that point to generate an improved parabola. This procedure results in significant savings compared to the already efficient parabola fitting algorithm. A description and code listing of this type of extrema search method is given in the book by Kuester and Mize.[37]

A number of approximation polynomials were investigated for the function approximation method. Since derivatives of the integrated Mie functions were not available the approximation polynomials had to be generated from the angular intensity data. Of the different possible approaches to generate polynomials from data points, the one based on collocation was selected. A collocating polynomial is one that coincides with the function to be approximated at certain specified points.[45] The other approaches, like the Chebyshev approximations, appeared to be very attractive for the present investigation.[45] However, the collocating polynomials were selected because they could make use of the large quantity of light scattering data already stored on magnetic tape[36] whereas the Chebyshev approximation could not.

*Additional points were calculated to search for the extremum when the interval would no longer contain the extremum.

Of the different collocating polynomials available, the ones based on Newton's formulas and Stirling's formulas[45] were used in this study. Newton's formulas are very useful to approximate data either at the beginning or the end of a tabulation. The Stirling's formulas are among the most frequently used forms of the collocation polynomial and use data spaced at both larger and smaller arguments. Since these polynomials have to accommodate the additional points from the extrema calculations, the formulas based on equispaced arguments can not be used. The parabola fitting algorithm was able to use equal spaced arguments in Stirling's formula of second degree because three new equal spaced points were calculated for each iteration. To allow new polynomials to be generated from unequal spaced data, as required in the function approximation methods, the divided difference versions of Newton's formulas and Stirling's formulas were used. The lengthy equations are fully described in the book by Scheid.[45]

The accuracy of the Stirling's polynomials in approximating the light scattering curves were then investigated. Since the polynomials using Newton's formulas were seldom required* only the Stirling's formulas were used in the accuracy study. However, the conclusions from the accuracy study will apply to the Newton's formulas as well since both methods will generate the identical polynomial from a given set of data points. The methods differ only in the way that the polynomial is generated.

---

*Since the scattering intensity pattern from 0^{o} to 180^{o} is repeated from 180^{o} to 360^{o}, the tabulations do not have a real beginning and end. The calculations in the present study were therefore able to use Stirling's formulas at the beginning and end of the table whenever the scattering intensities were tabulated to 0^{o} and 180^{o} respectively.

Figure 9 shows a comparison of the second and fourth degree Stirling's polynomials used to approximate the scattering intensity curve about a minimum. The intensity of the scattered light is plotted against the angle of observation. This figure is a blow-up of the scattering curve taken from Figure 7 for the particle size distribution characterized by P = 5 and Q = 0. The true scattering curve and the two Stirling's polynomial approximations are shown by the solid curve and the data points respectively. The second degree polynomial, which collocates with the scattering curve at 85^{o}, 90^{o} and 95^{o} shows only an approximate agreement with the scattering curve within this angular interval. Outside of this interval the second degree approximation deviates significantly. In contrast, the fourth degree polynomial, which collocates with the scattering curve at 80^{o} (5^{o}) 100^{o}, shows excellent agreement with the scattering curve over the twenty degree interval.

The extrema of the two approximation polynomials are then determined and the corrresponding scattering intensities calculated. An improved polynomial approximation is then generated from a new set of points using the newly calculated point and discarding the point farthest from this polynomial extremum. Figure 10 shows the improved polynomial for the second and fourth degree Stirling's polynomials. The second degree polynomial collocates with the true scattering curve at 85^{o}, 87.1^{o} and 90^{o} and shows very good agreement over this angular range. Outside of this range the approximation polynomial becomes increasingly less accurate. The fourth degree polynomial collocates with the true scattering curve at 80^{o}, 85^{o}, 87.0^{o}, 90^{o} and 95^{o} and shows excellent agreement within this angular range. Note that the extremum from the less accurate second degree polynomial was 87.1^{o} instead of 87.0^{o}.

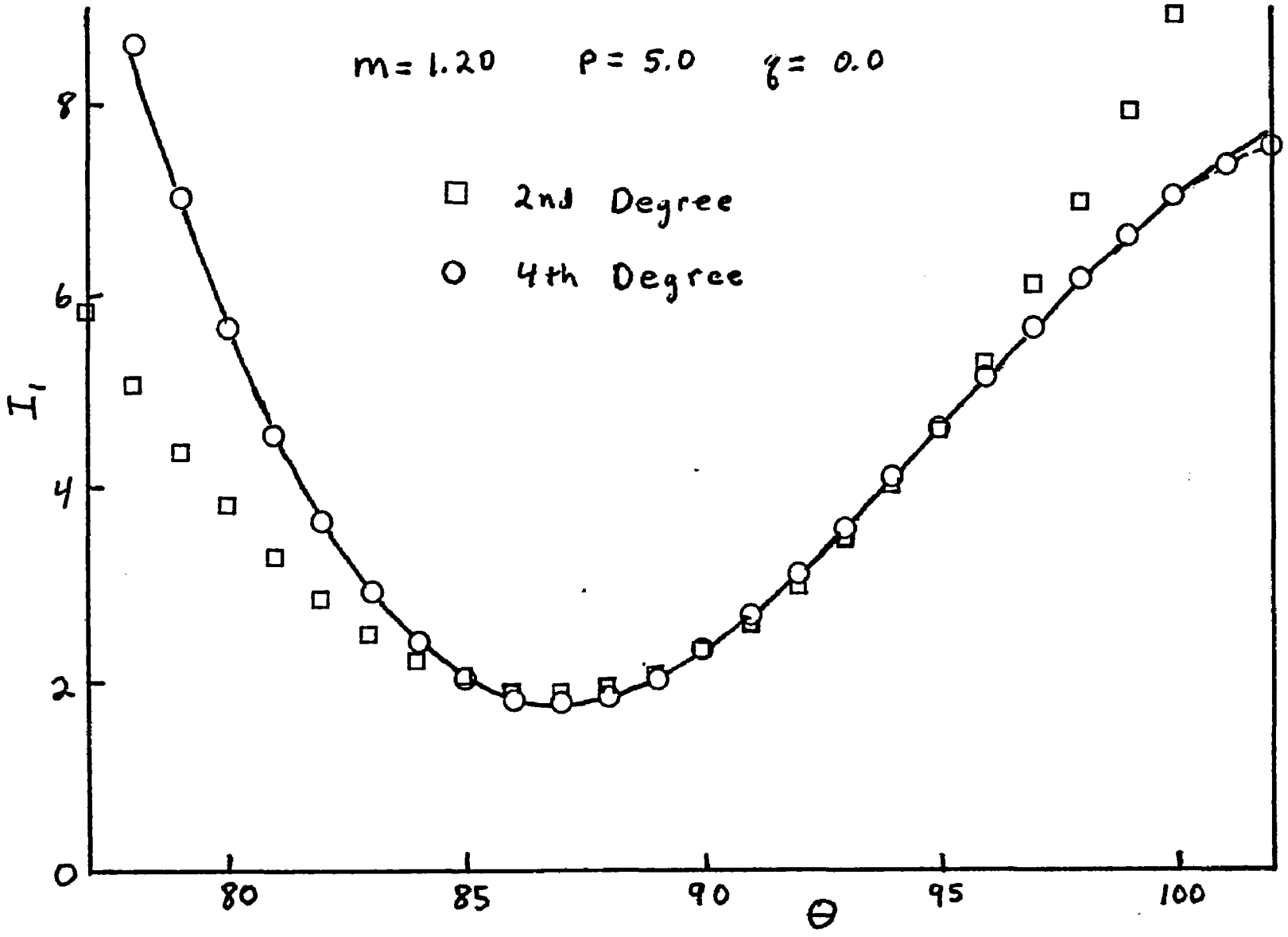

Fig. 9. Comparison of the Second and Fourth Degree Stirling's Polynomials in the First Approximation of the Scattering Intensity Curve About a Minimum

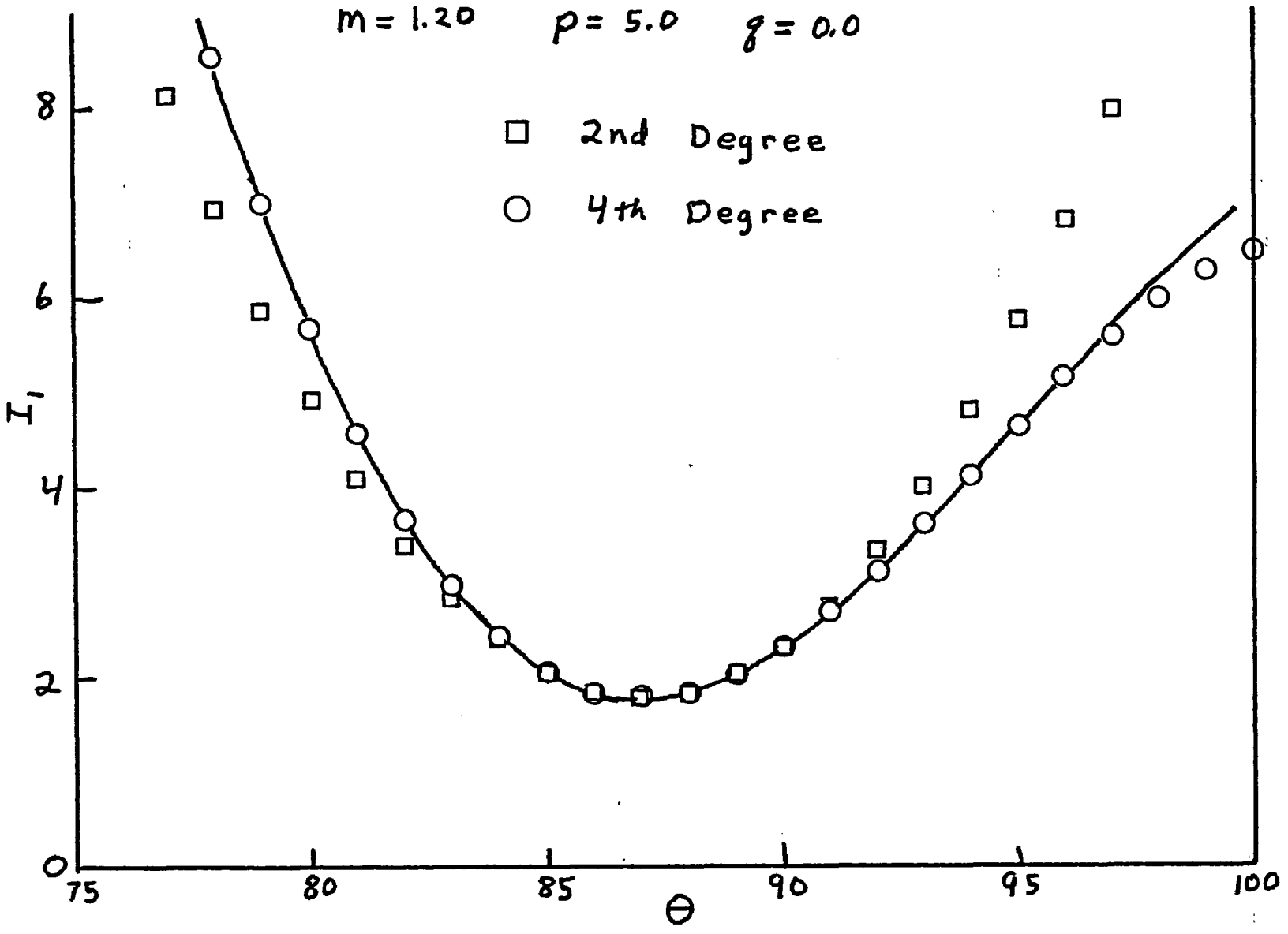

Fig. 10. Comparison of the Second and Fourth Degree Stirling's Polynomials in the Second Approximation of the Scattering Intensity Curve About a Minimum

The relative error for each degree polynomial was then determined for the original and improved polynomials shown in Figures 9 and 10 respectively. Figure 11 shows the percent relative error of the second degree polynomials plotted as a function of angle. The three points in each curve for which there is zero error represent the collocation points. The initial approximation (solid curve) and the improved approximation (dashed curve) show the same general behavior of a cubic curve. In general, the error will oscillate between positive and negative values within the angular range of the collocation points. Outside of this range the error will monotonically increase. Figure 11 shows the dramatic decrease in the percent relative error for the improved polynomial using the extremum from the previous polynomial. The extremum location is indicated by the arrow.

The corresponding percent relative error for the two fourth degree polynomials is shown in Figure 12. Note that the scale for the percent relative error is one tenth as large as in Figure 11. Both the initial approximation (solid curve) and the improved approximation (dashed curve) show the same general pattern of oscillating positive and negative errors within the angular region of the collocation points. Outside of this region, the error increases monotonically. The improved polynomial shows a large decrease in the percent relative error in the vicinity of the extremum. This improvement in the accuracy results from using the extremum of the initial approximation polynomial to generate an improved polynomial. As seen with the second degree polynomial, the improvement occurs primarily in the vicinity of the extremum.

Although both the second and fourth degree polynomials will provide

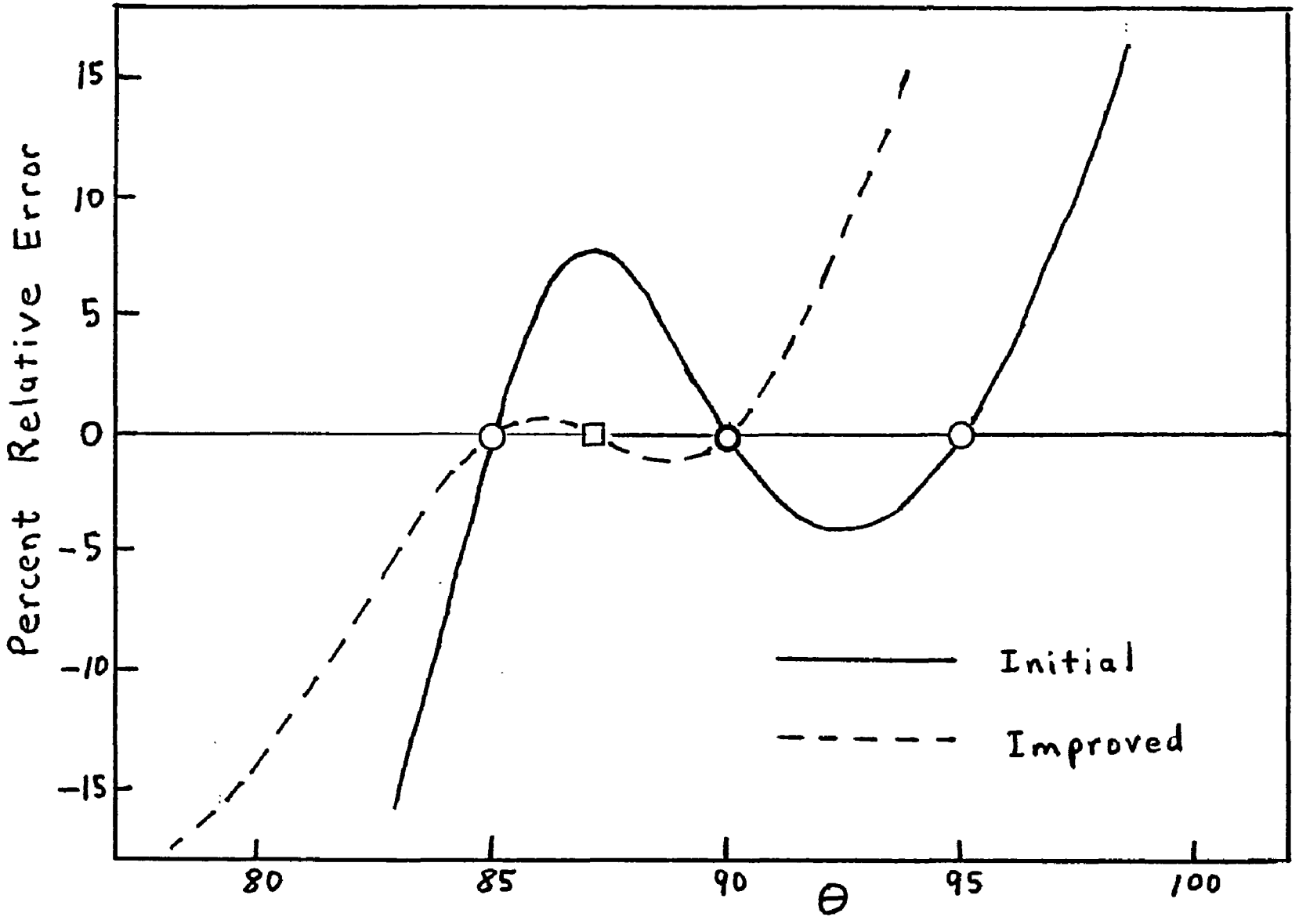

Fig. 11. Percent Relative Error of the First and Second Approximation of the Scattering Intensity Curve Plotted Against Angle θ Using Stirling's Second Degree Polynomial

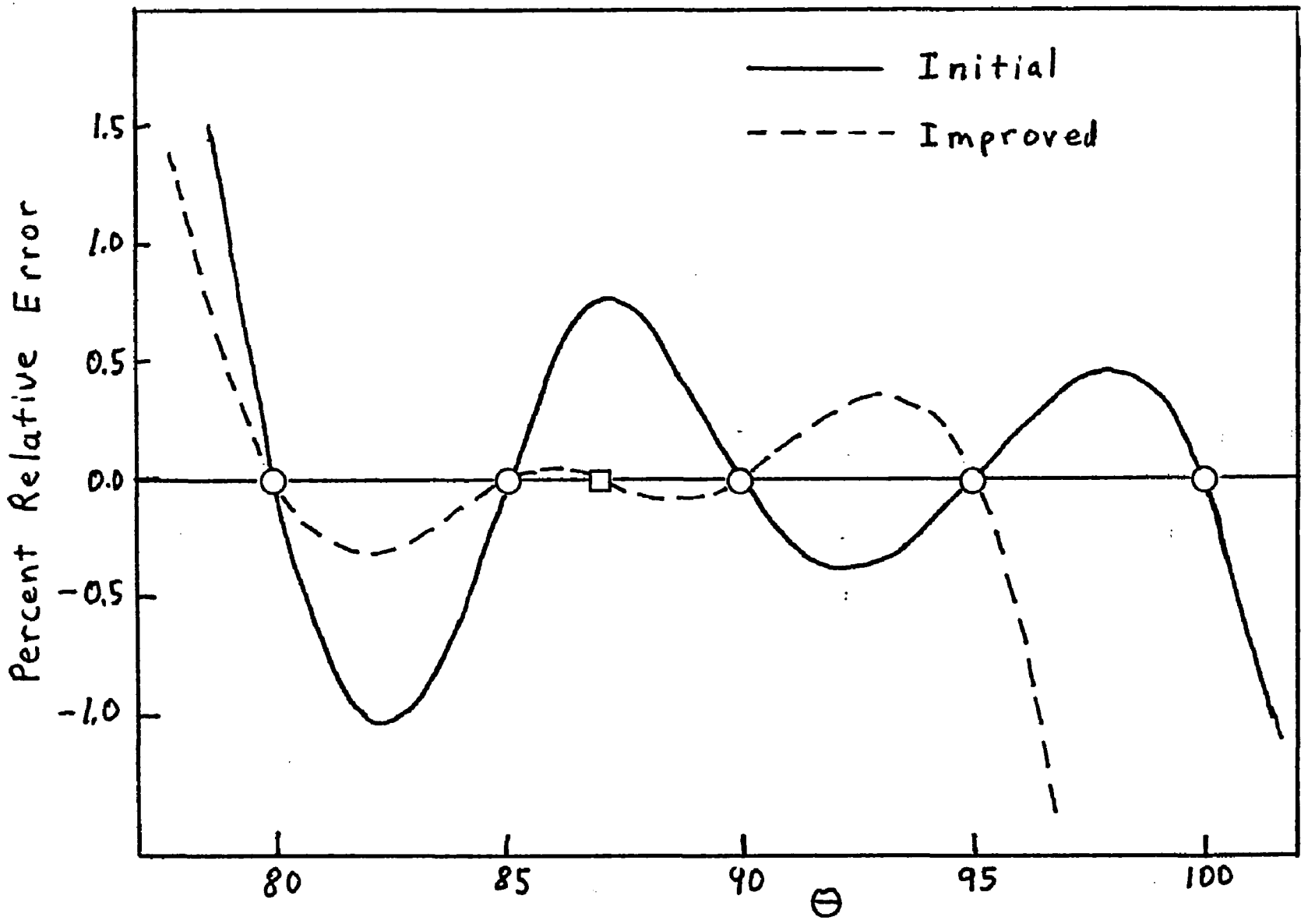

Fig. 12. Percent Relative Error of the First and Second Approximation of the Scattering Intensity Curve Plotted Against Angle Θ Using Stirling's Fourth Degree Polynomial

accurate extrema determinations, the fourth degree polynomial shows a much smaller relative error than the corresponding second degree polynomial. Figure 13 shows a comparison of the percent relative error for the improved second and fourth degree polynomials taken from Figures 11 and 12. The fourth degree polynomial has a much lower percent relative error and extends over a much wider angular range than the second degree polynomial. Another very important aspect to be considered in the present evaluation is the ability of the fourth degree polynomial to much better approximate the more assymetric extrema than considered in Figures 9-13. Based on these considerations, the light scattering extrema in the present investigation were determined by using the fourth degree Stirling's polynomial.

Unfortunately Stirling's polynomials were not used in the previous test which compared the number of points required to determine an extremum from an initial interval of $\pm 5^{\circ}$ to a final interval of $\pm 0.005^{\circ}$. However, a large number of tests on many different particle size distributions did show that the Stirling's fourth degree polynomial required an average of 1.2 points to determine an extremum from an initial interval of $\pm 5^{\circ}$ to a final interval of $\pm 0.1^{\circ}$. Another set of tests showed that the extrema were determined from an initial interval of $\pm 2.5^{\circ}$ to a final interval of $\pm 0.01^{\circ}$ using an average of 1.2 points per extremum. Based on these tests, the Stirling's fourth degree polynomial required about 80 points to determine the extrema in the comparison test in Figure 8. This represents a 90% reduction in the number of points required to determine the extrema compared to the Fibonacci method used initially.

D. Description of Computer Code and Accuracy of the Results

The preceding investigations on optimizing the light scattering

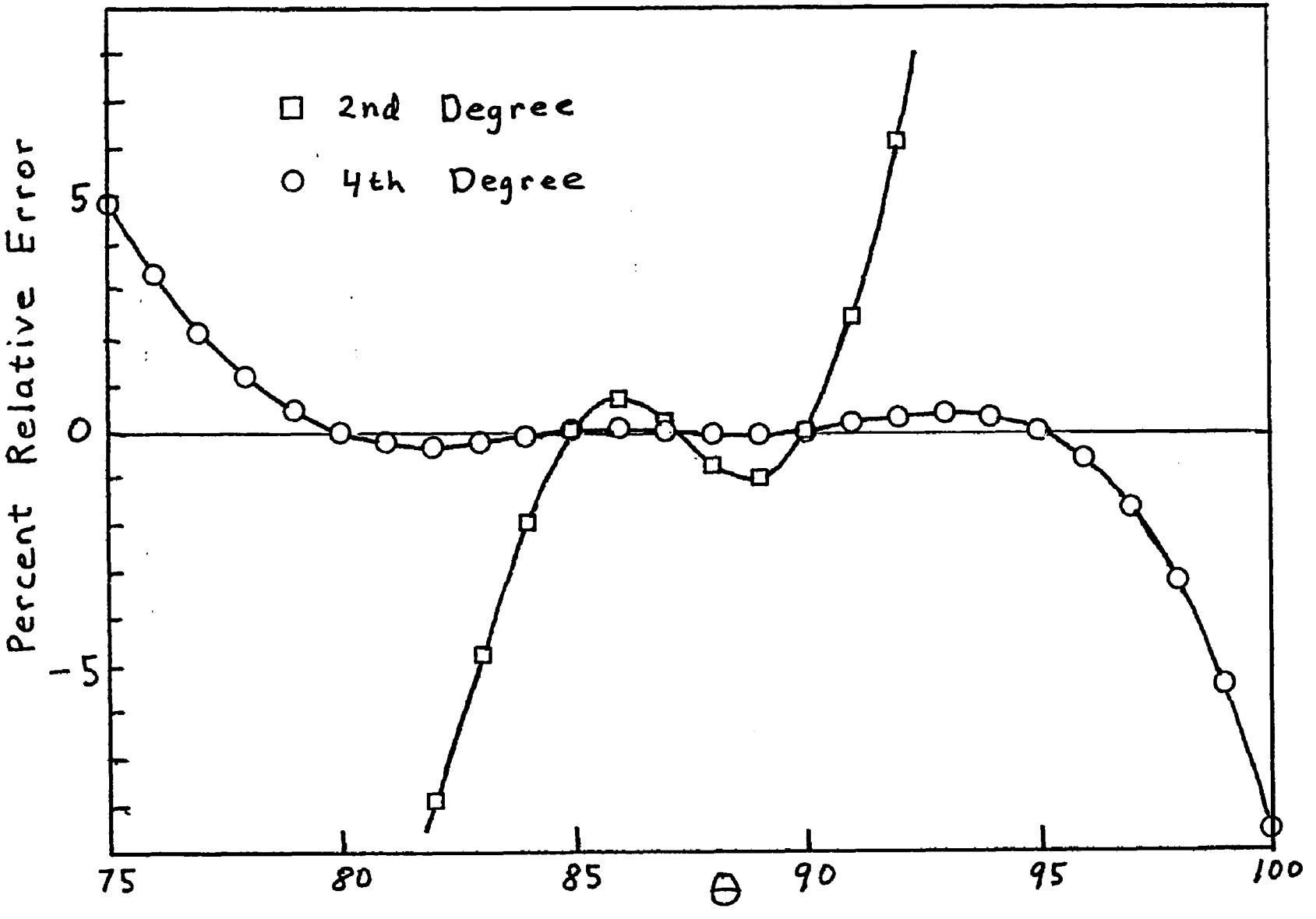

Fig. 13. Comparison of the Percent Relative Error from the Second Approximation of the Scattering Intensity Curve Using Stirling's Second and Fourth Degree Polynomial

intensities and developing the extrema search algorithms were used to write a computer code that calculates the angular extrema from heterodisperse distributions. A description of the code which is illustrated in the flow chart shown in Figure 14 will be presented in this section. The flow chart shows only the general functions of the code to make it easier to follow.

1. Primary Features of the Code

The first step in obtaining angular light scattering extrema is to generate for a particular set of parameters (m, ρ, q, polarization) the angular intensity at a number of angles (FC-3)*. To reduce the number of Mie calculations, the angular region between $\theta = 0^{\circ}$ and the first minimum was skipped. Since there are no extrema in this region, one can begin the angular search close to the first minimum in the forward direction.

The interval $\Delta\theta$ for the equally spaced angles was 5.0° if $\rho \leq 8.0$ and 2.5° if $\rho > 8.0$. This decrease in $\Delta\theta$ at higher ρ values (i.e., higher particle sizes) was required because the number of extrema for a given angular range increased as the particle size increases.

The next step involved using five consecutive Mie intensities $I(\theta)$'s centered about the angle θ_J to generate the derivative of a fourth degree polynomial (FC-4). The derivative is used because the extremum can be found directly from the zeros of the resulting third degree polynomial. Although the primary angular data were initially equispaced (FC-3), the addition of extrema points to this data (FC-7) resulted in unequal spacing. The Stirling's divided difference polynomial could handle both equal and unequal spaced arguments.

*The FC numbers in parentheses refer to the appropriate section of the flow chart.

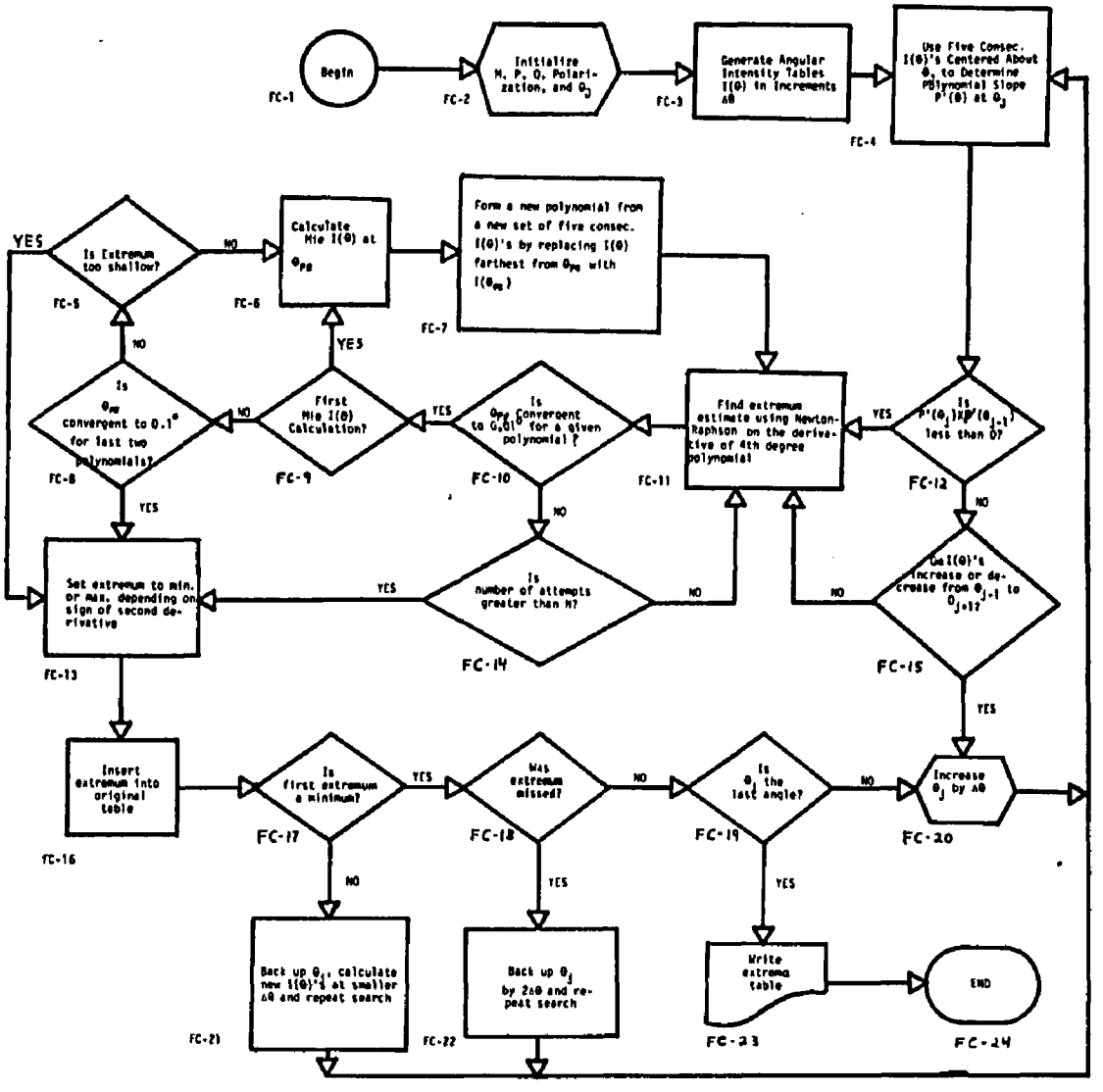

Fig. 14. Flow Chart of the Computer Code Used To Determine the Scattered Intensity Extrema

The slope, $P'(\theta_J)$, of the polynomial generated at the angle θ_J is then compared to the slope of the preceding polynomial generated at the angle θ_{j-1} (FC-12). If there is no preceding polynomial then the polynomial slope at the next angle must first be determined. A difference in the sign of the two consecutive slopes (i.e., product of the slopes is negative) will indicate the presence of an extremum.

On rare occasions the slopes of two consecutive polynomials will have the same sign although a point-by-point comparison of consecutive intensity data indicates the presence of an extremum. Therefore, to catch these extrema missed by the slope comparison, consecutive intensity values were also compared to see if they did not steadily increase or decrease from θ_{J-1} to θ_{J+1} (FC-15). It should be noted that the number of extrema missed by the polynomial slope method is much less than by the point-by-point comparison method. If both the slope comparison (FC-12) and the point-by-point comparison (FC-15) do not indicate the possibility of an extremum then the angle θ_J would be increased by $\Delta\theta$ (FC-20) and the extremum search continued at this new angle.

Once the possibility of an extremum was detected by either the slope comparison (FC-12) or the point-by-point comparison (FC-15), a detailed search was undertaken. The detailed extremum search consisted of repeatedly finding the extremum of a given polynomial (FC-11) and then using that extremum to generate a new, improved polynomial (FC-7). The extremum of the polynomial was determined using the Newton-Raphson method (FC-11) to find the zeros of the polynomial derivative. The Newton-Raphson method would be repeated until either two consecutive extrema for a given polynomial would differ by no more

than 0.01° (FC-10) or the number of repetitions exceeded a predetermined limit (FC-14).

The extremum angle θ_{PE} obtained in this manner pertains to the extremum of a given polynomial and not to the extremum of the angular light scattering function (θ_E). The angular location of the polynomial extremum θ_{PE} will converge to the true extremum θ_E as one of the five angular data used to generate the polynomial converges to the true scattering extremum. However, it is not necessary for all of the angular points to converge to the extremum.

This convergence can be accomplished by using the Mie intensity at the angular extremum θ_{PE} from one polynomial to generate a new polynomial (FC-6 and FC-7). Since the fourth order polynomial can only use five points, the point farthest from the extremum is discarded (FC-7). If the angular location of the extremum for two successive polynomials differed by no more than 0.1° then θ_{PE} obtained from the last polynomial would represent the angular location of the light scattering extremum θ_E (FC-8). However, if θ_{PE} from two successive polynomials differed by more than 0.1° then another polynomial would be generated (FC-6 and FC-7) using the Mie intensity at the last extremum angle θ_{PE} and the sequence repeated. The extremum at θ_E would then be designated as a maximum or minimum depending on the sign of the second derivative of the polynomial (FC-13).

To economize on the number of Mie calculations required, the Mie intensity $I(\theta)$ was not calculated for the last angular location of the extremum. The calculated intensity values will therefore not correspond to the associated extremum angle and thereby introduce an error into the intensity values.

However, this type of error would occur even if the last Mie intensity were calculated since the extremum angles were rounded to 0.1°.

After inserting the extremum into the original table (FC-16) the angle Θ_J was checked to see if it were the last angle (FC-19). If the angle Θ_J were not the last, then it would be increased by $\Delta\Theta$ (FC-20) and the search for an extremum continued (FC-4). A table of the angular position and the intensity of the extremum for a given set of parameters would be written when the last angle is reached. By systematically varying the different parameters (FC-2) all of the extrema would be produced.

2. Special Cases

While the method described proved most satisfactory both with regard to precision of the results obtained and the speed of computation, it was recognized that under certain circumstances it could either fail or produce questionable results. Steps were taken to exclude such contingencies. The complications which could present themselves under certain circumstances were (1) that extrema could be missed, or (2) that fake extrema were generated, or (3) that extrema were so shallow that their angular location could not be determined with sufficient precision.

a. Missing Extrema

Extrema can be missed only if the polynomial slope at Θ_J does not have an opposite sign compared to the preceding polynomial slope at Θ_{J-1} (FC-12) or if the intensity $I(\Theta)$ steadily increases or decreases from Θ_{J-1} to Θ_{J+1} (FC-15). The worst case occurs when a pair of shallow and closely spaced maximum and minimum are undetected by the above two checks (FC-12 and FC-15), since no subsequent test will detect them. In all cases these extrema can be detected by reducing the angular interval $\Delta\Theta$, although the number of Mie calculations

would then increase. However, in the majority of cases, one of the two extrema is detected and accurately located. The other extremum would then be detected in a subsequent check (FC-18) to insure that consecutive extrema alternate maximum and minimum. If this check reveals a missing extremum then an accurate search is undertaken in the appropriate angular range (FC-22) and the extremum located.

The alternating maximum and minimum check cannot indicate a missing extremum for either the first extremum in the forward direction or the last extremum in the backward direction. Since it is well established that the first extremum in the forward direction must be a minimum the calculated extrema were checked for this condition (FC-17). If the first extremum in the forward direction were not a minimum then a search was made in the appropriate region (FC-21) until the missing extremum was found.

The last extremum in the backward direction is also a minimum. However, in certain cases, the minimum lies within 0.1° of the backscatter at 180°, making its detection extremely difficult. Moreover, detecting the first minimum in the backward direction is very difficult because of the absence of a large intensity increase from this minimum to 180°, in contrast to the large intensity increase in the forward direction from the first minimum to 0°. No test was therefore made to determine a missing minimum in the backward direction. However, to improve the detection of this minimum, the angular increment $\Delta\theta$ was decreased by half in the region from 170° to 180°.

A small percentage of angular extrema were undetected by both the slope (FC-12) and the point-by-point (FC-15) comparison methods. These extrema were missed because the angular increment used to scan the intensity data would contain more than one extremum or be too large to detect the shallow

minimum in the backward direction. Reducing the angular increment so that it contained only one extremum would insure that all extrema were detected but greatly increase the number of computations. The angular increments used in the present investigation represent a compromise between minimizing the number of computations and maximizing the number of extrema detected.

Undetected extrema occur as the first minimum in the backward direction or as a pair of shallow minima and maxima separated by less than one angular increment. It was already pointed out that if one of the closely spaced extrema pair were detected, then the other would also be found. Special tests conducted at smaller intervals indicated that as high as 3% of the total number of extrema went undetected. The majority of the missing extrema occurred in pairs of maxima and minima having an average separation of 2.8° and a relative intensity difference of 0.74%. However, for practical purposes, the missing extrema are too shallow to be detected.

b. Fake Extrema

Fake extrema were generated in those extremely rare cases where the initial polynomial slope (FC-4) indicated the presence of an extremum (FC-12) although none actually existed. After determining the extremum of the polynomial using the Newton-Raphson method (FC-11), a new polynomial would be generated (FC-6 and FC-7) using the extremum θ_{PE} from the original polynomial. This new polynomial, however, would not have an extremum within the region indicated by the initial polynomial. The second application of the Newton-Raphson method would therefore not converge after N attempts (FC-14) and the extremum search would terminate. Since real extrema would sometimes converge so slowly that the number of attempts would also exceed N, there was no way of distinguishing between real and fake extrema by the convergence

test (FC-14). Whenever the extrema search terminated in this manner, a diagnostic message was written and the program proceeded to the next step (FC-13).

Figure 15 illustrates the typical case in which fake extrema are detected. This figure shows the angular variation of the scattered intensity from a heterodisperse distribution characterized by $m = 1.20$, $\rho = 5.0$ and $q = 1.2$ in which the incident light is polarized parallel to the plane of observation. The solid curve represents the actual scattered intensity while the dashed curve represents the polynomial approximation generated from the collocation points at 135^{o} (5^{o}) 155^{o}. Since the initial approximation indicates the presence of an extremum, a detail extremum search was undertaken although none was actually present.

After all of the computations were completed, the extrema listed in the diagnostic messages were reinvestigated in separate computations. The program performing these calculations was very similar to that shown in the flow chart except that angular increments $\Delta\theta$as small as 0.5^{o} were used to search a 10^{o} range about each questionable extremum. In about 75% of these cases the failure of θ_{PE} to reach convergence after N attempts was due to fake extrema, while in the remainder of cases real extrema were detected.

C. Shallow Extrema

The third complication in the normal sequence of extrema calculations was due to shallow extrema. Preliminary computations indicated that very shallow extrema would not only require several additional Mie calculations but would sometimes produce extrema that are in error by as much as 1.0^{o}. A special check (FC-5) was therefore incorporated in the program to detect those extrema that were too shallow for accurate determination. If such a

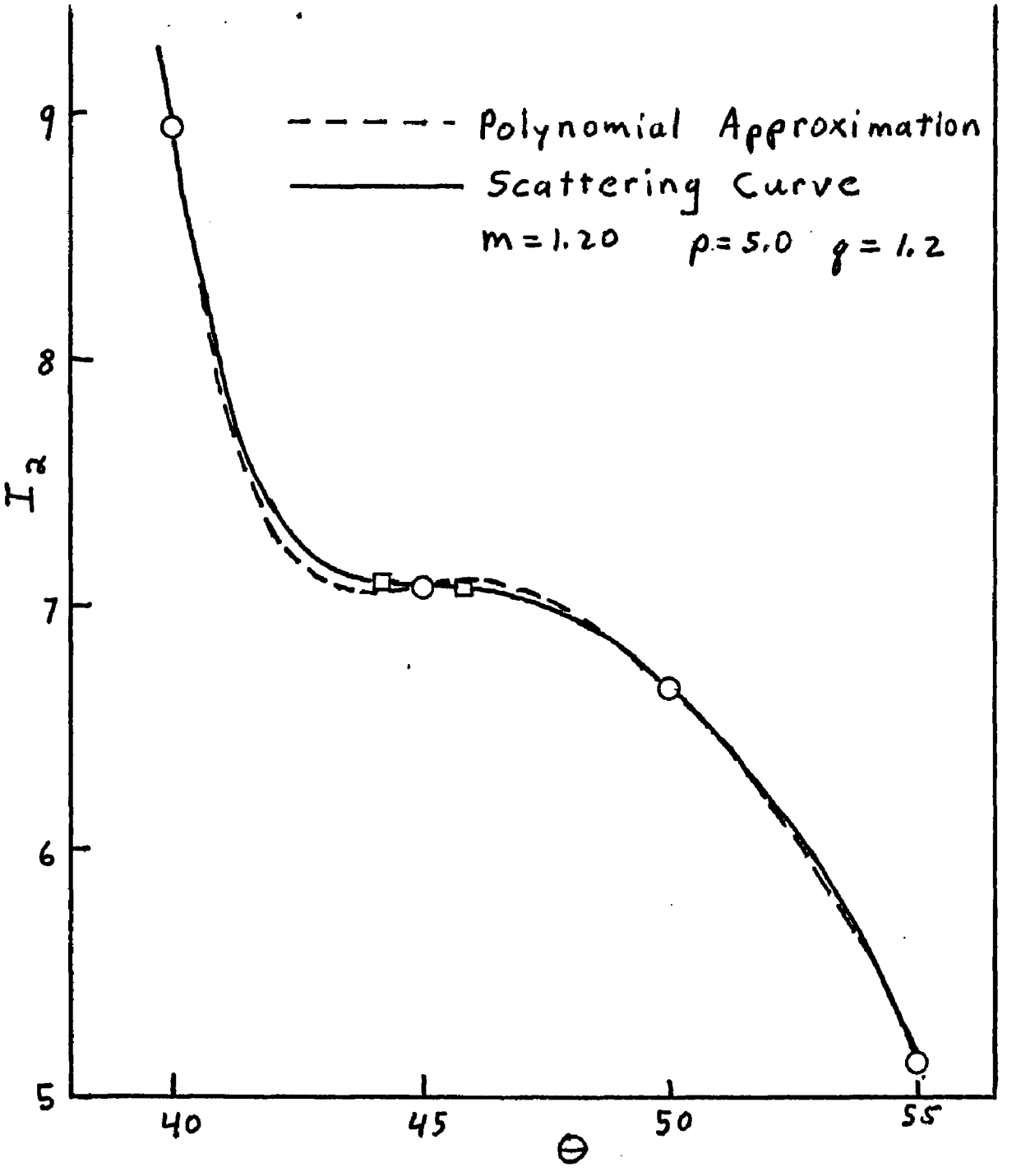

Fig. 15. Fake Extrema Obtained from the Polynomial Approximation

condition occurred, a diagnostic message was written, and the program proceeded to the next step (FC-12). After all of the computations were completed, the extrema listed in the diagnostic messages were reinvestigated using the same program used to investigate fake extrema. The occurrence of shallow and fake extrema were so infrequent that these reinvestigations proved to be more effective than trying to modify the computer code.

3. Accuracy of the Computations

The computer code just described was then used to perform a systematic study of the angular location of the intensity extrema as a function of refractive index, polarization of light and particle size distribution. The results of this study are presented in a book of light scattering tables published by the Wayne State University Press.[46] Also included in this book are 63 graphs that show the angular position of the intensity extrema plotted against the modal size for distributions having the same degree of heterodispersion. These graphs are a representative sample of the polarization, refractive index and degree of heterodispersion considered in the tabulations. The values of the variables m, p, and q considered in the tables are:

$$m = 1.05\ (0.05)\ 1.30,\ 1.333$$

$$p = 0.(0.2)\ 12.0$$

$$q = 0.(0.2)\ 2.0$$

These variables were computed for unpolarized incident light, I_u, for linearly polarized light with the electric vector vibrating perpendicular to the plane of observation, I_1, and for polarized light with the electric vector vibrating in the plane of observation, I_2.

The method of computation described earlier had been perfected to the point where an uncertainty in the extrema angles not in excess of $\pm$ 0.1° could be expected. In order to make certain that this objective had been reached, the extrema were recomputed for a representative sample of the ρ (4, 8, 12) and q (0 (.4) 2.0) values and all of the polarization and m values used in the tables.[46] These recomputations were made with a program identical to that shown in the flow chart with three exceptions. 1) The convergence for the extremum from a given polynomial was reduced from 0.01° to 0.001° (FC-10). 2) The convergence of the extrema from two consecutive polynomials was reduced from 0.1° to 0.01° (FC-8). 3) The angular increment $\Delta\theta$ used was throughout 2.5°. These change resulted in the angular location of extrema having an accuracy of .01°. Since no convergence tests were performed on the intensity values, similar accuracy values cannot be assigned to the extrema intensities. However, for obtaining the uncertainties of the intensity values in these tables, the recomputed intensities can, in the first approximation, be considered to have no error.

Subsequent comparison of these supplemental angular and intensity values with those listed in the tables[46] give, therefore, the absolute deviation of the latter from the true values. The results are listed in Tables II and III. Table II is concerned with the precision of the θ_{max} and θ_{min} values. The first column identifies the value of the variable which is kept constant using all of the data in these Tables, the second column identifies the size, S, of the sample, the third column gives the percent of those cases where the uncertainty in the value of an extremum angle was less than $\pm$ 0.1° and the fourth column gives the percentage of the total sample where the uncertainty amounted to $\pm$ 0.1°. One asterisk (*) in the fifth column indicates that in

TABLE II

Accuracy of Maxima and Minima Angles

	S	<0.1°	±0.1°	>±0.1°
m				
1.05	440	95.5	4.5	0
1.10	482	93.4	6.4	**
1.15	547	94.3	5.5	*
1.20	598	94.5	5.5	0
1.25	642	94.9	5.1	0
1.30	677	95.0	5.0	0
1.333	664	96.1	3.9	0
q				
0.0	676	96.3	3.7	0
0.4	713	95.5	4.5	0
0.8	726	94.8	5.2	0
1.2	733	94.7	5.2	*
1.6	661	93.5	6.4	**
2.0	541	94.1	5.9	0
p				
4	428	94.9	5.1	0
8	1304	90.1	9.7	*;**
12	2318	97.5	2.5	0
I_1	1538	95.3	4.7	0
I_2	1074	93.9	6.0	*
I_4	1438	95.1	4.8	**
θ_{max}	1870	95.0	4.9	*
θ_{min}	2180	94.7	5.2	**
θ_{both}	4050	94.8	5.1	*;**

TABLE III

Accuracy of Intensity Values at Extrema

	S	≤1	1–9	≥9
m				
1.05	440	76.8	21.6	1.6
1.10	482	87.6	12.0	0.4
1.15	547	86.1	13.7	0.2
1.20	598	86.5	13.2	0.3
1.25	642	86.3	13.4	0.3
1.30	677	80.6	18.6	0.8
1.333	664	80.3	18.9	0.8
%				
0.0	676	81.8	16.7	1.5
0.4	713	83.9	14.7	1.4
0.8	726	82.1	17.3	0.6
1.2	733	84.9	15.1	0.0
1.6	661	83.1	16.9	0.0
2.0	541	85.6	14.4	0.0
P				
4	428	97.7	2.3	0.0
8	1304	83.2	16.6	0.2
12	2318	81.0	18.0	1.0
I_l	1538	82.7	16.4	0.9
I_z	1074	84.0	15.2	0.8
I_u	1438	83.9	15.8	0.3
θ_{max}	1870	90.7	9.3	0.0
θ_{min}	2180	77.2	21.6	1.2
θ_{both}	4050	83.5	15.9	0.6

one instance the uncertainty was $\pm$ 0.2°. Two asterisks (**) indicate that in one instance the uncertainty was $\pm$ 0.3°. Thus, in 4050 cases more than 90% of all the results had an uncertainty of less than $\pm$ 0.1° and in only one case was the uncertainty at most $\pm$ 0.3°.

Table II indicates that ρ is the only parameter that affects the accuracy of the maxima and minima angles. The observed decrease in the accuracy as ρ increases from 4 to 8 is explained by the angular increment used to initially locate the extrema. Since the angular intensity was fixed at 5° the extrema were more difficult to determine as the ρ values increased from 0 to 8. This occurs because the higher ρ values have more extrema at smaller angular intervals. The increase in the accuracy for ρ = 12 is due to the smaller angular increment that was used for ρ = 8.2 to ρ = 12.0.

Table III gives a corresponding survey for the precision of the intensity values associated with the angular values in Table II. Here the third, fourth and fifth columns give the percentage of the cases where the uncertainty of the theoretical intensity value corresponding to the extremum angle differed in the last digit given by less than 1, between 1-9, and greater than 9. Table III shows that more than 75% of the intensity values given have more significant figures than the four given in the tables.[46] With a few exceptions listed in the fifth column, the intensity data are accurate to three digits.

A survey of Table III confirms the qualitative judgement that the extrema showing greater intensity changes will have greater errors. Except for m = 1.05 the accuracy of the intensity values tend to decrease as the relative refractive index increases. This follows from the sharper and more intense extrema

that occur for the higher m values. The reason for the unusually low accuracy at $m = 1.05$ is not known. As the heterodispersion q increases the extrema become less intense with some extrema even disappearing. The increased accuracy as q increases is especially pronounced in the column having less than three significant figures. The more intense and sharper extrema that occur for higher ρ values (see Figure 7) results in the lower accuracy seen in all the columns. Finally, Table III shows that the minimum intensities have a much lower accuracy than the maximum intensities. This trend occurs because, in general, the angular minima are very sharp while the angular maxima are quite broad. The difficulty encountered in determining the theoretical minima will be even more pronounced for measurements of the experimental minima.

IV. Study Of The Light Scattering Maxima and Minima

This chapter presents the results of a systematic study of the angular location of the intensity extrema as a function of relative refractive index, polarization of the incident light and particle size distribution. The computer code described in Chapter III was used to perform this study.

A. Effect Of Particle Size Distributions On The Angular Scattering Intensity

1. Previous Studies

The effect of particle size on the angular scattering intensity has been previously investigated by a number of different authors. Penndorf[33] has compiled an atlas of scattering diagrams showing the intensity of scattered light plotted against the angle of observation for different monodisperse particle sizes, relative refractive indexes and polarizations of the incident light. Much more comprehensive data has been published in the tables by Denman et al[38] for monodisperse spheres and Yajnik et al[36] for heterodisperse spheres. A review of the basic trends in the angular variation of the scattered intensity is found in Kerker's book[3]. In general, these previous investigations have shown that as the particle size increases, the number of maxima and minima increase and show a migration toward the forward direction. Heller and Nakagaki[11] have explained these trends using arguments based on the RGD theory. However, the complex pattern of the extrema in the backward direction did not fit into this simple picture. Except for Penndorf[33] and Patitsas[32] the scattering pattern in the backward direction was regarded as an unexplained deviation from the simple picture.

The effect of the heterodispersion on the angular intensity

(and related quantities) was also previously investigated by other researchers. Kerker et al[47] have shown that the magnitude of the oscillations in the polarization ratio* become obliterated as the distribution becomes more heterodisperse. They pointed out that the angular location of the maxima and minima of the polarization ratio remains approximately constant as the breadth of the distribution increases and consequently provides an average particle size which is independent of the width of the distribution. Wallace and Kratohvil[24] have applied Kerker's observation to develop a method for determining particle size distributions.

This important observation was possible because the size distribution function that they used maintained a constant mode while the width of the distribution increased. The extensive tabulations of heterodisperse distributions by Yajnik et al[36] also showed that the extrema in the angular intensities and scattering ratios** become washed out as the heterodispersion increases. However, the distribution function used in those tabulations (equation 5) does not maintain a constant mode (or any other average) as the breadth of the distribution increases. Consequently the angular location of the extrema would also shift as the heterodispersion increases.

This is illustrated in Figure 16, where the scattering ratio is plotted against the angle of observation for five heterodisperse distribu-

*The polarization ratio is defined as the ratio of the intensities of the two orthogonal components of light scattered by a sphere for incident unpolarized light.

** The scattering ratio is defined as the ratio of the scattered intensity from incident light polarized parallel to the plane of observation to that from incident light polarized perpendicular to the plane of observation.[48]

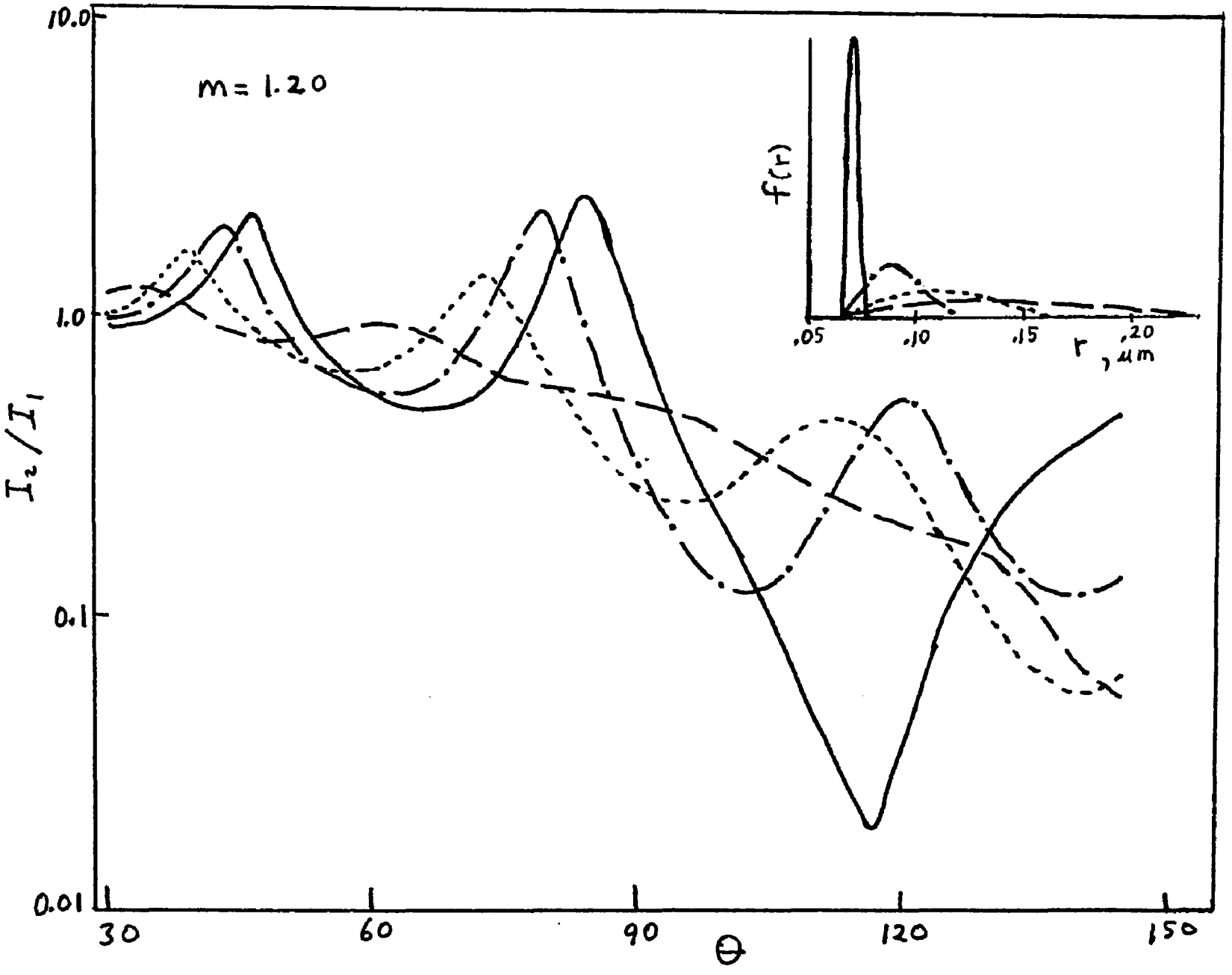

Fig. 16. Variation of the Scattering Ratio (I_2/I_1) With Angle θ from Size Distributions Having p=5 and Different q Values

tions having a constant p and different values of q. The graphs were drawn using the tabulated data by Yajnik et al[36]. The corresponding size distributions are shown in the same figure. Note that as the heterodispersion increases the average particle size also increases and the first two extrema migrate toward the forward direction. The complicated pattern in the backward direction is also seen. If the modal size (see equation 6) were constant then the extrema would remain at the same angular position as the width of the distribution changes.

2. Survey of I_1 Scattering Curves

The scope of the present investigation has allowed a more thorough examination of the effect of particle size distributions on the angular scattering intensity than was previously possible. A brief survey of these effects will be illustrated with graphs showing the intensity of scattered light plotted against the angle of observation. Although all of the graphs in this section of Chapter IV pertain to the relative refractive index m = 1.20, the conclusions and trends also apply to the other relative refractive indexes in the present study. The graphs shown in Figures 17-26 illustrate the effect of particle size and the degree of heterodispersion on the resulting angular scattering intensity. These figures show the angular scattering intensities from particle size distributions having a constant mode* and various degrees of heterodispersion. Figures 17-21 pertain to the light scattered I_1 from incident light that is polarized

*A constant mode was used for each figure because previous investigators[47, 24-26] have shown that this approach allows one to separate the effect on the angular scattering intensity due to the modal size and the distribution width. However very little data was presented in those studies to substantiate this separation and define the range of its validity.

perpendicular to the plane of observation while Figures 22-26 pertain to the light scattered I_2 from incident light that is polarized parallel to the plane of observation. All of the data for these graphs were obtained in separate calculations using equation 14 to determine the different size distribution parameters p and q to maintain a constant modal size α_M.

$$\alpha_M = p + q/\sqrt[3]{3} \qquad (14)$$

Scanning the I_1 graphs, one sees that the number of extrema steadily increase as the modal size α_M increases and that the extrema become washed out as the heterodispersion increases. Figure 17 shows that there are no extrema for the particle size distributions having $\alpha_M = 1.0$. This very small size almost approximates Rayleigh scattering[3], which shows a constant intensity as a function of angle. Note that as the heterodispersion increases for the constant mode $\alpha_M = 1$, the scattering becomes more pronounced in the forward direction, thus indicating a larger average size. This apparent increase in size is due to the much greater scattering intensity of the large particle sizes in the size distribution. The integrated scattering intensity (equation 11) will therefore resemble the intensity from primarily the large size fraction.

As the modal size increases to $\alpha_M = 3$ in Figure 18 a minimum and maximum appear. Increasing the heterodispersion for a constant mode now has a more symmetric effect on the resulting angular scattering curve. The minimum remains at the same angular location as the heterodispersion factor q increases from 0.0 to 0.5 while the maximum shows a slight shift. At q = 1.0 the maximum and minimum have both moved closer together and are almost washed out. A new shallow minimum has also appeared in the backward direction. For q = 2.0 the original extrema pair disappears completely

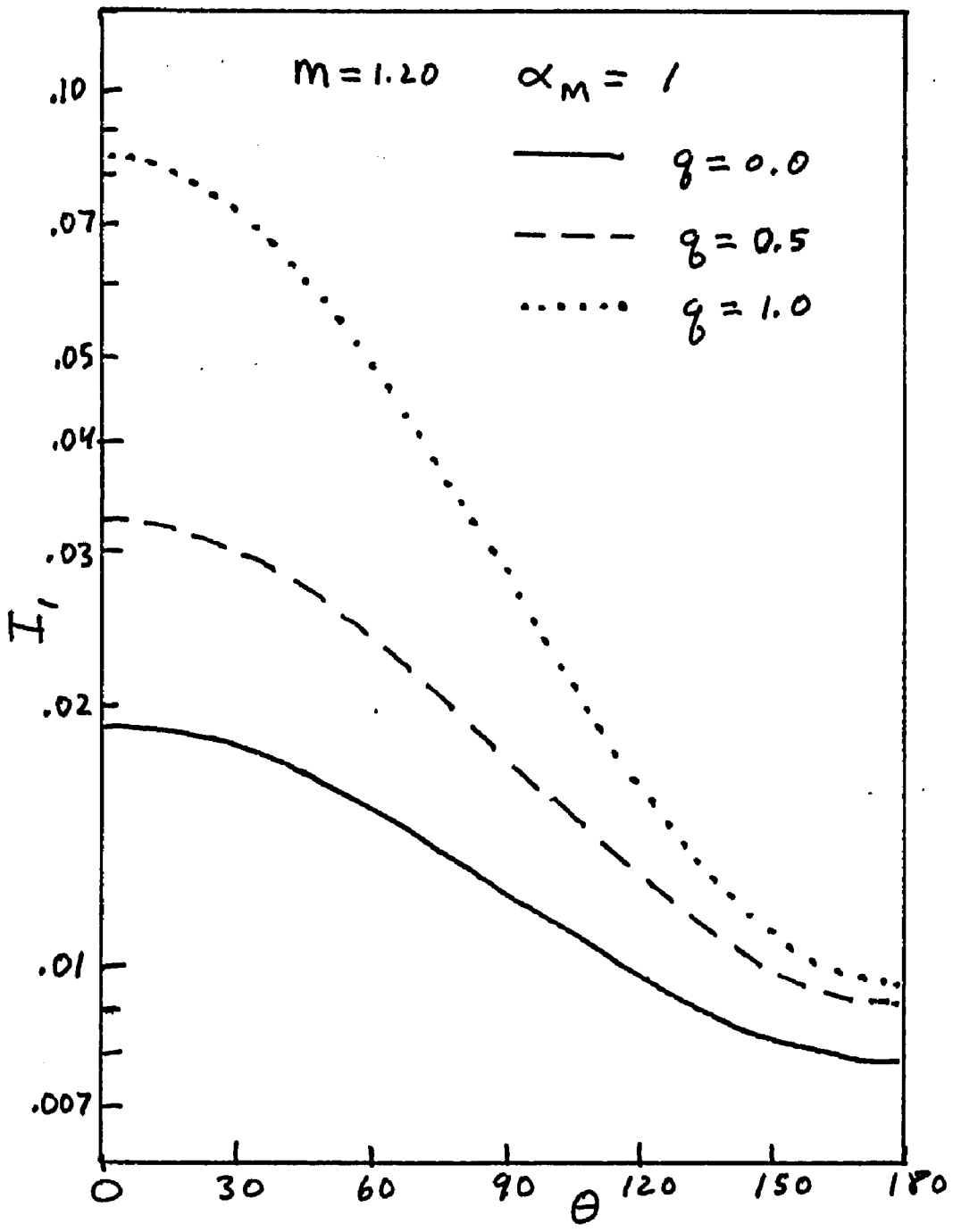

Fig. 17. Scattered Intensity I_1 as a Function of Angle for Size Distributions Having a Constant Mode α_M=1 and Different Distribution Widths

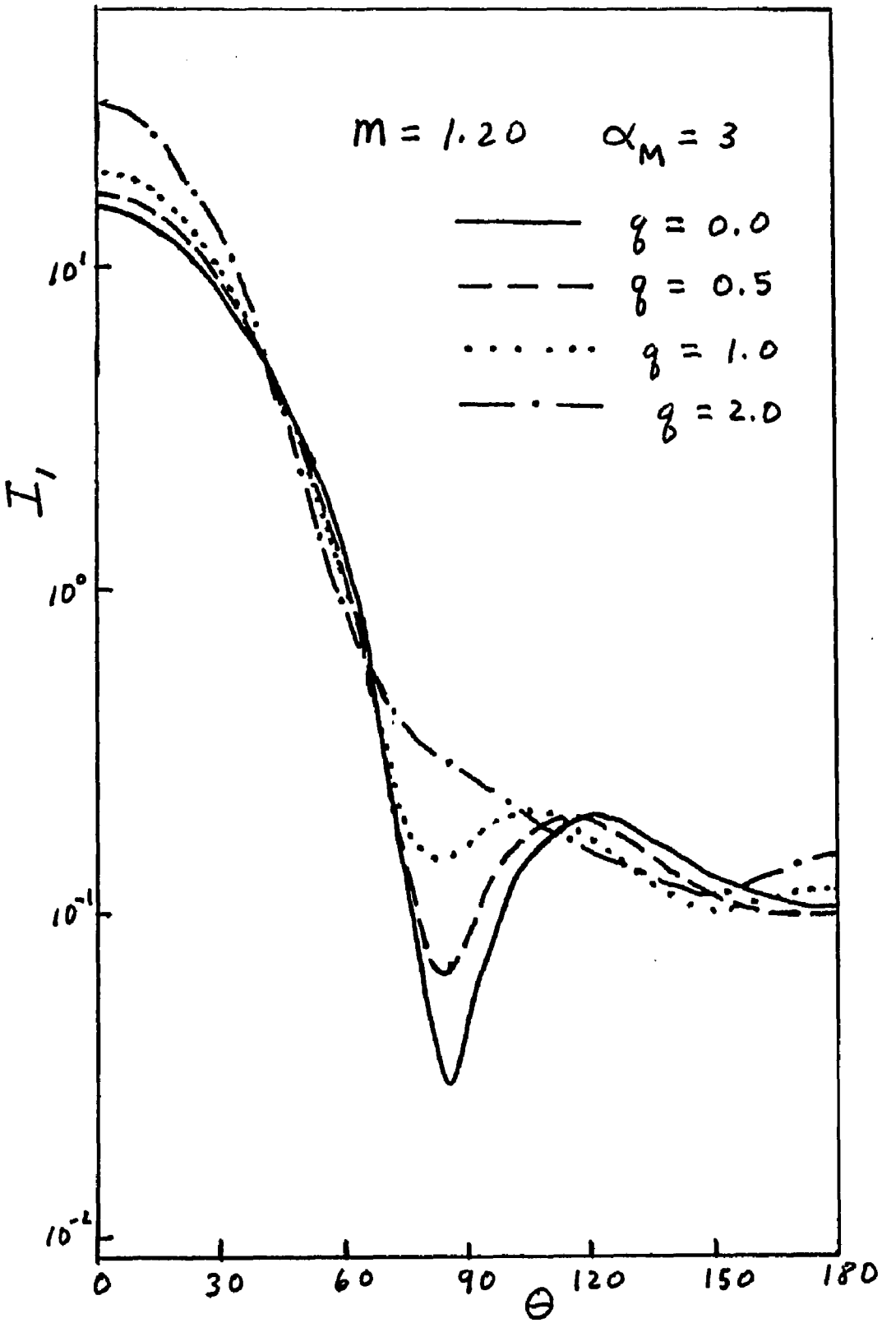

Fig. 18. Scattered Intensity I_1 as a Function of Angle for Size Distributions Having a Constant Mode $\alpha_M=3$ and Different Distribution Widths

while leaving the shallow minimum in the backward direction.

Proceeding to the next larger size, $\alpha_M = 5$ shown in Figure 19, one sees that the number of extrema have increased. There are now two maxima and minima pairs that show a systematic behavior as the degree of heterodispersion increases. The two minima remain at approximately the same angular position while the corresponding maxima migrate closer to the minima as the heterodispersion increases. Finally when q = 2.0 both extrema pairs disappear. The pattern in the backward direction is much more complicated. For a small increase in heterodispersion from q = 0.0 to q = 0.5 the general pattern in this region remains about the same with the minimum at 150° shifting slightly. However as the heterodispersion increases to q = 1.0 and larger, a new maximum and minimum appear. These new extrema remain at approximately the same angular position from q = 1.0 to q = 2.0 even after the extrema in the forward direction have disappeared.

The pattern of increasing number of extrema with increasing size is continued in Figures 20 and 21 where the scattering curves are plotted for $\alpha_M = 10$ and $\alpha_M = 15$ respectively. Several trends of the effect of increasing heterodispersion are seen in these figures. Looking at Figure 20, one sees that, in addition to the maxima and minima pairs in the forward direction, there are two pairs in the backward direction that also show a systematic behavior as the degree of heterodispersion increases. Note that the first maximum and minimum in the backward direction behave like the mirror image of the first maximum and minimum in the forward direction. In both cases the angular location and intensity of the maximum remains fixed while the minimum intensity increases. The second extrema pair in the backward direction also appears as a mirror image of the second extrema pair

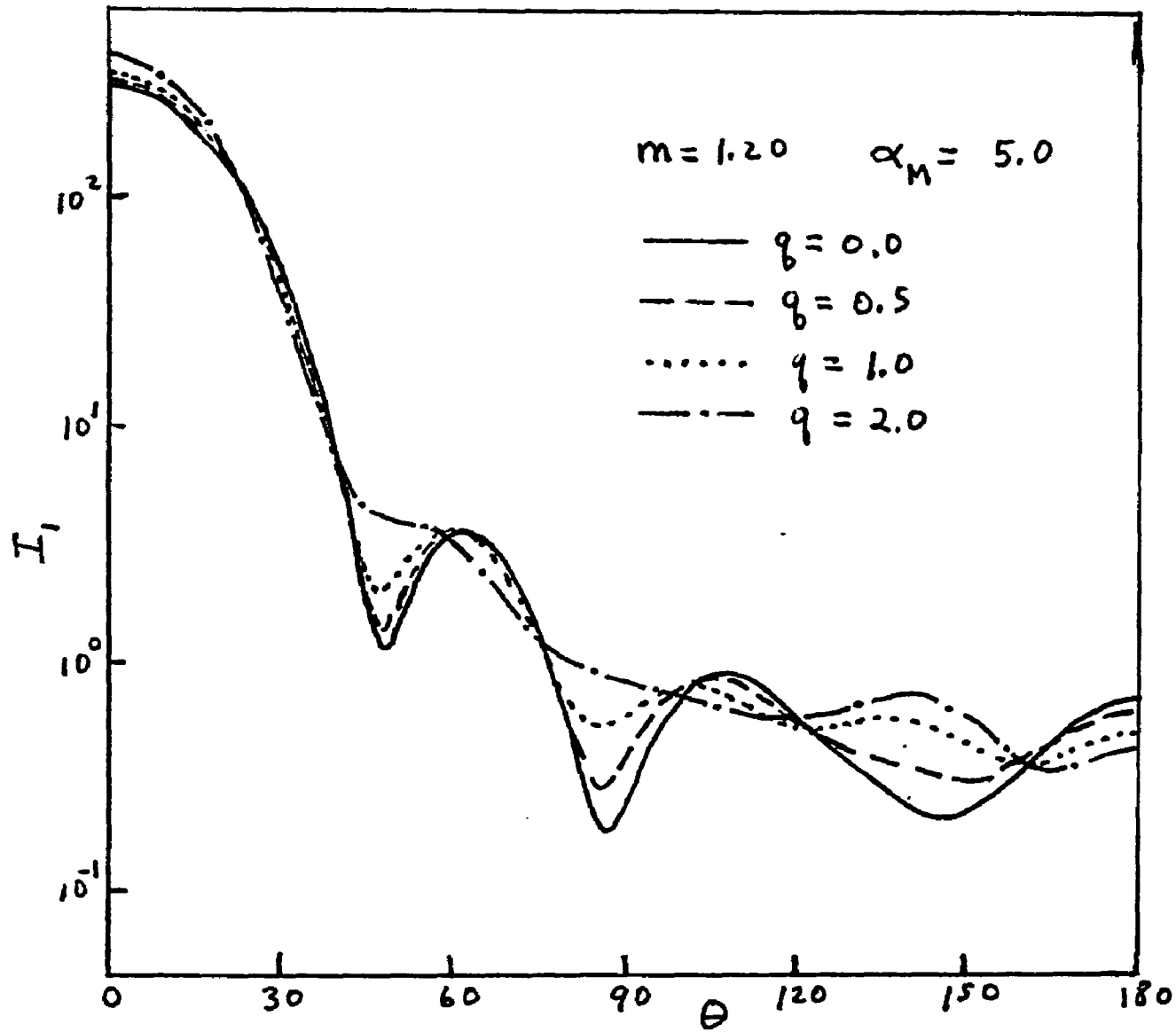

Fig. 19. Scattered Intensity I_1 as a Function of Angle for Size Distributions Having a Constant Mode α_M=5 and Different Distribution Widths

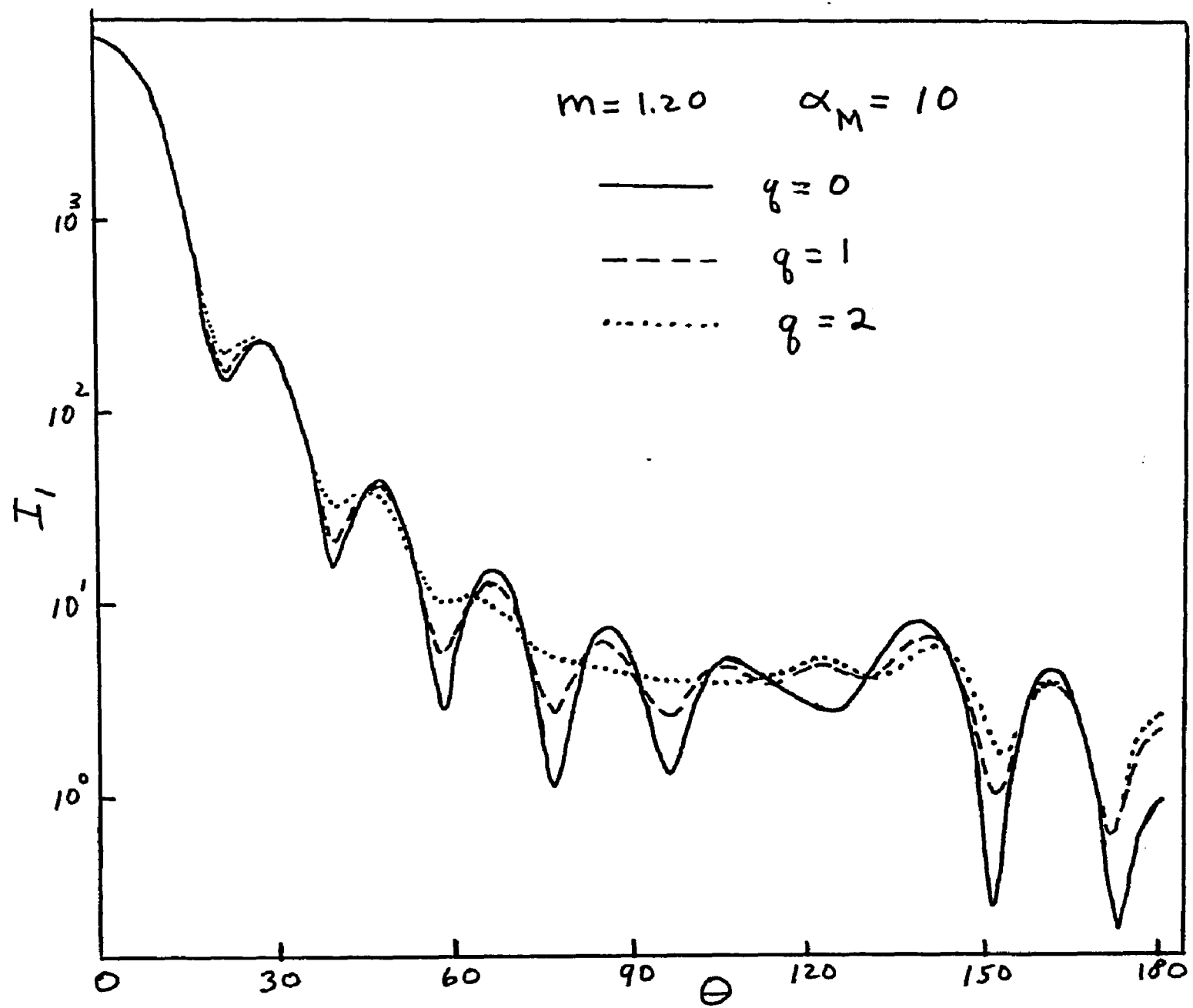

Fig. 20. Scattered Intensity I_1 as a Function of Angle for Size Distributions Having a Constant Mode α_M=10 and Different Distribution Widths

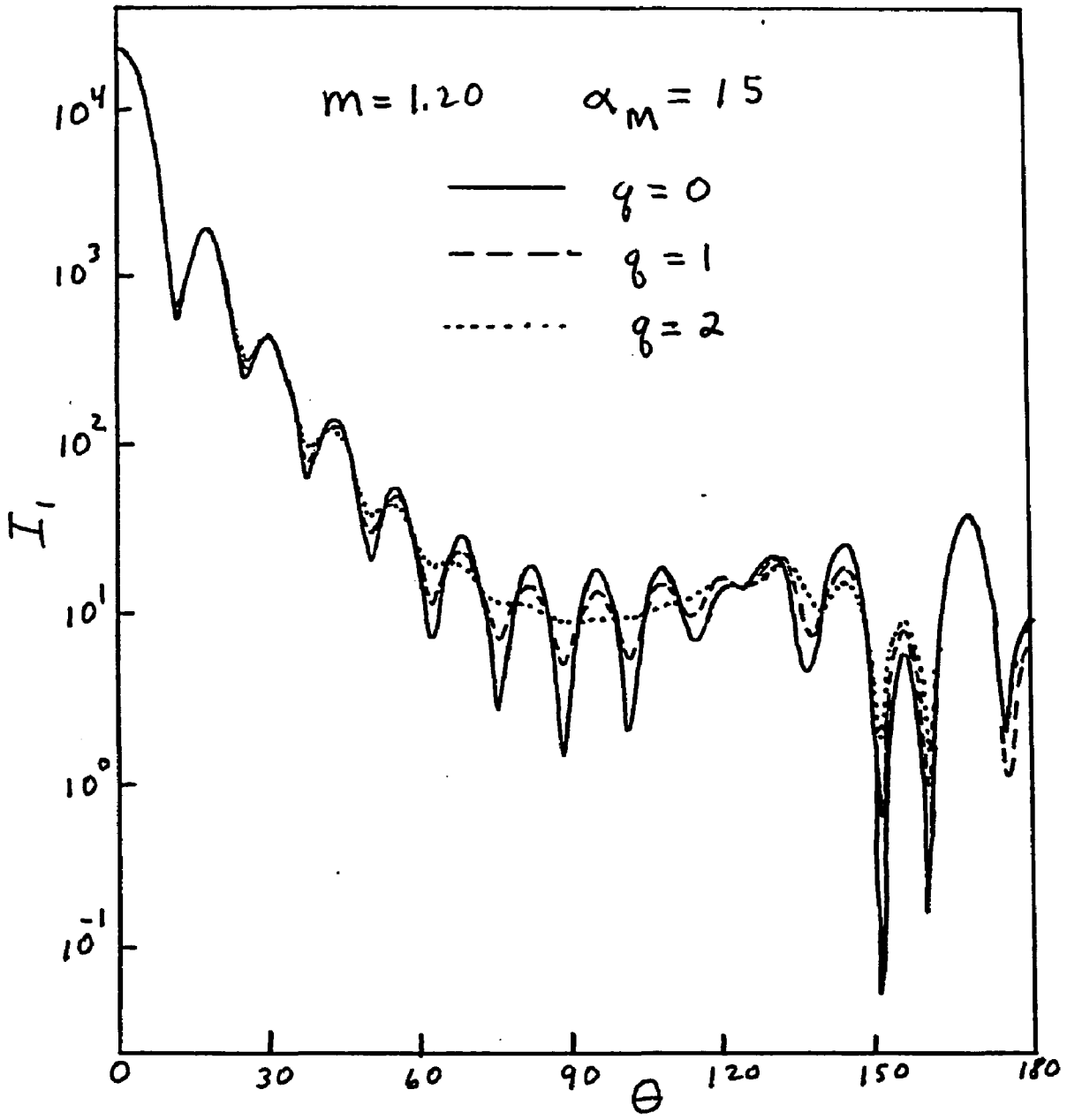

Fig. 21. Scattered Intensity I_1 as a Function of Angle for Size Distributions Having a Constant Mode α_M=15 and Different Distribution Widths

in the forward direction. However, compared to the corresponding extrema pairs in the forward direction, the extrema pairs in the backward direction show much sharper and deeper minima.

Another prominent feature in Figure 20 is the higher rate at which extrema in the central part of the scattering diagram become washed out as the heterodispersion increases. There is a gradual increase in the rate at which the extrema wash out as one compares successive extrema pairs beginning with the first pair in the forward direction. Figure 20 also shows a small region from 100^{o} - 120^{o} where the scattering curve has an irregular behavior as the heterodispersion increases. This region separates the regions in the forward and backward directions where the extrema show a systematic behavior. The analysis of the curves for $\alpha_M = 15$ in Figure 21 is very similar to the analysis just made for $\alpha_M = 10$ and therefore will not be repeated.

3. Survey of I_2 Scattering Curves

The corresponding I_2 light scattering curves are shown in Figures 22-26. The two prominent features in these graphs are the strong influence of the Rayleigh minimum for the small particle sizes and the very shallow extrema compared to I_1. An interesting observation of the latter item is that I_2 from monodisperse particles in the forward direction looks very similar to I_1 from heterodisperse particles.

The light scattered from small particle size distributions shown in Figures 22 and 23 are dominated by the Rayleigh minimum[3]. Figure 22 shows that the scattered intensity is greater in the forward direction than in the backward direction and has a deep minimum dispaced at larger

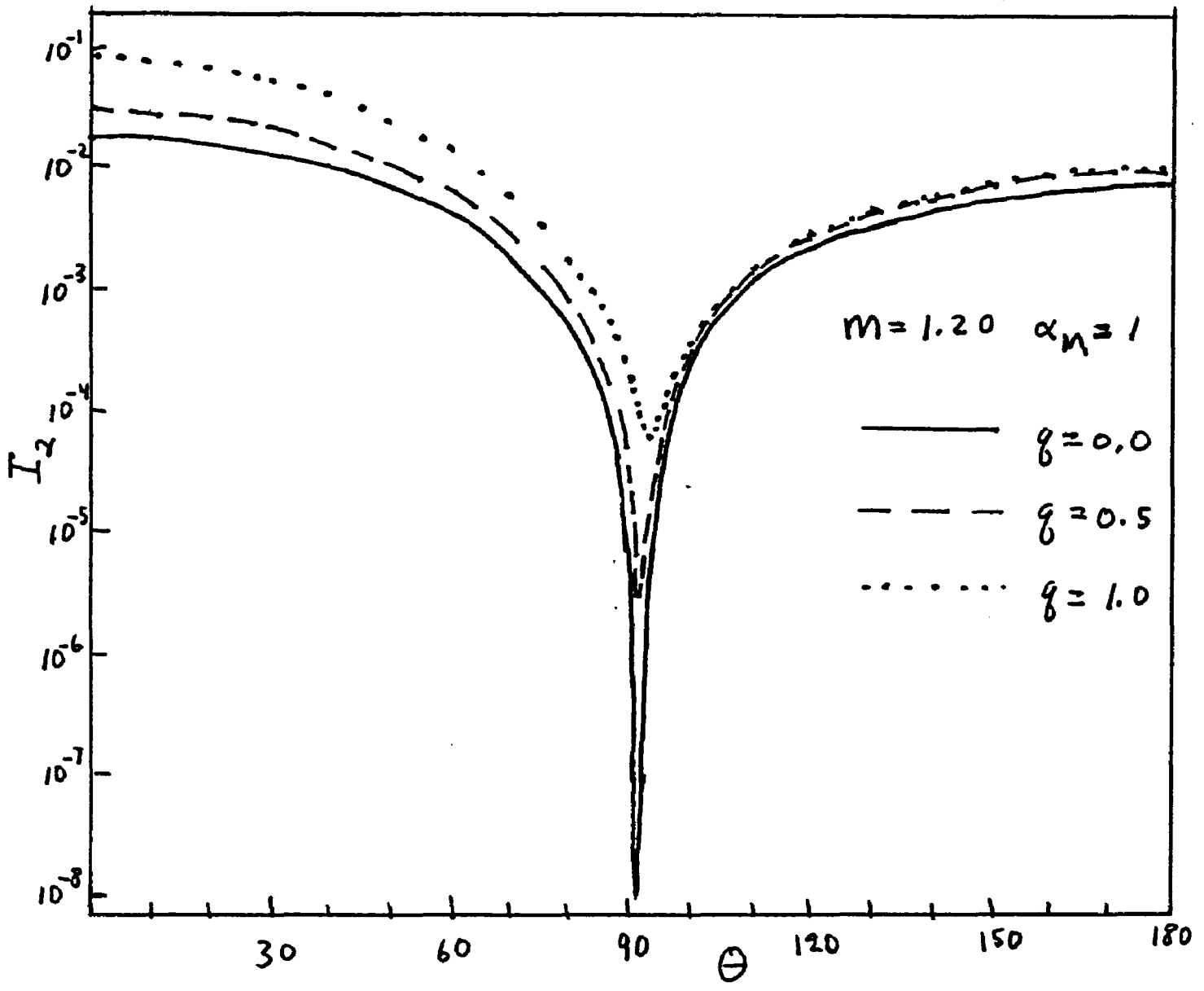

Fig. 22. Scattered Intensity I_2 as a Function of Angle for Size Distributions Having a Constant Mode $\alpha_m=1$ and Different Distribution Widths

angles from the true Rayleigh minimum at 90°. As the heterodispersion increases the Rayleigh minimum moves toward larger angles and the scattering becomes much greater in the forward direction than in the backward direction. This occurs because the integrated scattering is predominantly due to the larger particle sizes of the distribution.

The scattering curves for $\alpha_M = 3$ in Figure 23 show that the minimum has now moved more in the backward direction and is not as sharp as in the $\alpha_M = 1$ graph. In addition, the curve for $q = 0$ shows an inflection point in the location where I_1 in Figure 18 has an extrema pair. As the heterodispersion increases this inflection point becomes less pronounced. I_2 from monodisperse distributions thus appears to behave like I_1 from more heterodisperse distributions.

Proceeding to $\alpha_M = 5$ in Figure 24, one sees a very weak maximum and minimum in the forward direction for $q = 0$. As the heterodispersion increases the extrema pair is washed out and leaves only an inflection point. The corresponding region in Figure 19 for I_1 shows a very pronounced extrema pair. Comparing the same angular regions in Figures 19 and 24 shows once again that I_2 from monodisperse distributions looks like I_1 from heterodisperse distributions. However, this behavior does not hold in the backward direction where Figure 24 shows a very pronounced minimum that is gradually damped out as the heterodispersion increases.

The trend for very shallow extrema in the forward direction is also seen in Figure 25 where the scattering curves for $\alpha_M = 10$ are plotted. In contrast, a very pronounced scattering pattern occurs in the backward direction for angles larger than 110°. There appears to be a natural division of the I_2 curves into a forward and backward region as

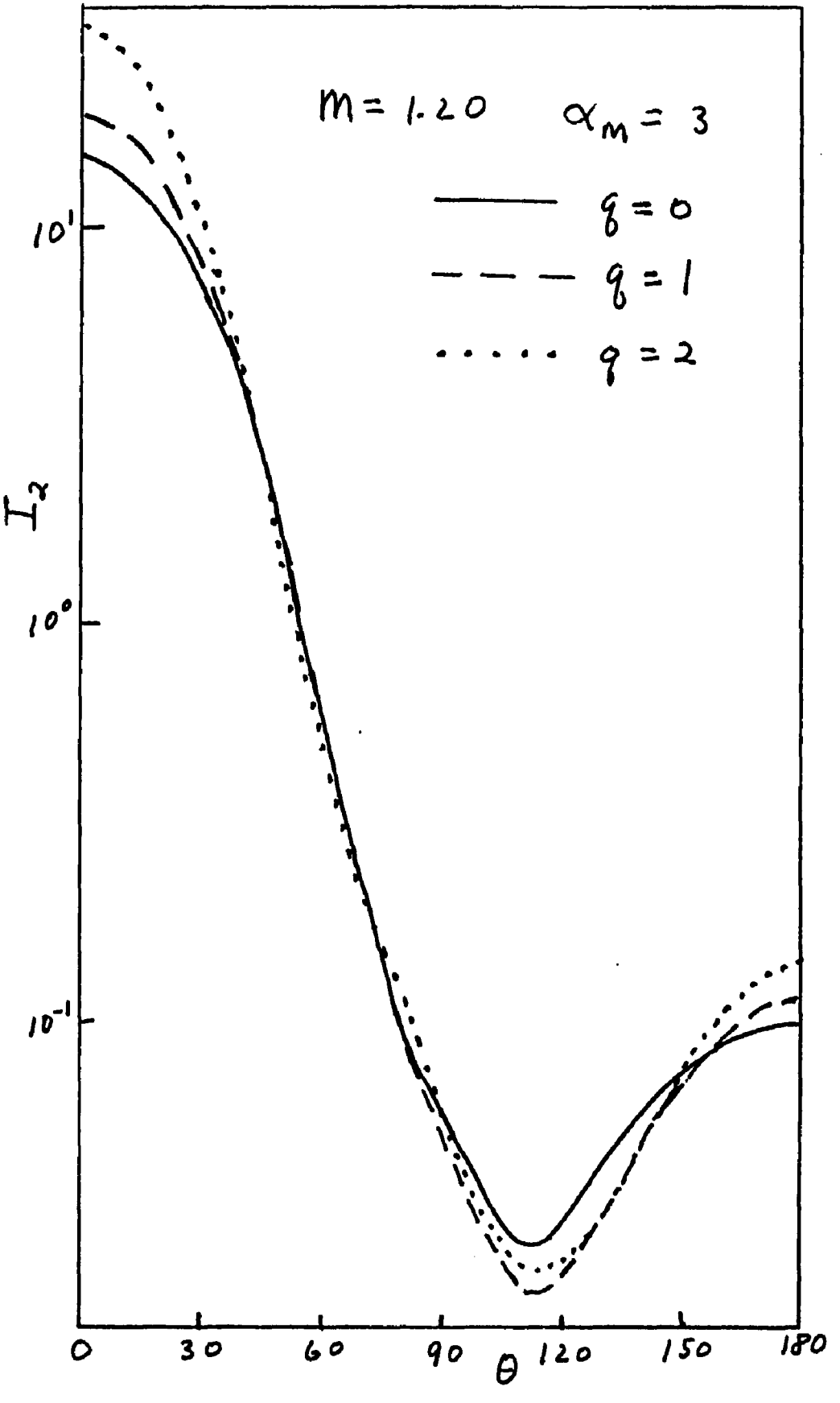

Fig. 23. Scattered Intensity I_2 as a Function of Angle for Size Distributions Having a Constant Mode $\alpha_M=3$ and Different Distribution Widths

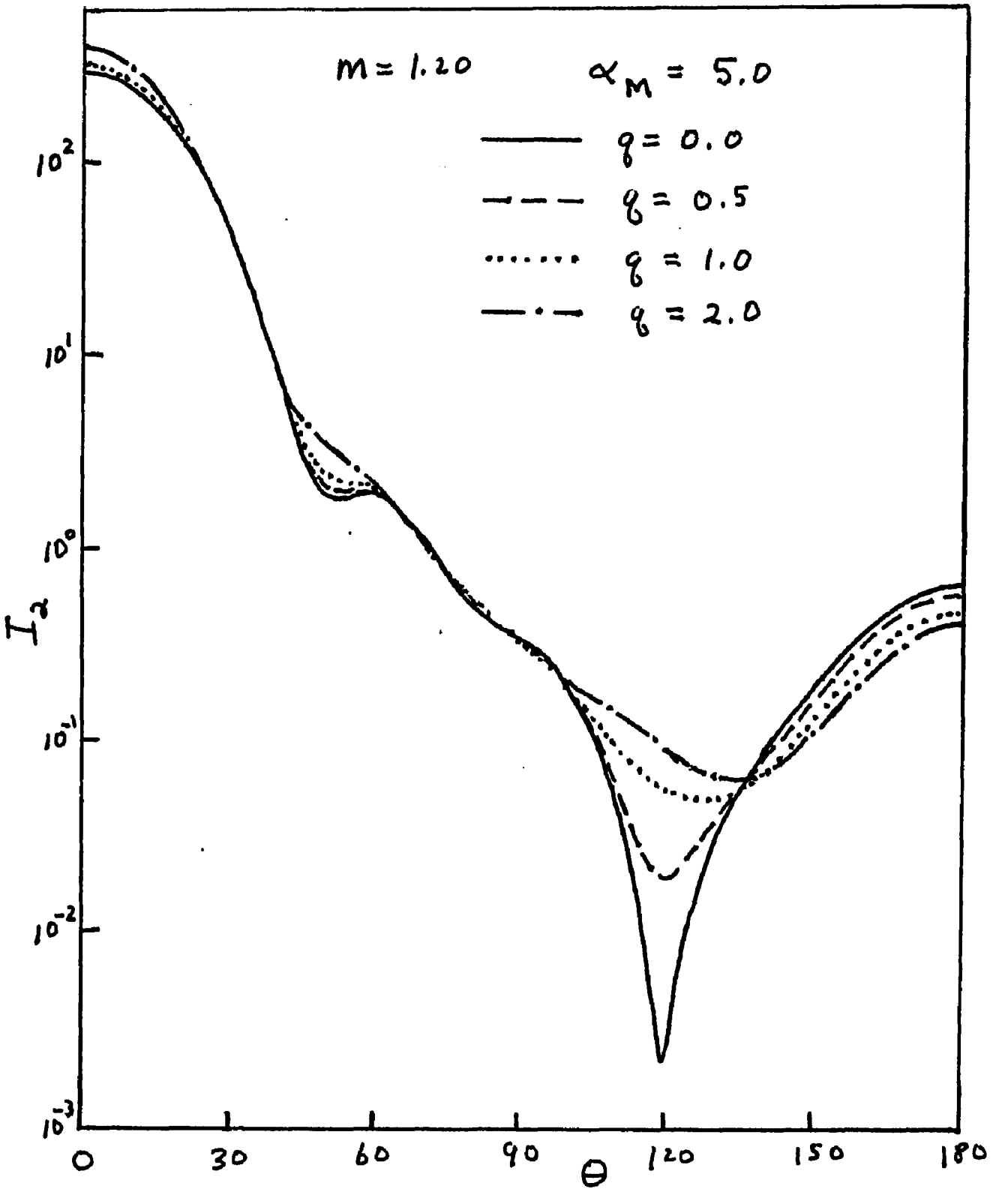

Fig. 24. Scattered Intensity I_2 as a Function of Angle for Size Distributions Having a Constant Mode α_M=5 and Different Distribution Widths

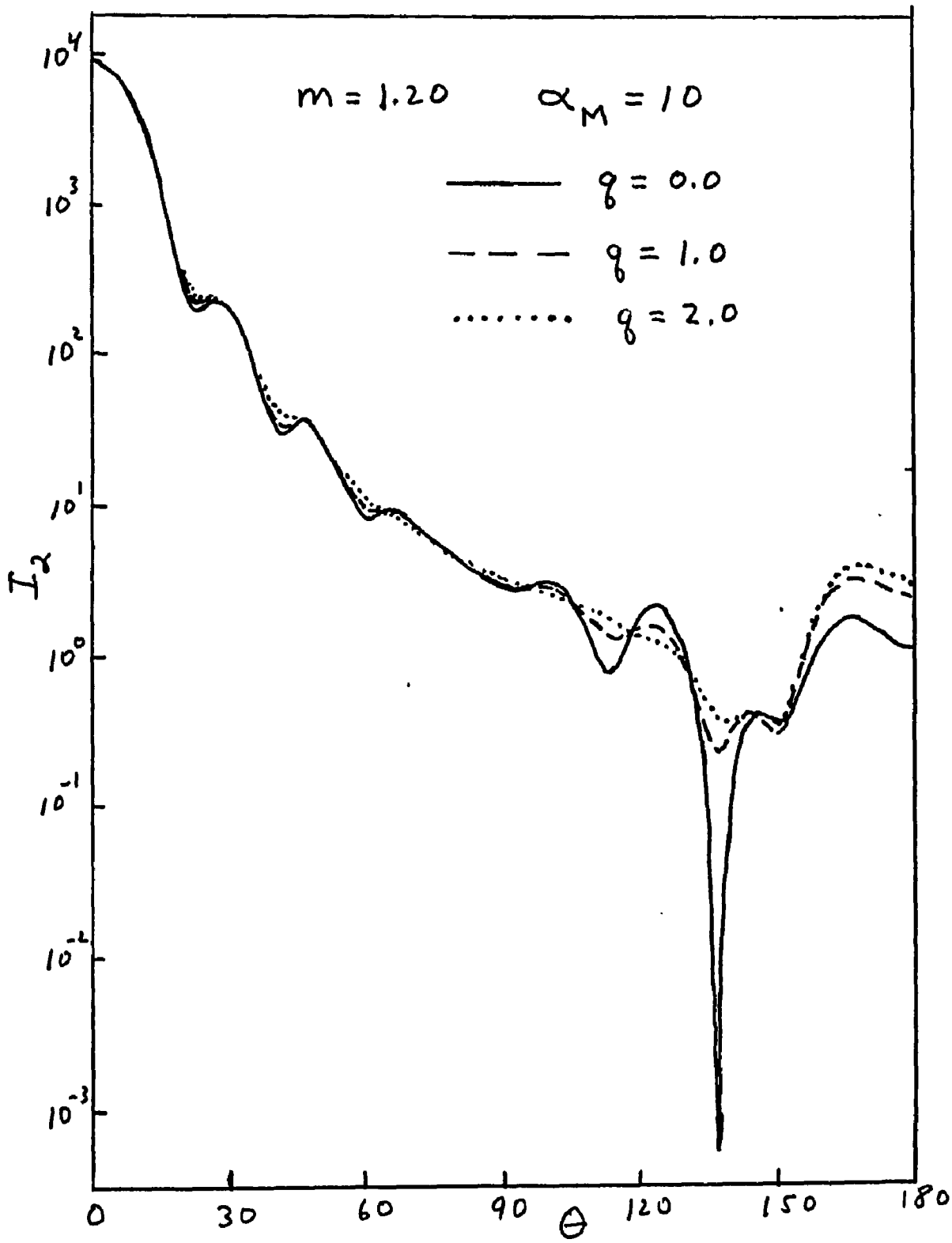

Fig. 25. Scattered Intensity I_2 as a Function of Angle for Size Distributions Having a Constant Mode α_M=10 and Different Distribution Widths

previously seen for the I_1 curves.

Figure 26 for $\alpha_M = 15$ shows a continuation of the same trend. The scattering in the forward direction shows highly damped maxima and minima while in the backward direction the scattering shows a very active oscillation pattern. An apparent exception to this trend is the first maxima and minima pair in the forward direction. This extrema pair for I_2 appears to have the same amplitude of oscillation as the first extrema pair for I_1. However, this apparent similarity is misleading because the amplitude of oscillation changes very little with the degree of heterodispersion for this extrema pair. The I_2 curves are, in fact, more damped than the corresponding I_1 curves.

4. Effect of Particle Size Distributions on the Number of Extrema

The relationship between the number of angular intensity extrema and the particle size (modal size for a distribution of particles) was then determined for the parameters used in the present investigation. Figure 27 shows the number of I_1 extrema from monodisperse systems having relative refractive indexes of m = 1.10 and m = 1.30 plotted against the modal size α_M. Both graphs show a step function relationship between the number of extrema and the modal size. Note that the number of extrema for m = 1.30 increases at a faster rate than for m = 1.10. Straight lines can be drawn through the data to show the overall linear behavior of the data.

An important aspect of Figure 27 is the step size used to increase the number of extrema. According to the Rayleigh-Gans-Debye (RGD)[3] theory, additional extrema enter the scattering diagram only one

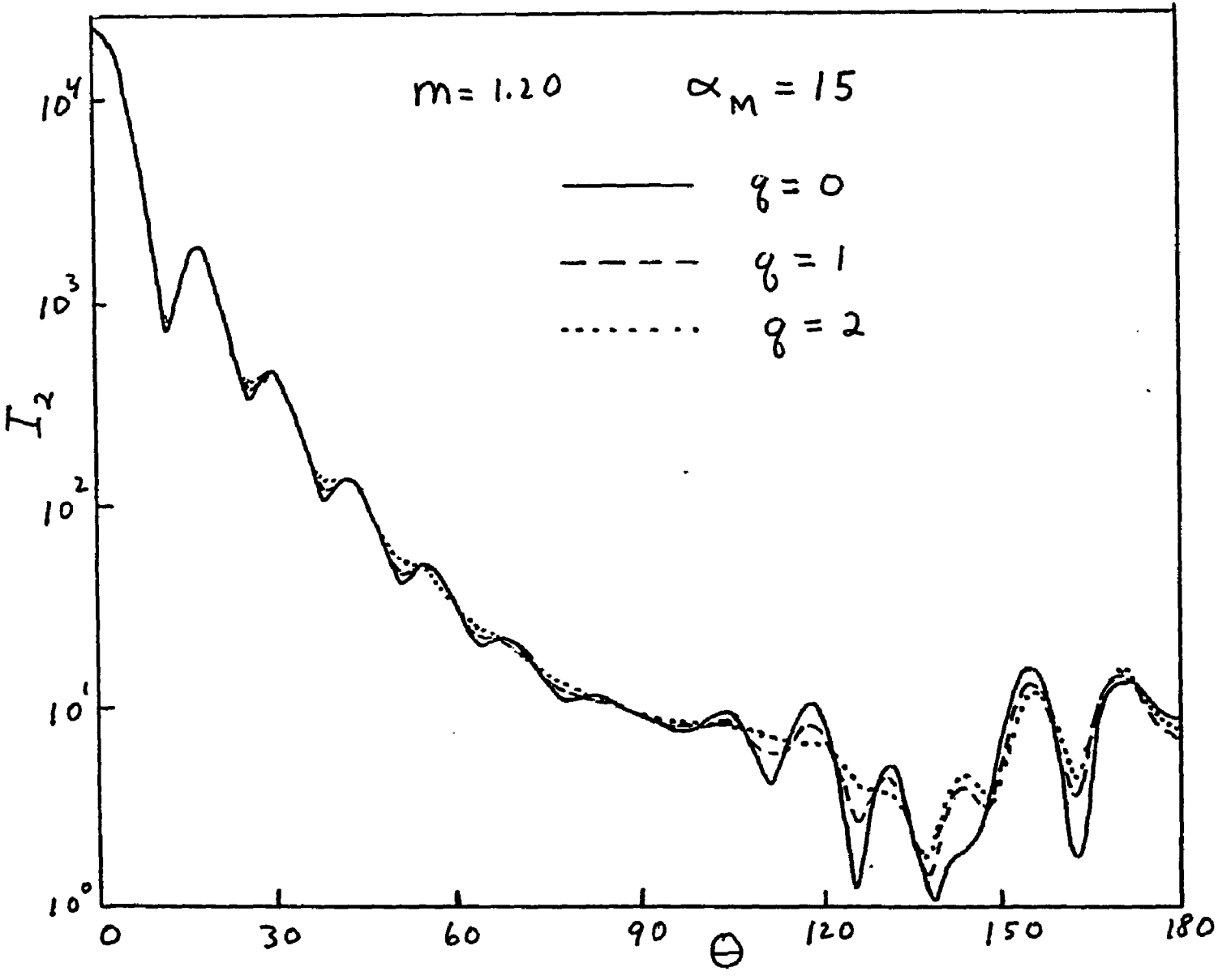

Fig. 26. Scattered Intensity I_2 as a Function of Angle for Size Distributions Having a Constant Mode α_M=15 and Different Distribution Widths

at a time as the particle size is increased. This can be seen in the extrema contour plots for low refractive indexes in the next section or in Figure 1 of the paper by Nakagaki and Heller[10]. The fundamental assumption in the RGD theory is that the optical phase shift corresponding to any point in the particle is small[3] i.e. that

$$\alpha (m - 1) \ll 1. \tag{15}$$

This means that neither the particle size , nor the relative refractive index m can become too large. Thus, if equation 15 holds, then the step size for increasing the number of extrema will be limited to one extremum.

Figure 27 shows that as the particle size increases for m = 1.10, the number of extrema increase in steps of one up to $\alpha_M = 9.2$ and in steps of two for larger sizes. This observation demonstrates the importance of equation 15 in assuming a negligible phase shift. At small values of . the phase shift is small and the RGD theory holds. However, as the size increases the phase shift becomes larger and the RGD theory no longer applies. For m = 1.30 the phase shift is sufficiently large even at small values of α that the number of extrema increases in steps of two for all of the particle sizes. Penndorf[33] and Rowell[32] had previously shown that all extrema after the first minimum enter the scattering diagram as maxima and minima pairs. The present study shows that this occurs only when the particle size or the relative refractive index becomes too large and results in a sizable phase shift.

The step functions in Figure 27 can be represented by straight lines if the discontinuous steps are averaged. This was done for various relative refractive indexes ranging from 1.00 to 1.333. The step function for m = 1.00 was obtained from the RGD theory. Figure 28

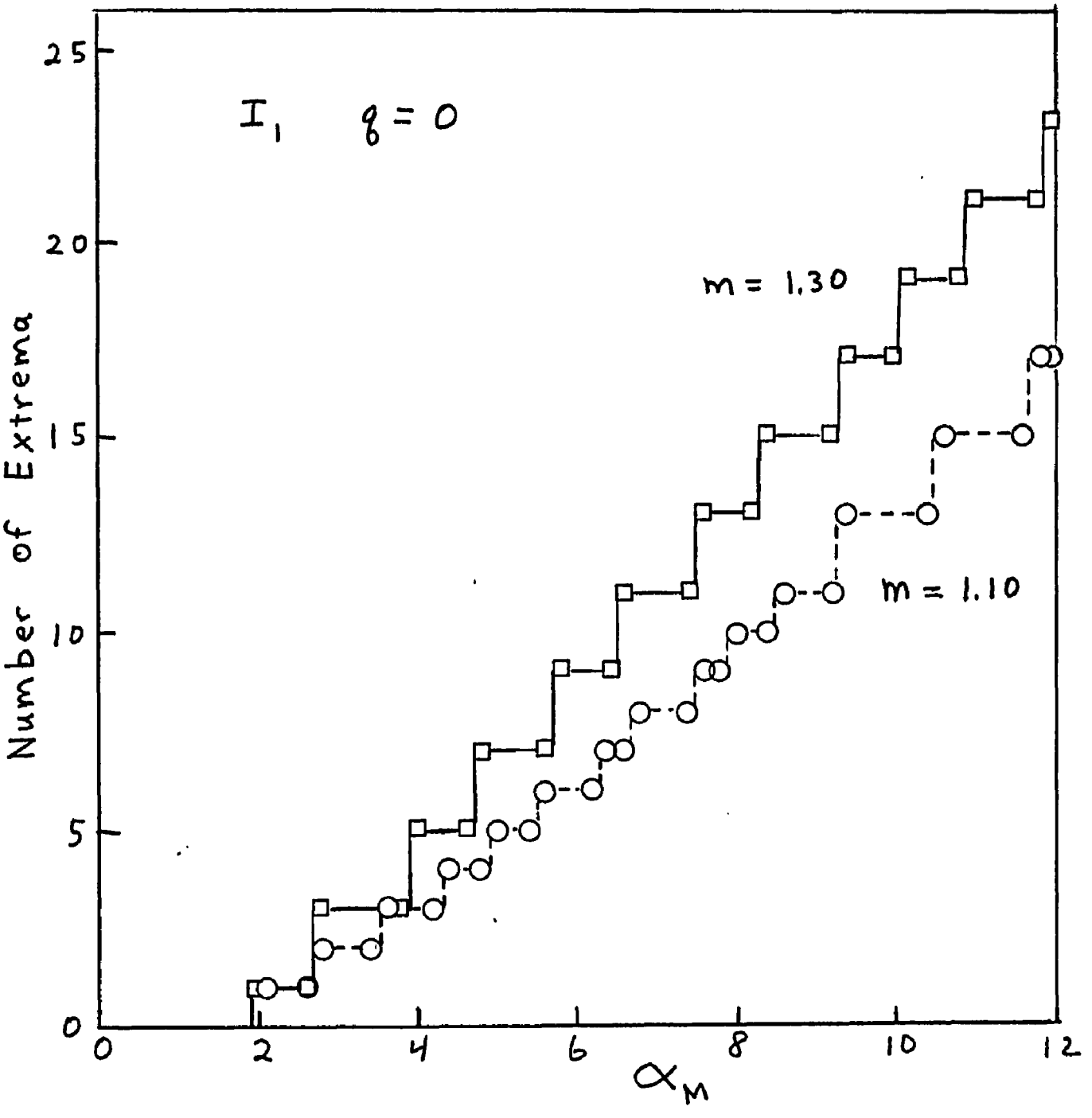

Fig. 27. Number of I_1 Extrema Plotted Against the Modal Size α_M for Monodisperse Systems with m=1.10 and 1.30

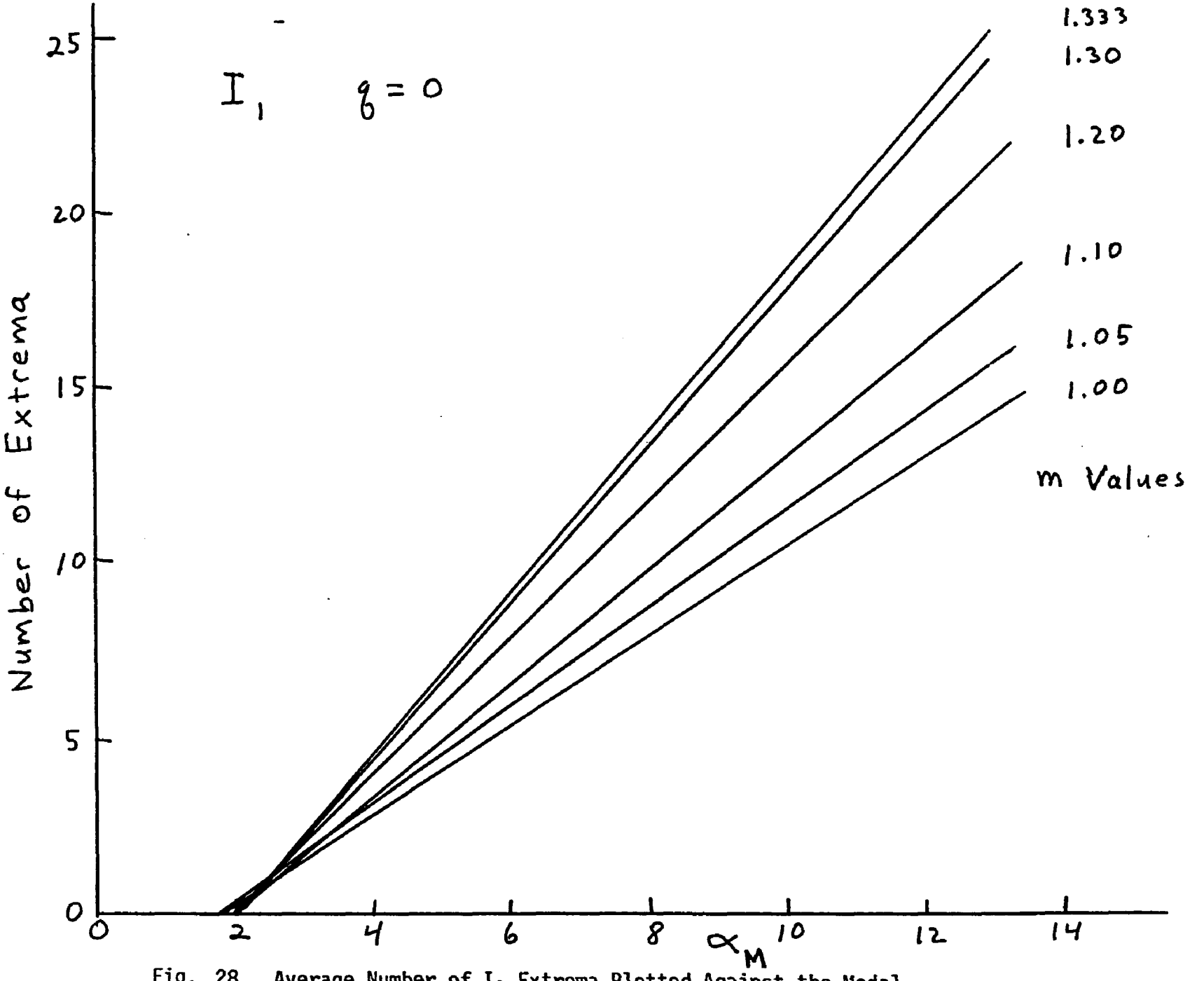

Fig. 28. Average Number of I_1 Extrema Plotted Against the Modal Size α_M For Monodisperse Systems with Different m Values

shows the resulting straight lines for the different relative refractive indexes. This figure represents the average number of extrema for different relative refractive indexes as a function of size. All of the data pertain to I_1 extrema from monodisperse systems. Note that the lines all begin at approximately $\alpha_M = 2$ and have greater slopes for the larger m values. These slopes vary linearly with m as seen in Figure 29.

The preceding discussion on the number of extrema was based on monodisperse particle sizes. For heterodisperse distributions the pattern has to be modified to account for the extrema being washed out. Figure 30 shows the number of I_1 extrema plotted against the modal particle size for three distributions characterized by q = 0, 1, 2 and m = 1.20. To allow easier viewing, the data for different q values have been displaced slightly on the ordinate axis and the complete step function drawn only for q = 0. One sees that all of the q values show a step function relationship between the number of extrema and modal size. Figure 30 shows that, with a few exceptions, the extrema for the different q values increase in steps of two as would be expected for the higher phase shift. The exceptions occur because the tabulated data[46] used to generate this figure had occassionally missed the minimum in the backward direction. The difficulty in detecting the first minimum in the backward direction was discussed previously in Chapter III.

Figure 30 shows that increasing q from 0 to 2 has only a minor effect on the number of I_1 extrema. The number of extrema remains constant from q = 0 to q = 1 and only decreases by one maxima and minima pair for q = 2. Note that the extrema disappear as the heterodispersion increases by the merging of a maxima and minima pair as seen in Figures

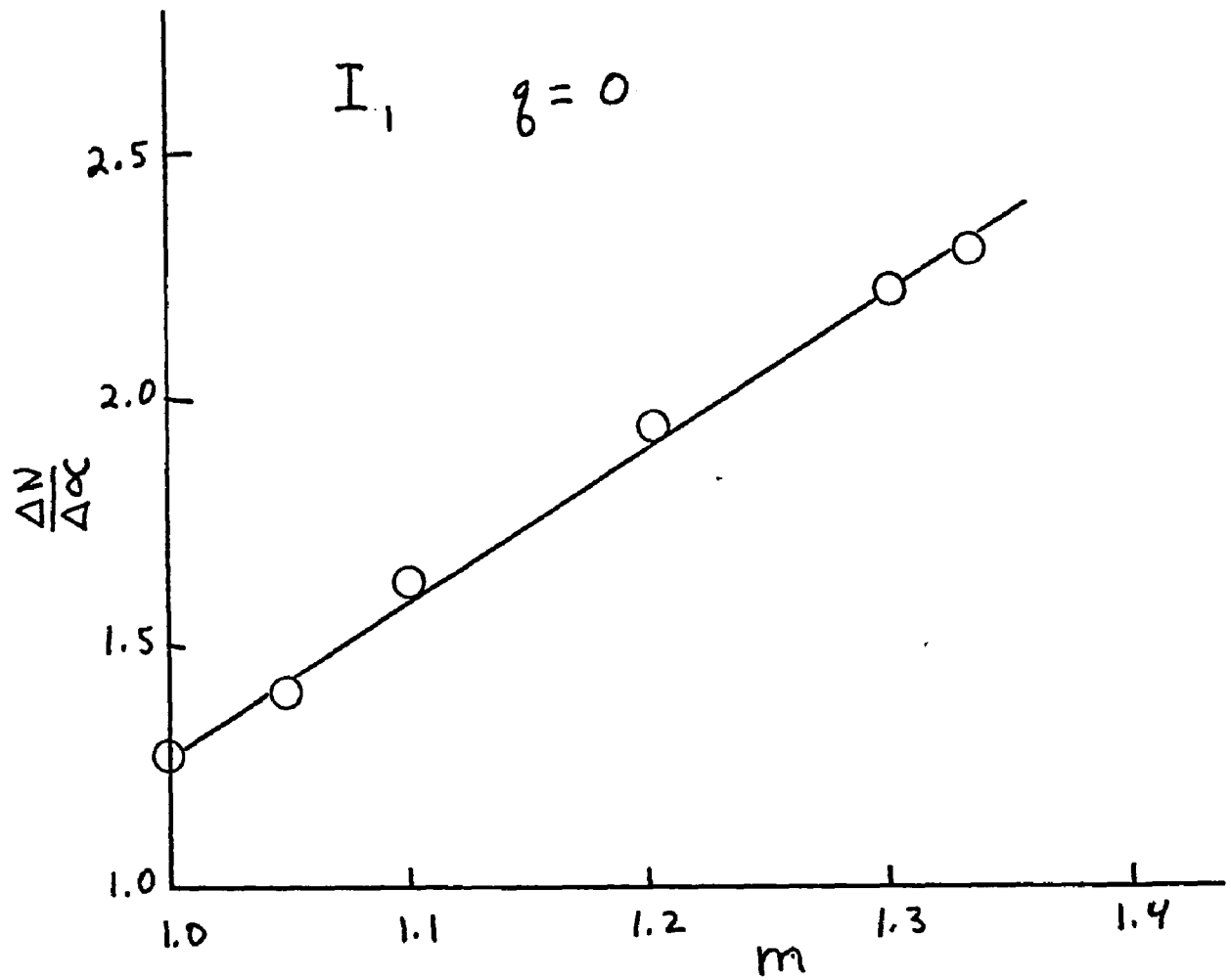

Fig. 29. Effect of m on the Change in the Number of I_1 Extrema with a Change in α_M

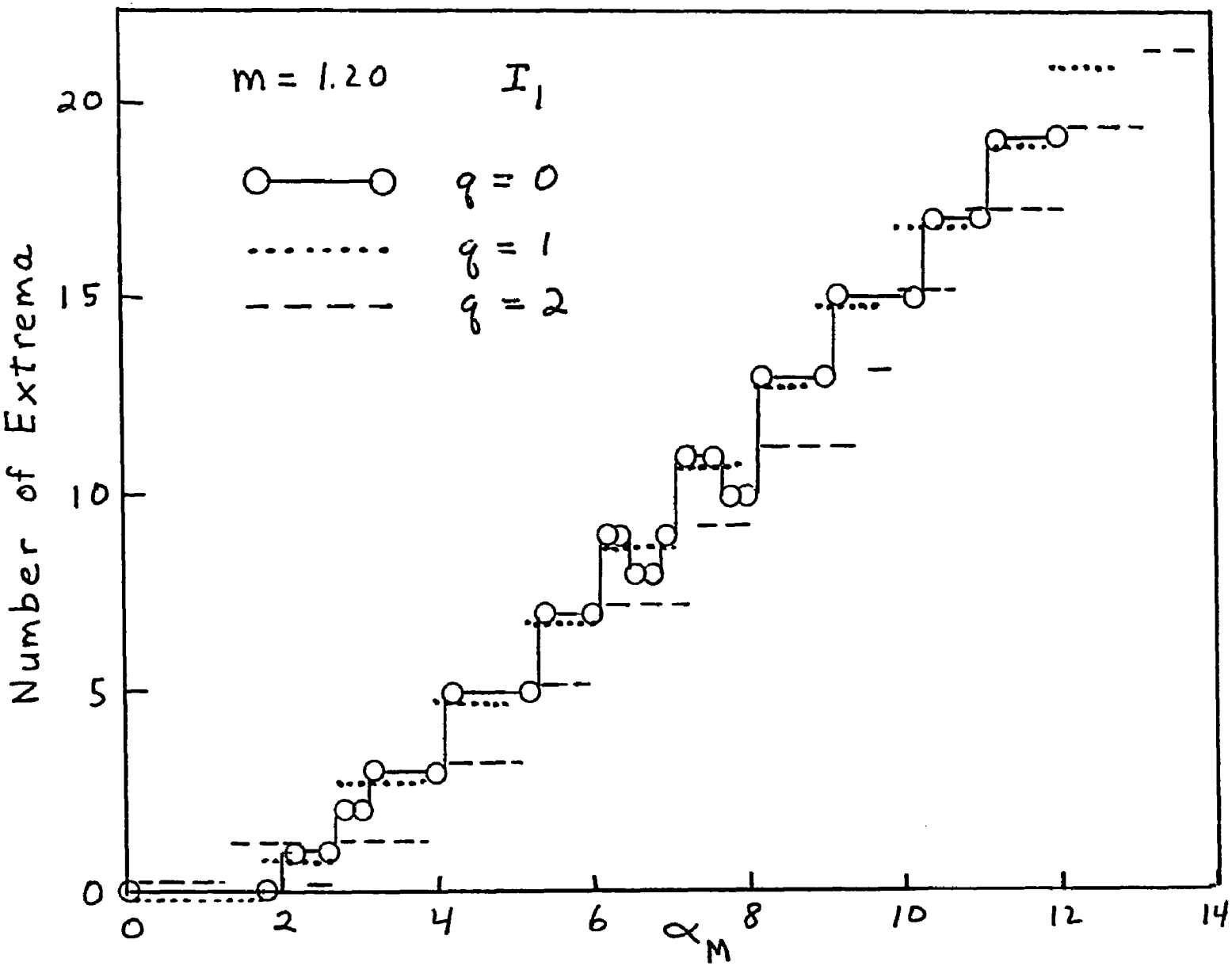

Fig. 30. Number of I_1 Extrema Plotted Against the Modal Size α_M for Different Heterodisperse Systems with m=1.20

17-26. Moreover, as the heterodispersion increases, the remaining extrema become more shallow and hence more difficult to detect.

A similar analysis of the number of I_2 extrema reveals a more complicated pattern. Figure 31 shows the number of I_2 extrema plotted against the modal size in the same fashion as in Figure 30 for m = 1.20 and q = 0, 1, 2. In general, the number of I_2 extrema both increases and decreases in steps of two as the modal size increases. However, the net change in the number of extrema shows an approximately linear increase with size. In addition, the number of extrema is greatly reduced when q is increased to 2.

The reason for the unusual behavior of the I_2 extrema increasing and decreasing by two was then investigated. A detailed extrema search verified that no extrema had been missed and the pattern shown in Figure 31 is indeed correct. This detailed extrema search indicated that the cause of the increase and decrease in the number of extrema was due to the formation and disappearance of extrema pairs in the backward direction.

Figure 32 shows the contours of the I_2 maxima and minima in the backward direction plotted on a graph having the size α as the ordinate and the angle θ as the abscissa. The maxima and minima are shown by the dashed and solid lines respectively. As the particle size increases from $\alpha = 0$, the Rayleigh minimum at 90° moves in the backward direction and undergoes a series of oscillations. New extrema pairs will then appear at the locations indicated by A and disappear at the locations indicated by D. This alternate appearance and disappearance of extrema pairs is the cause of the observed number of extrema increasing

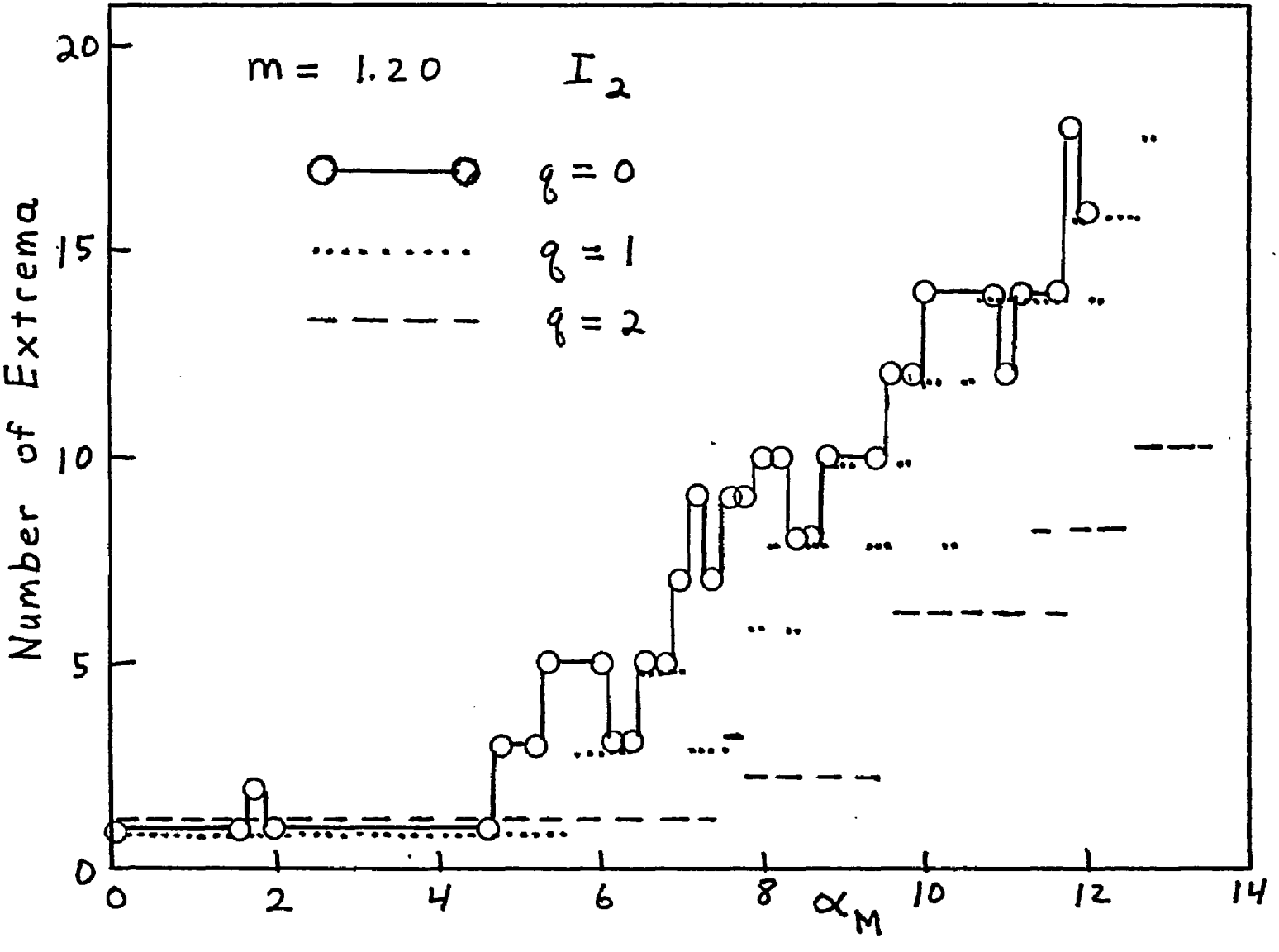

Fig. 31. Number of I_2 Extrema Plotted Against the Modal Size α_M for Different Heterodisperse Systems with m=1.20

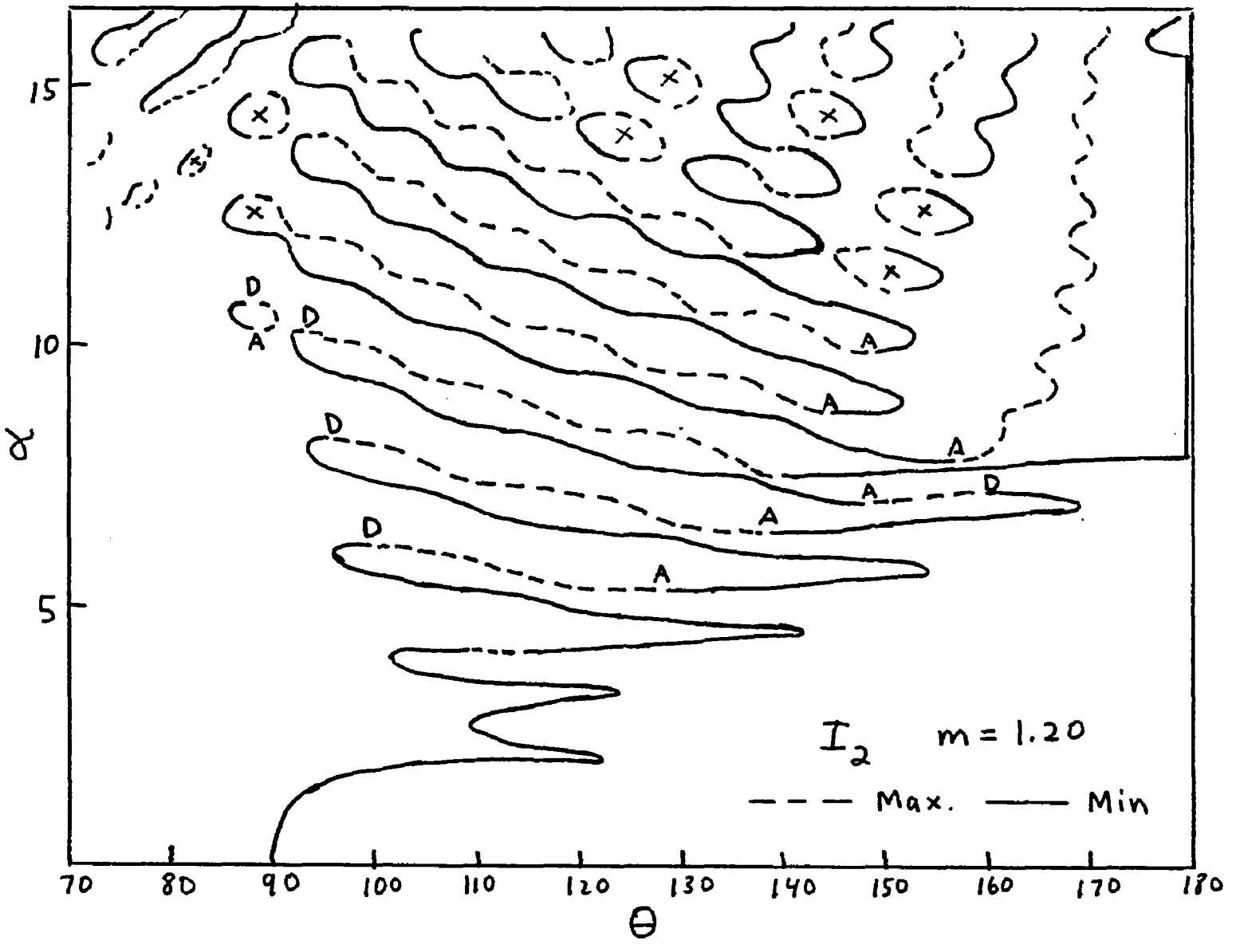

Fig. 32. Angular Location of I_2 Extrema Versus Modal Size α_M in the Backward Direction for Monodisperse Distributions with m=1.20

and decreasing in steps of two. Since the number of extrema pairs that are formed exceed the number of pairs that disappear, the overall number of extrema increase with size. In addition, the I_2 extrema pairs in the forward direction enter the scattering diagram in a systematic fashion and add to the cumulative total as seen in Figure 30 for the I_1 extrema.

When the particle size reaches $\alpha = 8$ a very strange behavior is seen in Figure 32 for the first minimum in the backward direction. This minimum moves rapidly toward $\theta = 180^{\circ}$ and remains fixed at that angle until the particle size is greater than 15. Detailed calculations have shown that the minimum actually occurs at 179.9°. Because of the close proximity to 180° this minimum was missed in the calculations of the tables[46]. Thus Figure 31 shows an increase of only one extremum at $\alpha = 8$.

The effect of increasing heterodispersion on the number of extrema is much more pronounced for I_2 than for I_1 as seen by comparing Figures 30 and 31. The primary cause of the increased rate at which the I_2 extrema wash out is due to the very shallow extrema initially present for even monodisperse distributions. As the heterodispersion increaseS from q = 0 to q = 1 the number of extrema decrease by an average of one extrema pair. The oscillation in the data indicates that the appearance and disappearance of I_2 extrema pairs is still occurring for q = 1. However, as q increases to 2 one sees a more uniform increase in the number of extema as the particle size increases. This indicates that the pattern of alternating extrema appearance and disappearance has given way to a less complicated pattern involving only extrema formation. Illustrations of these patterns will be given in the next section of this chapter.

The analysis of the number of extrema from the scattered intensity I_u using unpolarized incident light was also investigated. Figure 33 shows the number of I_u extrema plotted against the modal size for m = 1.20 and q = 0, 1, 2. Since I_u has a very close resemblance to I_1, the number of extrema should also be similar for the two uses. This is shown in Figure 33 where the number of I_u extrema for q = 0 and 1 are nearly identical with the I_1 data in Figure 30. The I_u data shows an additional extremum from the Rayleigh minimum at small sizes. Figure 33 also shows that increasing the heterodispersion to q = 2 has a large effect on reducing the number of I_u extrema compared to the I_1 extrema.

5. Constant Angular Location of Extrema with Increasing Heterodispersion

Another prominent characteristic in Figures 17-26 in addition to the number of extrema is the constant angular position of the extrema as the heterodispersion increases for a constant modal size. Demonstrating this behavior on a quantitative basis is very complicated and would offer little improvement over a qualitative explanation. The problem is to show that the angular location of the extrema from monodisperse intensities $i(\alpha,\Theta)$ is the same as the angular location from heterdisperse intensities in equation 11, rewritten below

$$I(p,q,\Theta) = \int f(\alpha,p,q)\ i(\alpha,\Theta)d\alpha. \qquad (11)$$

The size distribution is assumed to have a constant mode equal to the size of the monodisperse distribution.

A qualitative demonstration that the angular location of the intensity extrema will remain constant can be made using Figure 34.

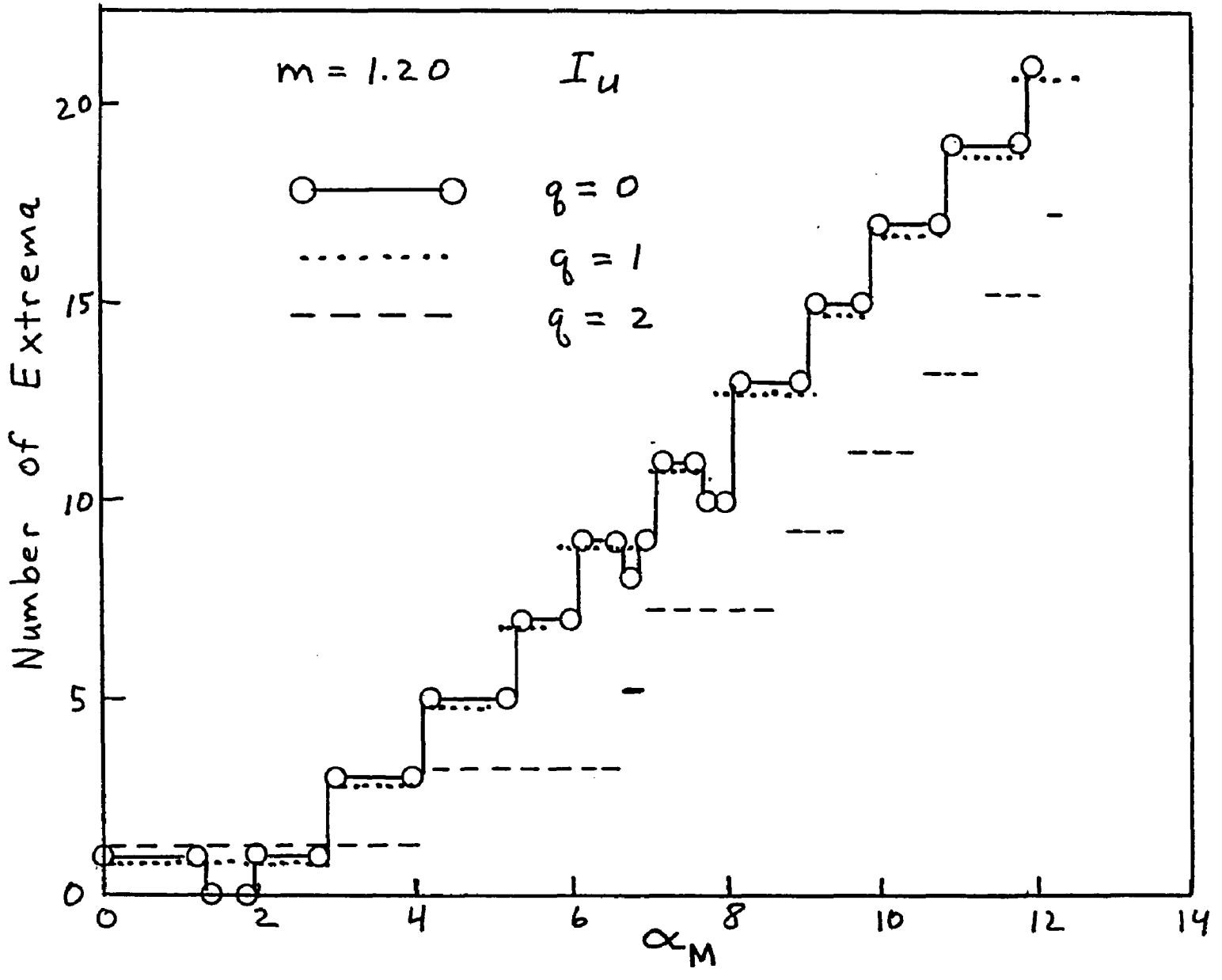

Fig. 33. Number of I_u Extrema Plotted Against the Modal Size α_M for Different Heterodisperse Systems with m=1.20

This figure shows the contours of the I_1 maxima and minima for mondisperse distributions with m = 1.20 plotted on a graph having the mode α_M for the ordinate and the angle θ for the abscissa. The maxima and minima are designated by circles and triangles respectively. Figure 34 therefore describes the same scattering system shown earlier in Figures 17-21.

A series of line segments were drawn through the extrema for $\alpha_M = 5$ and 10 to represent the size range of a heterodisperse distribution corresponding to q = 1. A more heterodisperse distribution would increase the line segment while a less heterodisperse distribution would decrease the line segment. If one assumes that the intensity along an extremum contour is constant within the size range of the heterodispersion (line segment in Figure 34) then a relatively simple explanation can be made for the constant angular location of the extremum as the heterdispersion increases.

The explanation will be illustrated using the minimum at $\theta = 48^\circ$ from the monodisperse distribution at $\alpha_M = 5$. For a distribution of particle sizes over the range indicated by the line segment, the fraction of particles greater than $\alpha_M = 5$ make the extremum angle smaller while the fraction of particles smaller than $\alpha_M = 5$ make the extremum angle larger. The two effects will cancel thus leaving the extremum from the heterodispersion fixed at the same location as the monodisperse distribution.

In a more quantitative description, the heterodisperse distribution has approximately a zero average deviation of the extremum angle $\overline{\Delta\theta}$, from the monodisperse extremum angle. The average deviation of the extremum angle is defined by

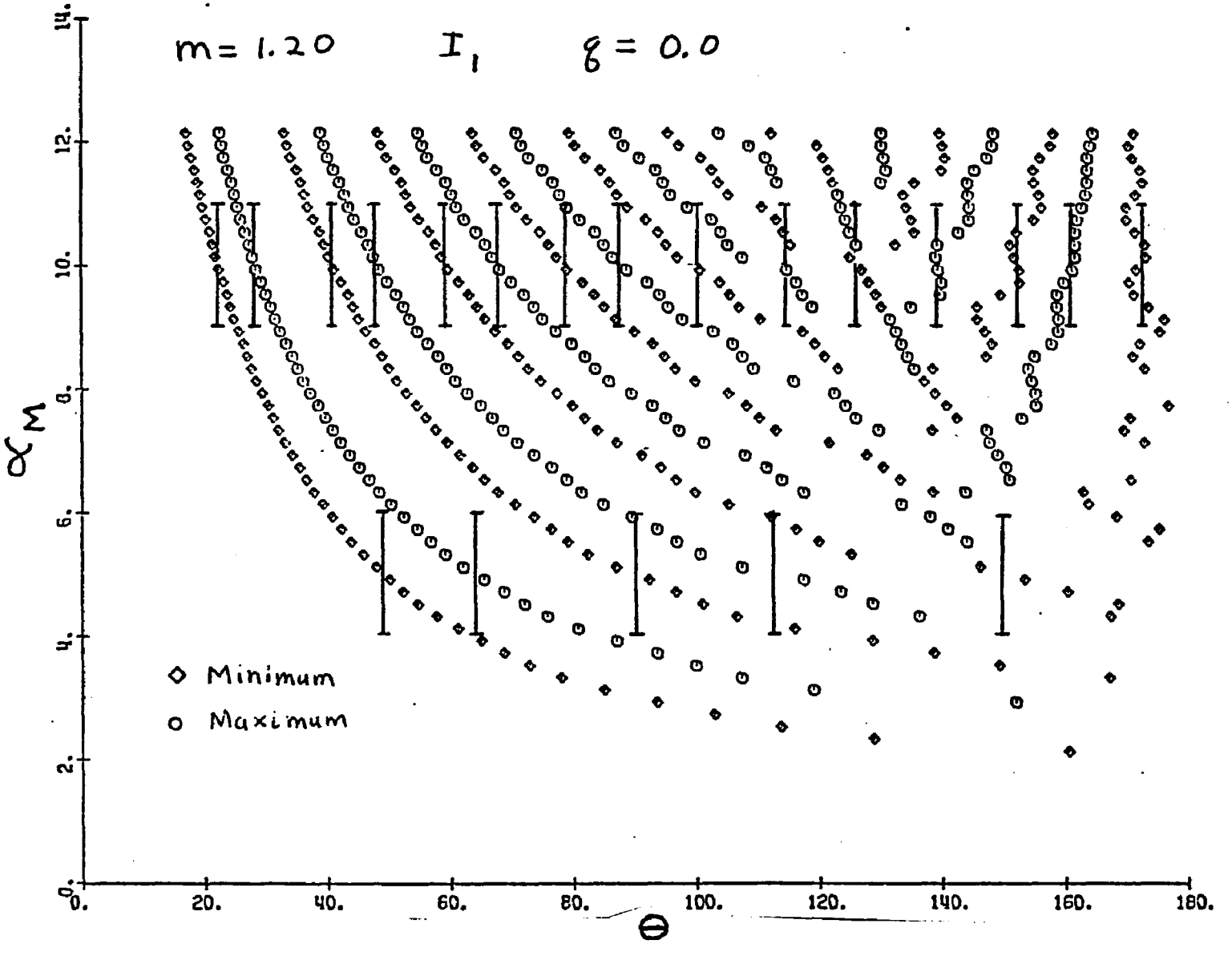

Fig. 34. Angular Location of I_1 Extrema Versus Modal Size α_M for Monodisperse Distributions with m=1.20

$$\overline{\Delta\theta} = \int (\theta_{\alpha} - \theta_{\alpha_M}) f(\alpha) d\alpha \qquad (16)$$

where θ_{α} is the angle of the intensity extremum for size α

θ_{α_M} is the angle of the intensity extremum for the monodisperse size α_M

$f(\alpha)$ is the number or particles having size α

If the angular shift from larger and smaller particle sizes are to cancel, the heterodisperse distribution must have a characteristic moment that equals the monodisperse particle size. A few preliminary tests using both the average and the mode showed nearly identical behavior. The mode was therefore chosen since it is much easier to identify than the average.

If the intensity along the extrema contour were constant then equation 16 would allow one to calculate the angular shift for any heterodisperse distribution compared to the monodisperse distribution. Unfortunately, the intensity is not constant within the extrema contour and requires an additional weighting function in equation 16. The problem must then be addressed in terms of the integrated intensities for heterodispersions in equation 11. However a qualitative interpretation of the extrema shift using equation 16 is satisfactory. Moreover, the equation becomes increasingly more accurate as the degree of heterodispersion decreases and as the extrema move in the forward direction. Both trends make the intensity along the contour more constant over the integration limits.

6. Other Trends in the Angular Scattering Intensity

The simple arguments used to explain the constant angular location of the extrema with increasing heterodispersion can also be used

to explain the other trends in the angular scattering intensity curves in Figure 17-26. In general, these trends are determined by the intersection angle of the extrema contours with the vertical integration lines in Figure 34. If the integration line cuts across several extrema contours then the extrema in the resulting heterodispersion will rapidly wash out and disappear. However, if the integration line runs nearly parallel to the extrema contours then the extrema in the resulting heterodispersion will show only a small damping effect.

Figure 34 shows that for a given particle size, the extrema contours in the forward direction are more parallel to the integration lines than in the central portion of the scattering diagram. Moreover there is a continual change in the slopes of the extrema contours relative to the integration lines from more vertical in the forward direction to more horizontal in the central portion. Thus, as the degree of heterodispersion is increased, the extrema in the forward direction will be slightly damped while the extrema at progressively larger angles will be increasingly damped and even disappear. These effects are illustrated in Figure 35, which is an enlargement of the first four extrema pairs taken from Figure 20. Figure 35 shows I_1 from different particle size distibutions having a constant mode of $\alpha_M = 10$. Note that the heterodispersion has an increasingly greater effect on washing out the extrema for the higher orders* of extrema pairs.

This trend becomes more pronounced for the larger particle sizes. Figure 36 shows I_1 from different heterodispersions having

*The order of an extrema pair is determined by counting the extrema pairs from the forward direction.

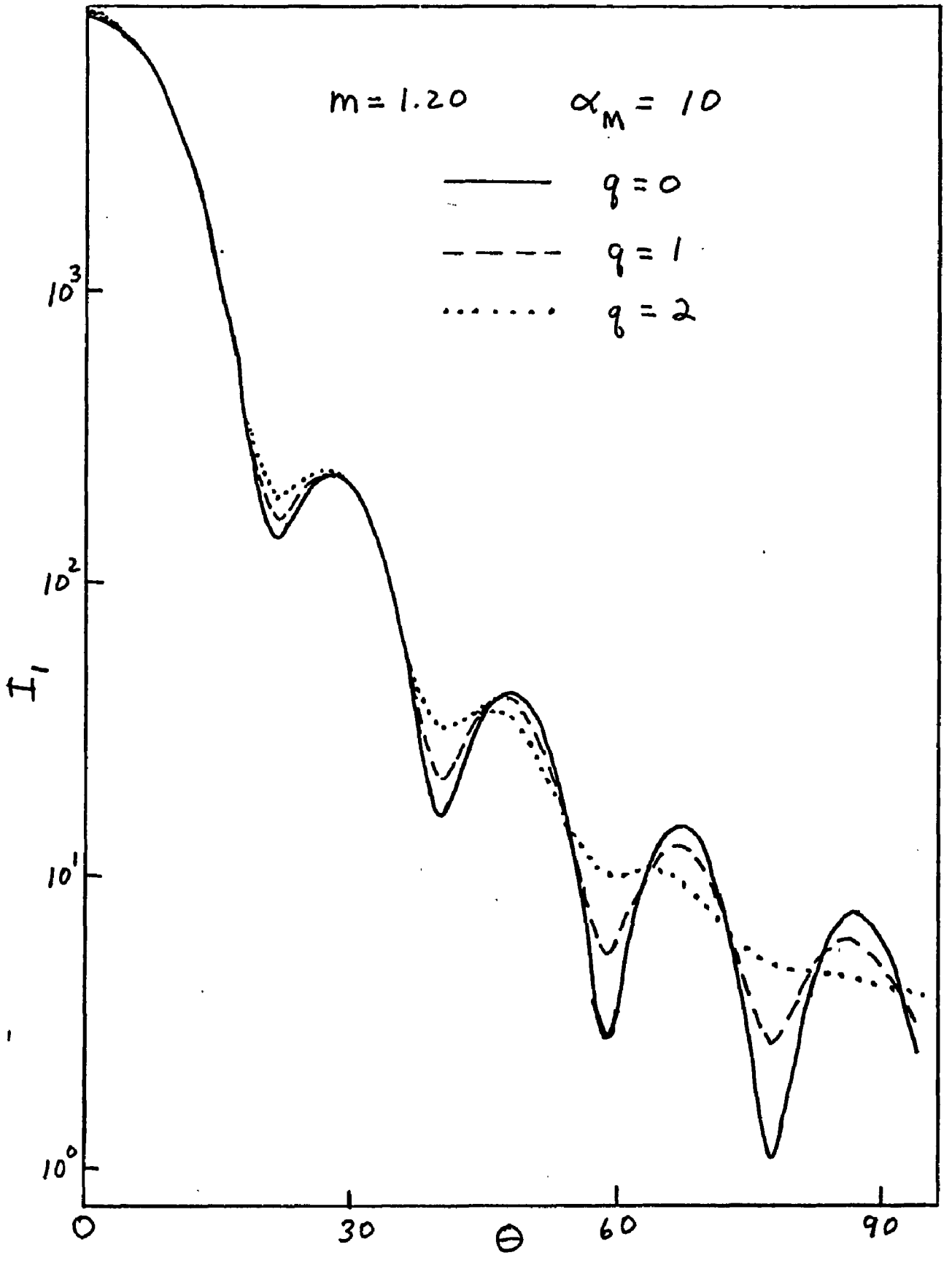

Fig. 35. Scattered Intensity I_1 as a Function of Angle Showing the First Four Extrema Pairs for Size Distributions Having a Constant Mode α_M=10 and Different Distribution Widths

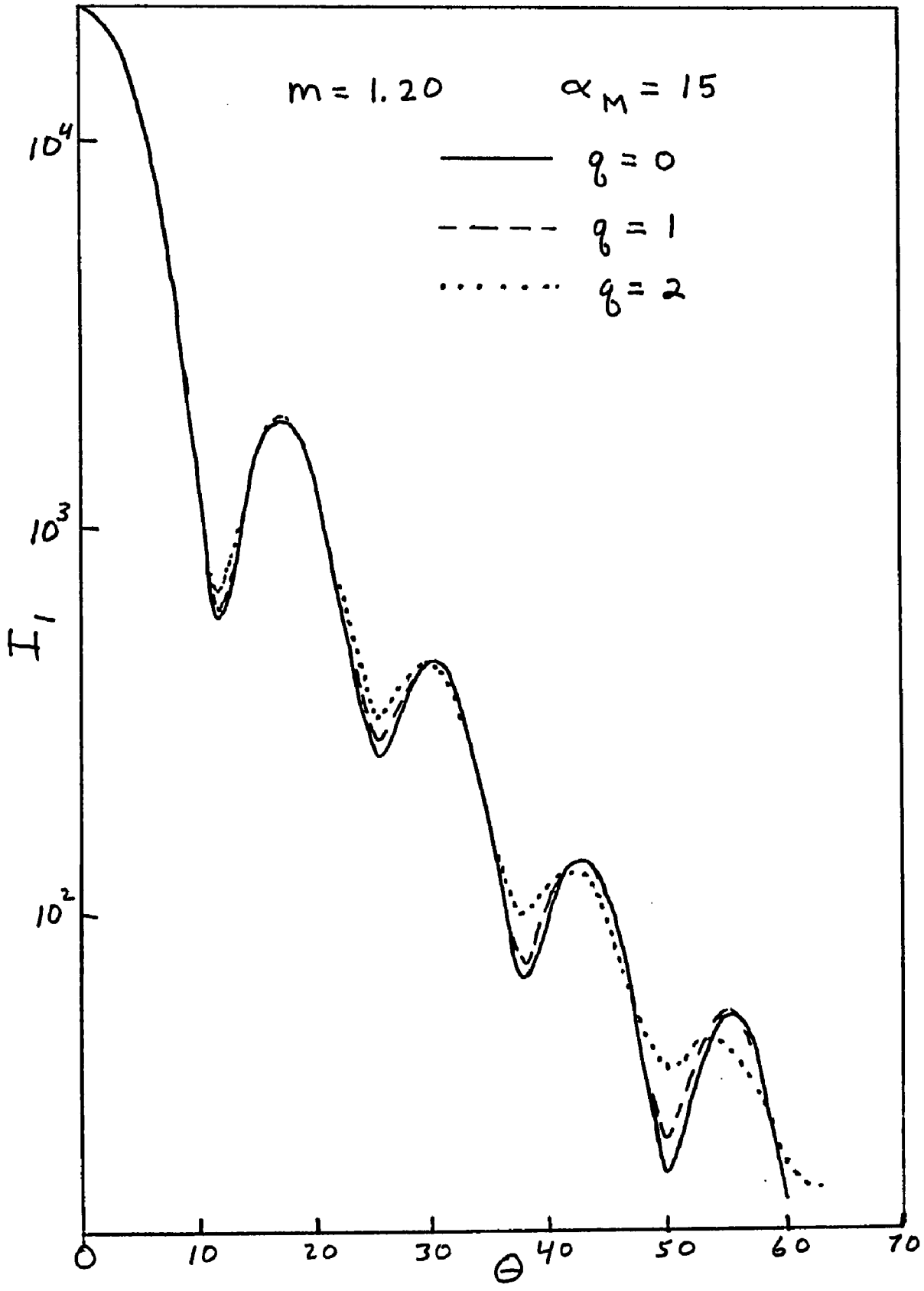

Fig. 36. Scattered Intensity I_1 as a Function of Angle Showing the Extrema Pairs in the Forward Direction for Size Distributions Having a Constant Mode α_M=15 and Different Distribution Widths

a constant mode of $\alpha_M = 15$. This figure is an enlargement of Figure 21 and shows the first few extrema orders in the forward direction. One sees that increasing the heterodispersion has very little effect on the first two extrema orders and only a moderate effect on the third extremum order. However, the higher orders, which are continued in Figure 37, show an increasingly greater sensitivity to the heterodispersion.

The extrema in the backward direction have a more complicated pattern. Figure 34 shows that for smaller particle sizes the extrema in the backward direction appear to have little if any pattern. However, for larger particle sizes the extrema in the backward direction show a definite migration toward the backward direction. A more detailed picture of the extrema contours in the backward direction of Figure 34 is shown in Figure 38. The formation of new extrema pairs with increasing particle size are shown on the graph with X's and numbered sequentially. This region is characterized by closely spaced maxima and minima and frequent reversals in the direction of the extrema contour migrations. Note that the angular location where the new extrema pairs originate moves toward the forward direction as the particle size increases.

Increasing the heterodispersion in the regions where new extrema pairs are formed will frequently result in major changes in the angular intensity plots. An example of this type of change is given in Figure 19, where the monodisperse distribution in the backward direction has a minimum intensity at 146°. As the heterodispersion increases this minimum moves to 151° and becomes more shallow. Further increase in the heterodispersion, however, results in a new maxima and minima pair appearing in the angular intensity diagram. The explanation for this addi-

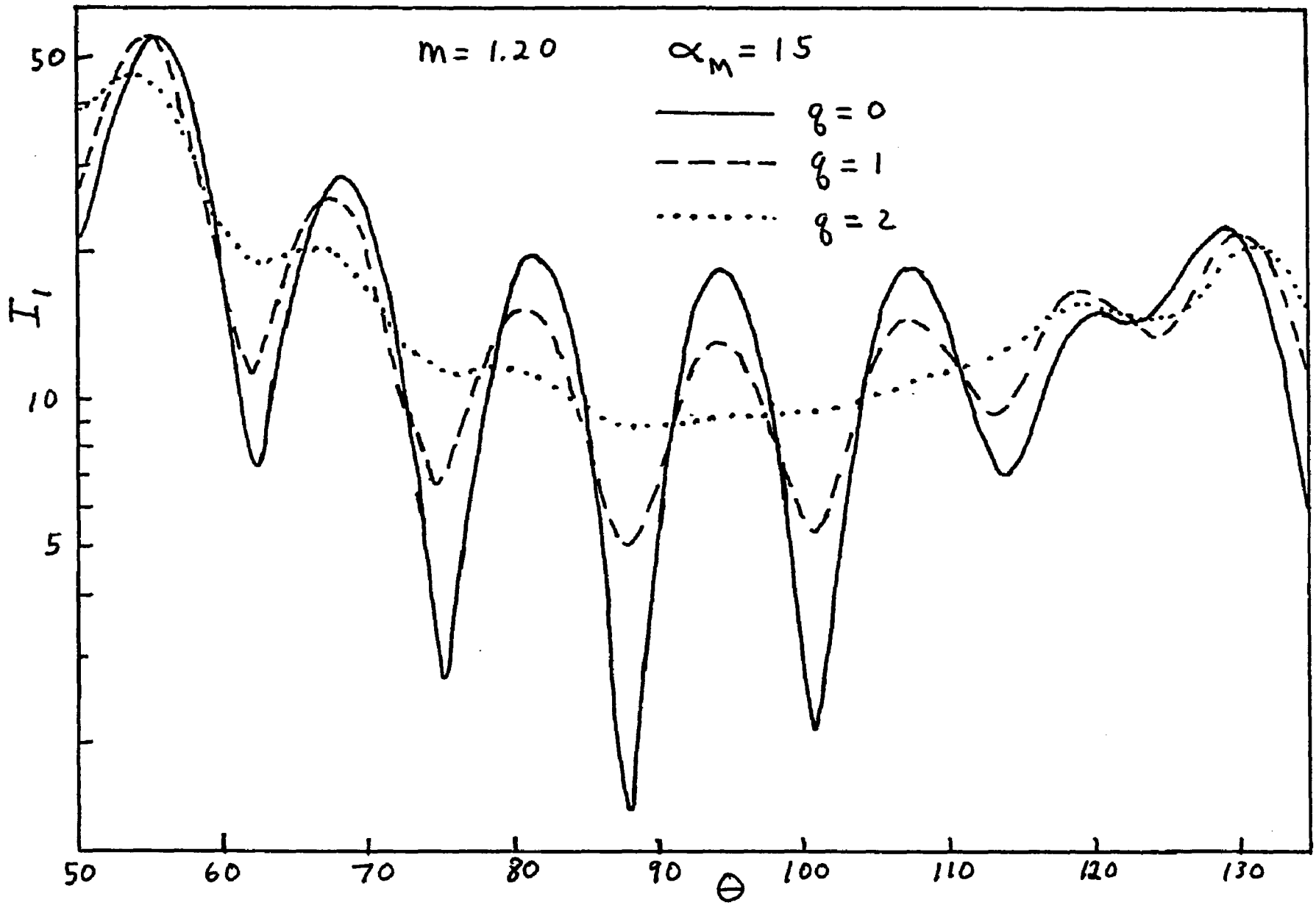

Fig. 37. Scattered Intensity I_1 as a Function of Angle Showing the Extrema Pairs in the Lateral Direction for Size Distributions Having a Constant Mode α_M=15 and Different Distribution Widths . . . . . .

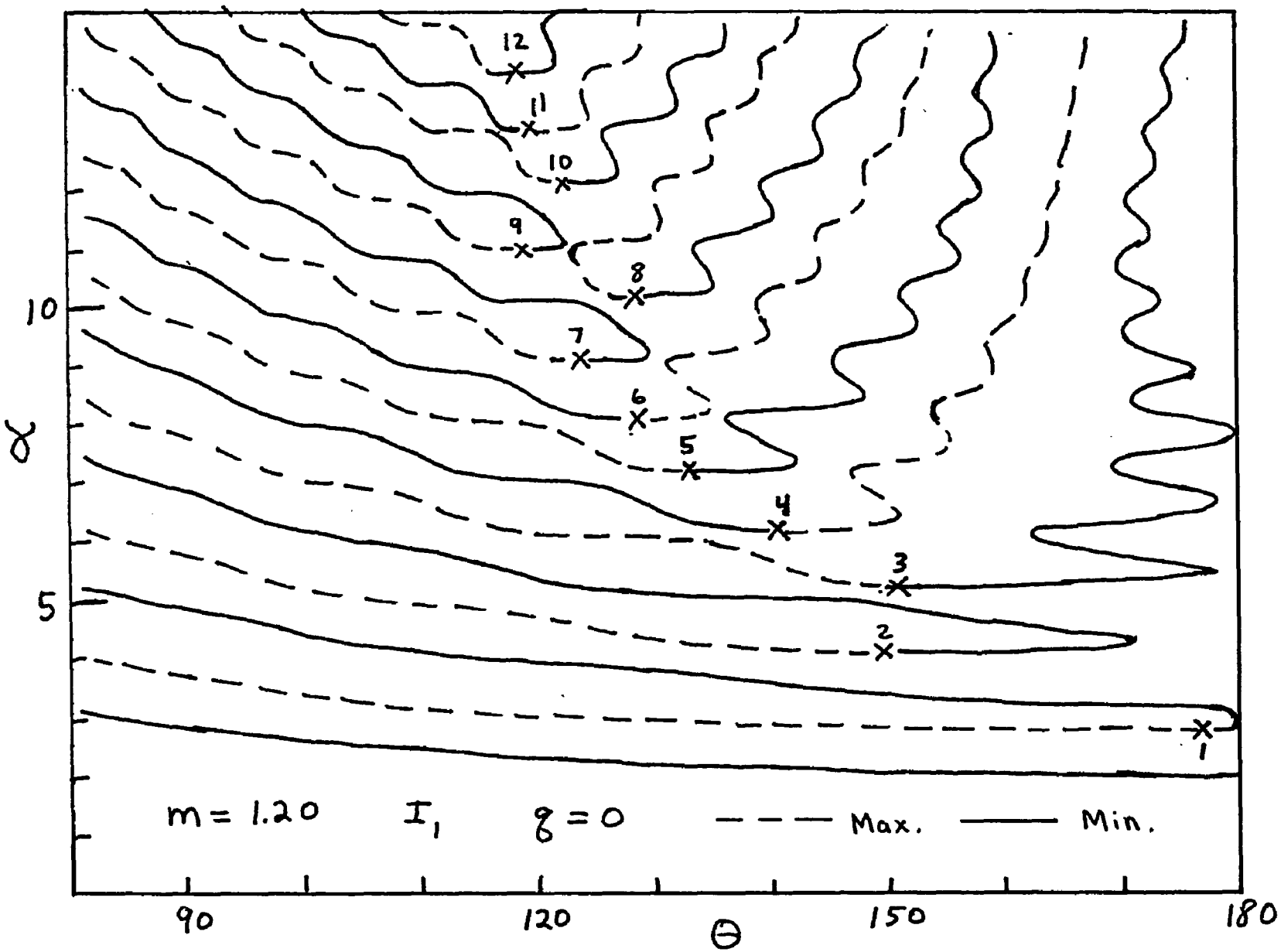

Fig. 38. Angular Location of I_1 Extrema Versus Modal Size α_M in the Backward Direction for Monodisperse Distributions with m=1.20 . . . . . .

tional extrema pair is seen in Figure 38 in the region defined by $\alpha = 5 \pm 1$ and $\theta = 120^{\circ}$ to 180°. As the heterodispersion increases the new extrema pair, indicated by the number 3 in Figure 38, will be included in the integration. When the heterodispersion has increased to q = 1 this new extrema pair dominates the angular range initially containing the minimum which has now been displaced to $\theta = 120^{\circ}$.

Another example of this type of behavior is seen in Figure 39 for the angular intensity curves having different heterodisperse distributions and a constant mode of $\alpha_M = 10$. This figure is an enlargement of the intensity curves in the backward direciton shown earlier in Figure 20. As the heterodispersion increases the intensity curves show the presence of a new maximum and minimum in the region from $\theta = 110^{\circ}$ to 135° which initially contained only a single minimum. A similar analysis to the preceding example showed that the new extrema pair indicated by the number 8 in Figure 38 was responsible for the observed changes in the integrated scattering intensity.

Figure 39 shows that the primary effect of the increasing heterodispersion is to increase the intensities of the minima. However, as the particle size increases, the I_1 extrema in the backward direction are less affected by the degree of heterodispersion as was seen earlier for the extrema in the forward direction. Figure 40 shows the I_1 curves for different heterodispersions having a constant mode of $\alpha_M = 15$. This figure is an enlargement of the scattering curves in the backward direction from Figure 21. The increasing heterodispersion has a much larger effect on the minimum than on the maximum. In addition the sensitivity of the extrema pairs to increasing heterodispersions becomes greater for

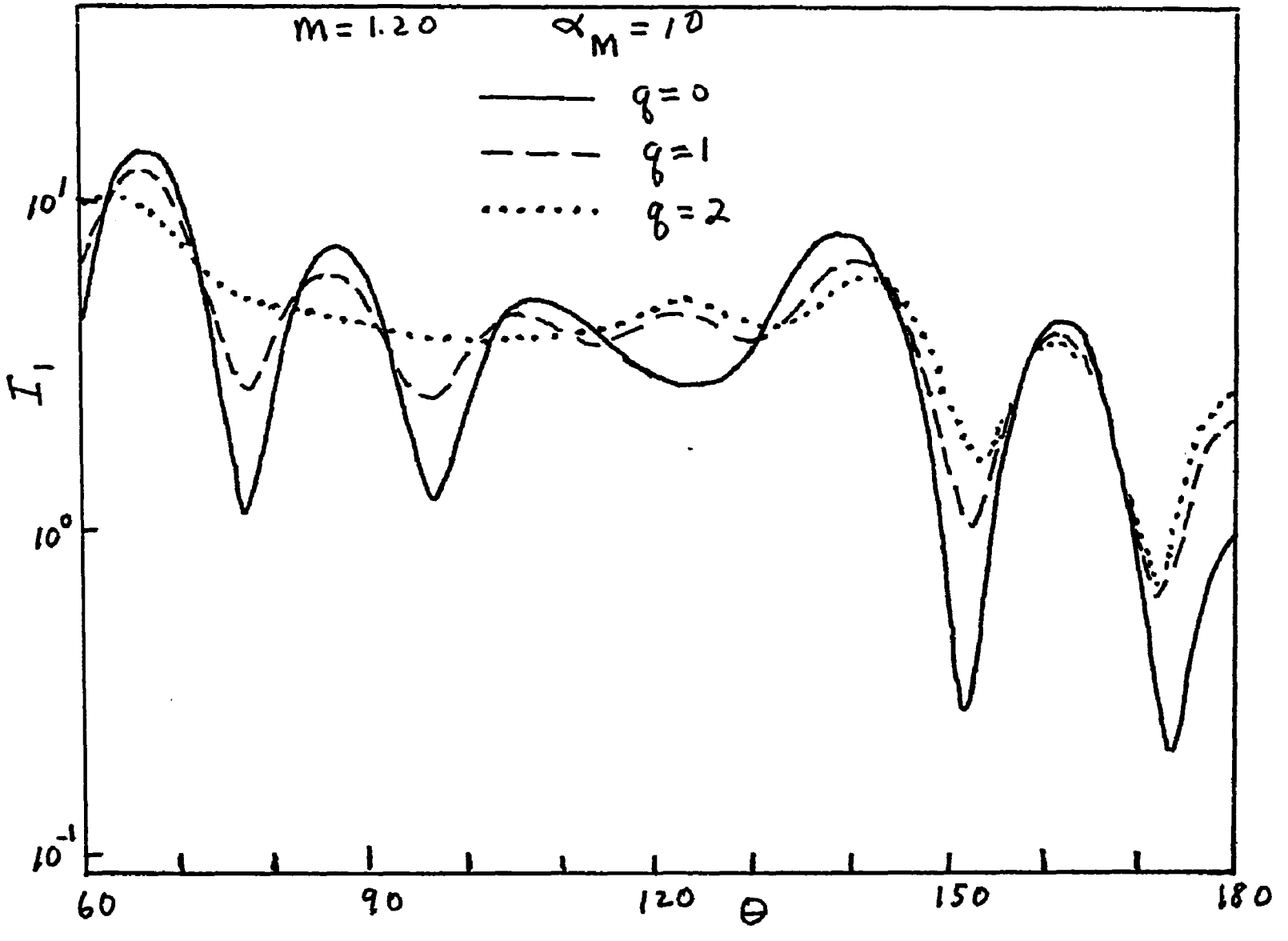

Fig. 39. Scattered Intensity I_1 as a Function of Angle in the Backward Direction for Size Distributions Having a Constant Mode α_M=10 and Different Distribution Widths

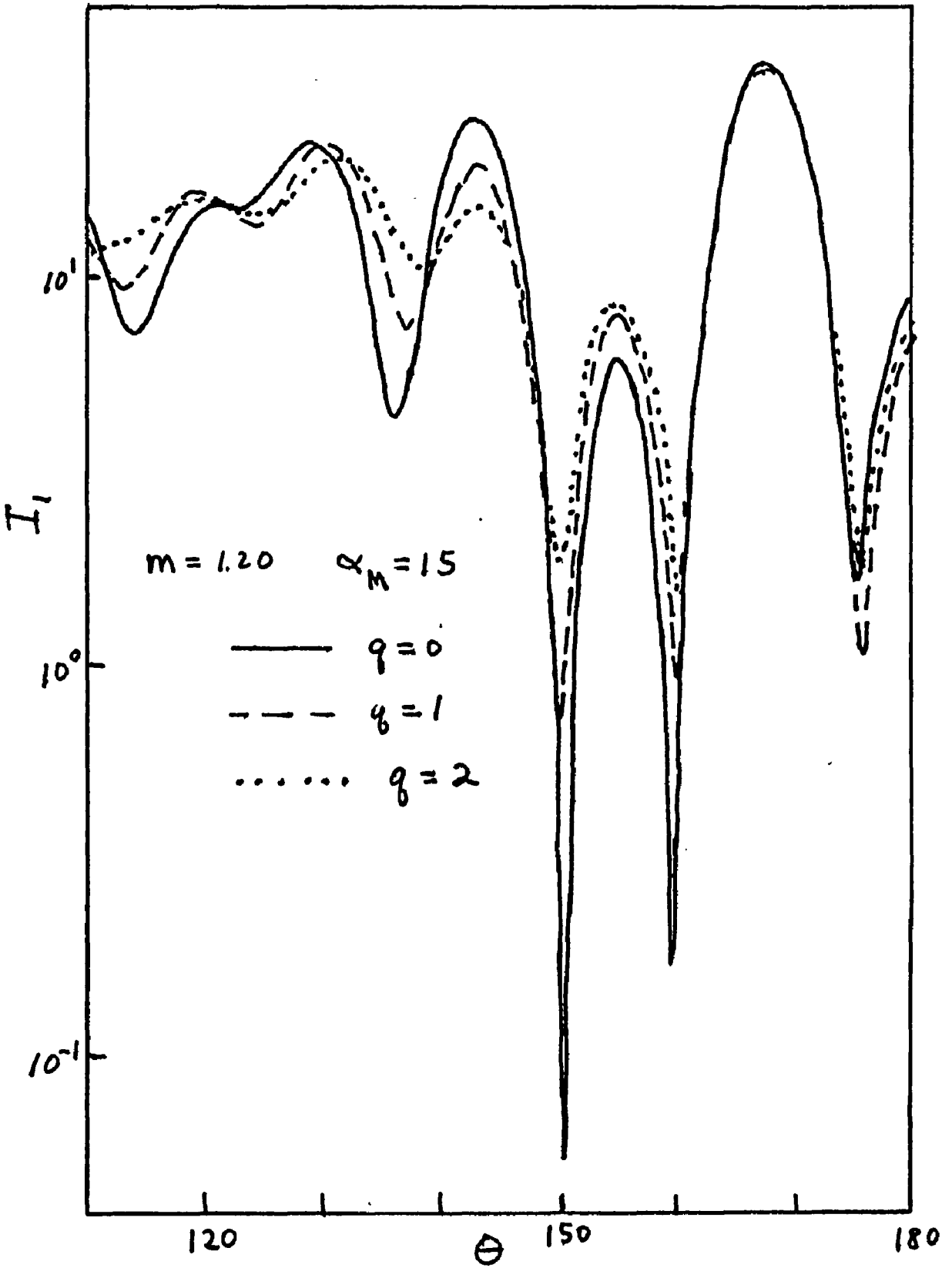

Fig. 40. Scattered Intensity I_1 as a Function of Angle in the Backward Direction for Size Distributions Having a Constant Mode α_M=15 and Different Distribution Widths

the extrema pairs farther from the backward direction. A similar trend was seen in the forward direction where the extrema pairs become more sensitive to increasing heterodispersion as the extrema pairs are farther from the forward direction.

The most striking feature of the angular variation of I_2 in Figures 22-26 is the very shallow extrema in the forward direction compared to I_1. Figure 41 shows the angular variation of I_1, I_2 and I_u for monodisperse distributions having size $\alpha = 5$. The curves for I_1 and I_2 were shown earlier in Figures 19 and 24 respectively. Note that the first minimum for I_2 is very shallow and the second minimum is completely washed out. This behavior would correspond to a very heterodisperse distribution for I_1.

For angles larger than $\theta = 100^\circ$ the scattering patterns for I_1 and I_2 no longer resemble each other which is not surprising in view of the large difference in the extrema contours shown in Figures 38 and 32. However, I_2 now shows a significant angular variation in the backward direction whereas in the forward direction the extrema are very shallow and even washed out. Figure 41 also includes the angular variation of I_u to show its close resemblance to the angular variation of I_1.

A similar pattern is seen in Figure 42 for the angular variation of I_1, I_2 and I_u for monodisperse distributions having a size $\alpha = 10$. Although the general pattern for the different curves in the forward direction are similar, the extrema from I_2 are very shallow compared to those from I_1. In fact, the fourth extrema pair, counting from the forward direction, for the I_2 curve is completely washed out and not seen. Once again the angular variation of I_2 for the monodisperse distribution

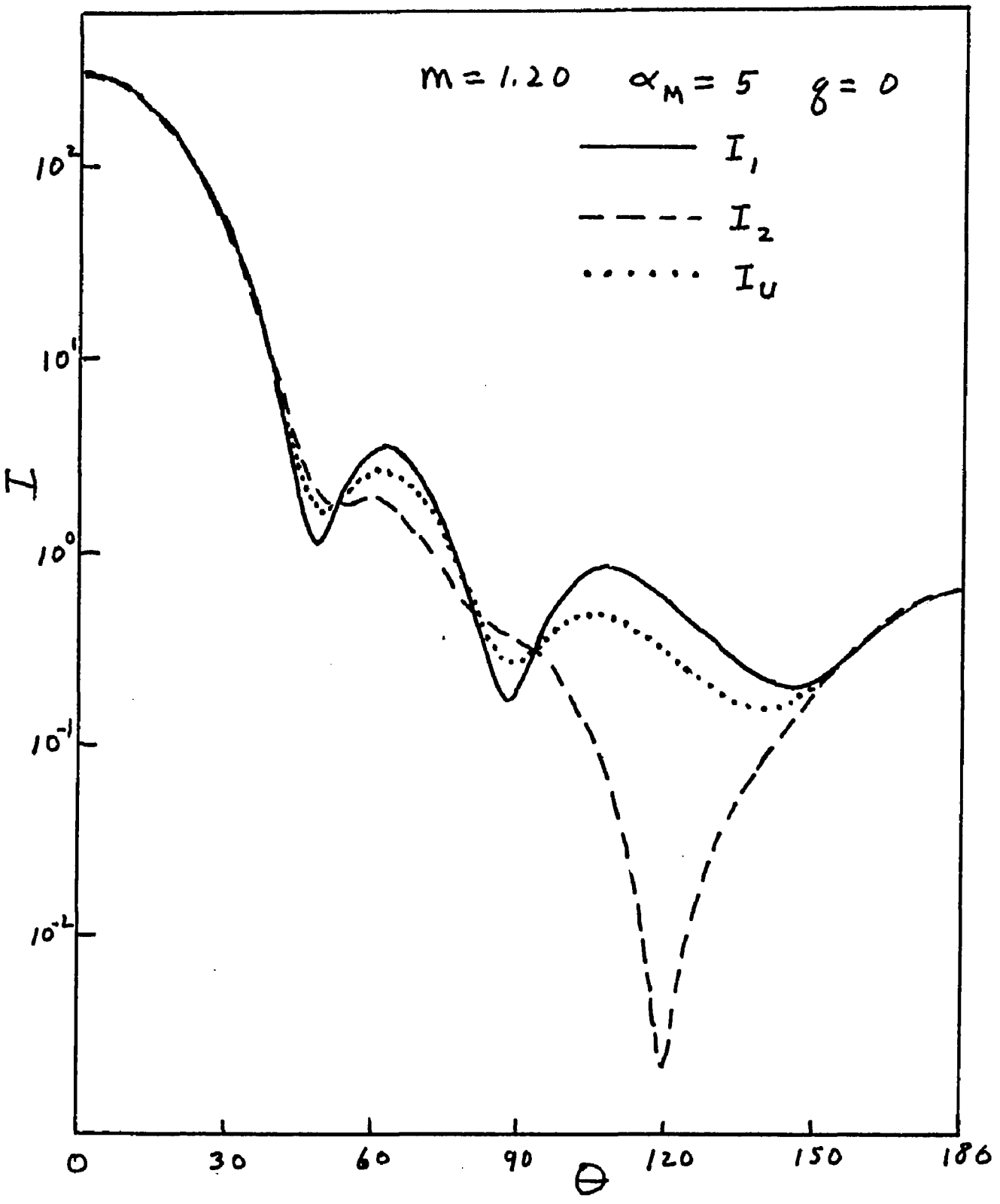

Fig. 41. Scattered Intensities I_1, I_2 and I_U as a Function of Angle for Monodisperse Size Distributions Having a Constant Mode α_M=5

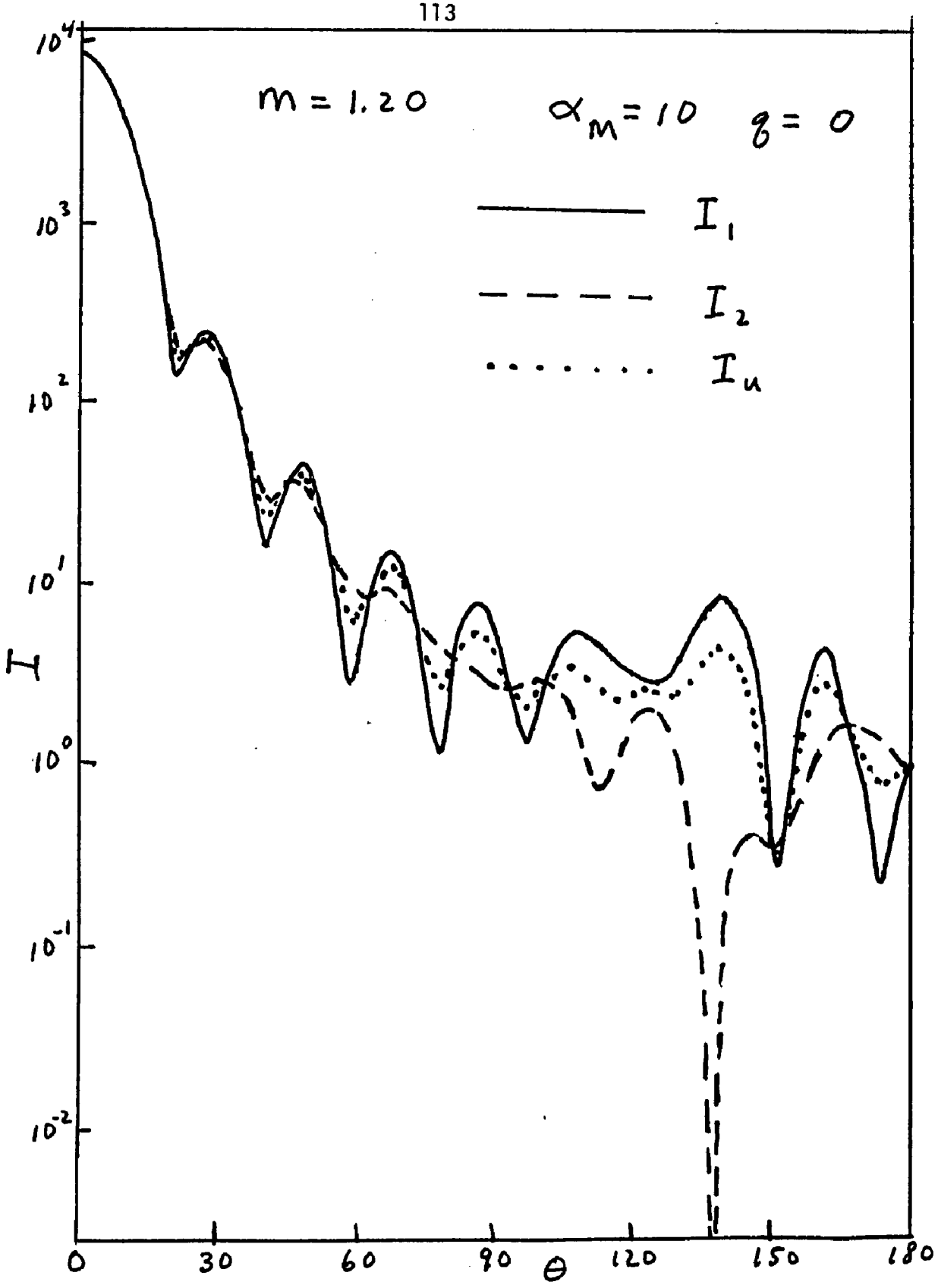

Fig. 42. Scattered Intensities I_1, I_2 and I_u as a Function of Angle for Monodisperse Size Distributions Having a Constant Mode α_M=10

shows a close resemblance to the coresponding angular variation of I_1 for a heterodisperse distribution. In contrast to the forward direction, the angular variation of I_2 from approximately $\theta = 100^\circ$ to 180° becomes very large and exhibits pronounced extrema. The curve for I_u was included in Figure 42 to show that the angular variation of I_u and I_1 are very similar.

Based on the previous observations, a general pattern for the angular intensity curves can be developed. This pattern has the angular scattering intensity divided into a forward and backward region. The angular location of the division is determined by the location of the new extrema pairs, which move from the backward direction toward the forward direction as the particle size increases. The new extrema pairs increase the total number of extrema in the scattering diagram. As the particle size increases, the extrema in the forward direction show a systematic migration toward the forward direction while the extrema in the backward direction show a systematic migration toward the backward direction. The extrema in both the forward and backward directions show a greater increase in damping as the heterodisperion increases for those extrema located close to the dividing region. This general pattern applies to I_1, I_2 and I_u although additional complications are seen for I_2 due to the Rayleigh minimum.

B. Effect of Particle Size Distribution, Relative Refractive Index and Polarization of Incident Light on the Angular Location of the Intensity Extrema

The previous section had been primarily concerned with investigating the effects of various parameters on the intensity of the angular scattering curves. This section will address the trends seen in the angular location of the intensity maxima and minima for a series of graphs having the angle of observation as the abscissa and the mode as the ordinate. The mode was chosen as the size parameter to be plotted because the angular location of the intensity minima remained approximately constant for a constant mode as the degree of heterodispersion increased. This allowed the effects due to the heterodispersion to be separated from the size effects. The graphs show the angular location of the maximum and minimum intensities plotted as circles and triangles, respectively. No curves were drawn through the points because, in those cases where lines would help interpret the pattern, there were an insufficient number of points to define the trend. In the remainder of cases, where there were a sufficient number of points, the pattern was readily seen without drawing a curve through the points.

1. Effect of m and q on I_1 Extrema Contours

A brief survey of the angular location of the intensity extrema will now be made for each polarization of the incident light. Figures 43-52 show the effect of the relative refractive index and the degree of heterodispersion on the extrema location of I_1. The extrema contours for m = 1.05 are shown in Figures 43-45. This value of m is

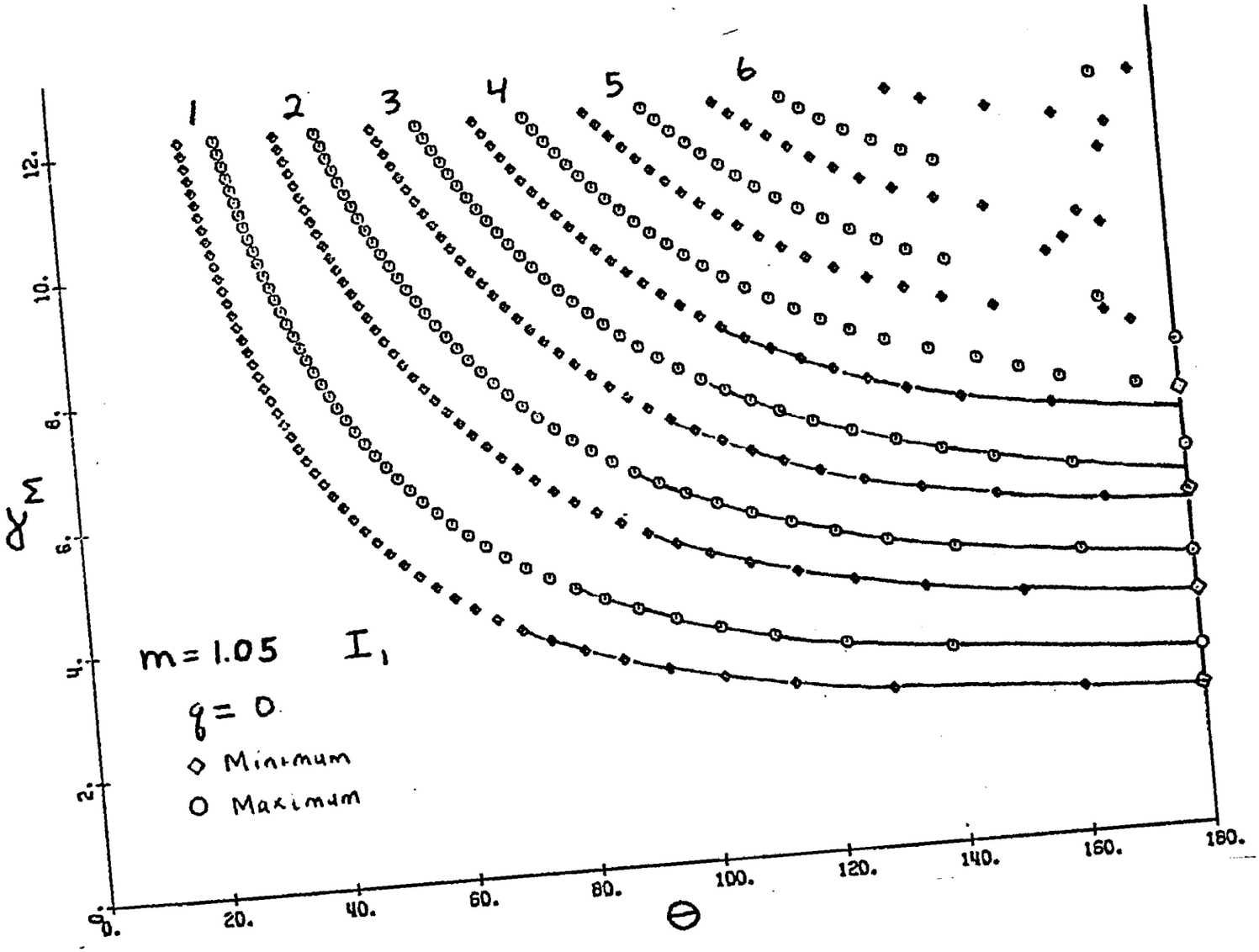

Fig. 43. Angular Location of I_1 Extrema Versus Modal Size α_M for Distributions with m=1.05 and q=0

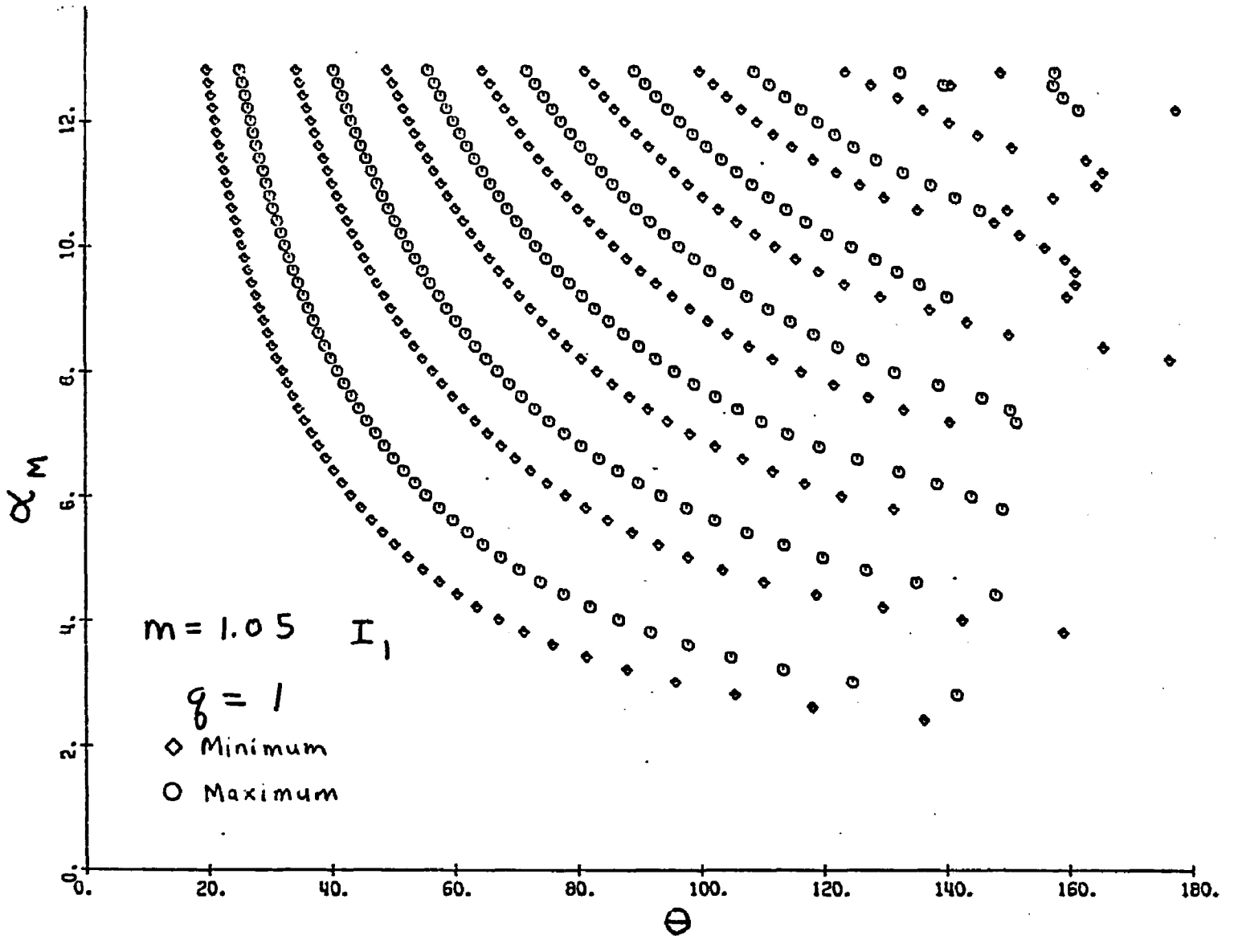

Fig. 44. Angular Location of I_1 Extrema Versus Modal Size α_M for Distributions with m=1.05 and q=1

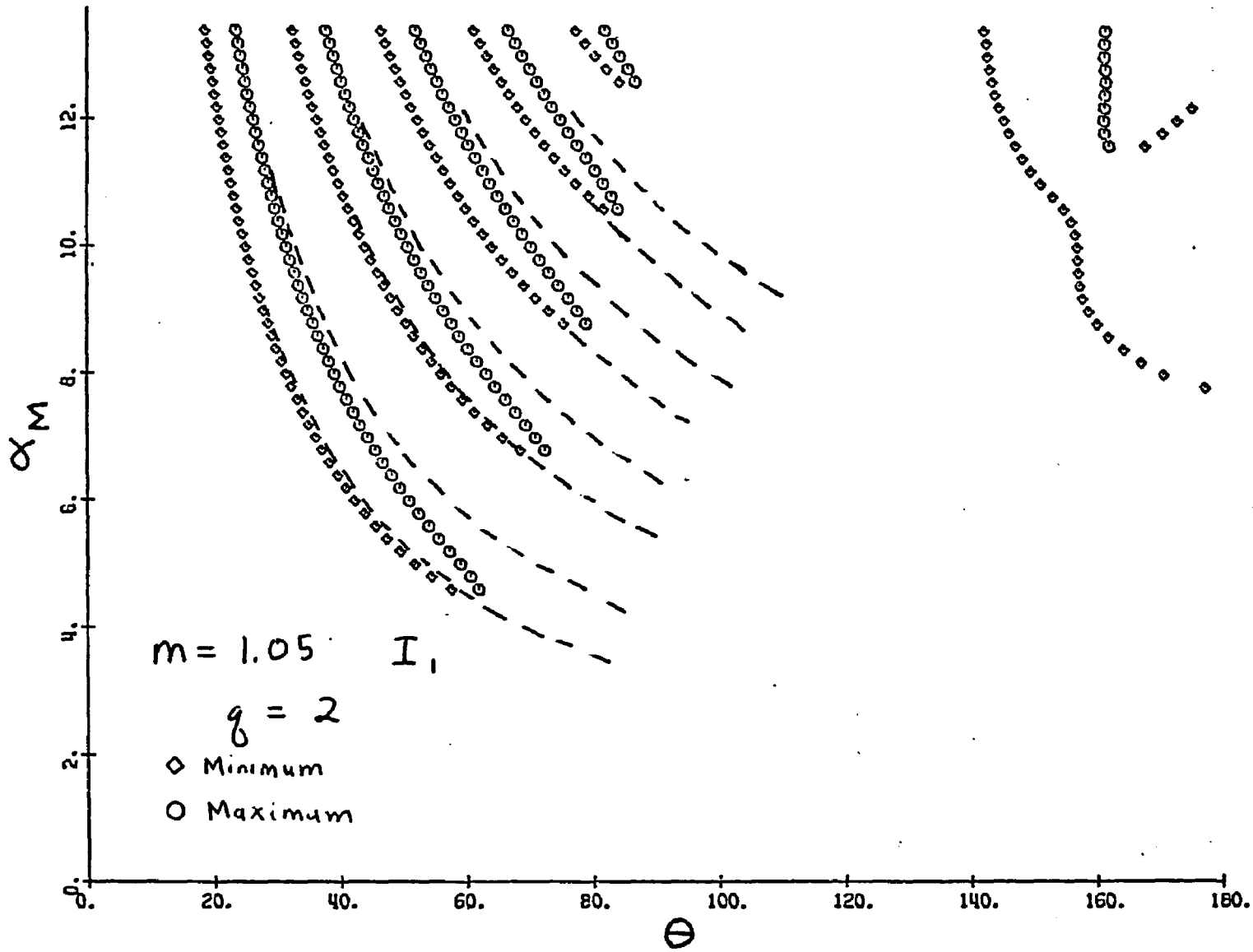

Fig. 45. Angular Location of I_1 Extrema Versus Modal Size α_M for Distributions with m=1.05 and q=2

very close to the limiting value of m = 1.00 where the RGD theory rigorously applies. As expected the angular extrema contours shown in Figure 43 for I_1 and q = 0 follows the RGD theory quite closely. No extrema are seen with increasing particle size until α = 2.25, where the first minimum appears at 180°.* Additional extrema enter individually from the backward direction alternating maximum and minimum. These extrema are frequently designated by the numerical order in which they appear in the scattering diagram. The orders are indicated by the numbers shown adjacent to the extrema contours.

Figure 43 shows that the first two orders of the maxima and minima extrapolate to the RGD values at θ = 180°. However, the extrapolation for the third extrema order shows a small deviation for the minimum and a significant deviation for the maximum. Higher extrema orders show an even greater deviation and, beginning with the sixth order, the extrema contours no longer originate at θ = 180°. These observations are in accord with the basic assumption in the RGD theory that the phase $\alpha(m-1) \ll 1$. Thus, one would expect major deviations from the RGD theory for larger particles even for small m values.

Increasing the heterodispersion to q = 1 has only a small effect on the extrema contours. Figure 44 shows that the pattern has washed out slightly in the backward direction for smaller sizes. A detailed comparison of Figures 43 and 44 also shows that for angles smaller than 140°, the minima remain constant while the maxima shift slightly toward the forward direction as the heterodispersion increases. The

---

*The extrema data shown at θ = 180° were obtained from the RGD theory.

magnitude of the shift decreases with increasing particle size.

As the heterodispersion increases to q = 2 in Figure 45, all of the central portion and most of the backward portion of the extrema contours has been washed out. The reason for the extrema washing out, as explained in the last section, is due to the integration lines crossing over successive maxima and minima. Figure 34 shows that the integration lines average the intensity over several maxima and minima in the central portion of the extrema plot. A similar integration in the forward direction or in the backward direction for large particle sizes averages the intensity over only one extremum. Although the extrema wash out faster with increasing heterodispersion in the central portion of the extrema plots, this does not mean that the extrema are more shallow in this region. This is seen in Figures 17-21.

Increasing the heterodispersion to q = 2 also results in a more uniform pattern for the extrema in the backward direction for large particle sizes. Figure 45 shows a new maxima and minima pair originating at about $\alpha_M \approx 11$ and $\theta = 160^\circ$. With increasing size, the maximum remains at the same angular location while the minimum migrates toward the backward direction. This type of behavior is representative of reflection phenomena.

Figure 45 also shows that the extrema in the forward direction wash out by merging the maximum and minimum of a given extrema order. Detailed comparisons with the monodisperse case in Figure 43 show that the merging is primarily due to the shift of the maxima toward the forward direction. In order to see this behavior, a portion of the monodisperse contours from the first four extrema orders in Figure 43 have been added

as dashed curves in Figure 45. Also note that the extrema pairs extend farther into the backward direciton for the larger particle sizes. This trend is a result of the increased slope of the extrema contours at a given angle for the larger particle sizes. Integrating over a given size range at that angle will therefore result in averaging over a fewer number of maxima and minima.

The extrema contour graphs for higher relative refractive indexes show an increasing deviation in the backward direction from the pattern seen for m = 1.05. This is not surprising since the scattering for m = 1.05 is very closely described by the RGD theory. Higher relative refractive indexes show that an increasing fraction of the extrema diagram is due to a reflection phenomenon which is absent in the RGD theory. Although true Fresnel and Snell's law reflection does not apply until particles become very large, the migration of the extrema toward the backward direction with increasing size is the pattern expected from a reflection phenomenon.

The prominent feature of the scattering diagram will now be presented for m = 1.20 which represents the middle of the m range considered in the present investigation. Figure 34 shows that the extrema contours in the forward direction appear very similar to those seen in Figure 43 for m = 1.05 and can be approximately represented by the RGD theory. However, an exact comparison of Figures 34 and 43 show that the extrema for m = 1.20 have a faster rate of migration toward the forward direction than the extrema for m = 1.05. This higher migration rate toward the forward direction with increasing m value had been previously incorporated into equations 2 and 3 by other investigators.[10, 11, 13-16] Figures 34

and 43 also show that for a given m and θ value, the rate at which extrema migrate toward the forward direction decreases with increasing order of the extrema.

Although increasing m shows a moderate effect on the extrema in the forward direction, the major effect is seen in the greatly increased region in the backward direction where reflection mechanisms control the scattering pattern. As a result of the reflection behavior in the backward direction, the sequence in which extrema appear in the scattering diagram differ considerably from the RGD theory. This theory predicts that the extrema will appear individually in the backward direction alternating maxima and minima, and then migrate toward the forward direction. Since the number of extrema in Figure 34 are insufficient to define the extrema behavior in the backward direction many additional calculations were made to resolve the pattern.

Figure 38 shows the extrema contours in the backward direction from the additional calculations. The angular location of I_1 maxima and minima are given by the dashed and solid curves respectively. One sees that the first extremum enters the backward direction at 180^o and $\alpha_M = 2.0$ and moves rapidly toward the forward direction as the particle size increases. However, as the size increases, new extrema appear in the scattering diagram as pairs. These extrema are shown by x's in Figure 38 and are numbered sequentially. As previously pointed out, the region where new extrema pairs originate are characterized by closely spaced maxima and minima and frequent reversals in the direction of the extrema contour migrations.

The migration pattern of the new extrema show one of two

trends. Either both of the extrema from the pair move in one direction or one extrema type moves in the forward direction while the other moves in the backward direction. In addition, the angular location where new extrema pairs originate moves in the forward direction as the particle size increases. These trends have been previously pointed out by Penndorf.[33] The contour of the origin of these extrema pairs serves as a boundary that divides the region of the scattering diagram where the extrema migrate in the forward direction from that where the extrema migrate in the backward direction. The region in the backward direction increases with size because the phase shift parameter $\alpha(m-1)$ increases. These two regions will be discussed in greater detail in terms of diffraction and reflection.

The extrema contours were then determined for particle sizes up to $\alpha = 30$ to see what changes would occur in the scattering diagram as one approaches the size where Fraunhoffer diffraction and Fresnel reflection are used to describe the optical behavior. Figure 46 shows that the resulting extrema contours continue the trends already pointed out. The location where new extrema appear has gradually moved to approximately $\theta = 90^{\circ}$ at $\alpha = 30$. Figure 46 also shows maxima and minima that appear and disappear over a small size range thus resulting in the closed circles designated by x. Rowell[32] had previously observed this behavior. These closed circles only occur in the region where new extrema form.

The most interesting feature of Figure 46 is the merging and disappearance of the first two extrema in the forward direction at $\alpha = 20.8$. This behavior was previously observed by Rowell[32] and

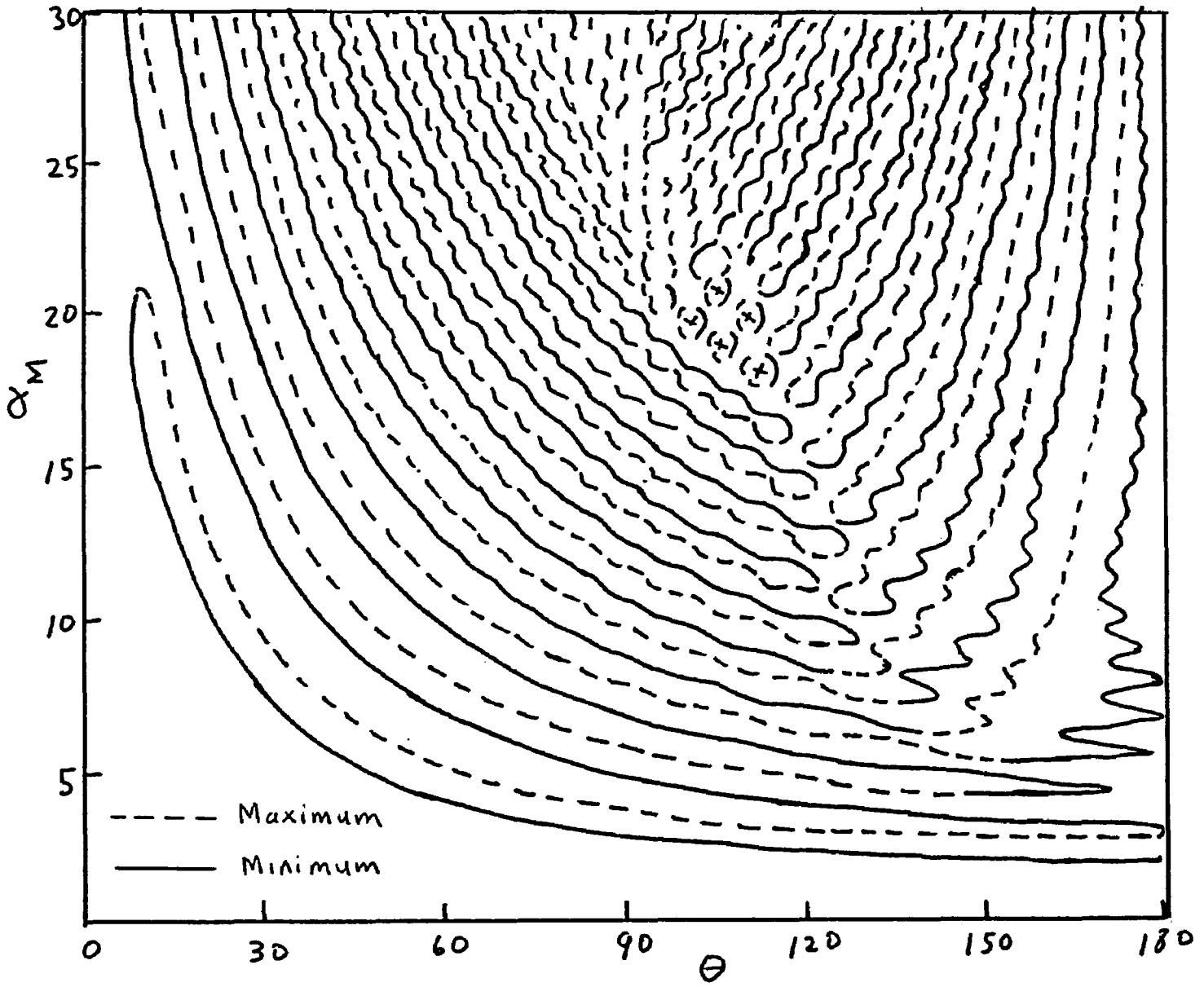

$m = 1.20$ I_1
$g = 0$

Fig. 46. Angular Location of I_1 Extrema Versus Modal Size α_M for Monodisperse Distributions with m=1.20

Patitsas.[21-23] Patitsas[21-23] has shown that the merging and disappearance of the extrema in the forward direction continues in a systematic fashion for higher extrema orders at larger particle sizes. Thus the first three extrema orders for m = 1.20 would disappear at α = 21, 38 and 55. The disappearance of the extrema will be explained in the next section in terms of the extrema pair in the forward direction merging into the main lobe of the Fraunhoffer diffraction pattern.

The description of the total light scattered by a particle in terms of the diffraction of light passing near the particle and the scattering (refraction, reflection, etc.) of light striking the particle is strictly not correct for the particle sizes considered in the present study. Such a separation of the scattering process can only be used for very large particles where the laws of geometric optics apply.[28] However for approximate solutions of the scattering from moderately sized particles ($\alpha \approx 10$) one can assume that the diffracted light and the light striking the particle can be separated.

Hodkinson and Greenleaves[49] have shown that the scattering of light in the forward direciton up to $\theta = 40^\circ$ from a particle size distribution of α = 10 to 15 can be approximated by the diffraction of light passing near the particle and the transmission and reflection of light striking the particle. Hodkinson[50] had also shown that the shape of the forward scattering lobe at $\theta = 0^\circ$ to 30° is closely approximated by Fraunhoffer diffraction for paticles as small as α = 2. In both of these cases the scattering was approximated by optical laws which are generally used for much larger particle sizes.

The effect of increasing the heterodispersion to q = 1 on

the extrema contours for m = 1.20 is seen in Figure 47. Compared with the monodisperse case in Figure 34, the region in Figure 47 where the extrema migrate toward the backward direction has increased significantly. Also note that the oscillations in the monodisperse curves have been damped out significantly, especially in the backward direction. Close inspection of the data also reveals that, compared to the monodisperse case, the minima in the forward direction remain constant while the maxima migrate slightly toward the forward direction. This migration is larger for the smaller particle sizes. One cannot say whether a similar trend occurs for the extrema in the backward direction because the monodisperse case in Figure 34 shows large oscillations.

Increasing the heterodispersion to q = 2 in Figure 48 shows that a large fraction of the extrema that migrate toward the forward direction have been washed out. In contrast, the region where the extrema migrate toward the backward direction has increased considerably. In fact, it now includes a portion of the region where the extrema for monodisperse distributions had migrated toward the forward direction. This reversal in the direction of the extrema migration with increasing heterodispersion is due to the washing out of very shallow extrema that had migrated toward the forward direction. These shallow extrema had been superimposed over another extrema pattern migrating toward the backward direction.

Figure 48 also shows the extrema contours for the monodisperse distribution added as dashed curves. One sees that increasing the heterodispersion causes the maxima to migrate toward the forward direction while the minima remain constant. This trend does not occur for the extrema migrations in the backward direction. Also note that the

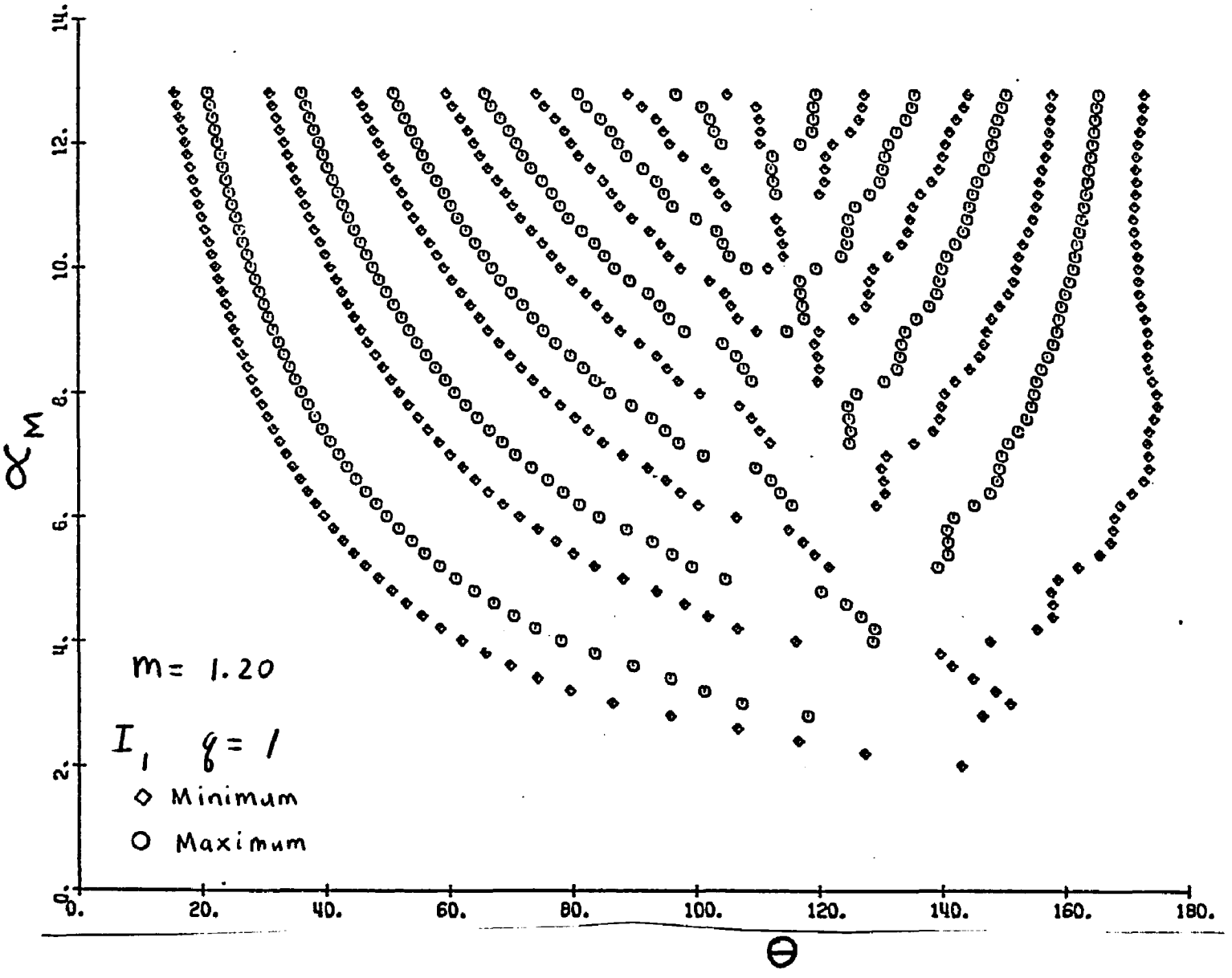

Fig. 47. Angular Location of I_1 Extrema Versus Modal Size α_M for Distributions with m=1.20 and q=1

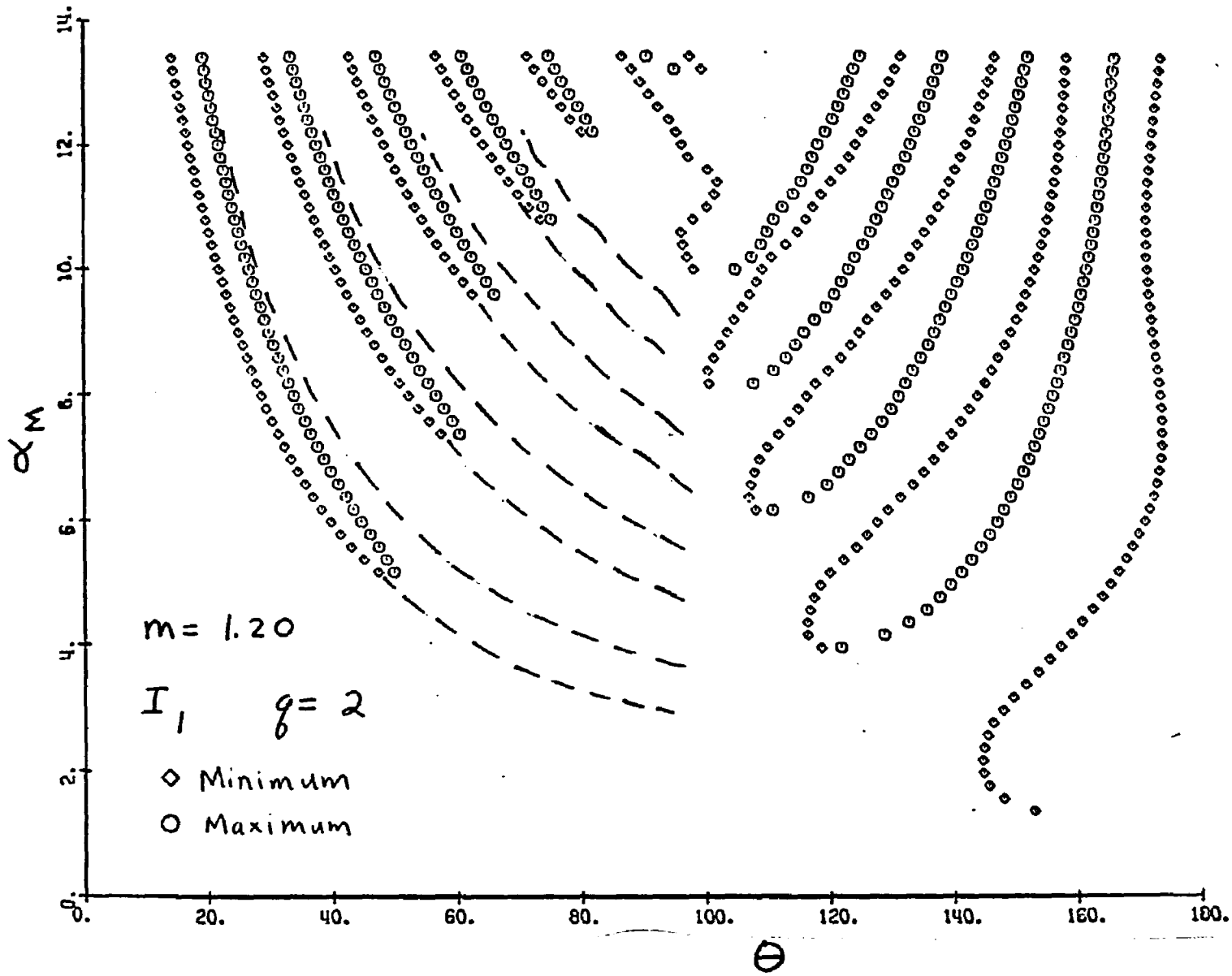

Fig. 48. Angular Location of I_1 Extrema Versus Modal Size α_M for Distributions with m=1.20 and q=2

extrema that migrate toward the forward direction extend farther into the backward direction for the larger particle sizes. The same explanation used for m = 1.05 applies here as well.

The extrema contours for m = 1.333, which is the largest value considered in the present investigation, are shown in Figures 49-51. In general, these figures show an acceleration of the trends seen for m = 1.05 and m = 1.20 toward smaller particle sizes. The extrema contours for the monoddisperse distributions in Figure 49 show a larger region where the extrema migrate toward the backward direction and extends to the smaller particle sizes. This behavior is expected from the increase in the relative refractive index which increases the fraction of light scattered due to reflection. Compared to smaller m values the extrema contours for the monodisperse case in Figure 49 show an increased oscillation in the forward direction and a decreased oscillation in the backward direction.

Increasing the heterodispersion to q = 1 in Figure 50 smoothens out the oscillations in both the forward and backward direction and shows the scattering pattern clearly divided into the separate forward and backward region. In addition, the merging and disappearance of the first extrema pair in the forward direction is now seen at $\alpha_M = 12.5$. Increasing the relative refractive index from m = 1.20 to m = 1.333 has decreased the size at which the first extrema pair disappears from $\alpha_M = 20.6$ to $\alpha_M = 12.5$.

A further increase in the heterodispersion to q = 2 in Figure 51 shows that the extrema in the forward direction wash out while those in the backward direction become more pronounced. As seen in the previous cases the extrema in the forward direction wash out by the mi-

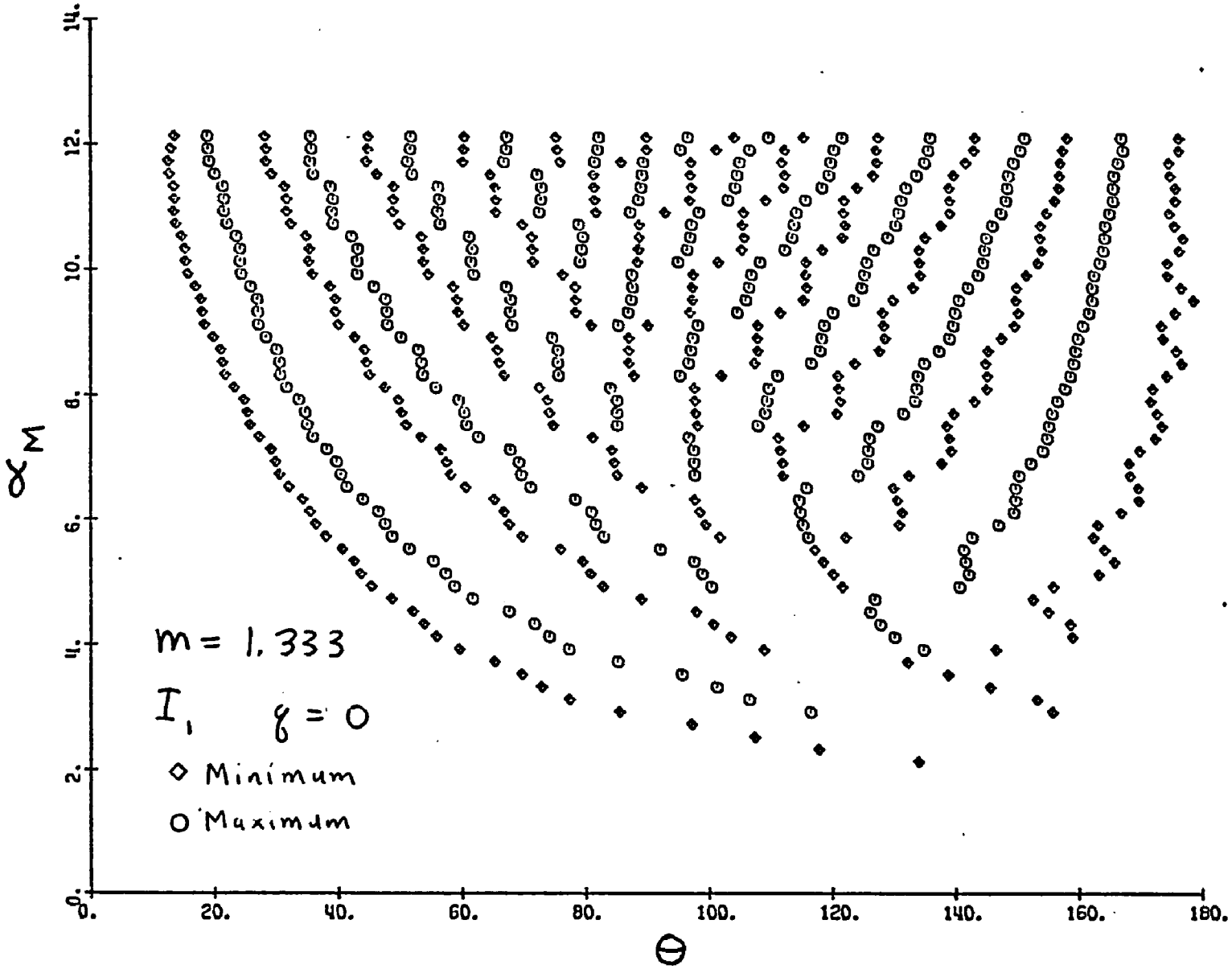

Fig. 49. Angular Location of I_1 Extrema Versus Modal Size α_M for Distributions with m=1.333 and q=0

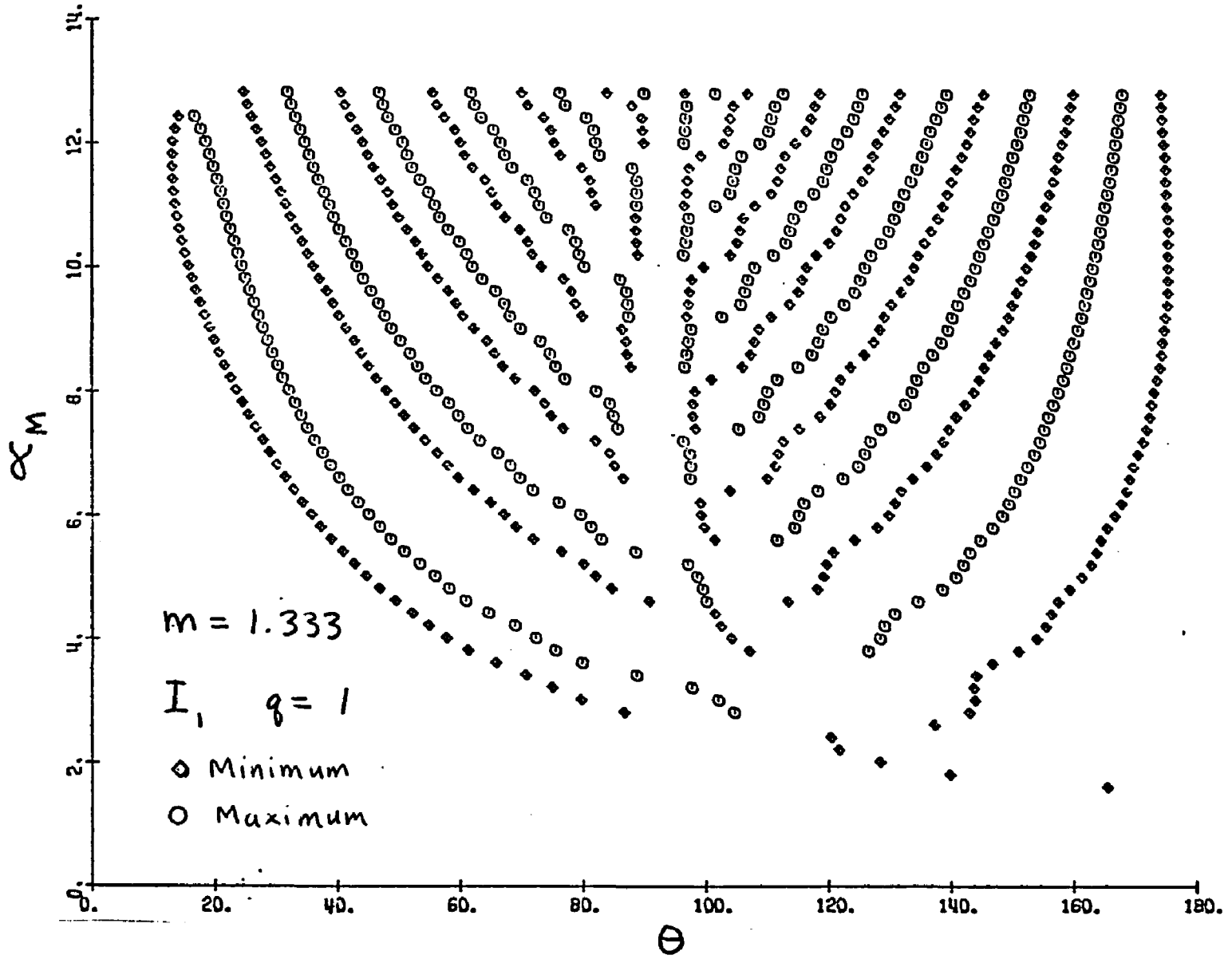

Fig. 50. Angular Location of I_1 Extrema Versus Modal Size α_M for Distributions with m=1.333 and q=1

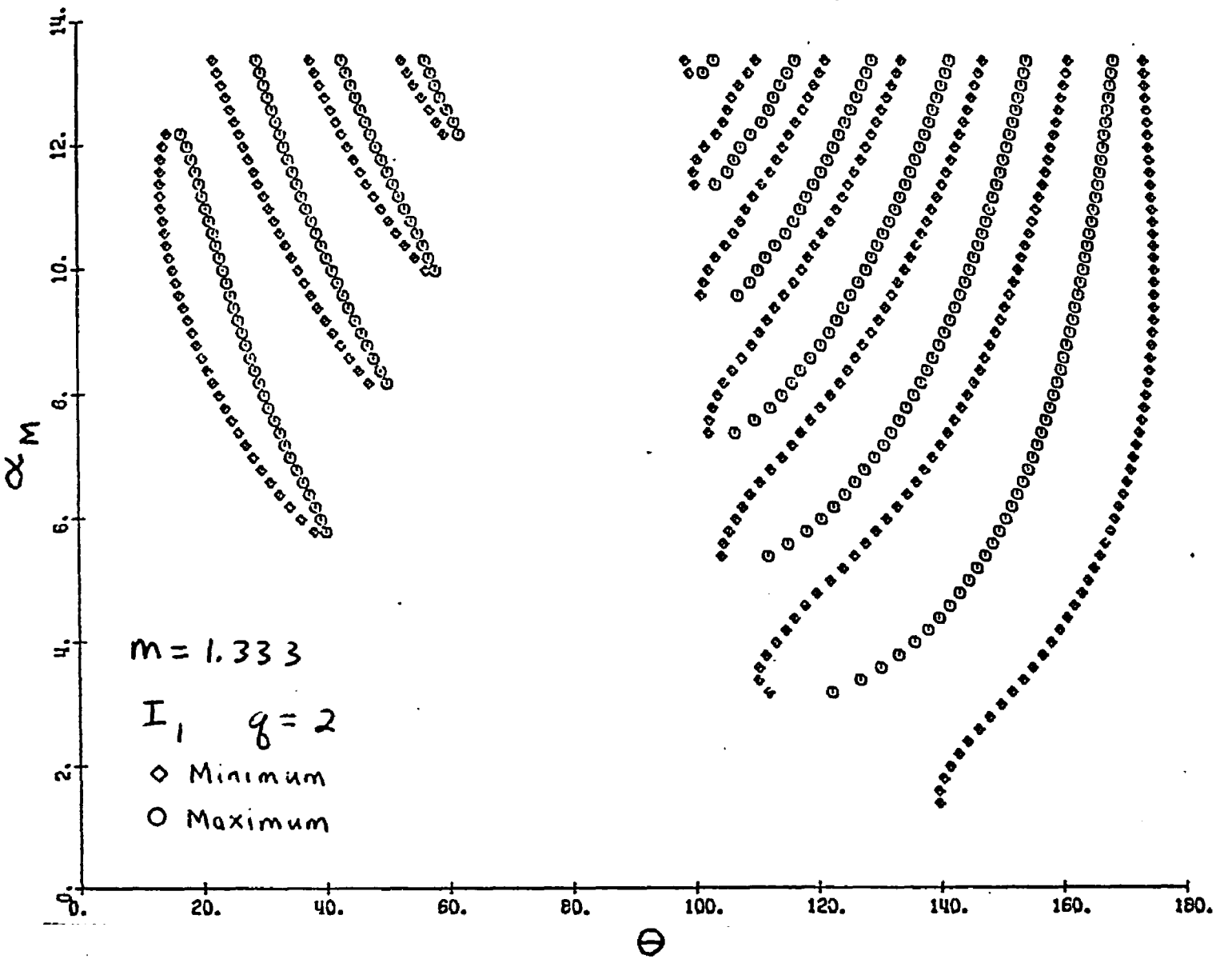

Fig. 51. Angular Location of I_1 Extrema Versus Modal Size α_M for Distributions with m=1.333 and q=2 . .

gration of the maxima toward the fixed minima. Although this does not occur in the backward direction, both maxima and minima have shifted slightly toward the forward direction as q increased from 1 to 2.

Surveying the extrema contours for I_1 in Figures 43-51 reveals several trends. Increasing the relative refractive index at a fixed degree of heterodispersion increases the region of the scattering diagram where extrema migrate toward the backward direction and decreases the region where extrema migrate toward the forward direction. In addition, the larger m values compress the extrema contours to smaller particle sizes. This suggests that a scheme may be devised for superimposing the extrema contours from different m values on a single graph as done for total extinction curves having different relative refractive indexes.* Attempts to plot the angular location of the extrema against $\alpha(m-1)$ were not successful. However, the analogous scheme of plotting a number of different heterodispersions using the mode for the size parameter was very successful.

The general trends in Figures 43-51 also show that the extrema that migrate toward the forward direction are washed out with increasing heterodispersion. The disappearance of these extrema first occurs near the boundary of the forward and backward regions and then gradually moves toward the forward direction as the heterodispersion increases. Note that for an increase in the heterodispersion from $q = 0$ to $q = 2$, the extrema in the forward direction are reduced to a

---

*Penndorf[51] had shown that the total extinction curves for different m values can be approximately superimposed by plotting the extinction against the parameter $\alpha(m-1)$.

smaller region as the m value increases. In contrast, the region where the extrema migrate toward the backward direction show a small increase as the heterodispersion increases.

2. Effect of m and q on I_2 Extrema Contours

The extrema contours for I_2 have a more complicated pattern than the corresponding contours for I_1 because of the additional Rayleigh minimum at $\theta = 90^\circ$. Since this minimum carries over into the RGD theory, one expects that for low m values the minimum will affect the extrema contours for even large particle sizes. Figure 52 shows the very pronounced effect of the Rayleigh minimum on the I_2 extrema contours from monodisperse distributions with m = 1.05. The solid lines have been added to Figure 52 to help interpret the observed pattern. These lines were taken from the corresponding extrema contours for I_1 in Figure 43. The extrema contours for I_2 can therefore be interpreted as the basic pattern for I_1 modified by superimposing a minimum at 90° for all sizes. This interpretation represents the RGD theory for I_2 since

$$I_{2,RGD} = I_{1,RGD} \cos^2 \Theta \qquad (17)$$

Adding a minimum at 90° to the I_1 contours is easily accomplished for small particle sizes up to the first extrema pair. Since the 90° minimum (also called the Rayleigh minimum) must then cross the extrema pair, the normal extrema contours shown by the solid lines are considerably distorted. The effect of the Rayleigh minimum crossing the extrema contours resembles a "pinching" behavior where the maxima contours are squeezed onto the minima contours. Note that only the maxima have shifted

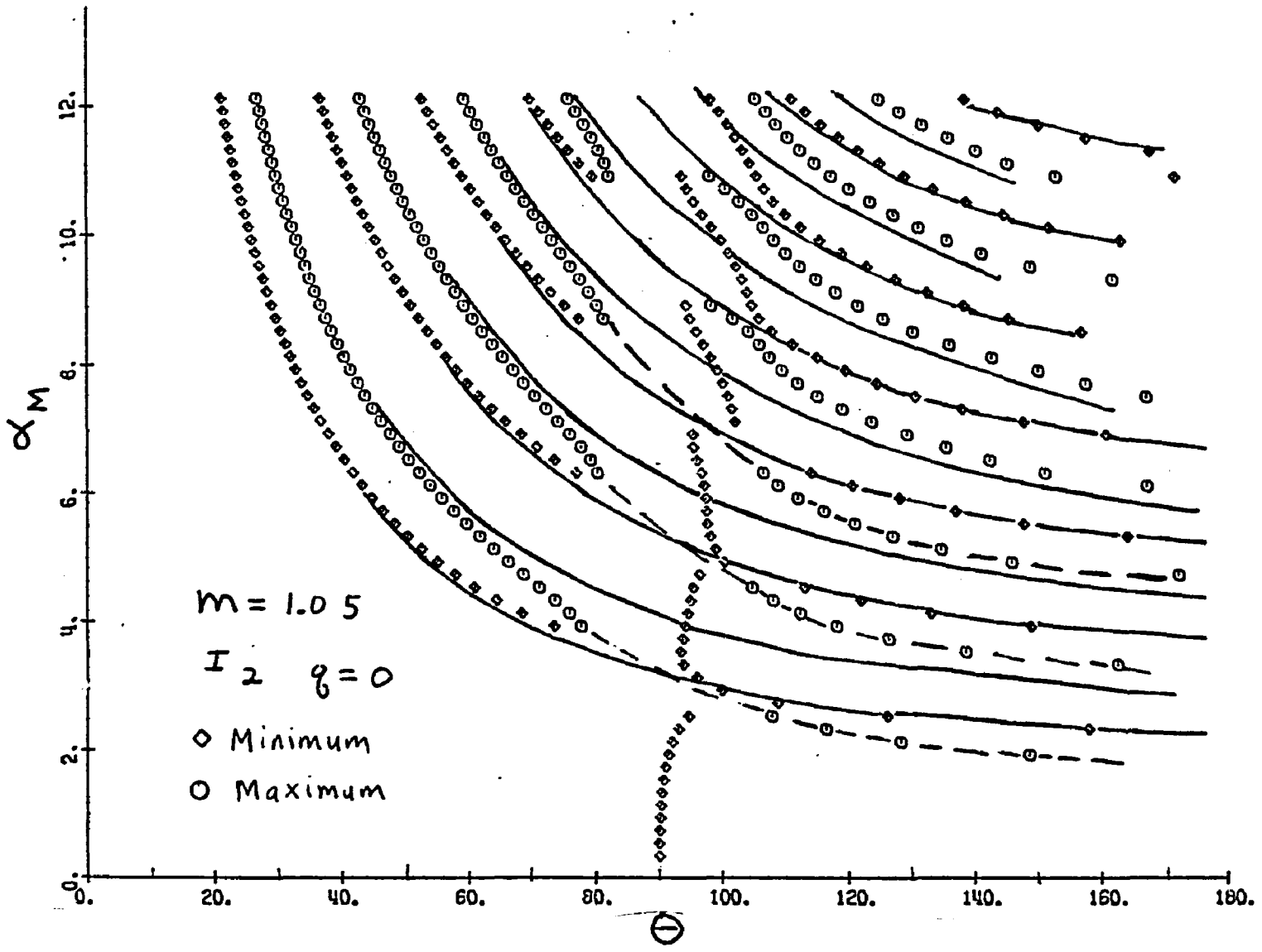

Fig. 52. Angular Location of I_2 Extrema Versus Modal Size α_M for Distributions with m=1.05 and q=0

from the solid lines while the minima remain constant. The maxima and minima contours would then intersect at $\theta = 90^{o}$ forming an X over the Rayleigh minimum.

Figure 52 shows the general appearance of this intersection for the first three extrema pairs. The extrema contours do not extend completely to the Rayleigh minimum as indicated by the dashed lines because of deviations from the RGD theory. Also note the bending of the Rayleigh minimum as it crosses the intersection. For scattering obeying the RGD theory, the Rayleigh minimum would appear as a straight line at 90^{o} showing no deviation as it crosses the extrema contours. This follows from equation 17 which shows that I_2 goes to 0 at 90^{o}. However for scattering from systems having m values larger than 1.00 the intensity of the Rayleigh minimum has a finite value and will therefore shift when it approaches other extrema.

The description of the scattering pattern in terms of the intersection of the extrema contours becomes less accurate as the particle size increases. Figure 52 shows that the maxima and minima in the forward direction merge and disappear before reaching the Rayleigh minimum. The merging and disappearance of the I_2 extrema for monodisperse systems show the same behavior as the I_1 extrema for heterodisperse systems shown in Figures 45 and 48. Figure 52 also shows that the slope of the line segments representing the Rayleigh minimum approaches the slope of the extrema contours as the particle size increases. These line segments then merge with the minima contours in the backward direction and form extrema pairs similar to those in the forward direction.

Increasing the heterodispersion to q = 1 in Figure 53

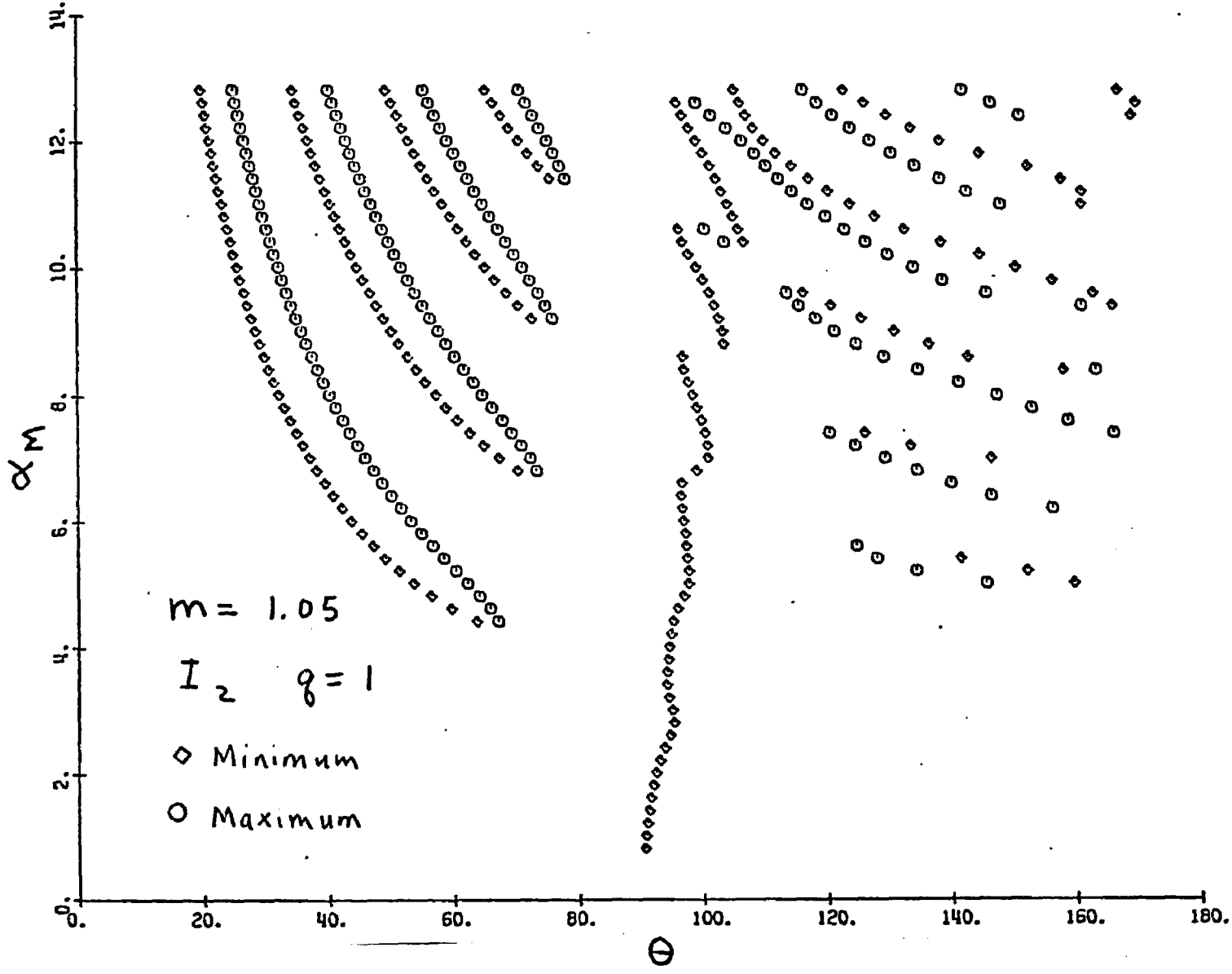

Fig. 53. Angular Location of I_2 Extrema Versus Modal Size α_M for Distributions with m=1.05 and q=1

shows the expected results from averaging over a given size range. The Rayleigh minimum now forms a continuous curve at the smaller particle sizes, and the extrema pairs in both the forward and backward direction wash out near the Rayleigh minimum. In addition, the first extrema pair in the backward direction has completely washed out. Further increase in the heterodispersion washes out nearly all of the structure in the backward direction. Figure 54 shows that the remaining extrema in the backward direction at large particle sizes migrate toward the backward direction. These extrema originate from a reflection phenomenon. The Rayleigh minimum for the heterodisperse system now forms nearly a straight line. Figure 54 also shows the familiar pattern of the extrema washing out in the forward direction. The dashed lines which represent the monodisperse case in Figure 52 have been added for comparison.

As the relative refractive index increases to m = 1.20 the Rayleigh minimum is only seen for the very small particle sizes although it greatly affects the extrema contours for even large particle sizes. The most prominent and easily recognized influence of the Rayleigh minimum is the absence of any extrema in the angular region slightly greater than 90^{o} for small and moderate size particles. Figure 55 shows the extrema contours for I_2 from monodisperse systems having m = 1.20. Note that the Rayleigh minimum is readily seen only for particles smaller than $\alpha_M = 2$. The rest of Figure 55 shows the behavior described earlier for the large particles having m = 1.05. In that description the Rayleigh minimum had merged with the minima contours in the backward direction to form extrema pairs. This behavior which was observed for the large particle sizes having m = 1.05 is now seen for the small particle sizes having m = 1.20.

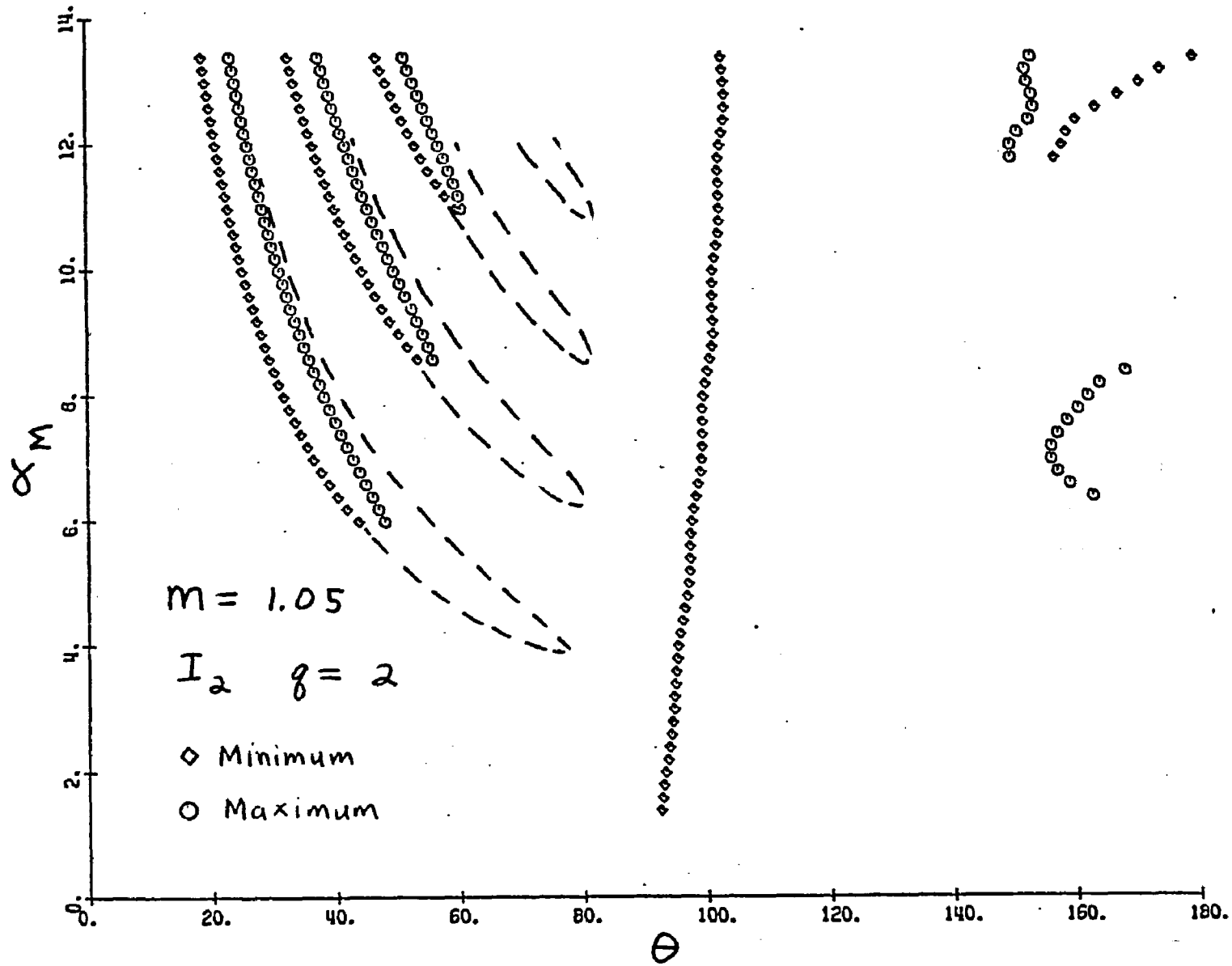

Fig. 54. Angular Location of I_2 Extrema Versus Modal Size α_M for Distributions with m=1.05 and q=2

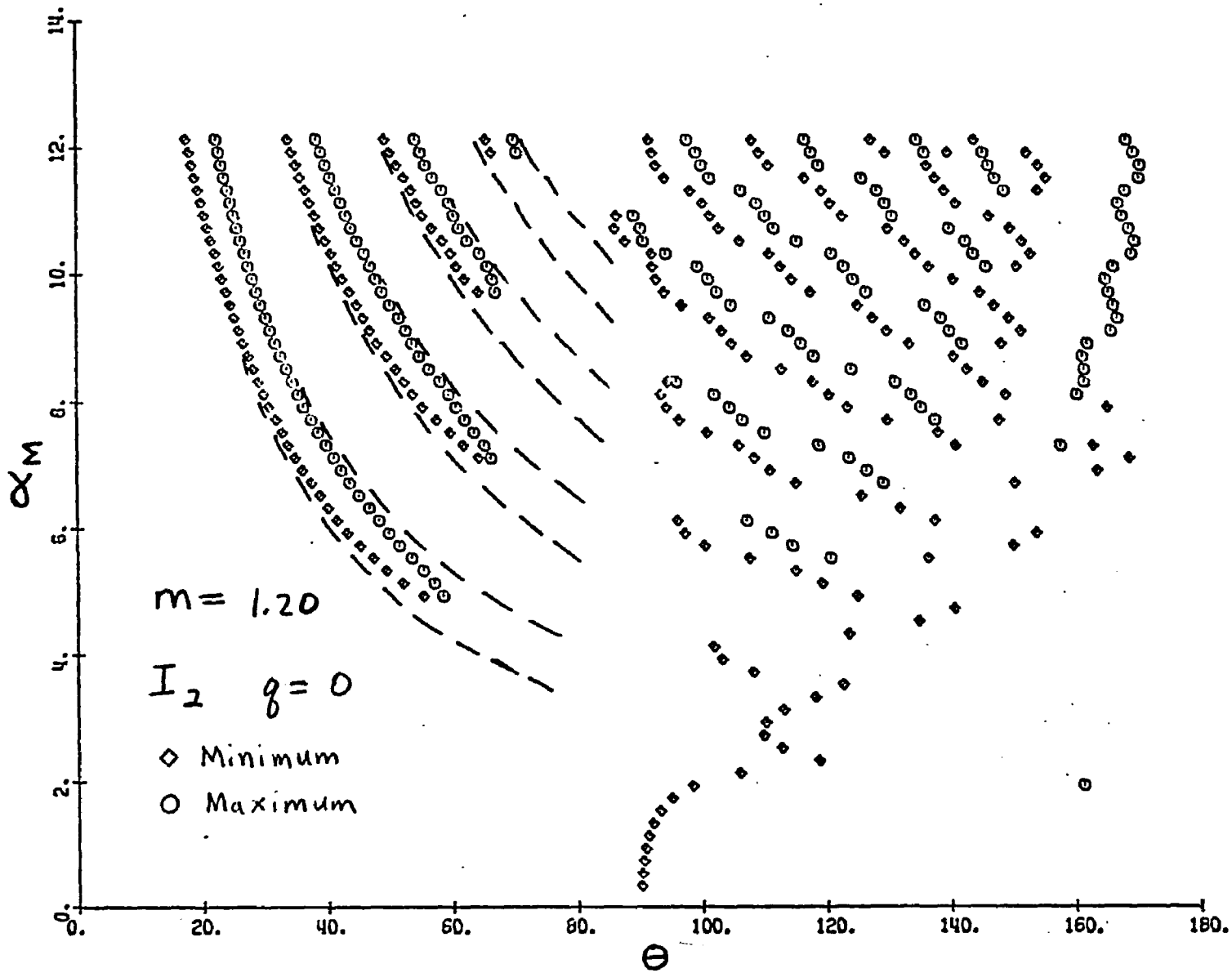

Fig. 55. Angular Location of I_2 Extrema Versus Modal Size α_M for Distributions with m=1.20 and q=0

Once again, similar scattering properties are observed by systems having similar values of $\alpha(m-1)$.

The extrema pairs in the forwad direction are similar to those described for m = 1.05 but now occupy a smaller portion of the scattering diagram. Dashed lines were added to Figure 55 in the forward direction to compare the extrema contours for I_2 with the corresponding extrema contours for I_1 taken form Figure 34. As seen for m = 1.05 the extrema contours for I_2 from a monodisperse system appear very similar to the heterodisperse curves for I_1. However, the minima contours for I_1 and I_2 are no longer identical.

In contrast to the smooth extrema pairs seen in the backward direction for m = 1.05 the extrema pairs for m = 1.20 are highly oscillatory. Figure 55 also shows the pronounced migration of a maximum contour toward the backward direction for the large particle sizes. These two observations are related to the increased contribution of reflection to the scattering that occurs for m = 1.20. An enlargement of the backward region of Figure 55 is shown in Figure 32 where the dashed lines represent maxima contours and the solid lines represent minima contours. Except for the first extrema pair in the backward direction all of the extrema pairs in Figure 32 migrate toward the forward direction. This type of migration is characterized by diffraction.

A reflection pattern is superimposed over this forward migration and results in the oscillations seen in the extrema contours. These oscillations increase as the particle size increases until the maxima and minima contours make contact and form the closed circles indicated by x's in Figure 32. This pattern shows a continual increase

in the contribution to the total scattering due to reflection as the particle size increases. Whenever the extrema contours show a closed circle the reflection and diffraction systems make about equal contributions to the scattering pattern. These closed circles were seen previously in Figure 46 in the region where new extrema form.

The transformation of the scattering pattern in the backward direction from one dominated by diffraction to one dominated by reflection is shown in Figure 56. As the particle size increases, the oscillations in the extrema contours increase until the curves are broken up into circles and closed loops. Further increase in the particle size show the circles opening up and forming oscillatory extrema contours that migrate toward the backward direction. These oscillations dampen out as the size increases and the diffraction contribuiton to the scattering pattern vanishes.

Figure 56 shows a very unusual effect for the first minimum in the backward direction. After a very rapid movement toward the backward direction around $\alpha_M = 8$ the minimum remains constant at $\theta = 179.9^{\circ}$ until the particle size has increased beyond $\alpha_M = 15$. The reason for this behavior is not know although it may be related to the Rayleigh minimum. Note that for particle sizes larger than $\alpha_M = 15$ the influence of the Rayleigh minimum has also disappeared in the scattering pattern.

Comparing the extrema contours for I_2 in Figure 56 with those for I_1 in Figure 46 shows that the extrema contours in the forward direction are identical for particle sizes larger than $\alpha_M = 10$. Note the disappearance of the first extrema pair for I_2 in the forward direction. Similarly the corresponding extrema contours for I_1 and I_2 in the back-

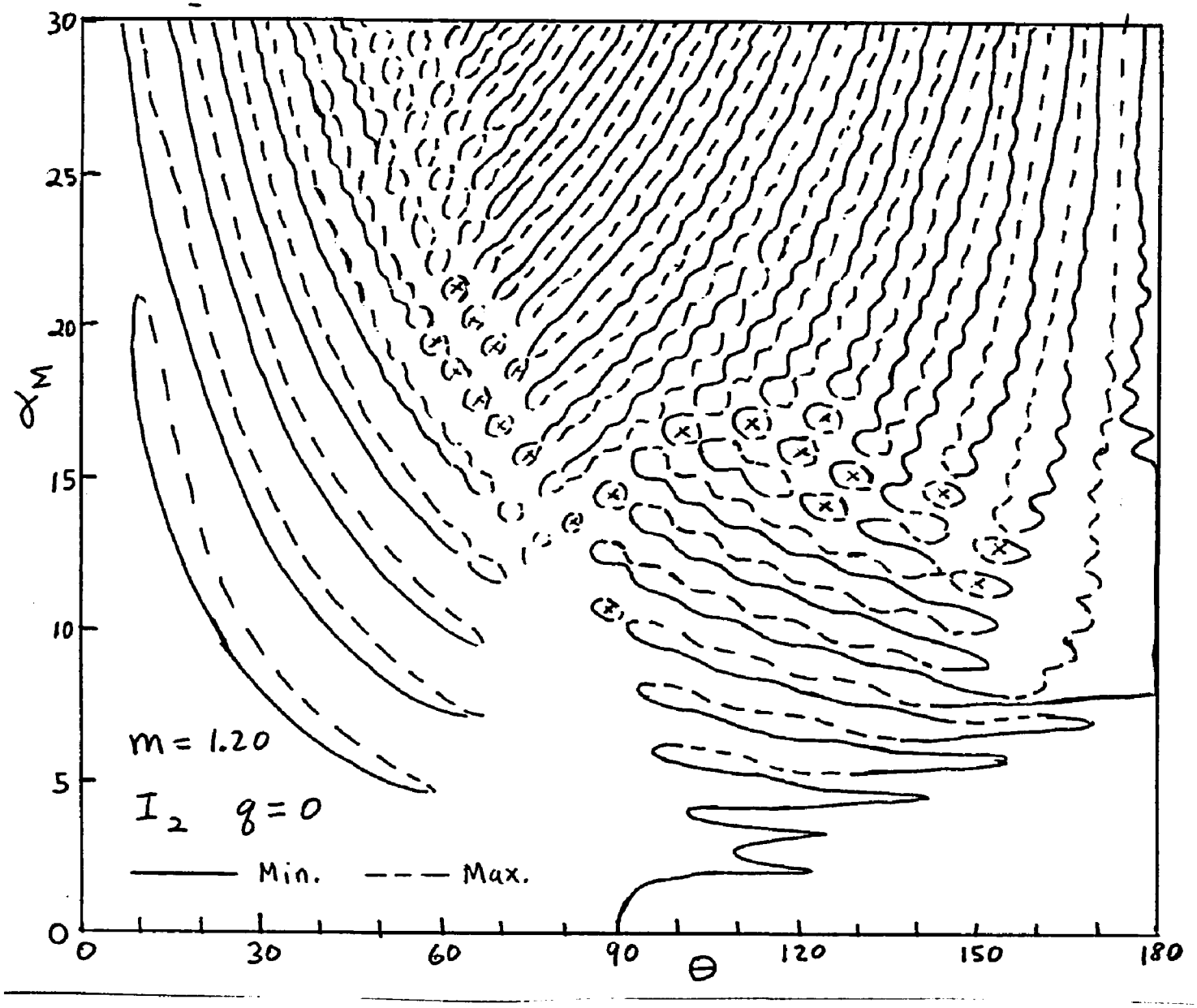

Fig. 56. Angular Location of I_2 Extrema Versus Modal Size α_M for Distributions with m=1.20 and q=0

ward direction are nearly identical for particle sizes larger than $\alpha_m = 15$. The maxima contours show better agreement than the minima contours because they have smoother curves. The minima contours tend to oscillate about a common curve.

Another interesting observation from comparing the extrema contours for I_1 and I_2 shows that the region where extrema migrate toward the backward direction is much greater for I_2 than for I_1. The boundary dividing the extrema contours into regions of forward and backward migration for particle size of $\alpha = 30$ occurs at $\theta = 90^\circ$ and 50° for I_1 and I_2 respectively. The boundary in both cases moves toward the forward direction with increasing particle size.

Increasing the heterodispersion of the extrema contours to $q = 1$ in Figure 57 shows the typical pattern in the forward direction where the minima contours remain constant while the maxima contours shift toward the forward direction. This reduces the region in the forward direction that contain extrema. The increasing heterodispersion in the backward direction has washed out the pattern of the forward migration and formed a series of closed circles as well as extrema contours that migrate in the backward direction. These closed circles represent retions of the scattering diagram where approximately equal reflection and diffraction patterns are superimposed. The extrema contours for I_1 and $m = 1.20$ had previously shown a tendency for reversing the extrema pattern from diffraction to reflection as the heterodispersion increased. However, this reversal only occurred near the boundary of the reflection and diffraction regions. Figure 57 also shows the Rayleigh minimum forming an oscillating curve that migrates toward the backward direction.

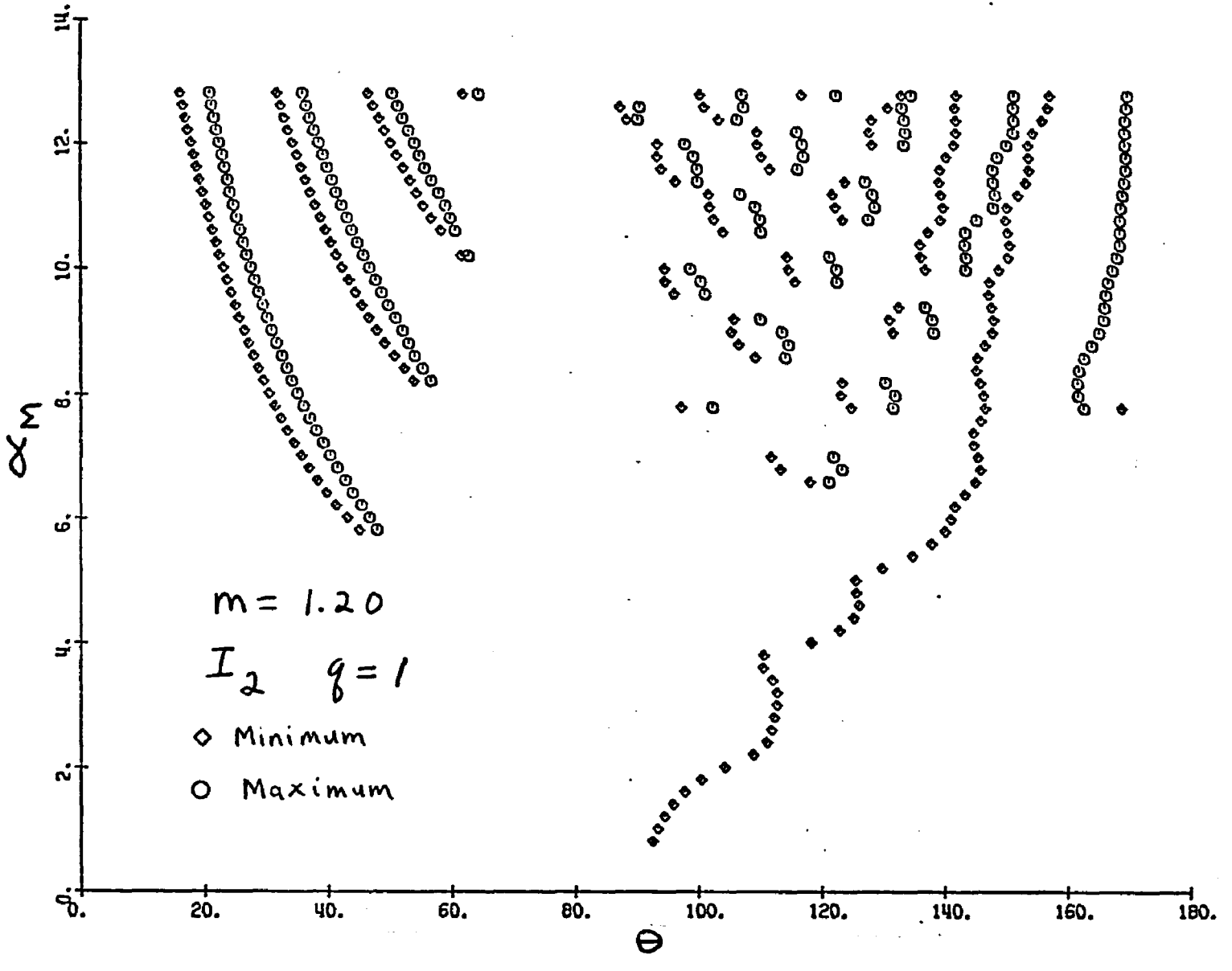

Fig. 57. Angular Location of I_2 Extrema Versus Modal Size α_M for Distributions with m=1.20 and q=1

Increasing the heterodispersion to q = 2 in Figure 58 shows that most of the extrema contours have been wahsed out except for those in the backward and forward regions at large particle sizes. However the backward region contains a greater number of extrema. Dashed lines have been added to the region in the forward direction to show the effect of increasing the heterodispersion from q = 0 to q = 2. Note that the minima remain constant while the maxima shift toward the forward direction. Figure 58 also shows the pronounced migration of the Rayleigh minimum toward the backward direction.

As the relative refractive index is increased to m = 1.333 the previously observed pattern for m = 1.20 is now seen at smaller particle sizes. Figure 59 shows that the extrema in the backward direction no longer have a clear pattern of migrating toward the forward direction. The extrema contours for particle sizes below $\alpha_M = 9$ resemble a region where both diffraction and reflection patterns are superimposed. For particles larger than $\alpha_M = 9$ the extrema contours show a definite migration toward the backward direction as expected when the influence of the Rayleigh minimum has become negligible. The minimum close to 180° also becomes measurable for sizes larger than $\alpha_M = 9$.

Figure 59 indicates that the fraction of the scattering diagram where the extrema migrate in the forward direction has been reduced compared to smaller m values. Note that the second extrema pair shows an oscillation pattern and the third extrema pair has degenerated to a series of closed circles. These observations indicate that the reflection pattern extends into the forward direction up to the second extrema pair.

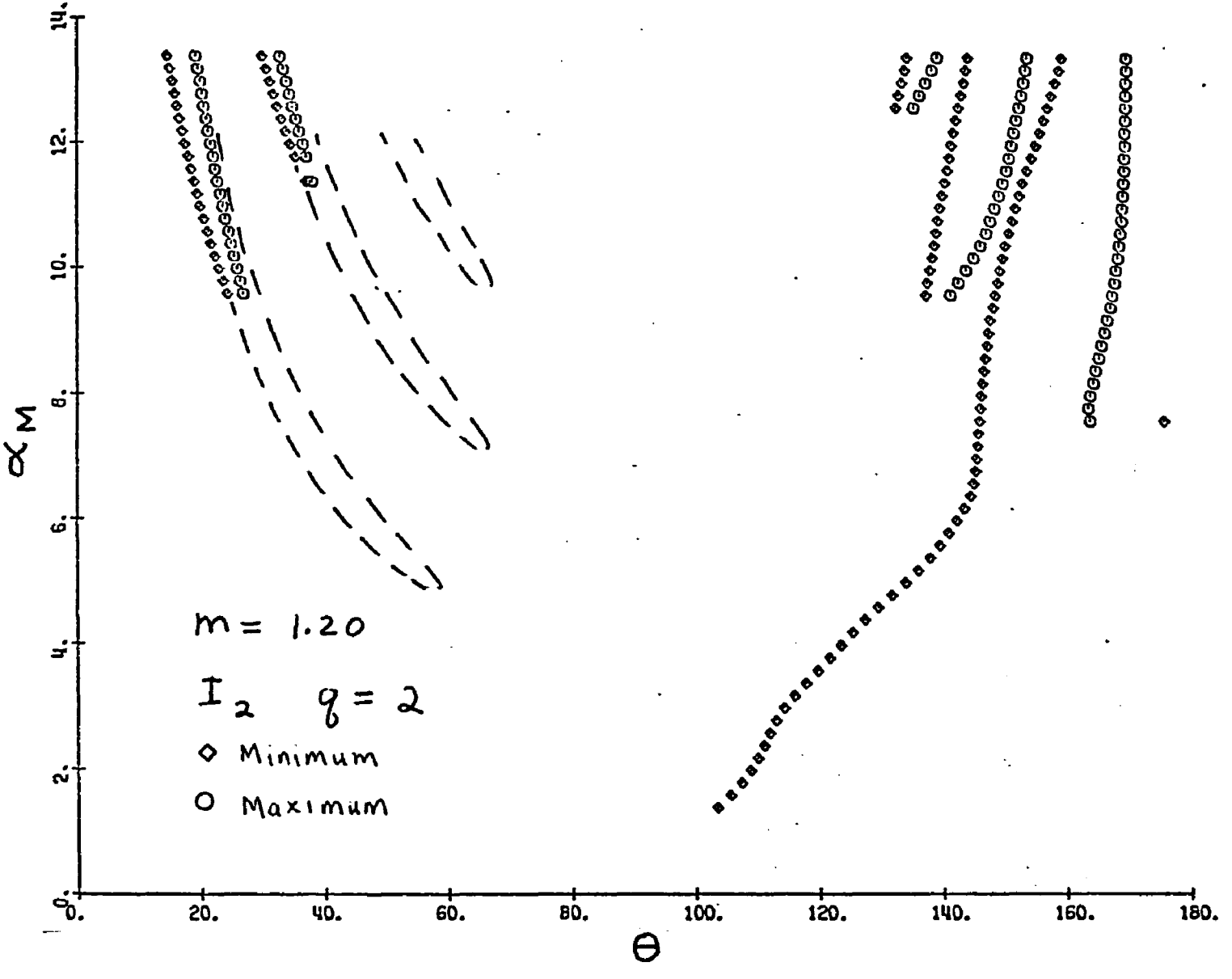

Fig. 58. Angular Location of I_2 Extrema Versus Modal Size α_M for Distributions with m=1.20 and q=2

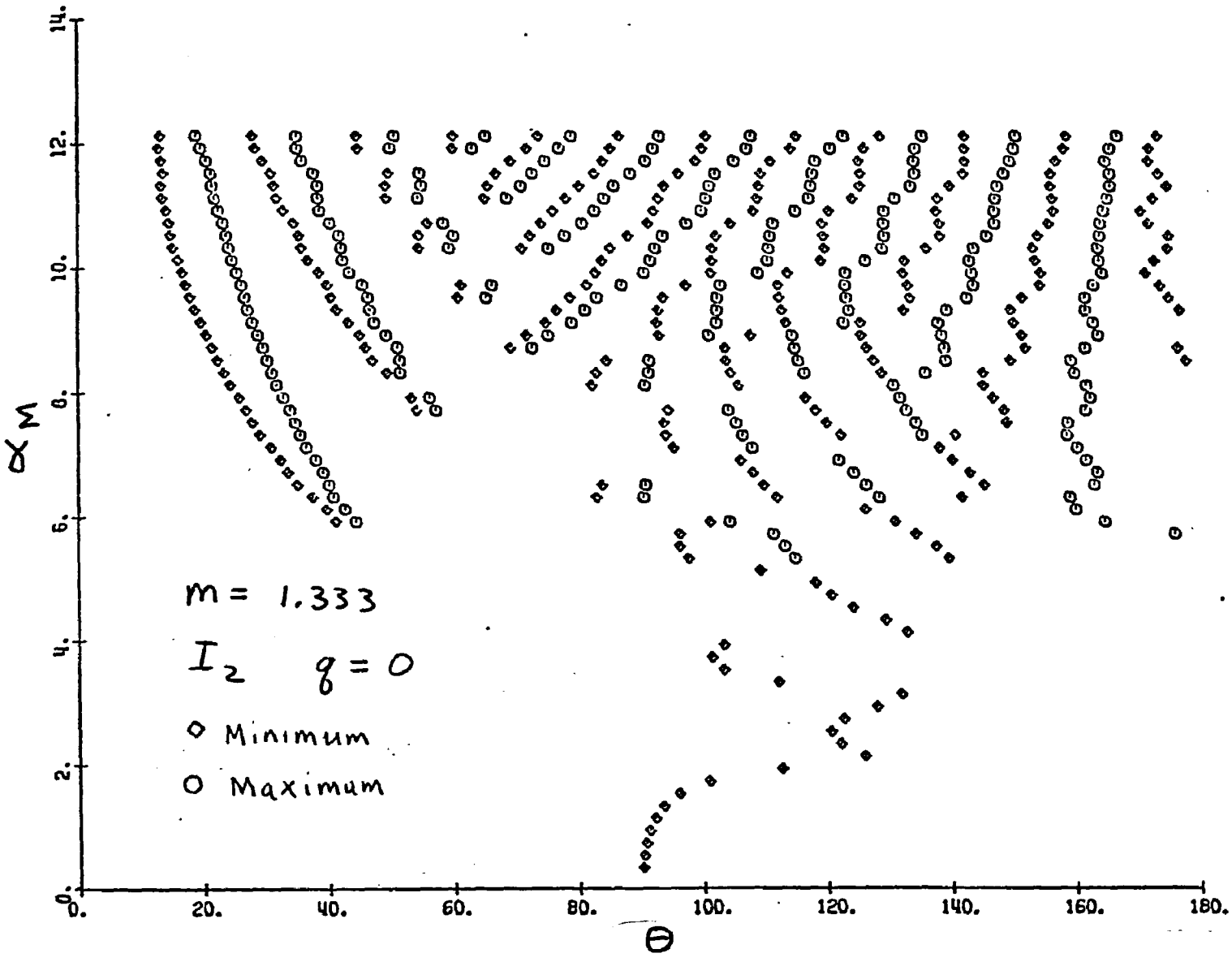

Fig. 59. Angular Location of I_2 Extrema Versus Modal Size α_M for Distributions with m=1.333 and q=0

Increasing the heterodispersion to q = 1 in Figure 60 enhances the reflection pattern and the resulting migration of the extrema contours toward the backward direction. In contrast, the increase in the heterodispersion in the forward direction enhances the diffraction pattern and makes the forward migration more pronounced. The increase of either the diffraction or reflection pattern with an increase in the heterodispersion results from washing out the weaker pattern of the superposition of both patterns. Figure 60 also shows the disappearnace of the extrema between the regions where extrema migrate in the forward and backward directions. Also note the merging and disappearance of the first extrema pair at $\alpha_M \approx 12.5$. Increasing the heterodispersion to q = 2 in Figure 61 shows the standard trends of smoothing the extrema contours and washing out the shallow extrema in the area between the reflection and diffraction regions.

The explanation for the I_2 extrema in the forward direction being so shallow appears to be closely related to the Rayleigh minimum. This explanation can be illustrated on a qualitative basis using the extrema contour plots for m = 1.20 shown in Figures 48 and 55. Figure 48 shows the extrema contours for I_1 from a heterodisperse size distribution having q = 2. A very similar pattern is seen in Figure 55 which shows the extrema contours for I_2 from a monodisperse system. The extrema in the forward direciton in Figure 48 have been washed out because of the averaging effect of the scattered intensities from a distribution of particles. In contrast, the corresponding extrema in Figure 55 appear washed out because the Rayleigh minimum has forced the maxima and minima contours to cross over each other. This crossing over effect is clearly

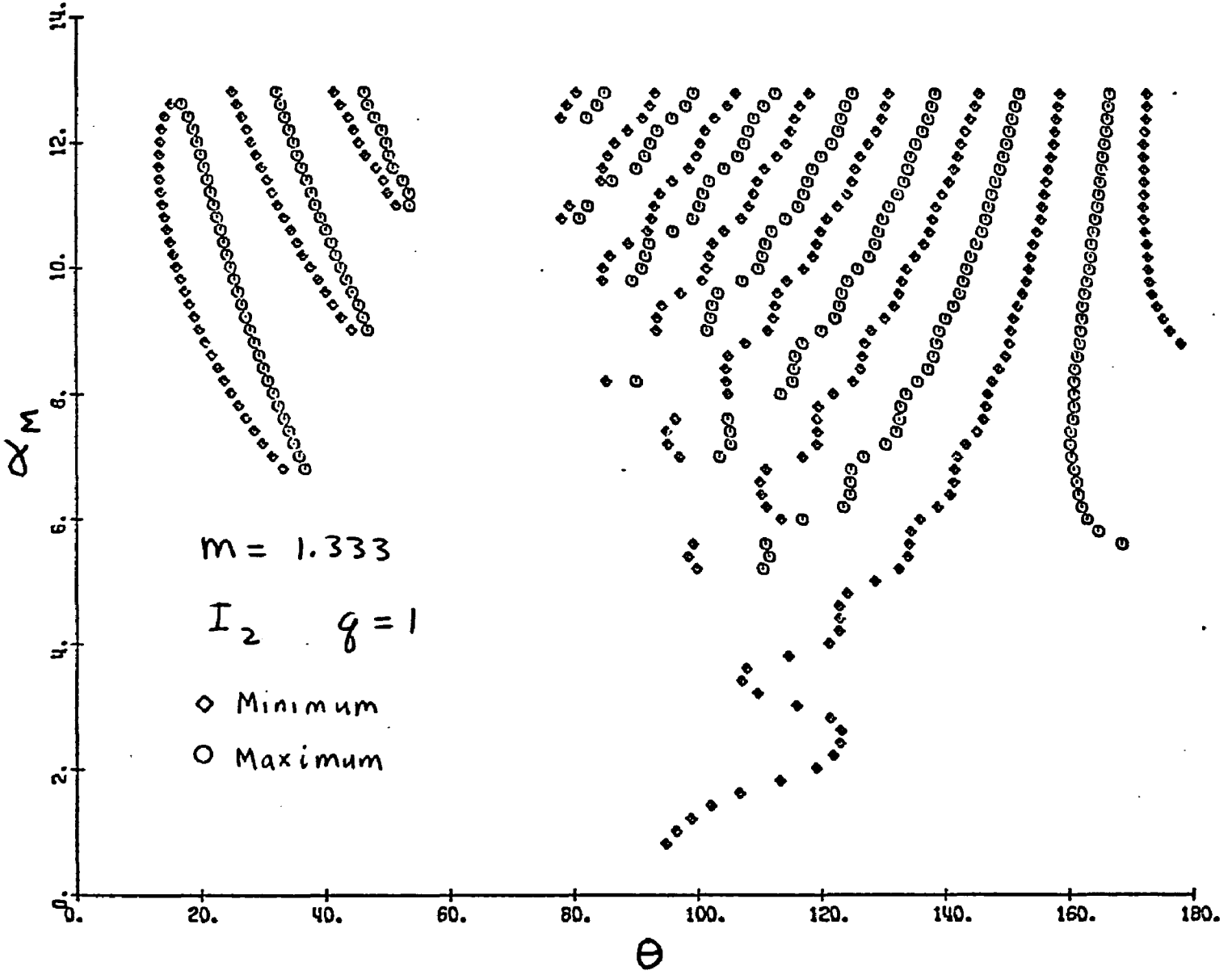

Fig. 60. Angular Location of I_2 Extrema Versus Modal Size α_M for Distributions with m=1.333 and q=1

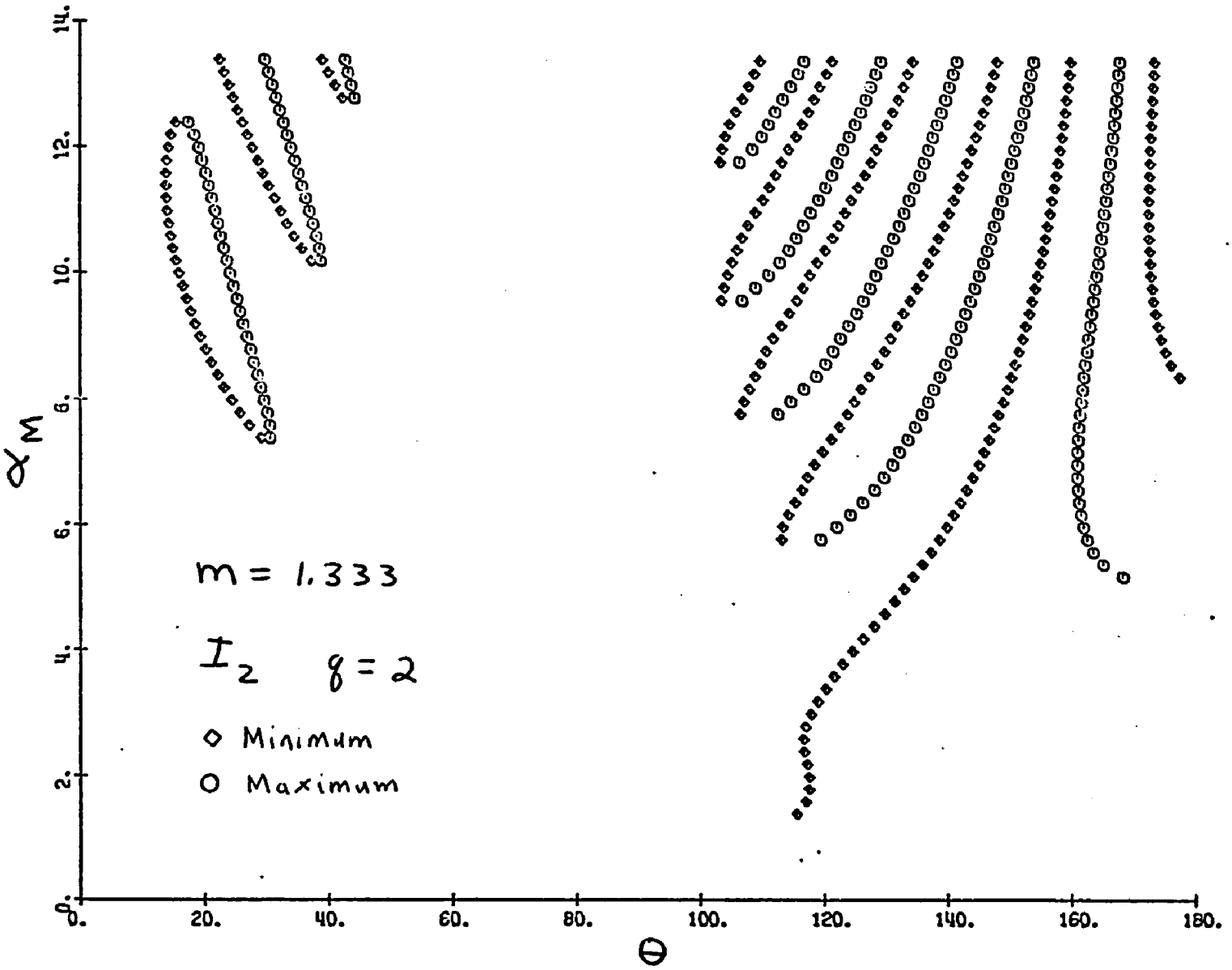

Fig. 61. Angular Location of I_2 Extrema Versus Modal Size α_M for Distributions with m=1.333 and q=2

seen in Figure 52 for the I_2 scattering from monodisperse systems having m = 1.05.

A comparison of the angular intensity curves for I_1 from a heterodisperse distribution and I_2 from a monodisperse distribution shows that increasing the heterodispersion has the same effect in washing out the diffraction extrema as the Rayleigh minimum. This comparison is shown in Figure 62 where the angular intensity curves in the forward direction are plotted for I_1 at q = 2 and I_2 at q = 0. Similar results are seen for other particle sizes and other relative refractive indexes.

A survey of the extrema contour for I_2 in Figures 52-61 reveals many of the same trends seen for I_1. Increasing the relative refractive index increases the region of the scattering diagram where extrema migrate toward the backward direction. The region where the extrema migrate toward the forward direction is simultaneously reduced. The larger m values also compress the extrema contours to smaller particle sizes. Thus, trends in the scattering pattern seen in large particle sizes for systems having low m values are seen in smaller particle sizes for systems having larger m values.

The effect of increasing heterodispersion on the I_1 extrema contours in the forward direction is also very similar for the I_2 extrema contours. In both cases the minima contours remain constant while the maxima contours shift toward the forward direction with increasing heterodispersion. However the I_2 extrema contours have a similar appearance to the I_1 extrema contours for a more heterodisperse system.

The primary influence on the I_2 extrema contours is the Rayleigh minimum. At low m values the Rayleigh minimum is easily seen

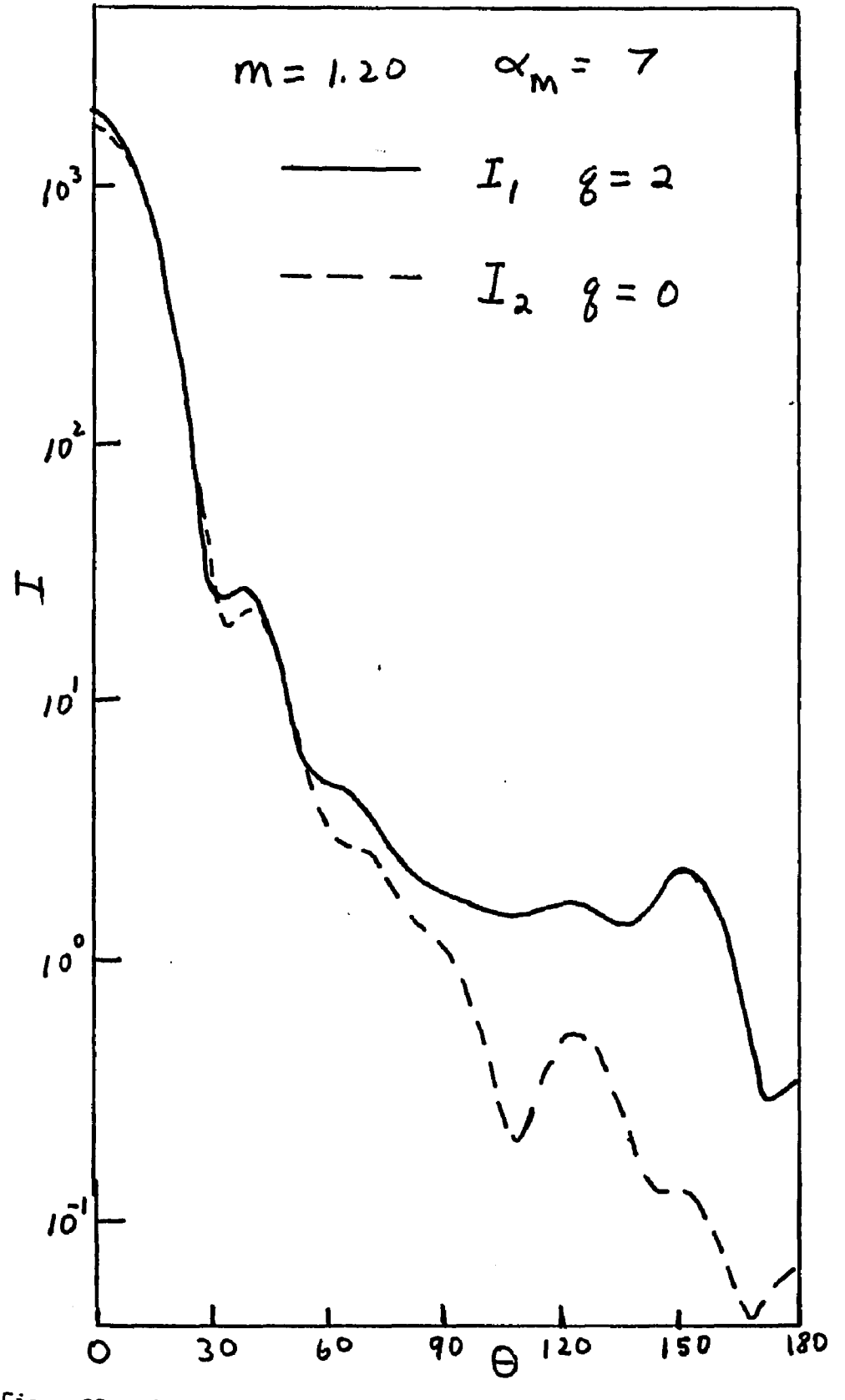

Fig. 62. Comparison of the Scattered Intensity I_1 from a Heterodisperse Distribution with the Scattered Intensity I_2 from a Monodisperse Distribution Having the Same Mode $\alpha_M = 7$

crossing the middle of the scattering diagram. For higher m values, segments of the Rayleigh minimum merge with other minima contours that migrate toward the forward direction. However this forward migration changes to a backward migration with increasing heterodispersion. The reversals in the direction of the extrema migration reveals the frequent superposition of both diffraction and reflection patterns. The Rayleigh minimum also creates a region extending into the forward direction from $\theta = 90^{o}$ that contains no extrema. This region decreases in size as the relative refractive index increase.

3. Effect of m and q on I_u Extrema Contours

The extrema contours for I_u are shown in Figure 63-71. Since these contours are nearly identical to the extrema contours for I_1 a separate analysis of Figures 63-71 is not necessary. The previous description of the I_1 curves will also apply for the I_u curves. However two additional features must be added to the previous discussion which applies to I_u. These two features result from the definition of I_u which is the average of I_1 and I_2. In general this average is nearly equal to I_1. However since the I_2 extrema are more shallow than the corresponding extrema for I_1 the average of the two will also be more shallow than I_1.

Thus one of the primary differences between I_u and I_1 is the higher rate at which the I_u extrema wash out with increasing heterodispersion. A comparison of the extrema contours for I_1 and I_u for a system with m = 1.20 and q = 2.0 is shown in Figure 68. The dashed curves in this figure represent the extrema contours for I_1. This figure shows that for the same degree of heterodispersion the extrema contours for I_u have washed out to a greater extent than the corresponding extrema con-

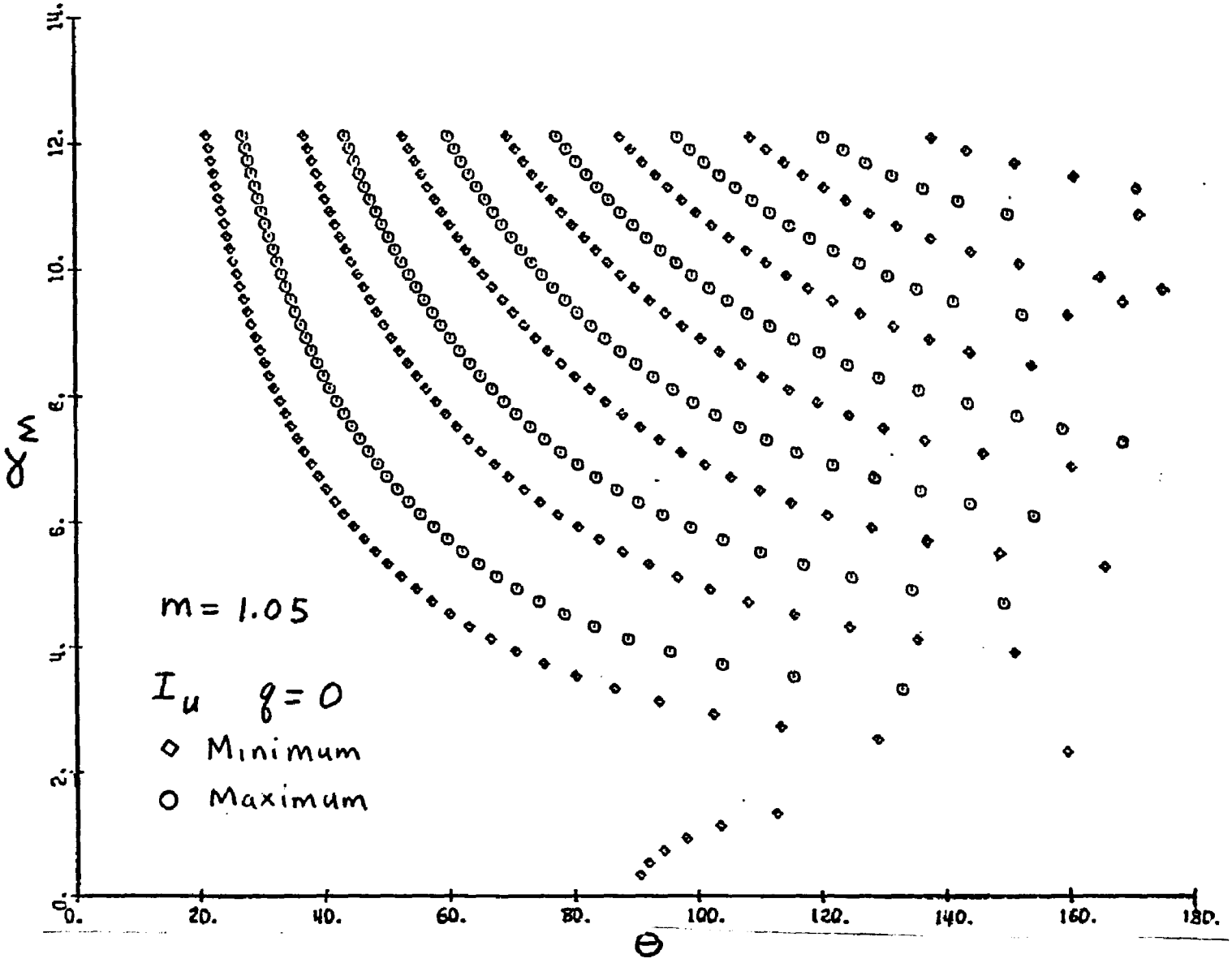

Fig. 63. Angular Location of I_u Extrema Versus Modal Size α_M for Distributions with m=1.05 and q=0

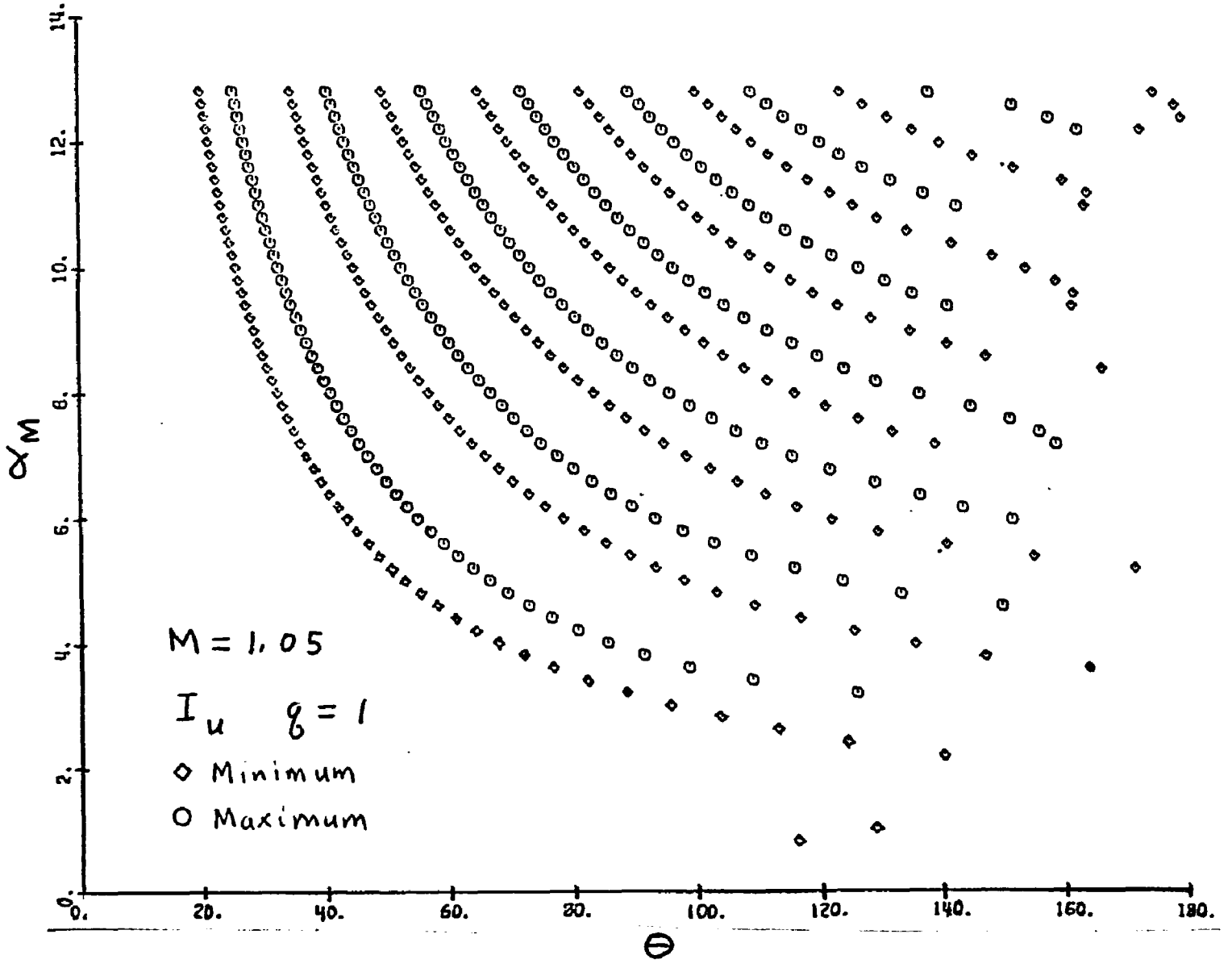

Fig. 64. Angular Location of I_u Extrema Versus Modal Size α_{iM} for Distributions with m=1.05 and q=1

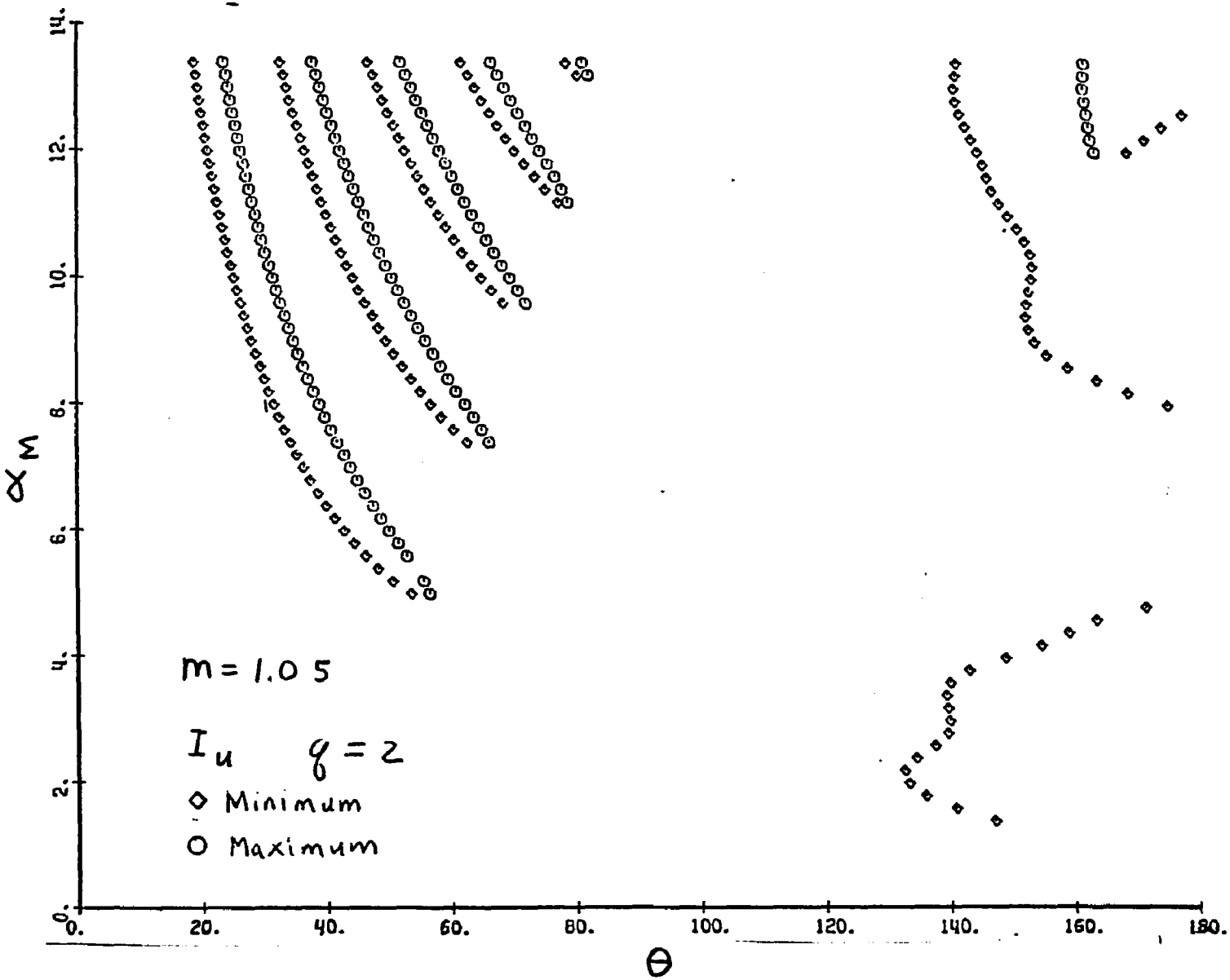

Fig. 65. Angular Location of I_u Extrema Versus Modal Size α_M for Distributions with m=1.05 and q=2

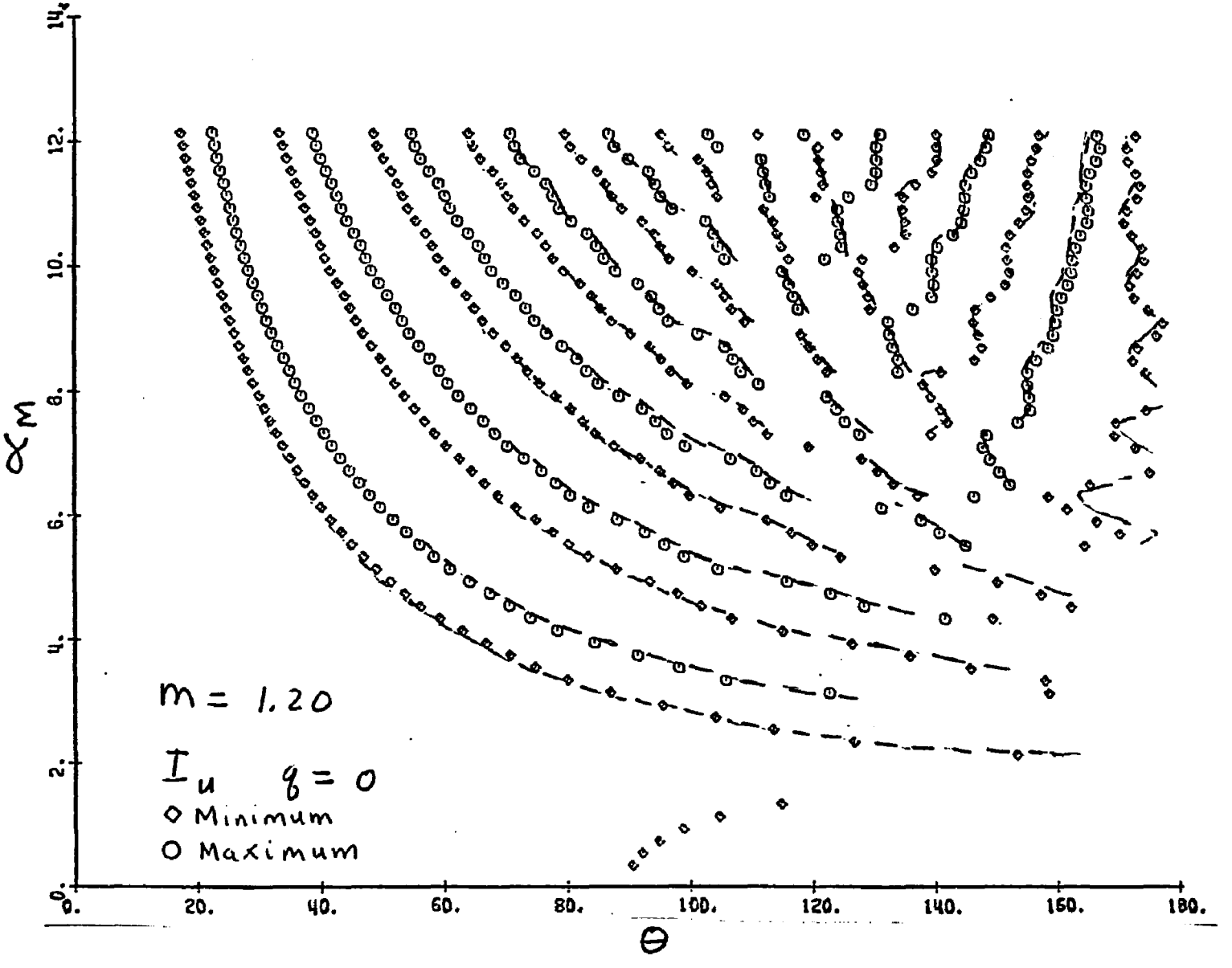

Fig. 66. Angular Location of I_u Extrema Versus Modal Size α_M for Distributions with m=1.20 and q=0

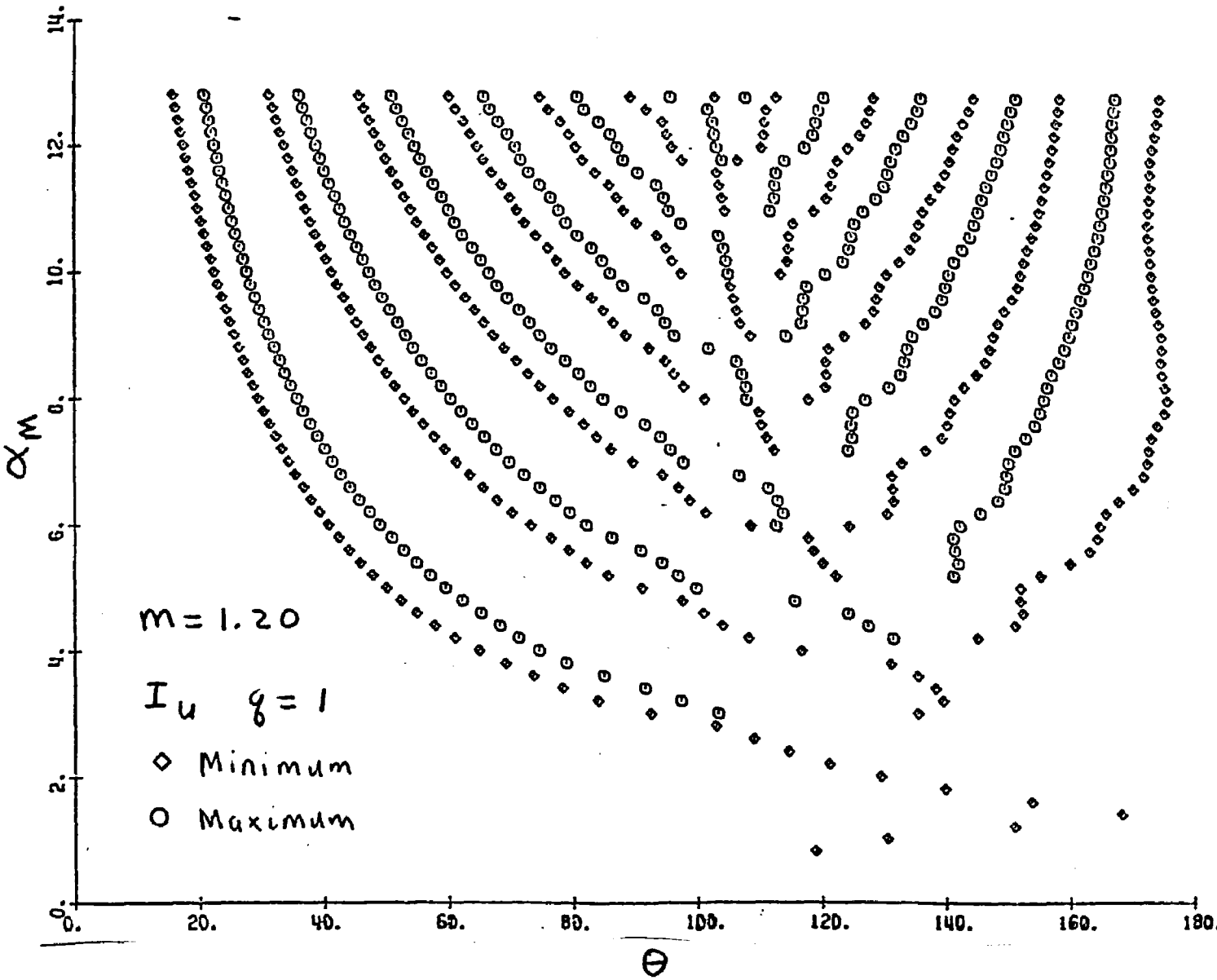

Fig. 67. Angular Location of I_u Extrema Versus Modal Size α_M for Distributions with m=1.20 and q=1

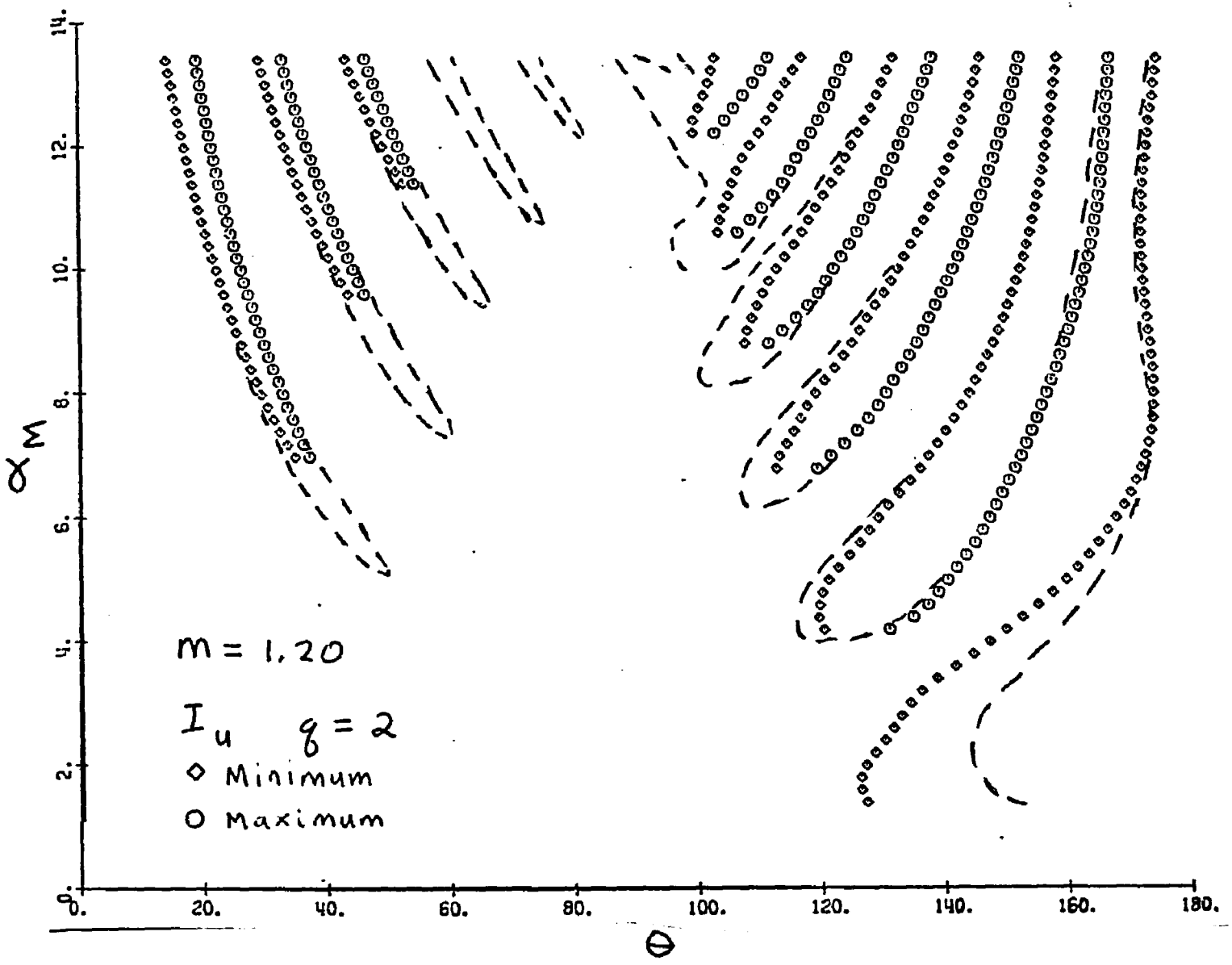

Fig. 68. Angular Location of I_u Extrema Versus Modal Size α_M for Distributions with m=1.20 and q=2

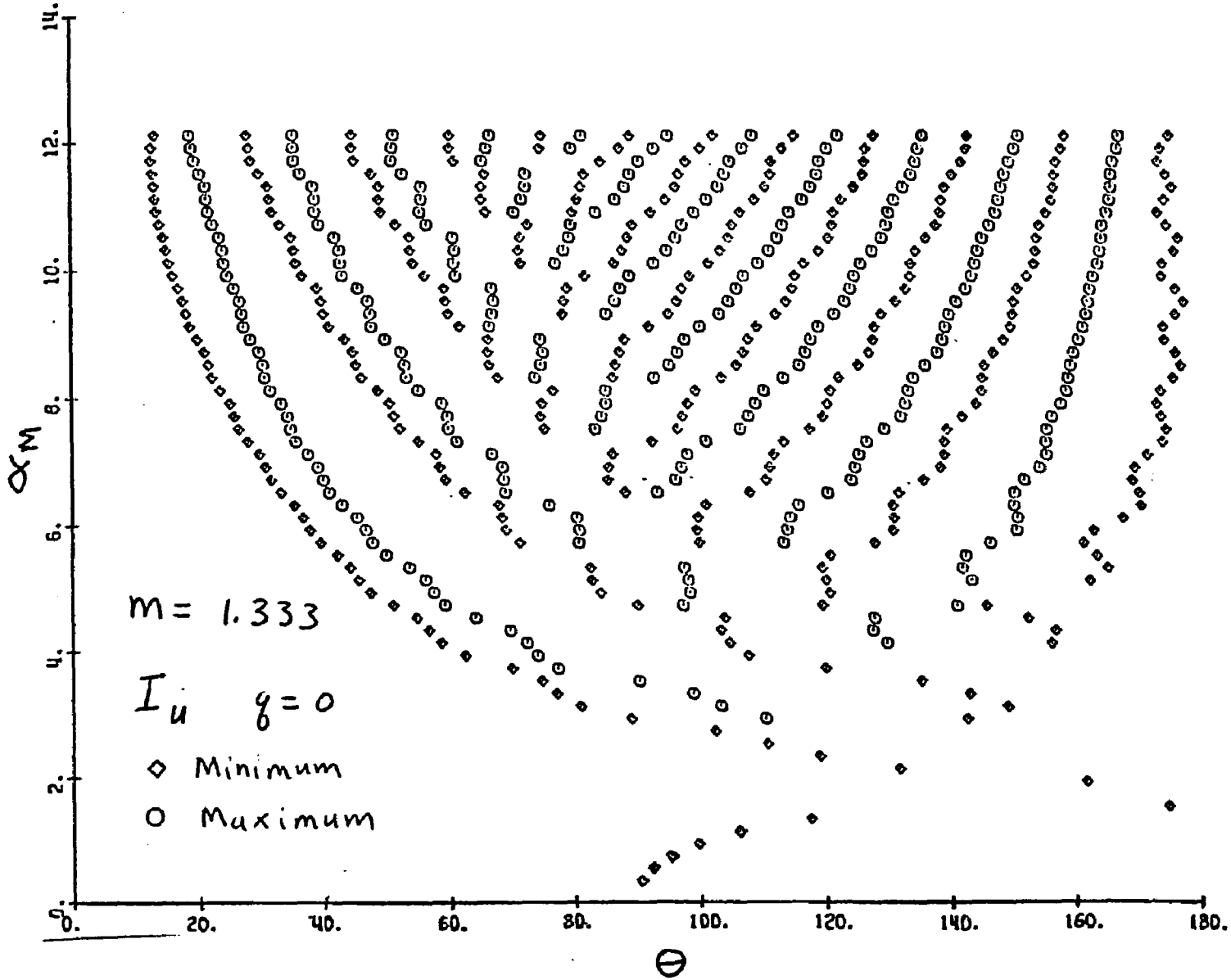

Fig. 69. Angular Location of I_u Extrema Versus Modal Size α_M for Distributions with m=1.333 and q=0

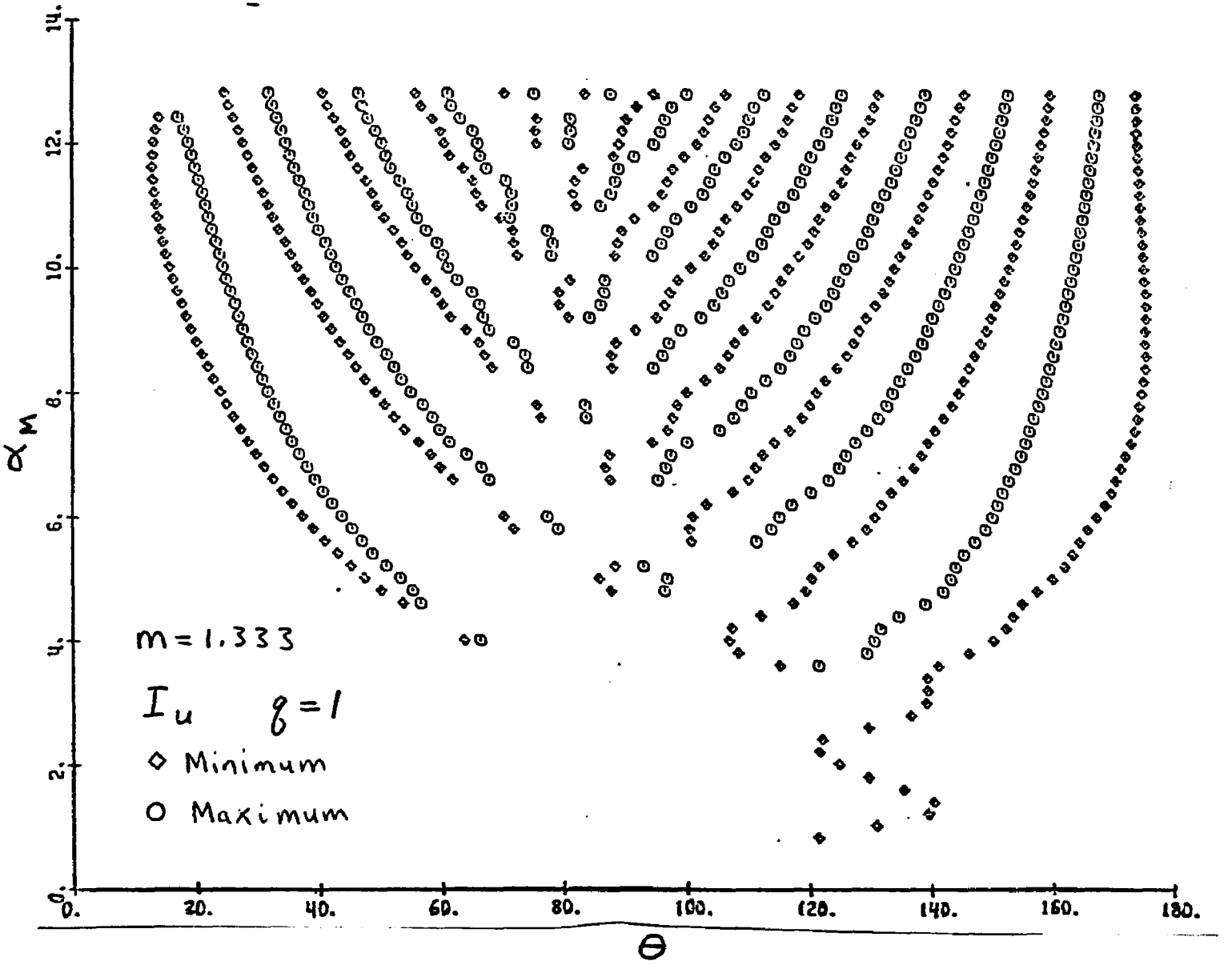

Fig. 70. Angular Location of I_u Extrema Versus Modal Size α_M for Distributions with M=1.333 and q=1

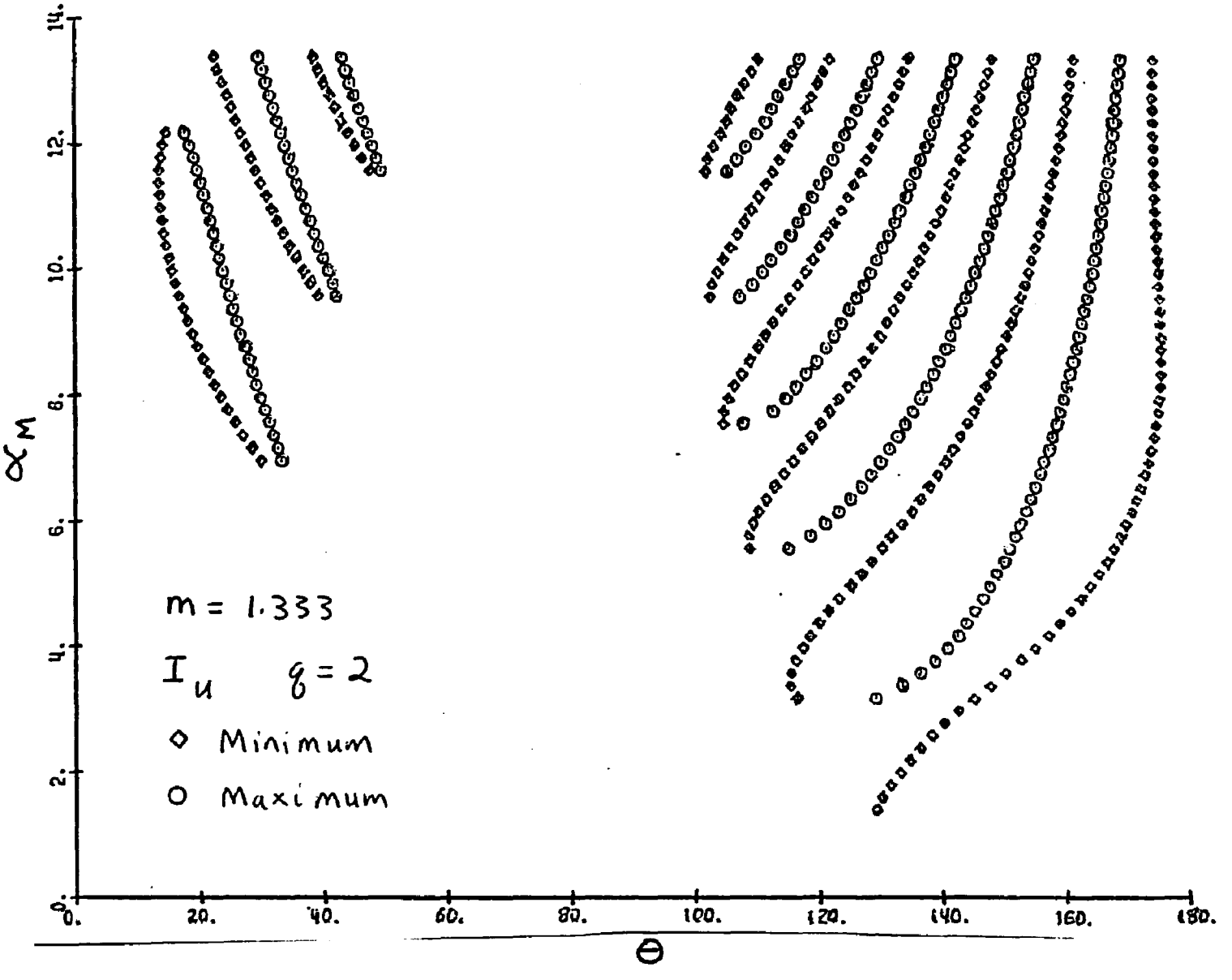

Fig. 71. Angular Location of I_u Extrema Versus Modal Size α_M for Distributions with M=1.333 and q=2

tours for I_1. The deviation between I_1 and I_u for the same m values are equal to or less than that shown in Figure 68. Also note the large difference between the two curves for the first minimum in the backward direction, especially at small particle sizes. This difference is due to the Rayleigh minimum.

The second major difference between the extrema contours of I_1 and I_u is the presence of the Rayleigh minimum in the I_u contour. Figure 66 shows the extrema contours for I_u with m = 1.20 and q = 0. The corresponding extrema contours for I_1 are superimposed on Figure 66 as dashed curves. Note that except for a few minor deviations in the backward direction, the two sets of extrema contours differ by the additional Rayleigh minimum for I_u. Figure 66 shows that this minimum shifts quickly to larger angles and then disappears with increasing size.

C. Interpretation of the Scattering Pattern in Terms of Diffraction and Reflection Phenomena

The previous discussions have been concerned with the trends in the extrema contours considering each polarization of the incident light separately. However a common pattern is seen when the extrema contours from I_1, I_2 and I_u are compared together. This pattern shows the approximate independence of the incident polarization on the diffraction and reflection systems in the scattering diagram. If one compares the extrema contours in the forward direction at a given m value for I_1, I_2 and I_u and all q values then the extrema will fall within a small region of the scattering diagram. The boundary of this region is defined by the

extrema contours for I_1 at q = 0.

This behavior is illustrated in Figure 55 which shows that the extrema contours for I_2 at q = 0 fall within the boundary indicated by the dashed lines. Similarly, Figure 48 illustrates that the extrema contours for different q values will also fall within the boundary of the I_1 extrema contours. In both cases the maxima and minima contours merge and wash out at large angles within the boundary of the I_1 extrema contours. If all of the extrema contours for m = 1.20 having different polarizations and q values were plotted in Figure 48, the entire region between the dashed lines would be filled with points. All of the m values show the same trend although the defining boundaries are different for each. An apparent exception to this trend is seen in Figure 45 for m = 1.05 where the extrema curves for q = 2 fall slightly outside of the defining boundary.

1. Forward Scattering Described in Terms of Diffraction

a. General Description

The common pattern of the extrema contours in the forward direction for I_1, I_2 and I_4 at various q values provides a strong motivation to consider the forward scattering in terms of a diffraction phenomenon. This does not mean that the scattering in the forward direction is described by Fraunhoffer diffraction. Rather the forward scattering is described in terms of a diffraction phenomenon because it has very similar properties to the Fraunhoffer diffraction. Figure 72 shows the extrema contours of the angular maxima and minima intersities obtained from the Fraunhoffer diffraction theory. The difraction maxima and minima are indicated by the dashed and solid lines respectively. Note that

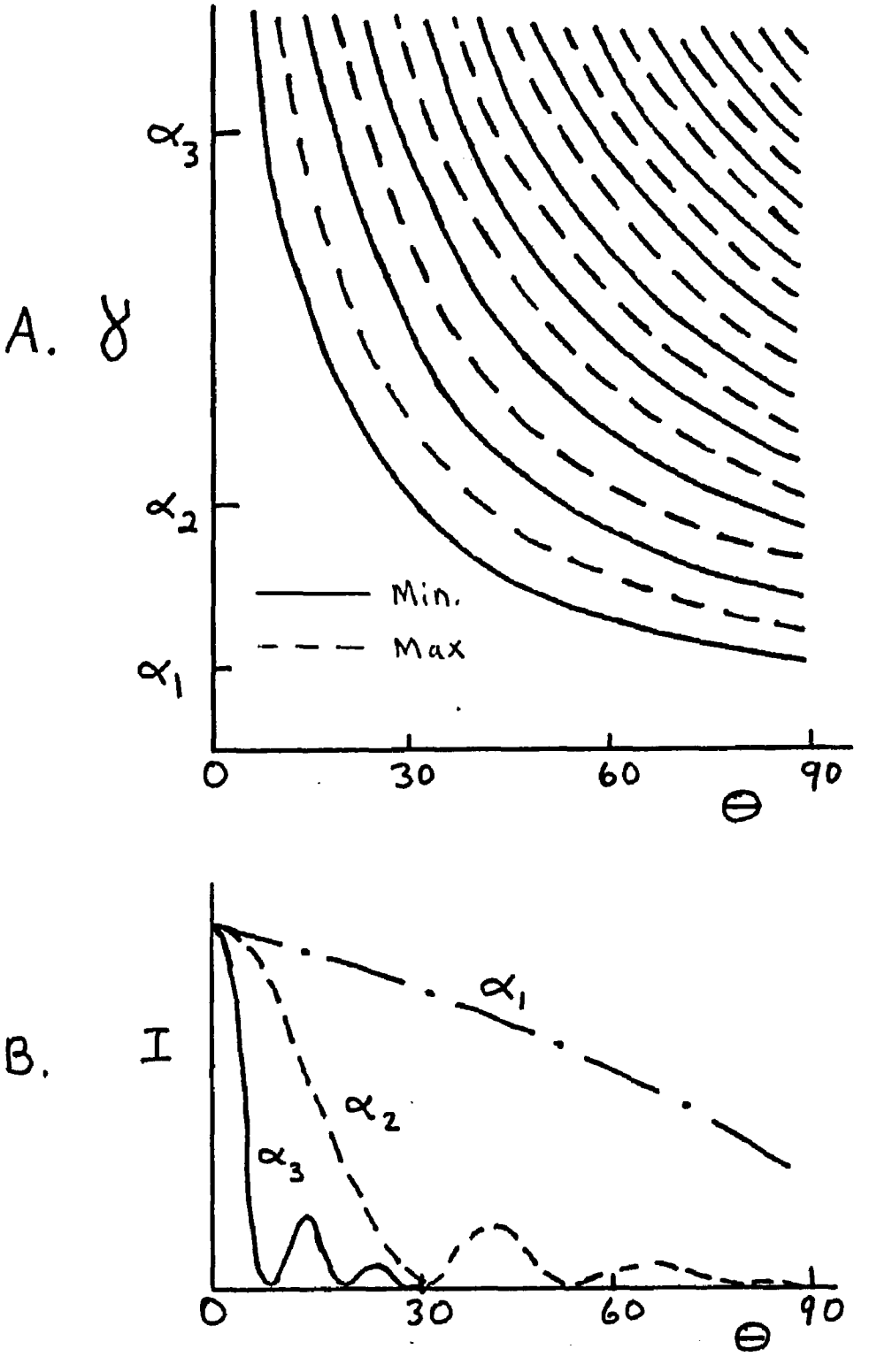

Fig. 72. Fraunhoffer Diffraction. (A) Angular Location of Intensity Extrema Versus Modal Size for Monodisperse Distributions. (B) Diffracted Intensity as a Function of Angle for Three Particle Sizes

the extrema contours only extend from the forward direction to $\theta = 90^{o}$. Figure 72 also shows the angular intensity of diffracted light normalized at $\theta = 0^{o}$ for three particle sizes as a separate graph.

In the limit of very large particle sizes the forward scattering merges into the Fraunhoffer diffraction. Although the forward scattering in the systems studied is approximately independent of the incident polarization it does depend on the relative refractive index. In contrast, the Fraunhoffer diffraction is independent of both the incident polarization and the relative refractive index.

As stated in Chapter II previous investigators[27,28,29-31,50] had interpreted the scattering in the forward direction in terms of diffraction. Although these investigators were well aware that the Fraunhoffer diffraction theory only applies for very large particles they still used that theory to describe the light scattering behavior in the forward direction. The scattering in the forward direction was described as a diffraction phenomenon if the maxima and minima contours would have approximately constant $\propto\theta$ values[27,28] or constant $\propto \sin\theta$ values.[29-31] These arguments were chosen because the angular maxima and minima of the Fraunhoffer diffraction have constant values of $\propto\sin\theta$. For very small angles the term $\propto\sin\theta$ would then reduce to $\propto\theta$. Although the extrema curves in those studies did not have constant values of $\propto\theta$ or $\propto\sin\theta$, the curves did meander about the classical diffraction maxima and minima.

The present investigation uses an expanded definition of diffraction to describe any scattering process in which the maxima and minima contours migrate toward the forward direction with increasing particle size. The RGD theory is therefore considered basically a diffraction

theory under this expanded definition. This is not unreasonable, considering the fundamental assumption of the RGD theory that the phase shift parameter $\alpha(m-1) \ll 1$. Physically this assumption implies that the incident wave front passes through the particle without distortion or phase retardation. For very large particles one would say that the assumption implies no refraction or reflection. The strong similarity between the extrema contours for the RGD theory and the Fraunhoffer diffraction theory is seen by comparing Figures 43 and 72 in the region from $\theta = 0^{\circ}$ to 90°.

The diffraction pattern for the particle sizes used in the present investigation are described much better by the RGD theory than by the Fraunhoffer diffraction theory, which is the correct theory in the limit of large particle sizes. The scattering patterns were therefore described as a diffraction pattern if the maxima and minima contours have approximately constant $\alpha \sin(\theta/2)$ values. Patitsas[21] had previously plotted the extrema contours in graphs of $\alpha \sin(\theta/2)$ versus α in order to obtain empirical improvements in equation 1 for the RGD theory. He found that these graphs show a series of curves that decrease approximately linearly with increasing α and have a sharp decrease at smaller α values. To prevent the sharp decrease at small α values, Patitsas used $\alpha(\theta/2)$ in his plots instead of $\alpha \sin(\theta/2)$. The present investigation will show that the series of extrema curves that decrease linearly with increasing α are diffraction extrema and those with a sharp decrease at small α are reflection extrema.

The extrema contours in Figures 43-71 were replotted in graphs of $\alpha \sin(\theta/2)$ versus α to indentify the extrema that are characterized as

diffraction extrema. Figure 73 shows the extrema contours for I_1 having m = 1.05 and q = 0.0. The maxima and minima are again designated by circles and triangles respectively. Note that all of the extrema data appears in a lower triangle defined by the line $\alpha \sin(\theta/2) = \alpha$. This limiting line occurs because the largest value of $\sin(\theta/2)$ is 1. Numbers have been added identifying the orders of the extrema contours to allow comparisons with the same extrema contours plotted in Figure 43 as α versus θ. The lines defining constant θ angles are also shown on this graph.

Figure 73 shows that the extrema contours form straight horizontal lines at nearly constant $\alpha \sin(\theta/2)$ values as expected from the RGD theory. The extrema contours can therefore be considered as diffraction extrema. However the lines for the lower extrema orders show a small decrease for increasing α values. The corresponding lines for m = 1.00 in the RGD theory would have no decrease with increasing size α. Figure 73 also shows deviations from the horizontal lines in the backward direction ($\theta = 180^{\circ}$) for larger particle sizes. These deviations which are seen as an abrupt change in the slope from a constant $\alpha \sin(\theta/2)$ to an approximately constant θ are due to reflection rather than diffraction phenomena. Increasing the heterodispersion to q = 2, as shown in Figure 74, washes out the diffraction extrema at smaller particle sizes and enhances the reflection extrema. Note the clear distinction between the diffraction extrema that lie nearly horizontal and the reflection extrema that slope at approximately constant θ angles in the backward direction.

Increasing the relative refractive index to m = 1.20 for the monodisperse system shown in Figure 75 has several effects on the I_1 extrema contours. All of the diffraction lines have shifted to smaller

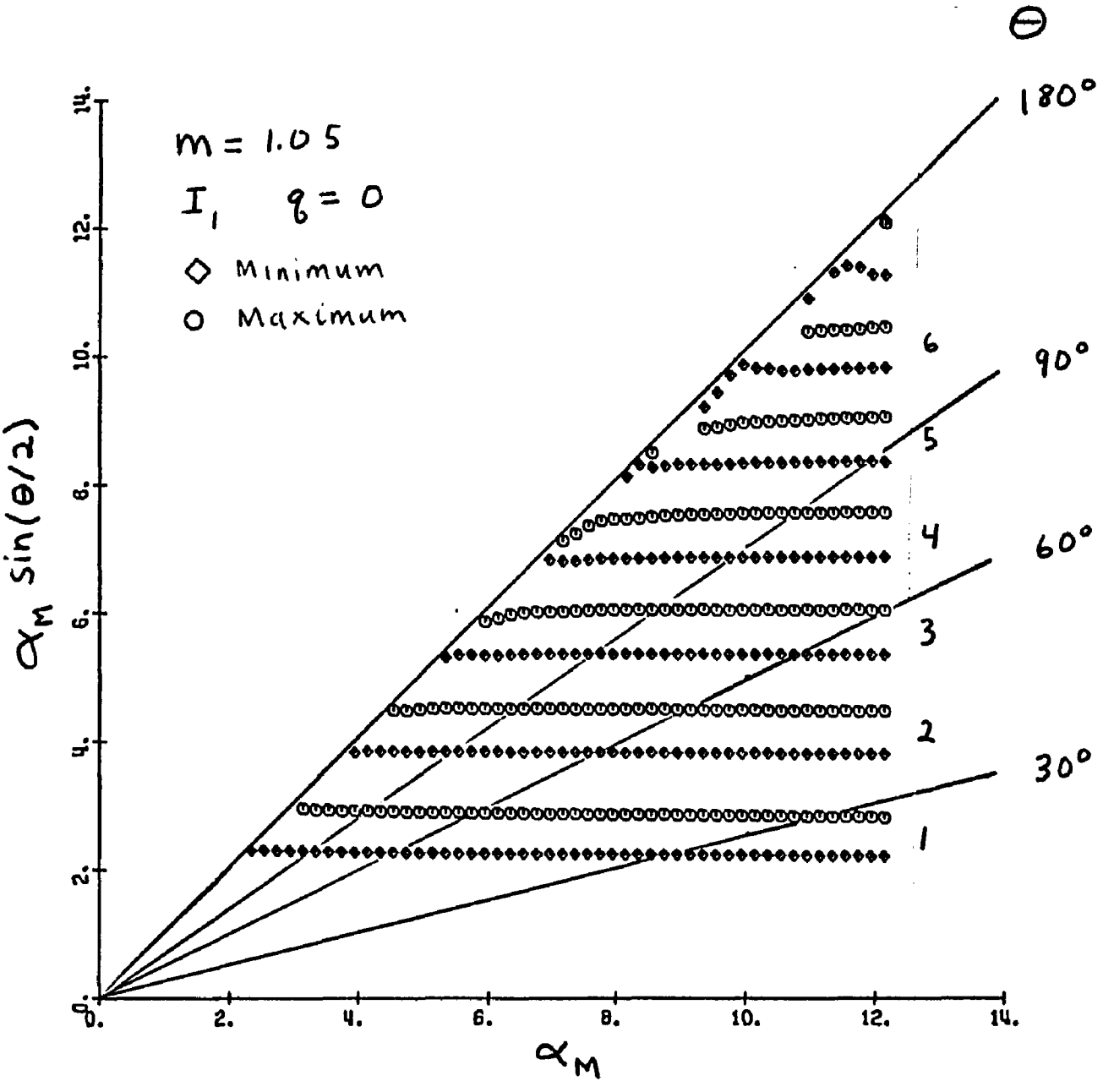

Fig. 73. Angular Location of I_1 Extrema for m=1.05 and q=0 Plotted as $\alpha \sin(\theta/2)$ Versus α

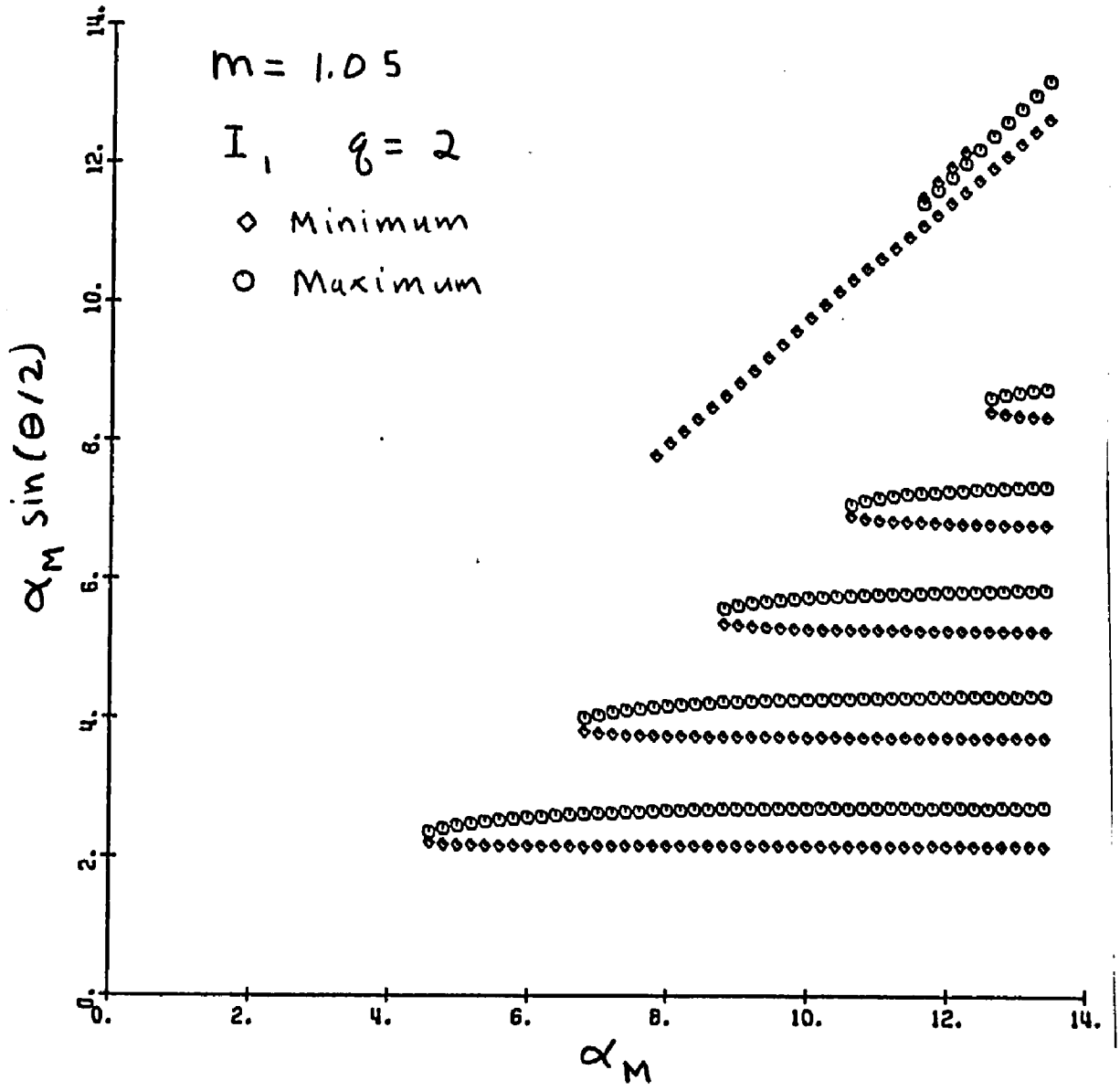

Fig. 74. Angular Location of I_1 Extrema for m=1.05 and q=2 Plotted as $\alpha\sin(\theta/2)$ Versus α

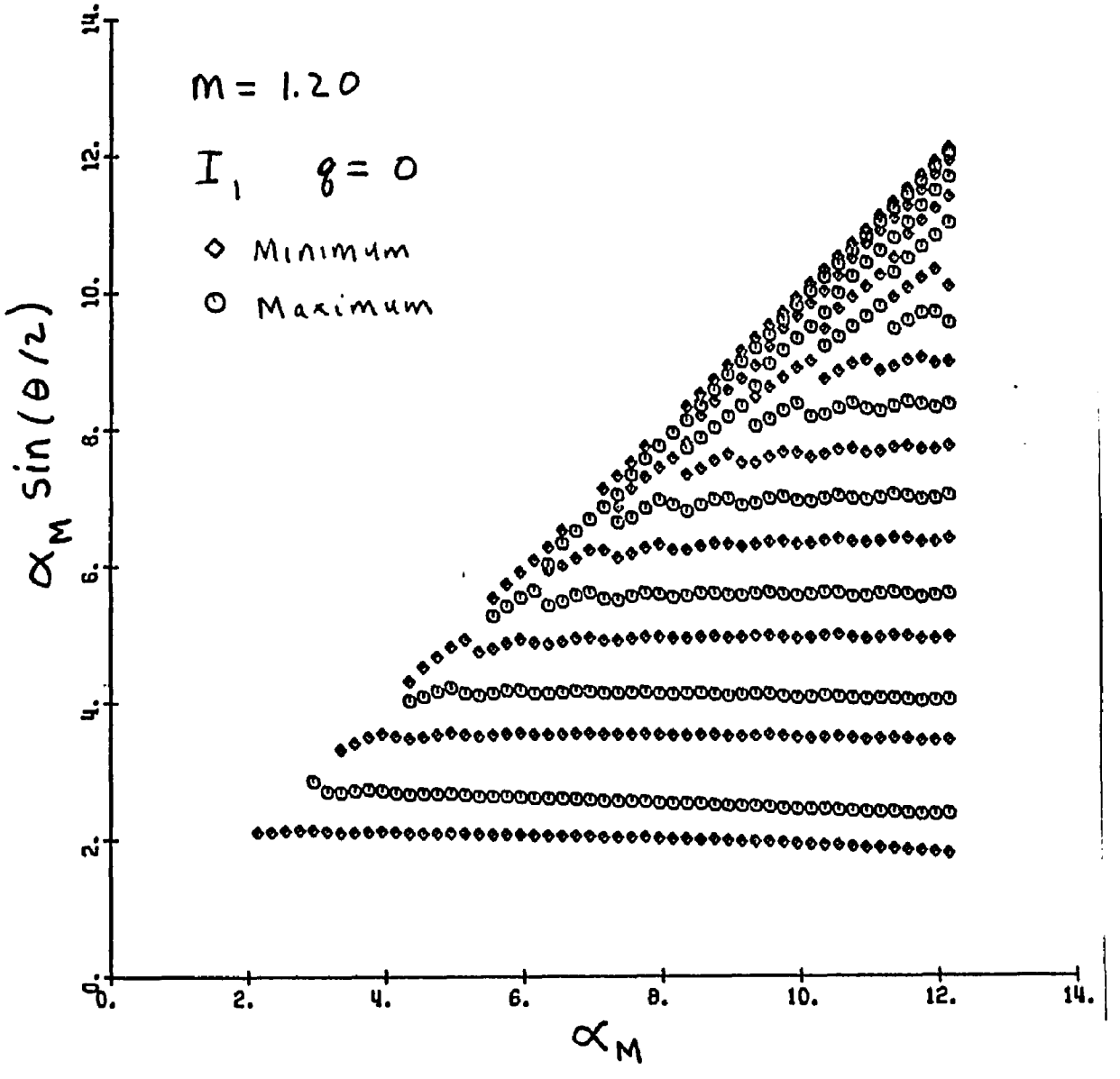

Fig. 75. Angular Location of I_1 Extrema for m=1.20 and q=0 Plotted as $\alpha \sin(\theta/2)$ Versus α

$\alpha \sin(\theta/2)$ values while maintaining the same spacing between the maxima and minima lines. Smaller values of $\alpha \sin(\theta/2)$ cause the extrema contours to migrate toward the forward direction at a faster rate with increasing particle size. In addition to the downward shift, the lines for the lower extrema orders have a larger negative slope compared to the corresponding lines for smaller m values. The magnitude of this negative slope decreases for the higher extrema orders. Figure 75 also shows a considerable increase in the number of extrema lines adjacent to the limiting diagonal. Note that the horizontal lines for the higher extrema orders show oscillations which indicate a contribution from the reflection system. When the heterodispersion is increased to q = 2 the diffractive extrema wash out at smaller particle sizes and the region corresponding to reflection increases. These trends are shown in Figure 76.

A similar analysis for m = 1.333 shows a continuation of the trends seen for m = 1.05 and m = 1.20. The I_1 extrema contour plots for m = 1.333 and q = 0 are shown in Figure 77. One can readily identify the first three extrema orders as diffraction extrema although the increasing orders show greater oscillations which indicate a reflection contribution. Beyond the third extrema pair (counting from the bottom) the oscillations are too great to identify the extrema as originating from diffraction. Note that the oscillations have a saw tooth pattern consisting of a series of small line segments. The slope of these line segments indicate that they originate from a reflection phenomenon. These line segments gradually merge into continuous lines for large particle sizes in the region close to the limiting diagonal (i.e., the backward direction).

In addition to the decreased region characterized

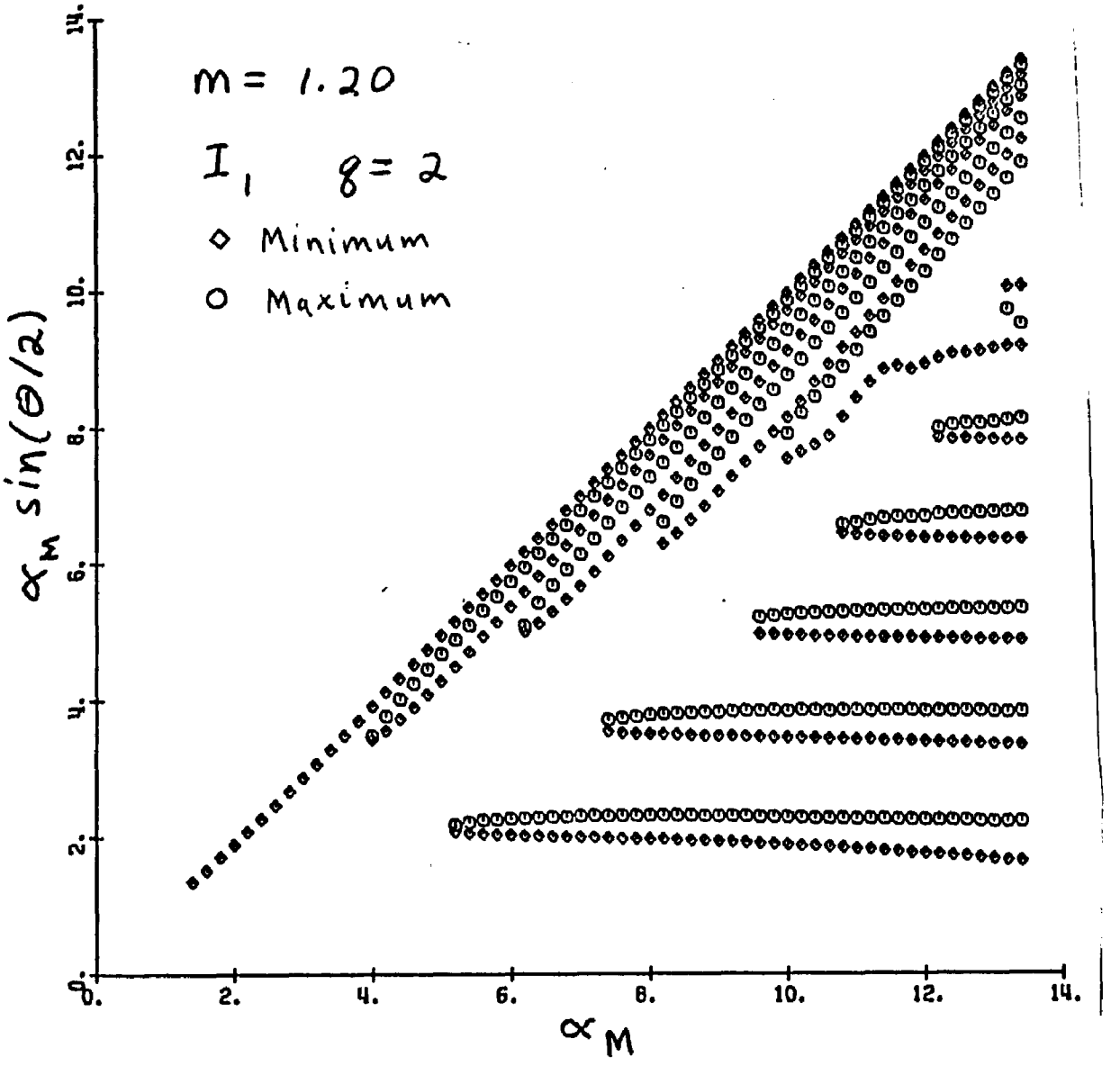

Fig. 76. Angular Location of I_1 Extrema for m=1.20 and q=2 Plotted as $\alpha \sin(\theta/2)$ Versus α

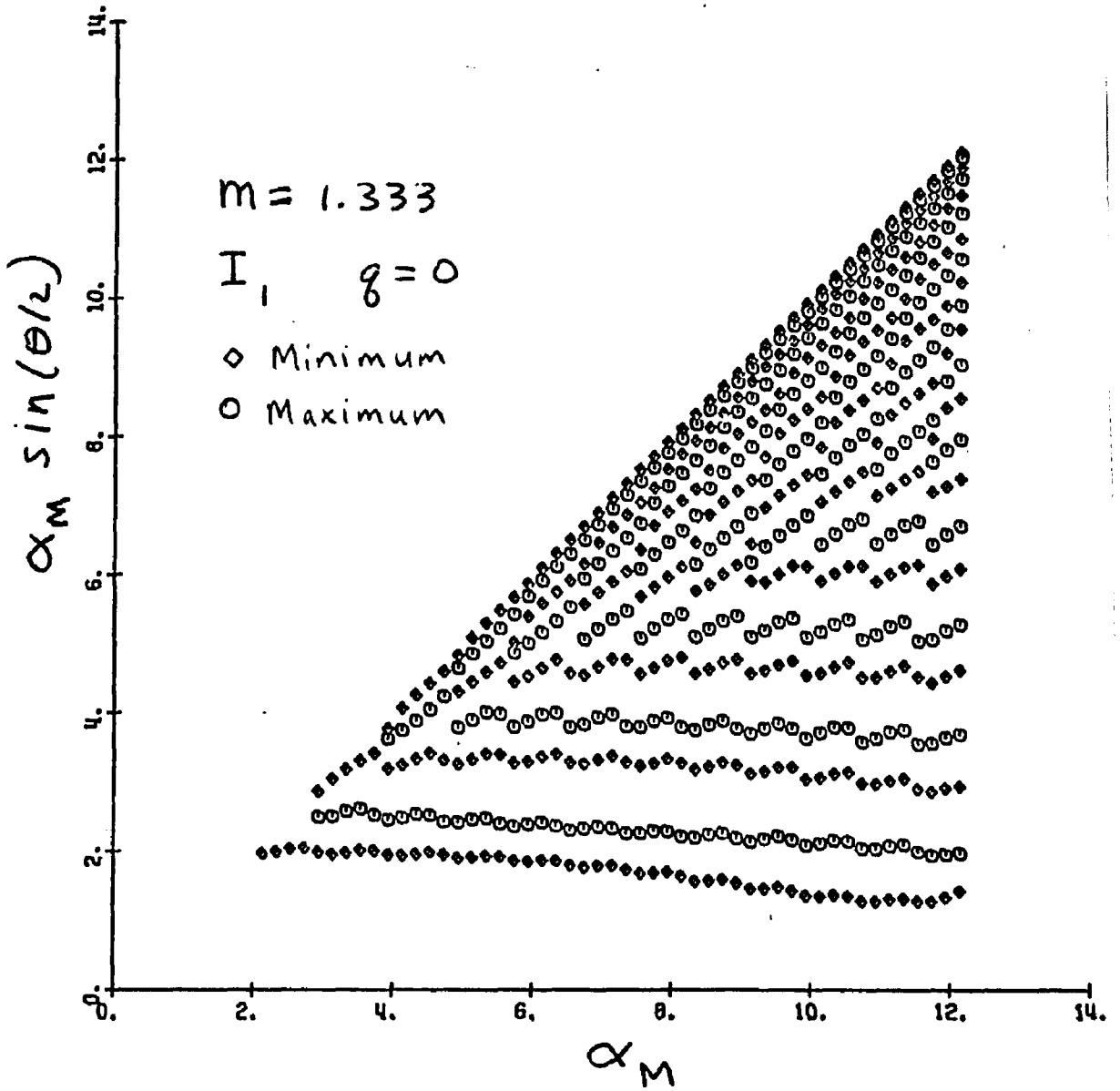

Fig. 77. Angular Location of I_1 Extrema for m=1.333 and q=0 Plotted as $\alpha\sin(\theta/2)$ Versus α

by diffraction. Figure 76 shows the shift of the three extrema pairs toward smaller $\alpha \sin(\theta/2)$ values compared to the corresponding curves from m = 1.20. The lower extrema orders also show a larger negative slope which drives the extrema even faster toward the forward direction. Note that the diffraction extrema curves now have a slight downward curvature. The curve for the lowest order minimum has, in addition, an upward bend around $\alpha_M = 12$ because it disappears with the first order maximum shortly after. Increasing the heterodispersion to q = 1 in Figure 78 smooths out the oscillations in the extrema curves and allows a better identification of the diffraction extrema. The disappearance of the first extrema pair is clearly seen. Figure 79 shows that a further increase in the heterodispersion to q = 2 washes out the diffraction extrema at smaller particle sizes.

b. Empirical Extensions of the RGD Theory

Plotting the extrema contours on graphs of $\alpha \sin(\theta/2)$ versus α also allows one to obtain empirical corrections to the RGD theory in addition to readily identifying the diffraction extrema. Patitsas[21] had previously plotted I_1 extrema in this fashion to obtain empirical equations for monodisperse distributions. He tried to fit all of the extrema to a series of straight lines. As seen in Figures 73, 75 and 77 straight line fits are possible for the diffractive extrema. However, these lines would not fit the extrema in the backward direction. Patitsas found that replacing $\alpha \sin(\theta/2)$ with $\alpha(\theta/2)$ would prevent the extrema in the backward direction from turning downwards at small α values and thereby allow a better fit of the data.

A more accurate approach to obtaining empirical equations from the extrema would treat the diffraction and reflection systems

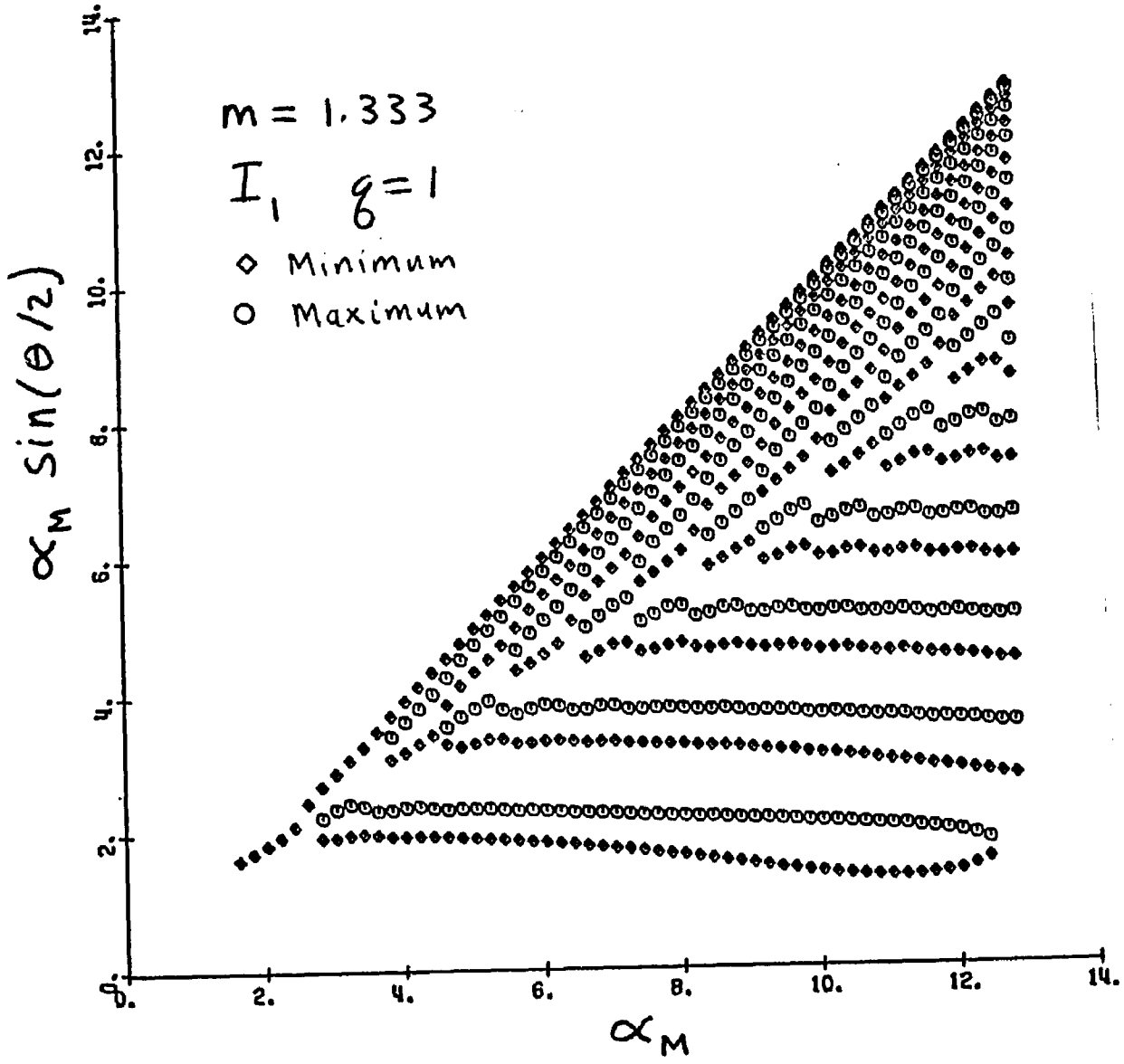

Fig. 78. Angular Location of I_1 Extrema for m=1.333 and q=1 Plotted as $\alpha\sin(\theta/2)$ Versus α

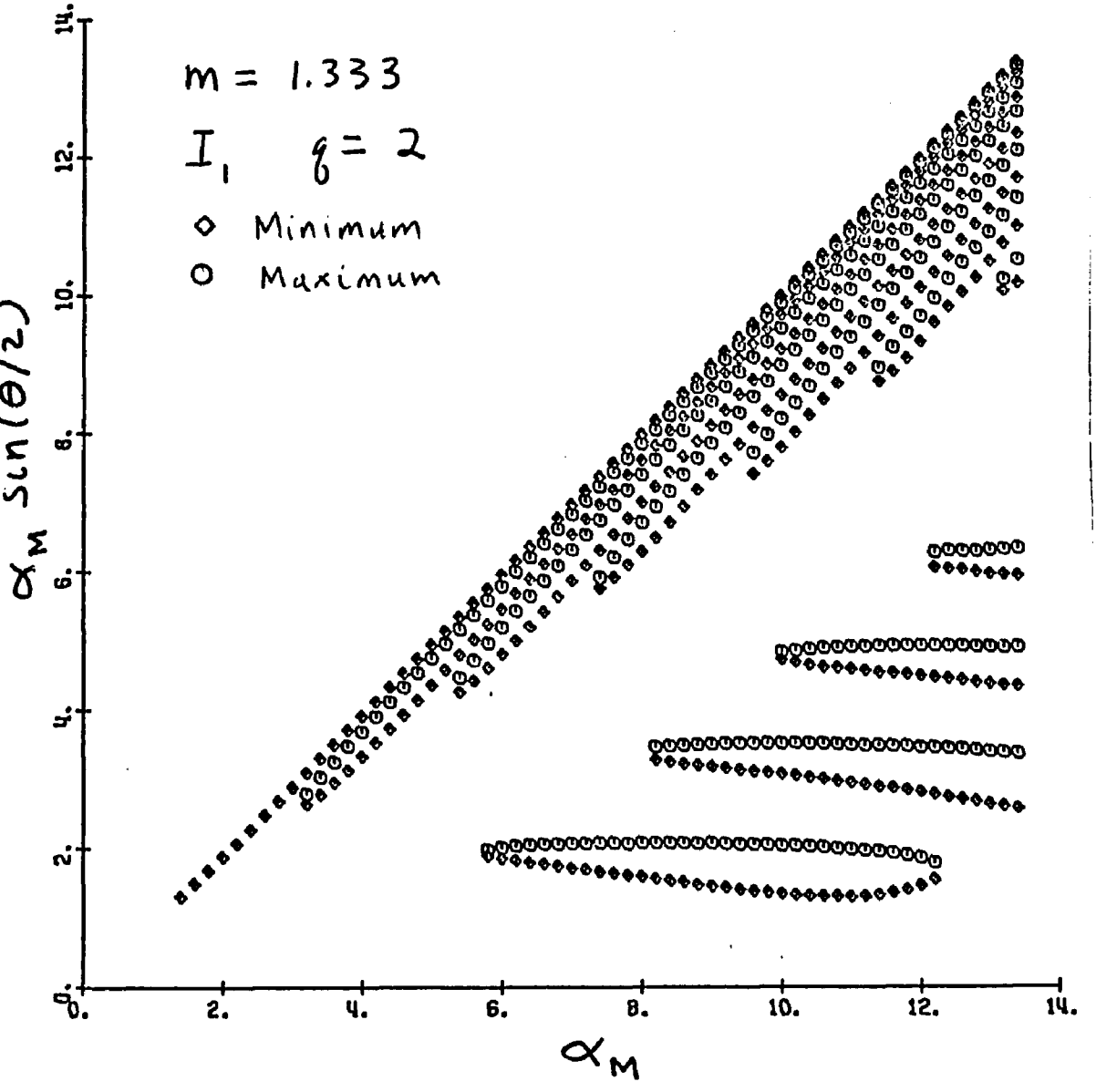

Fig. 79. Angular Location of I_1 Extrema for m=1.333 and q=2 Plotted as $\alpha\sin(\theta/2)$ Versus α

separately. Based on the trends observed for the diffraction extrema from monodisperse systems one can write the following equation

$$\alpha \sin(\theta/2) = K_{0i} - K_{1i} \tag{18}$$

where i is the order of the extrema

K_{oi} and K_{1i} are empirical constant.

The constant K_{oi} increases with the order i and generally decreases with increasing m. In the limit of m = 1.00, these constants equal the RGD values shown in the paper by Heller and Nakagaki[11]. The constant K_{1i} decreases with increasing i and increases with increasing m. A family of equations can therefore be described by specifying the constants K_{0i} and K_{1i}. Table IV shows the values of the constants for the first order minima and maxima for m = 1.05, 1.20 and 1.333. The values of these constants were determined from Figures 73, 75 and 77.

More detailed calculations were then made using conventional least squares fitting techniques to determine the coefficients K_{0i} and K_{1i} in equation 18. The results of the calculations are shown in Figures 80 and 81 for the angular minima. Similar results are seen for the corresponding maxima. Figure 80 shows the value of the coefficients K_{oi} for the extrema orders from i = 1 to 5 plotted against the relative refractive index. In general, the data shows a linear relationship with increasing m. However, there is an increasing scatter for the higher orders and larger relative refractive indexes that result from the larger oscillations in the extrema contours. Also note that the extrapolations to m = 1.00 have systematically smaller values than the RGD values. The The reason for this is not known.

TABLE IV

Empirical Constants for Equation 18

	Minimum		Maximum	
m	K_{01}	K_{11}	K_{01}	K_{11}
1.05	2.38	.013	3.00	.016
1.20	2.25	.031	2.88	.042
1.333	2.31	.093	2.81	.068

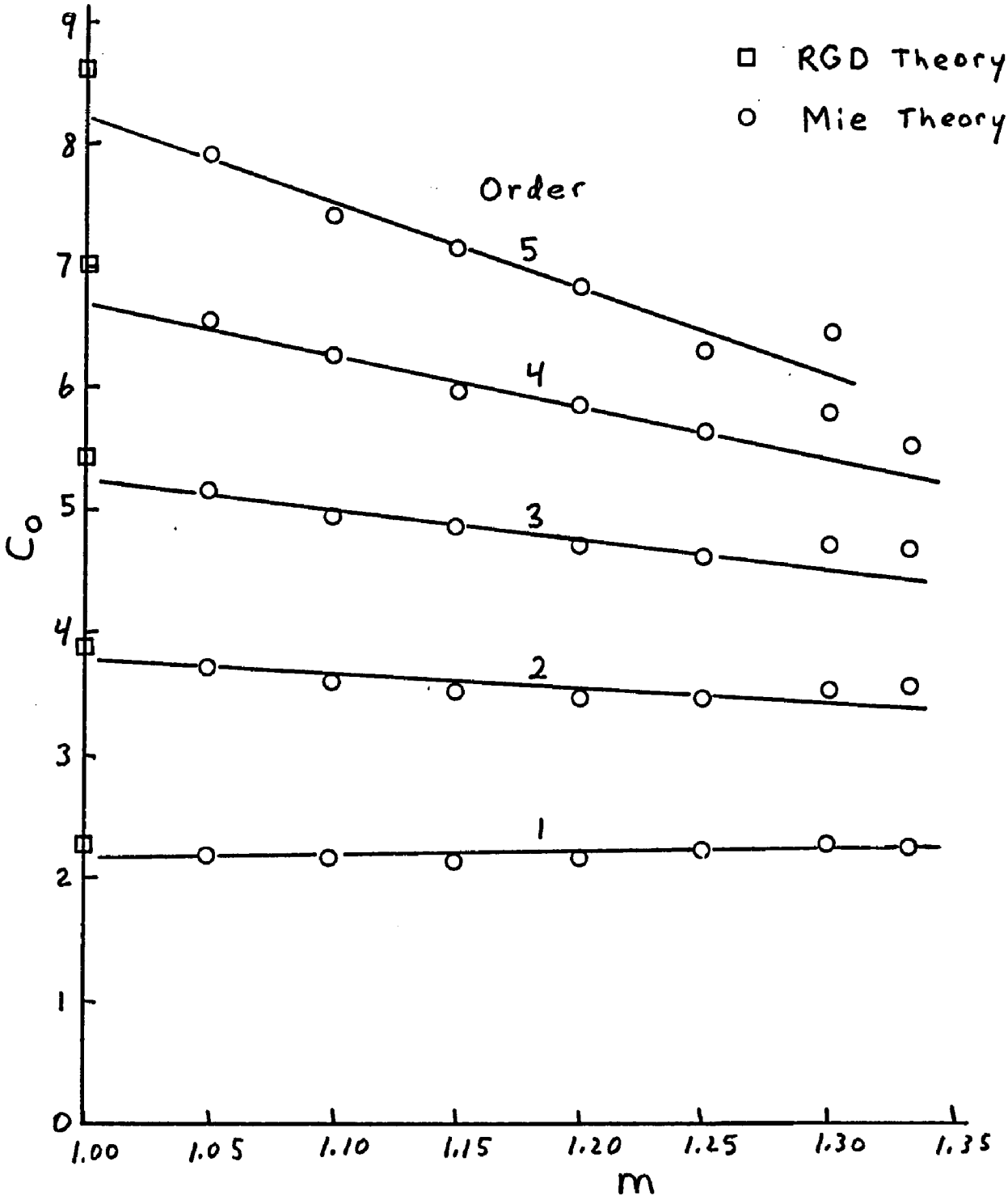

Fig. 80. Values of the Coefficient K_{oi} in Equation 18 for Intensity Minima of Order i=1 to 5 As a Function of m

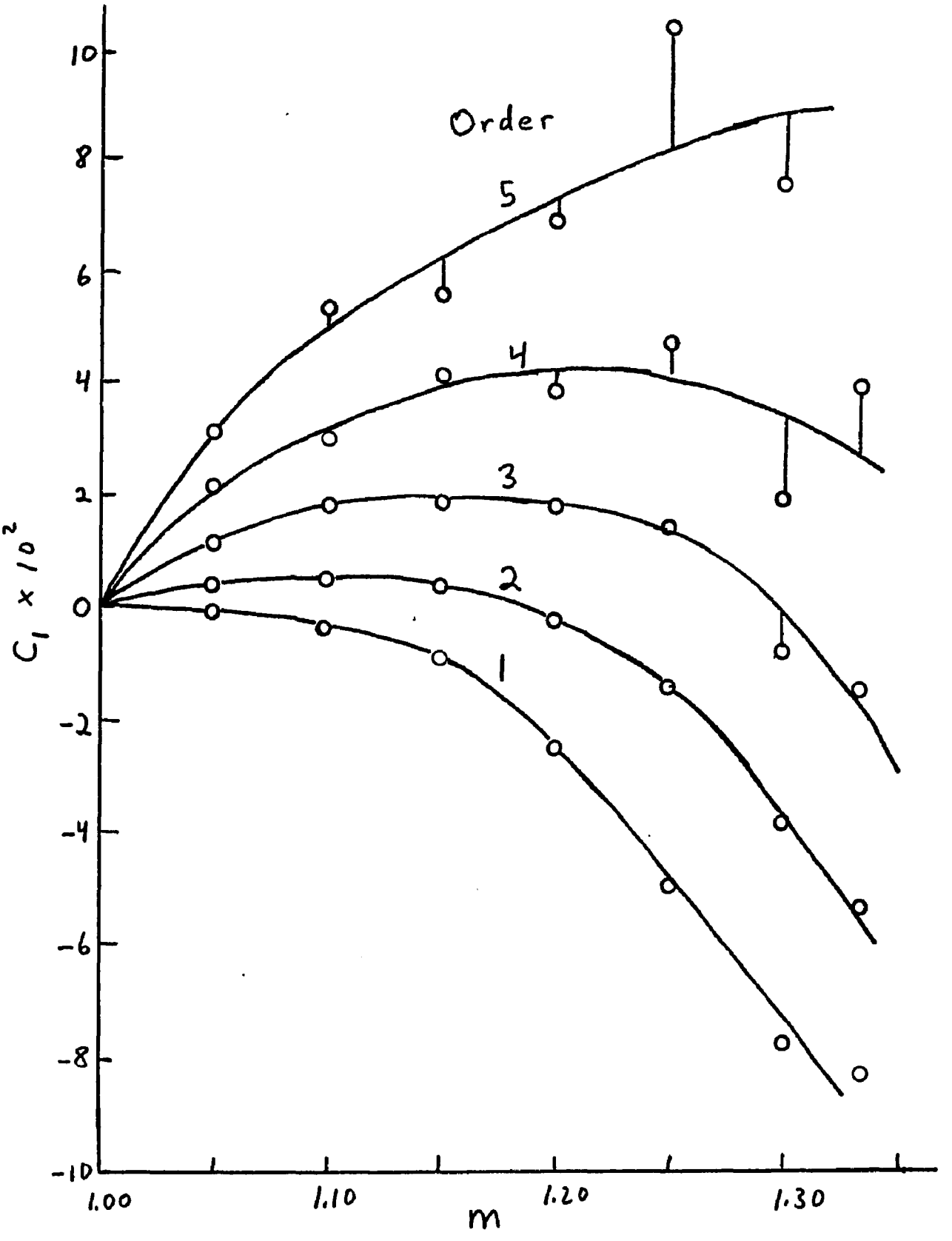

Fig. 81. Values of the Coefficient K_{1j} in Equation 18 for Intensity Minima of Order i=1 to 5 as a Function of m

Figure 81 shows the coefficients K_{1i} for extrema orders from i = 1 to 5 plotted against the relative refractive index. This data shows a quadratic behavior and has a considerable amount of scatter for the higher extrema orders. Note that all of the curves extrapolate to zero as the relative refractive index approaches 1.00. This follows because the extrema in the RGD theory obeys equation 1 exactly. The values of the coefficients in Figure 81 were determined from the slope of the extrema contours when plotted as shown in Figures 73 - 79. However, these extrema contours have a small curvature which can affect the slope of a linear approximation. Since the high extrema orders have a much smaller size range for obtaining an average slope, it is possible that the coefficient values for the higher orders in Figure 81 are too high.

To resolve this problem, equation 17 was modified by adding the term $K_{2i}\alpha^2$ and performing a least squares fit on the extrema contours using the modified equation. Although the resulting equations fit the data much better, the behavior of the coefficients was complicated and did not lend itself to a general equation. The extrema contours would then be described by a large number of empirical equations. Alternatively a series of coefficients could be tabulated as shown in Table IV.

A theoretical explanation of the observed size dependence in equation 18 was then made using Van De Hulst's[28] theory on anomalous diffraction. He had shown that the scattered intensity for values of α (m - 1) that were larger than permitted in the RGD theory was given by

$$i = 2\pi\alpha^6 (m - 1)^2 \frac{J_{3/2}^2 (Y)}{Y^3} \tag{19}$$

where $$Y = 2\alpha [(m - 1)^2 + \sin^2 (\theta/2)]^{1/2} \tag{20}$$

and $J_{3/2}$ is the Bessel function of order 3/2. Equation 19 thus represents the scattering from systems that show small deviations from the RGD theory. The RGD theory is given by equations 21 and 22.

$$i = 2\pi\alpha^6 (m - 1)^2 \frac{J_{3/2}^2 (U)}{U^3} \tag{21}$$

where $$U = 2\alpha \sin (\theta/2). \tag{22}$$

As shown previously by Heller and Nakagaki[11], the contours of the minimum intensities for the RGD theory occur at the zeros of the Bessel function while the contours of the maximum intensities occur at the zeros of the Bessel function derivative. In both cases the extrema contours are determined by

$$U = K_i = 2\alpha \sin (\theta/2) \tag{23}$$

where the constant K_i is the appropriate zero of the Bessel function or its derivative. In a similar fashion it can be shown that the extrema contours from equation 19 are determined by

$$Y = K_i = 2\alpha [(m - 1)^2 + \sin^2 (\theta/2)]^{1/2} \tag{24}$$

where K_i has the same value as in equation 23. Rearranging equation 24 one has

$$\alpha \sin (\theta/2) = [K_i^2/4 - \alpha^2 (m - 1)^2]^{1/2} \qquad (25)$$

Comparing this theoretical equation with equation 18 obtained from empirical fits shows several common features. The most significant of these features is the decrease in $\alpha \sin (\theta/2)$ with increasing α. Equation 25 also predicts the observed increase in the empirical constant K_{1i} with increasing m. However, it does not show the effect of the higher orders on K_{1i}. Since K_i in equation 25 is comparable to K_{0i} in equation 18, the two equations will also show similar trends for these parameters.

Although equation 25 shows many of the trends seen in equation 18, it does not give a quantitatively correct result. Equation 25 predicts an extremum migration toward the forward direction with increasing particle size that is much greater than actually occurs. This can be seen by determining the size α at which the right side of equation 25 goes to zero. Thus for m = 1.20 and $K_i = 2.25$ the first minimum will reach $\theta = 0^\circ$ when the particle size reaches $\alpha = 5.6$. In contrast, equation 18 shows a slightly slower rate of forward migration with increasing particle size than actually occurs. For example, for m = 1.20 at $\alpha = 15$, the first minimum has moved to $\theta = 11.7^\circ$ while equation 18 predicts only $\theta = 13.6^\circ$. The agreement of equation 18 is much better at smaller particle sizes. At $\alpha = 5$ and 10, equation 18 predicts the first minimum to be at $\theta = 47.8^\circ$ and 21.9° respectively. The exact

Mie calculations predicts that the first minimum will be at $\theta = 47.9^{o}$ and 21.8^{o} respectively.

c. Variation in Trends Due to Different Polarizations

The previous analysis of the diffraction extrema were all based on the extrema contours for I_1. However, as pointed out in the beginning of this Section the diffraction extrema from I_1, I_2 and I_u are very similar. The trends observed for I_1 will therefore also apply to the diffraction extrema for I_2 and I_u. Recall that the I_1 maxima and minima contours for a given extrema order serve as a boundary in which the extrema for I_2 and I_u are contained. The extrema for I_2 have two additional features that affect the appearance of the diffraction extrema: the shallow extrema and the Rayleigh minimum. The very shallow I_2 extrema from monodisperse systems have the appearance of I_1 extrema that are washed out from heterodispersion. It was previously shown that the shallow I_2 extrema were caused by the Rayleigh minimum.

These two features of the I_2 extrema contours result in a deviation from the pattern seen previously in Figures 73-79 for the diffraction extrema. Figure 82 shows the I_2 extrema for m = 1.05 and q = 0 plotted as $\alpha \sin(\theta/2)$ versus α. The Rayleigh minimum is seen as a series of diagonal line segments close to the 90^{o} line and divides the extrema pattern into two parts. The diffraction extrema in the bottom portion of the graph have the appearance of the corresponding I_1 extrema shown in Figure 74 for q = 2. Note that the extrema in the upper portion of the graph are approximately horizontal lines indicating a contribution from diffraction. Increasing the heterodispersion to q = 2 in Figure 83

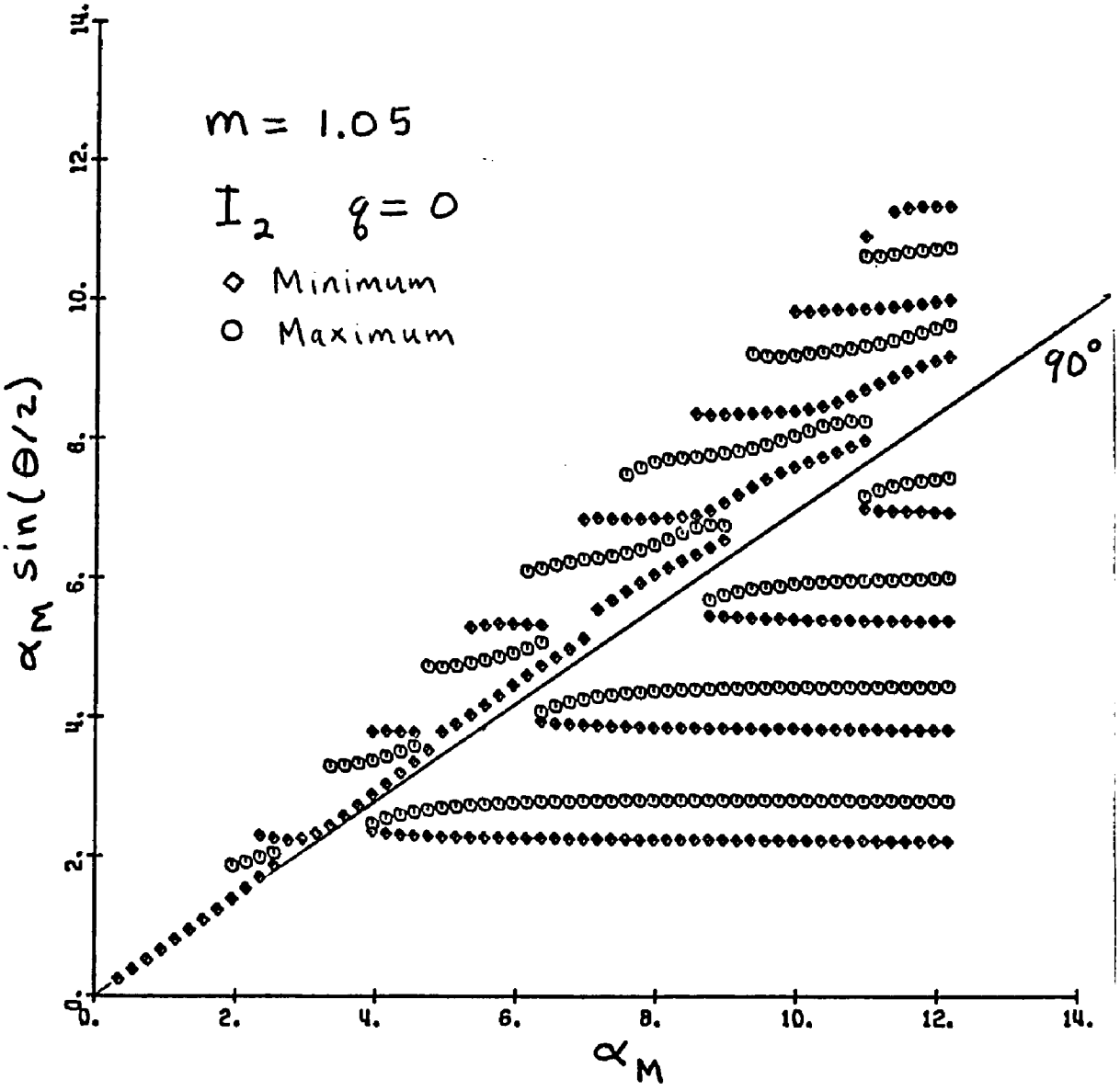

Fig. 82. Angular Location of I_2 Extrema for m=1.05 and q=0 Plotted as $\alpha \sin(\theta/2)$ Versus α

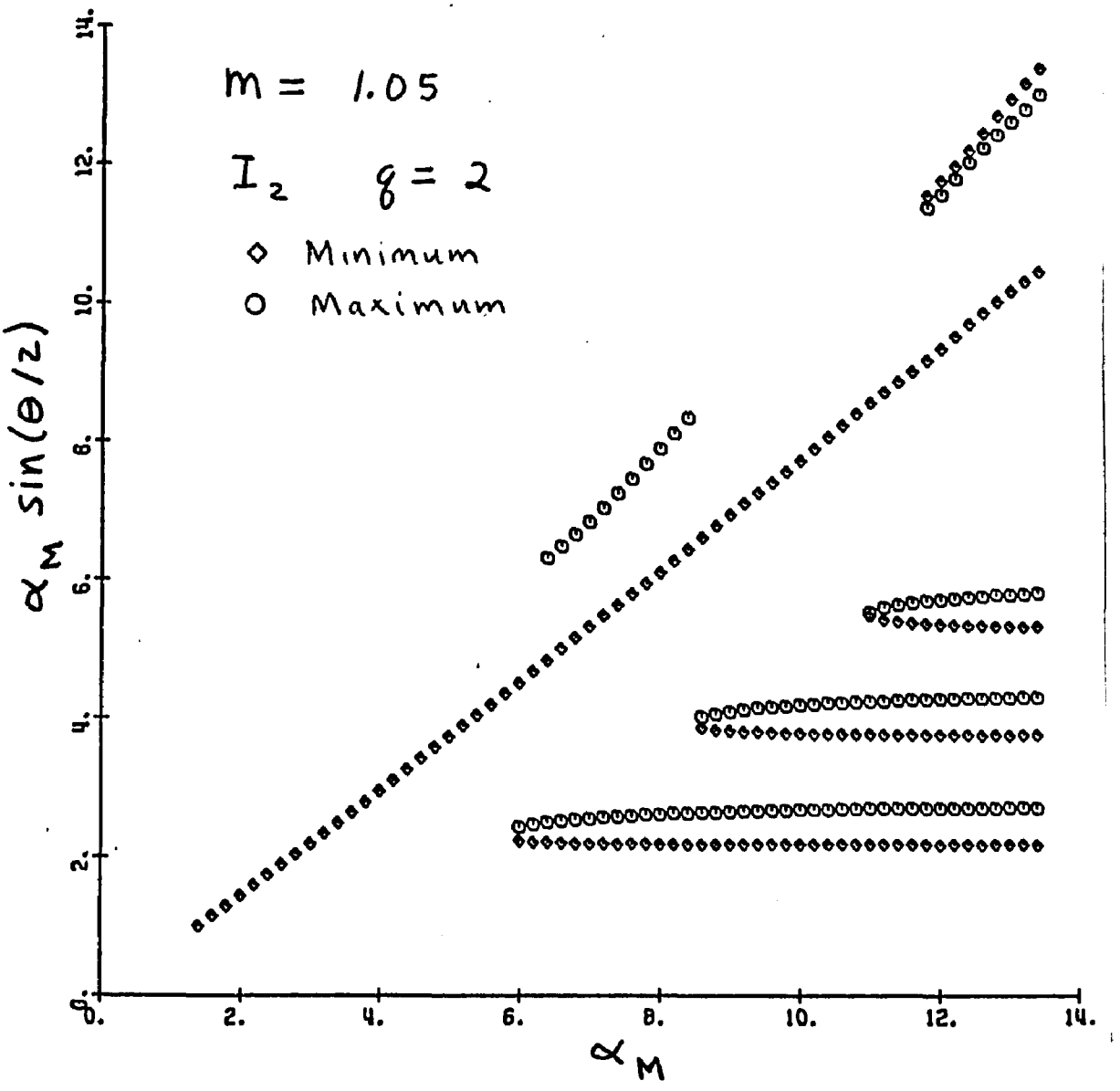

Fig. 83. Angular Location of I_2 Extrema for m=1.05 and q=2 Plotted as $\alpha\sin(\theta/2)$ Versus α

shows the typical behavior seen previously for the I_1 extrema except for the additional line from the Rayleigh minimum.

The Rayleigh minimum becomes less apparent for the higher relative refractive indexes and is generally seen only at the small particle sizes. Figure 84 and 85 show the monodisperse I_2 extrema contours for m = 1.20 and m = 1.333 respectively. The diffraction extrema in both cases show the typical washed out pattern. Note that Figure 84 has several extrema pairs in the backward direction that behave like diffraction extrema. However these extrema also show a strong reflection trend and wash out as the heterodispersion increases. The I_2 extrema show the same general pattern for increasing heterodispersion as seen previously for the I_1 extrema and therefore do not require separate figures. In addition, no separate figures will be shown for the I_u extrema contours because they are nearly identical to those seen for I_1 in Figures 73-79.

d. Explaining the Disappearance of the Extrema Pairs in the Forward Direction

In classifying the RGD theory as a diffraction it is important to note that the Fraunhoffer diffraction is only a portion of the total scattering process whereas the RGD theory (within its region of validity) describes the entire scattering process. Additional terms must therefore be included with the Fraunhoffer diffraction to describe the total scattering. Using arguments based on geometric optics, Hodkinson and Greenleaves[49] have shown that the scattering of light in the forward direction from a particle size distribution of α_M = 10 to 15 can be approximated by the diffraction of light passing near the particle and

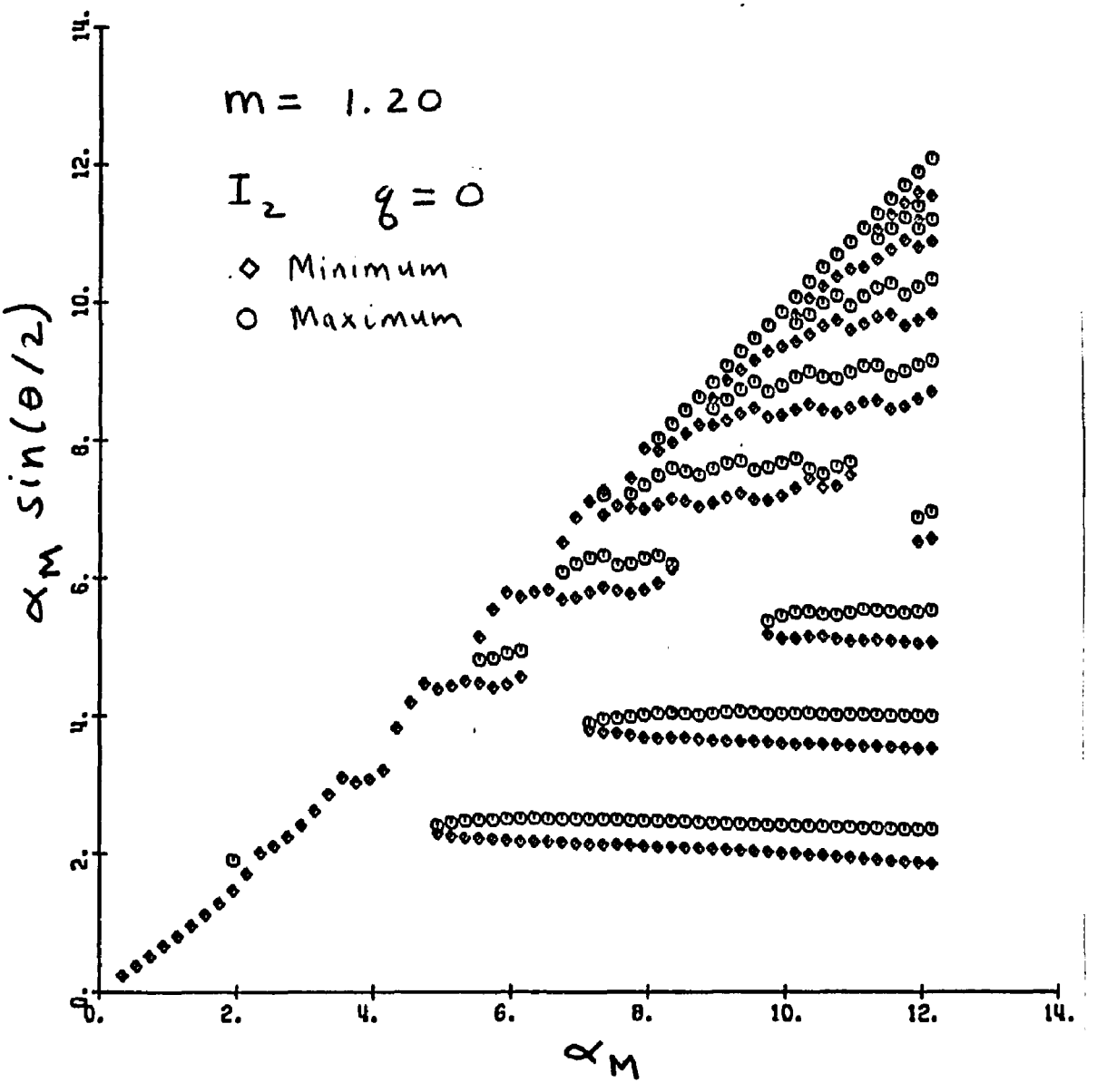

Fig. 84. Angular Location of I_2 Extrema for m=1.20 and q=0 Plotted as $\alpha \sin(\theta/2)$ Versus α

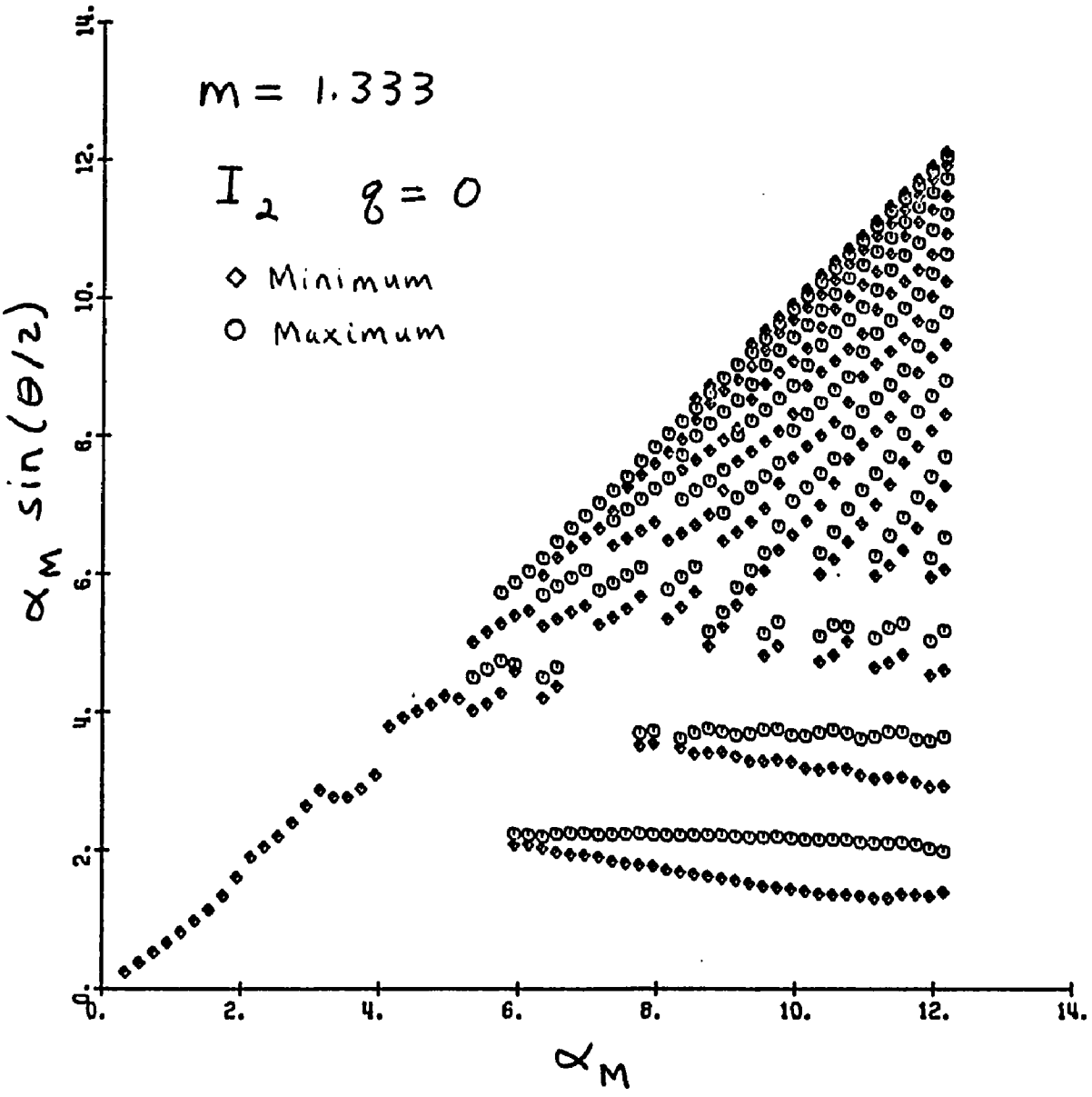

Fig. 85. Angular Location of I_2 Extrema for m=1.333 and q=0 Plotted as $\alpha\sin(\theta/2)$ Versus α

the transmission and reflection of light striking the particle. Although the Mie theory gives the correct light scattering results, it does not allow a separation of the total scattering into light diffracted by and incident on the particle.

However such a separation of the total light scattered can be approximated in a similar manner shown by Hodkinson and Greenleaves[49]. This approach describes the total light scattered as the sum of the light incident on the particle and the light diffracted by the particle. Since the diffracted light makes a negligible contribution to the total scattered light at larger angles, the total scattering is then approximated by the light incident on the particle. Instead of using geometrical optics for this scattering, a better approximation would be to use the RGD theory or an empirically improved RGD equation. The scattering in the forward direction would then be obtained by adding the Fraunhoffer diffraction term.

This type of approximation was used to successfully predict the merging and disappearance of the extrema in the forward direction. The intensity of the light scattered by a particle is approximated by

$$I = I_s + I_D \tag{26}$$

where I_s is the scattering from light striking the particle

I_D is the light diffracted by the particle

The scattering from the light striking the particle can be approximated by the RGD theory while the light diffracted by the particle is described by Fraunhoffer diffraction.

Both the RGD theory and the Fraunhoffer diffraction theory show maxima and minima that migrate toward the forward direction as the particle size increases. However the extrema from the RGD theory migrate at a faster rate toward the forward direction than the corresponding extrema from the Fraunhoffer diffraction. A particle size is eventually reached where the extrema curve from the two systems intersect. Since this intersection occurs close to the forward direction, the diffracted light makes a significant contribution to the total light scattered. One can then use arguments related to the Rayleigh criterion for resolving two overlapping diffraction patterns to predict where the first extrema pair disappears. According to the Rayleigh criterion, two overlapping diffraction patterns are no longer resolvable when the center of one Airy disk falls on the first minimum of the other Airy pattern. A similar approach shows that the first extrema pair in the forward direction disappears when the first maximum of the RGD theory falls on the first minimum of the Fraunhoffer diffraction theory.

The gradual change in the total scattering intensity as the first maxima and minima pair disappear in the forward direction is seen in Figure 86. This figure shows the scattered intensity using Mie theory calculations plotted against the angle of observation for several different particle sizes ranging from $\alpha = 15$ to $\alpha = 21$. The range of particle size and angular distribution corresponds to the region in Figure 46 where the first extrema pair disappears in the forward direction. Assuming that equation 26 is a good approximation for interpre-

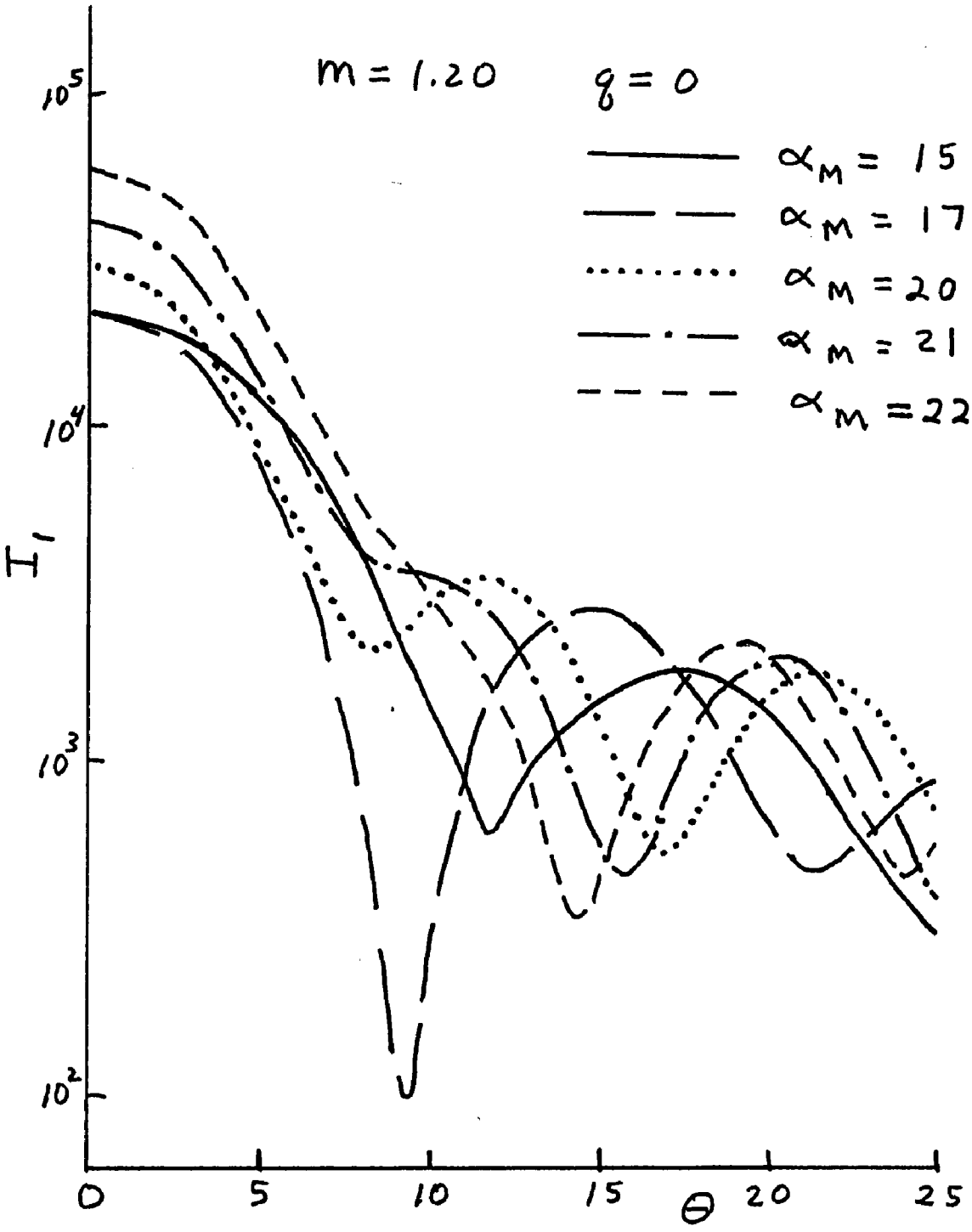

Fig. 86. Scattered Intensity I_1 as a Function of Angle for Different Monodisperse Distributions in the Size Range Where the First Extrema Pair Disappears

ing the actual scattering curves, one can follow the migration of the first extrema pair toward the forward direction.

Figure 86 shows that as the particle size increases from $\alpha = 15$ to $\alpha = 17$ the first extrema pair shifts to smaller angles and the minimum becomes much deeper. The very large decrease in the minimum occurs when the minimum for I_s coincides with the minimum for I_D. Increasing the particle size to $\alpha = 20$ shows the first minimum becoming very shallow. Note that the maximum has shifted 3.1° toward the forward direction while the minimum has only shifted 1°. These observations are consistent with the minimum for I_s moving past the minimum for I_D and into the range where I_D has a very rapid rise in intensity. Increasing the particle size to $\alpha = 21$ shows only an inflection point since the maximum of I_s now lies on the minimum of I_D. Further increase in particle size gradually reduces the inflection point to a small bend in the curve and then disappears as the first extrema pair moves into the first lobe of the diffraction pattern.

The explanation for the first extrema pair washing out was then tested using equation 18 to describe the extrema migration for I_s and the Fraunhoffer diffraction theory to describe the extrema migration for I_D. The first minimum contour for the Fraunhoffer diffraction theory is given by

$$\alpha \sin \theta = 3.83 \tag{27}$$

combined with equation 18 one has two equation in two unknowns.

$$\alpha \sin (\theta/2) = K_{oi} - K_{1i} \tag{18}$$

Since the extrema pairs wash out very close to the forward direction one can approximate sin with its argument. Eliminating the angle θ from the two

equations, one has

$$\alpha_{Max} = (K_{0i} - 1.915)/K_{1i} \qquad (28)$$

The values of K_{0i} and K_{1i} must correspond to the maxima contours.

Using the constants shown in Table IV in equation 28 one can predict that the first order extrema disappear at α = 67.8, 23.0 and 13.2 for m = 1.05, 1.20 and 1.333 respectively. The Mie calculations in the present study show that the first order extrema for m = 1.20 and 1.333 disappear at α = 20.6 and 12.5 respectively. No calculations were available to determine the size at which the first order extrema disappear for m = 1.05. However, the close agreement between the predicted and actual disappearance of the extrema in the forward direction indicates that the proposed explanation represents a reasonable approximation.

A comparison of Figures 46 and 56 for m = 1.20 and Figures 50 and 60 for m = 1.333 indicate that the extrema disappearance is independent of the polarization of the incident light. In addition Patitsas[21-23] has shown that the higher extrema orders also disappear in the forward direction in a systematic fashion. The continued disappearance of the higher order extrema pairs is not surprising since the rate of migration of the I_s extrema pair toward the forward direction is faster than the migration of the diffraction extrema. A particle size is eventually reached where the I_s extrema overtake the diffraction extrema and disappear in the manner previously outlined.

2. Backward Scattering Described in Terms of Reflection

a. General Description

The interpretation of the extrema that migrate toward the

backward direction in terms of a reflection phenomenon was first proposed by Penndorf[33]. Kerker[3] has reviewed a number of other investigations that have explained the scattering at $\theta = 180^{o}$ in terms of reflection using geometrical optics. These studies showed a remarkably good agreement between the backscatter from geometrical optics and that from the Mie theory even for the very small particle sizes where geometrical optics is generally not considered applicable. However the investigations reviewed by Kerker did not consider the angular variation of the scattered intensity in the backward direction.

Penndorf[33] reasoned that a portion of the light scattered in the forward direction undergoes a reflection when crossing the particle surface. If the scattered intensity in the forward direction has a maximum characterized by a constant $\alpha \sin\theta$ value then there will also be an intensity maximum in the backward direction having a constant $\alpha \sin(\pi - \theta)$ value. Increasing the particle size α will then cause the maximum in the forward direction to move farther into the forward direction while the maximum in the backward direction moves farther into the backward direction. Penndorf had shown that the diffraction extrema were seen in plots of $\alpha \sin\theta$ versus α as curves having approximately constant $\alpha \sin\theta$ values. In a similar fashion the reflection extrema were seen in plots of $\alpha \sin(\pi - \theta)$ versus α as curves approximately constant $\alpha \sin(\pi - \theta)$ values.

The present investigation also interpreted the extrema that migrate toward the backward direction with increasing particle size in terms of a reflection phenomenon. However instead of using $\alpha \sin(\pi - \theta)$ to describe the contours of these extrema the present investigation used $\alpha \sin[(\pi - \theta)/2]$. This term was used because the diffraction extrema in the present study were described by the RGD theory where the extrema contours

have constant $\alpha \sin(\theta/2)$ values instead of the Fraunhoffer diffraction theory where the extrema contours have constant $\alpha \sin\theta$ values. A reflection of the diffraction extrema at the particle surface will therefore result in extrema having constant $\alpha \sin[(\pi-\theta)/2]$ or $\alpha \cos(\theta/2)$ values. Reflection extrema will then be seen in plots of $\alpha \cos(\theta/2)$ versus α as curves having constant values of $\alpha \cos(\theta/2)$. Patitsas[22] had previously shown that the extrema contours in the backward direction for large particles having large relative refractive indexes can be described by constant values of $\alpha \sin[(\pi-\theta)/2]$. Unfortunately he treats this observation only as a convenient empirical relation for describing the extrema contours in the backward direction. He does not recognize the significance of constant values in terms of a reflection pehnomenon.

Figures 87-92 show the I_1 extrema contours plotted on graphs of $\alpha \cos(\theta/2)$ versus α for the range of m and q values considered in the present investigation. The graphs are similar to those seen previously for the diffraction extrema in that the extrema data appears only in the lower triangle. However the limiting line is now defined as $\alpha \cos(\theta/2) = \alpha$ and represents $\theta = 0^{\circ}$. The lines representing other angles are shown in Figure 87. Note that the sequence of angles is now reversed for the reflection plots compared to the diffraction plots. The diffraction extrema will now be seen as inclined lines while the reflection extrema will be seen as horizontal lines. Figure 87 shows that the extrema contours for m = 1.05 and q = 1 have no reflection extrema since all of the lines have large slopes and represent diffraction extrema. The lack of any reflection extrema is not surprising because of the low m value. Increasing the heterodispersion to q = 2 in Figure 88 washes out many of the diffraction extrema and shows the emergence of reflection extrema for the larger particle sizes.

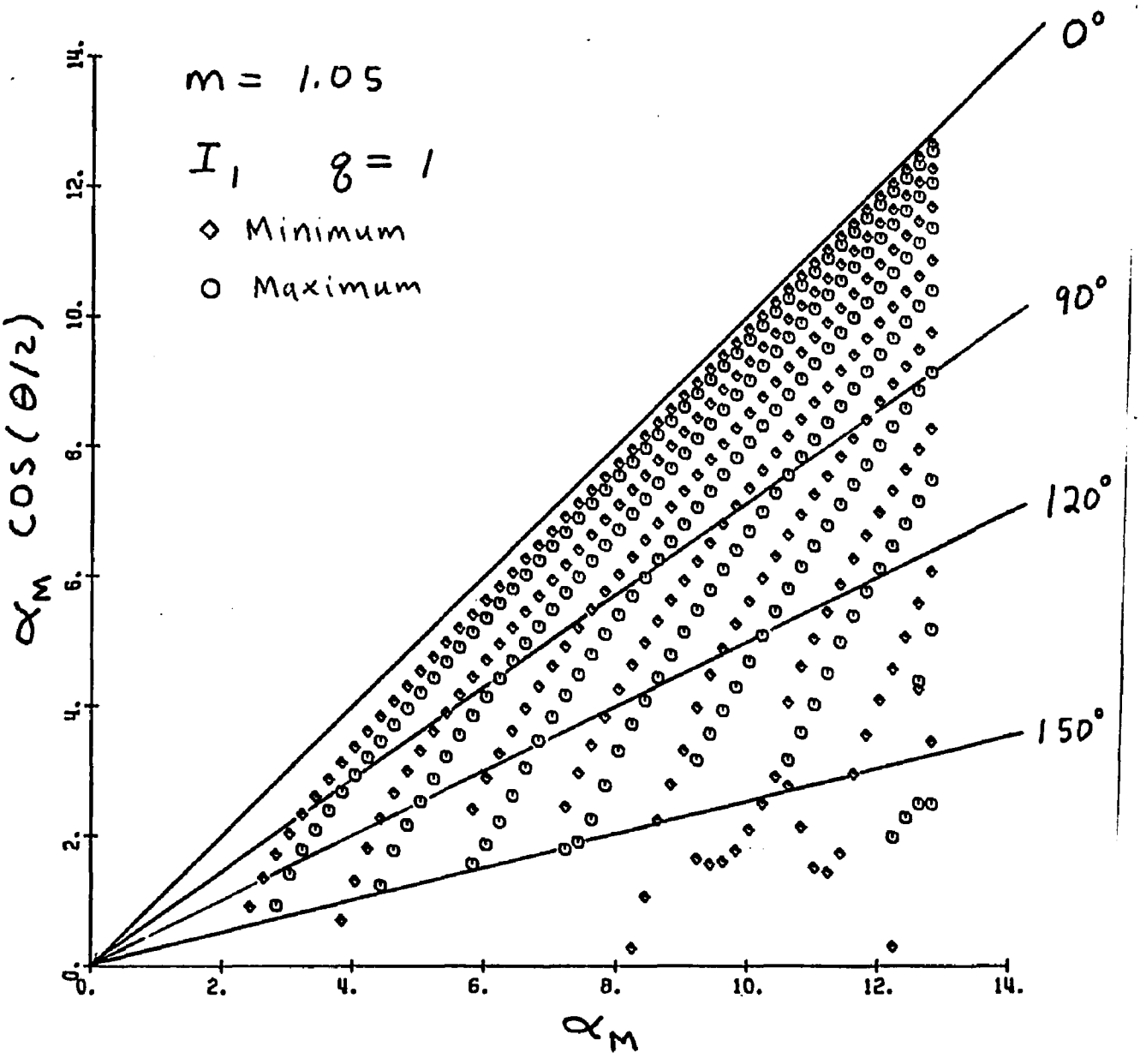

Fig. 87. Angular Location of I_1 Extrema for m=1.05 and q=1 Plotted as $\alpha\cos(\theta/2)$ Versus α

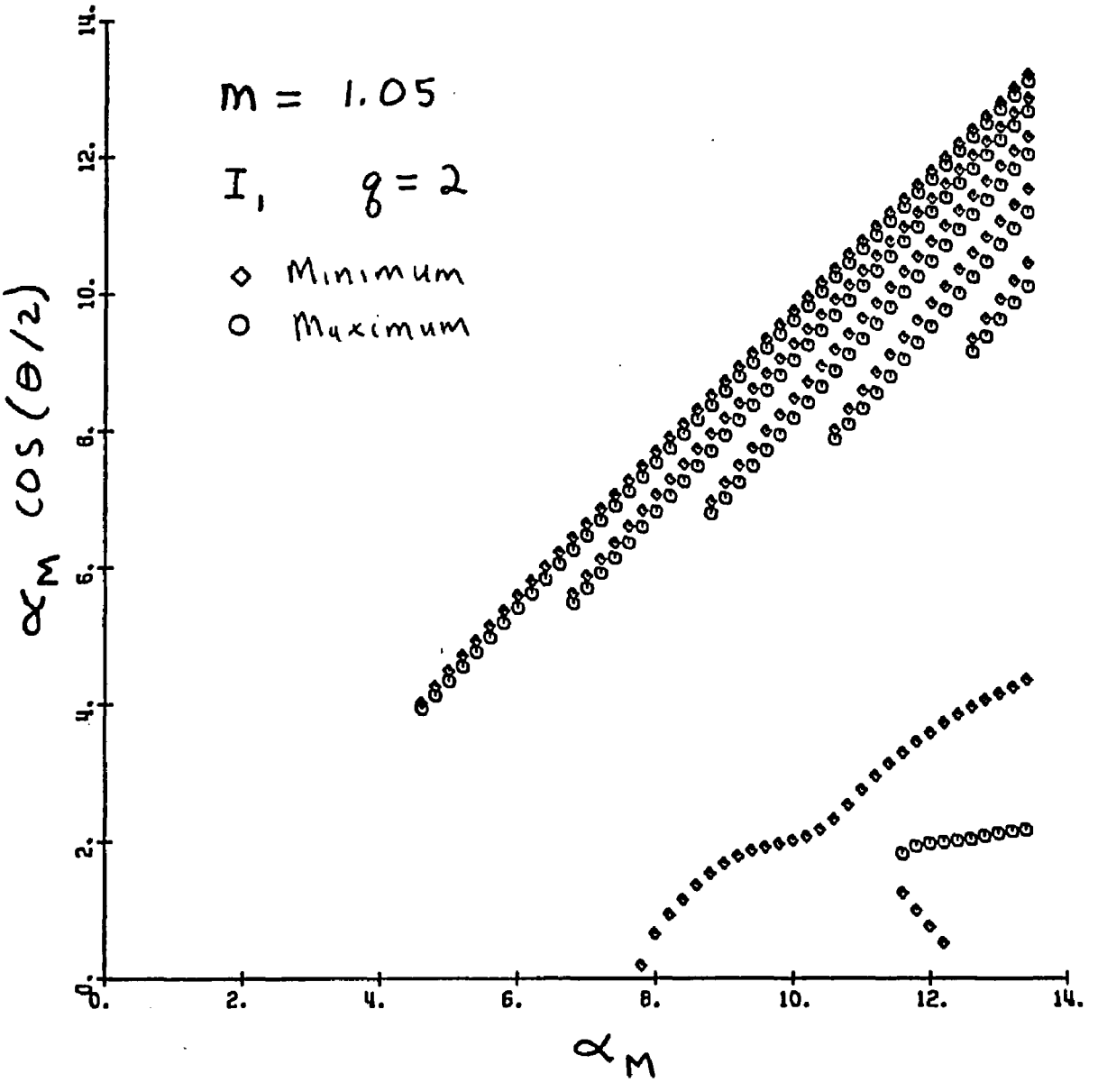

Fig. 88. Angular Location of I_1 Extrema for m=1.05 and q=2 Plotted as $\alpha\cos(\theta/2)$ Versus α

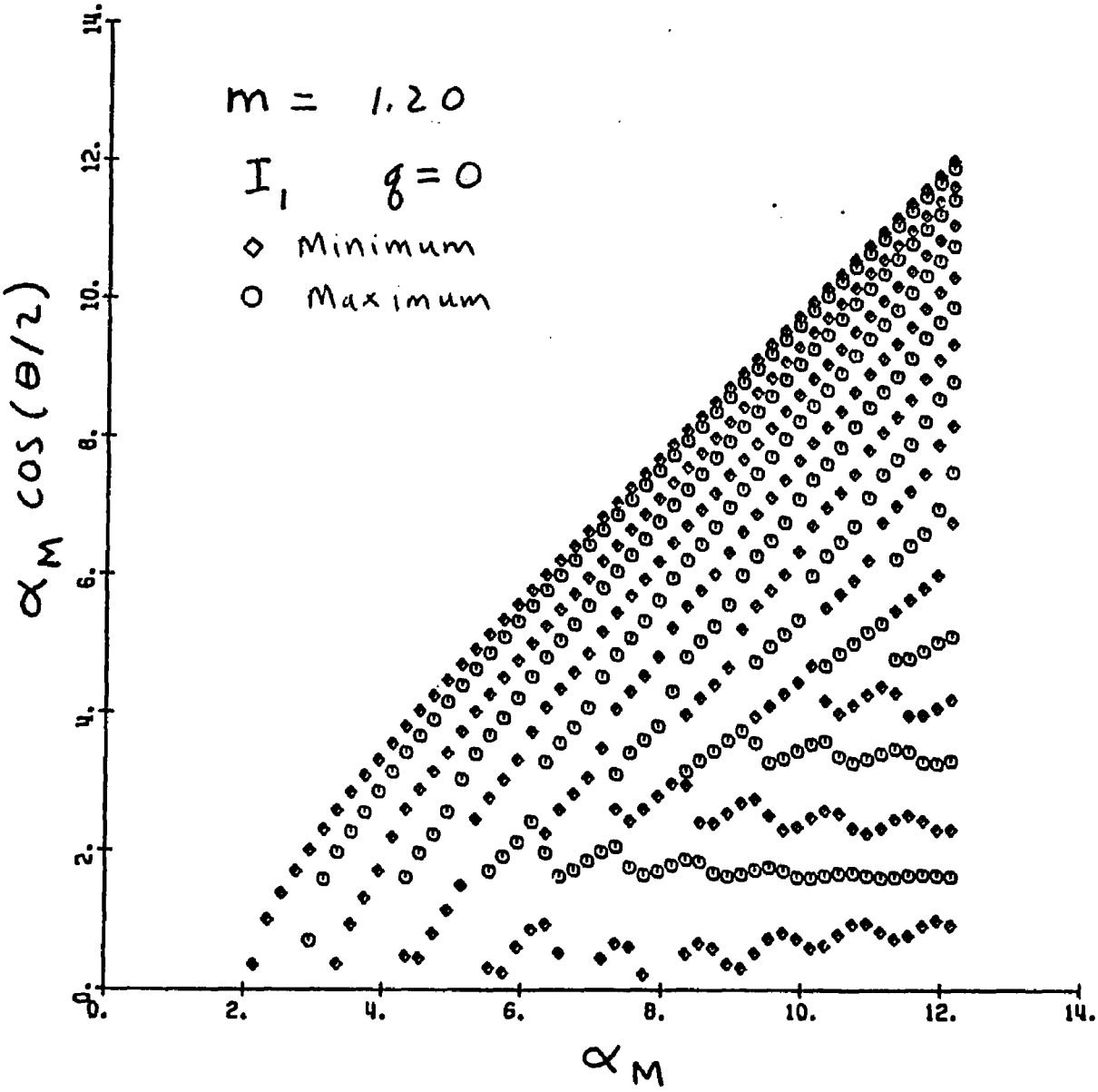

Fig. 89. Angular Location of I_1 Extrema for m=1.20 and q=0 Plotted as $\alpha\cos(\theta/2)$ Versus α

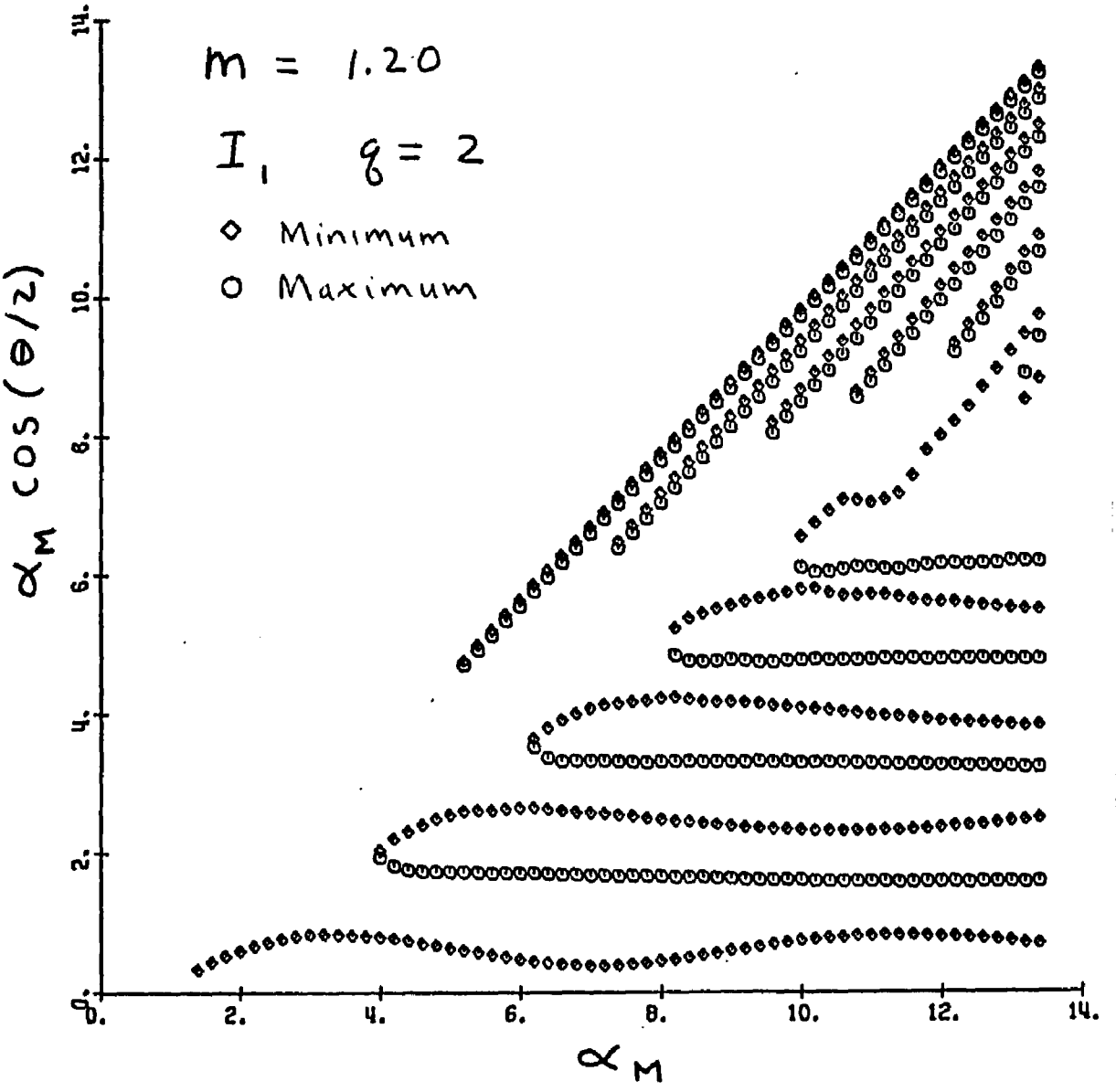

Fig. 90. Angular Location of I_1 Extrema for m=1.20 and q=2 Plotted as $\alpha\cos(\theta/2)$ Versus α

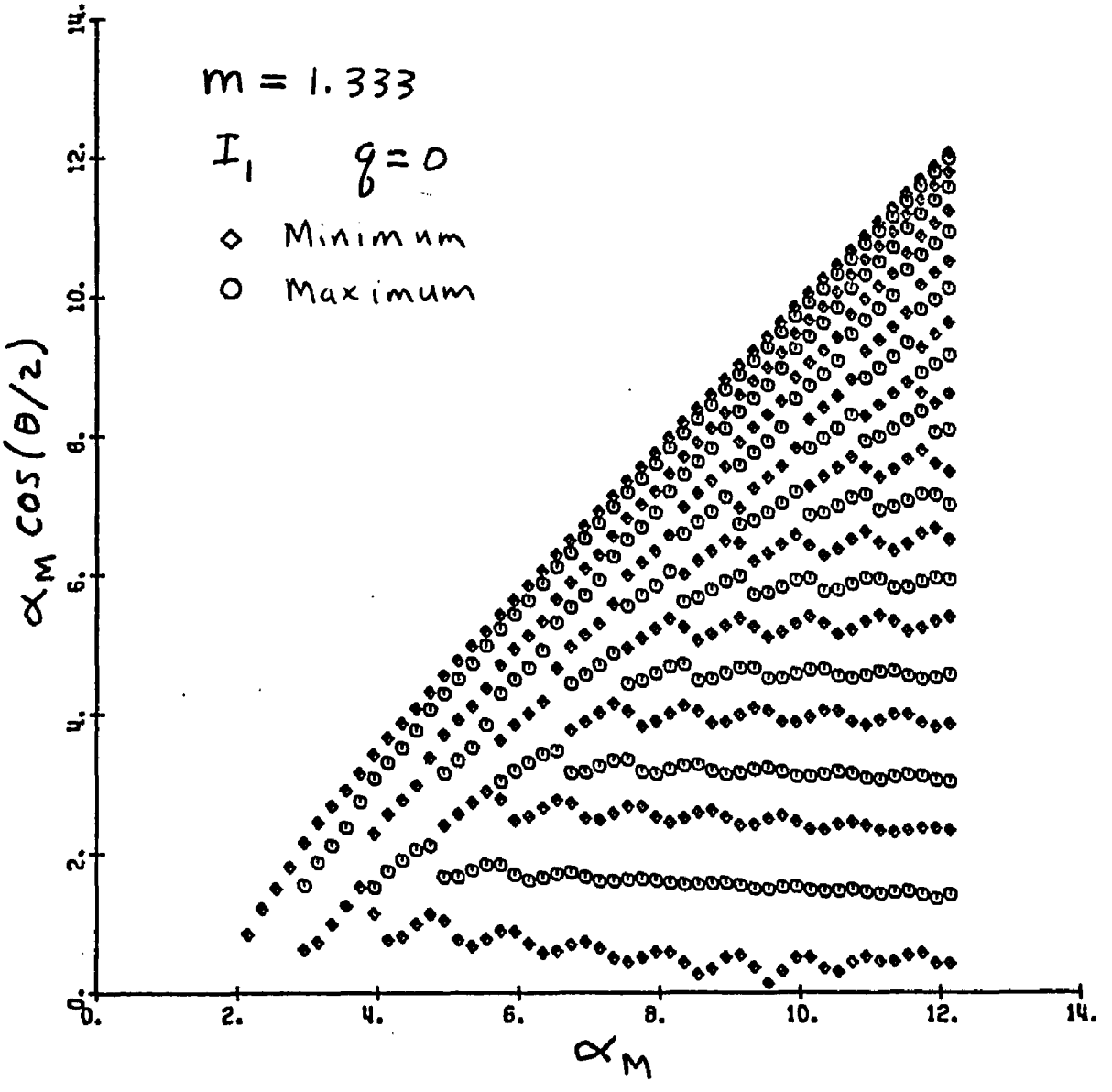

Fig. 91. Angular Location of I_1 Extrema for m=1.333 and q=0 Plotted as $\alpha\cos(\theta/2)$ Versus α

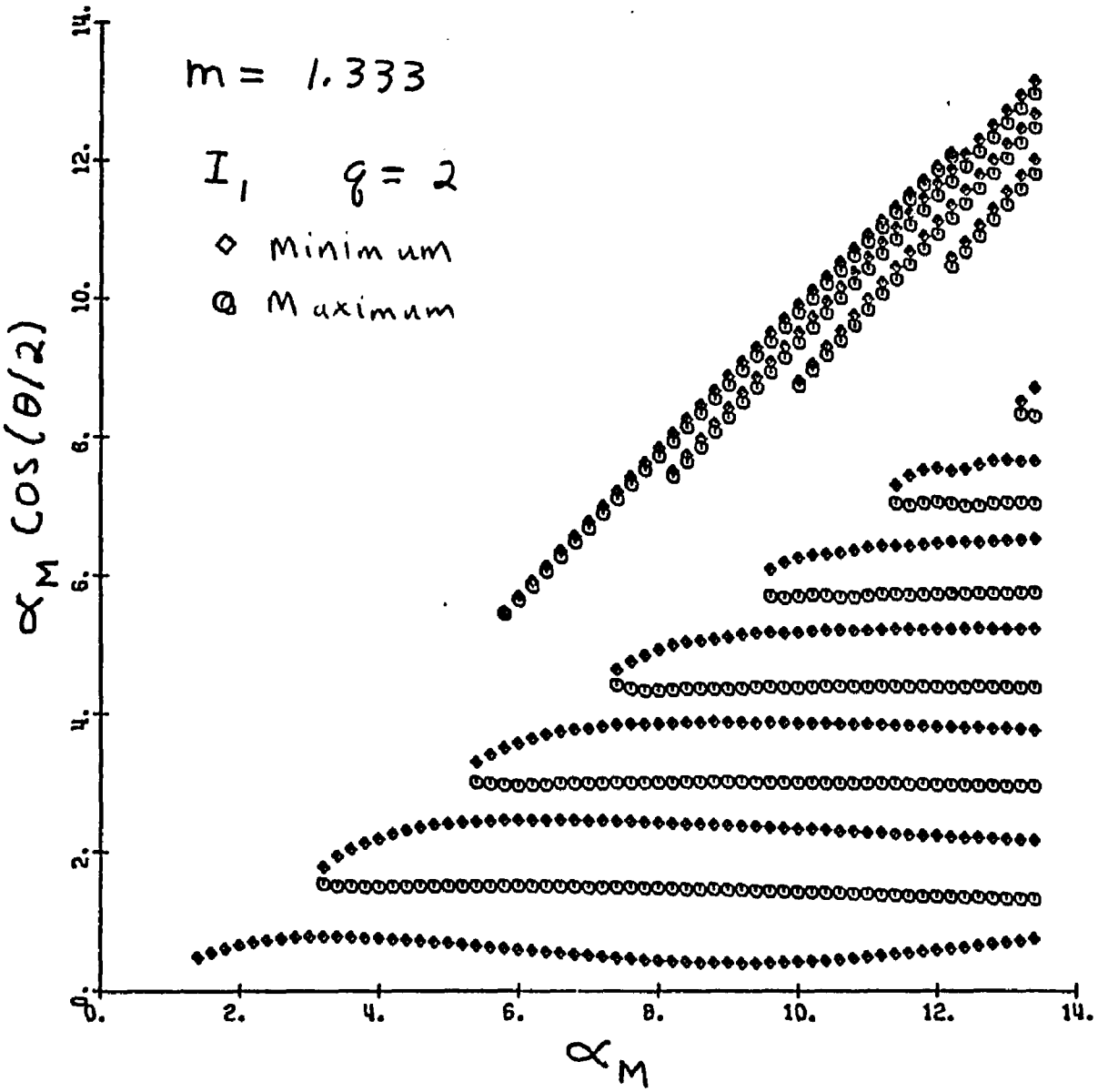

Fig. 92. Angular Location of I_1 Extrema for m=1.333 and q=2 Plotted as $\alpha\cos(\theta/2)$ Versus α

The reflection extrema become more pronounced as the relative refractive index increases. Figure 88 shows the definite appearance of several reflection extrema for m = 1.20 and q = 0 at the larger particle sizes as indicated by the horizontal lines. Note that the minima contours for the reflection extrema show a much higher oscillation than the maxima contours. This trend is expectred since the reflection pattern is produced from finite intensities and not the lack of intensities. The reflection minima contours will therefore be strongly influenced by the diffraction system. Increasing the heterodispersion to q = 2 in Figure 89 greatly enhances the reflection extrema and washes out a portion of the diffraction extrema. Again note that the reflection maxima show very constant horizontal lines while the minima have smooth oscillations. Increasing the relative refractive index to m = 1.333 shows a greater number of extrema characterized by reflection. Figures 90 and 91 show the reflection extrema as horizontal lines for q = 0 and q = 2 respectively.

The same trends in the reflection extrema are also seen for the extrema from I_2 and I_u. However the I_2 and I_u extrema have an additional extremum due to the Rayleigh minimum. The I_2 extrema for m = 1.05 and q = 0 in Figure 92 shows this Rayleigh minimum as a very pronounced diagonal line. Since the Rayleigh minimum also appeared as a diagonal line in the diffraction plots, one can say that the Rayleigh minimum is neither a reflection nor a diffraction extremum. The other aspects of the I_2 and I_u reflection extrema are similar to those already discussed.

The physical interpretation of the reflection phenomenon in the previous discussions is made in the following manner. The incident radiation induces oscillating electric dipoles within the particle which radiates in the manner described by the RGD theory. A portion of this radia-

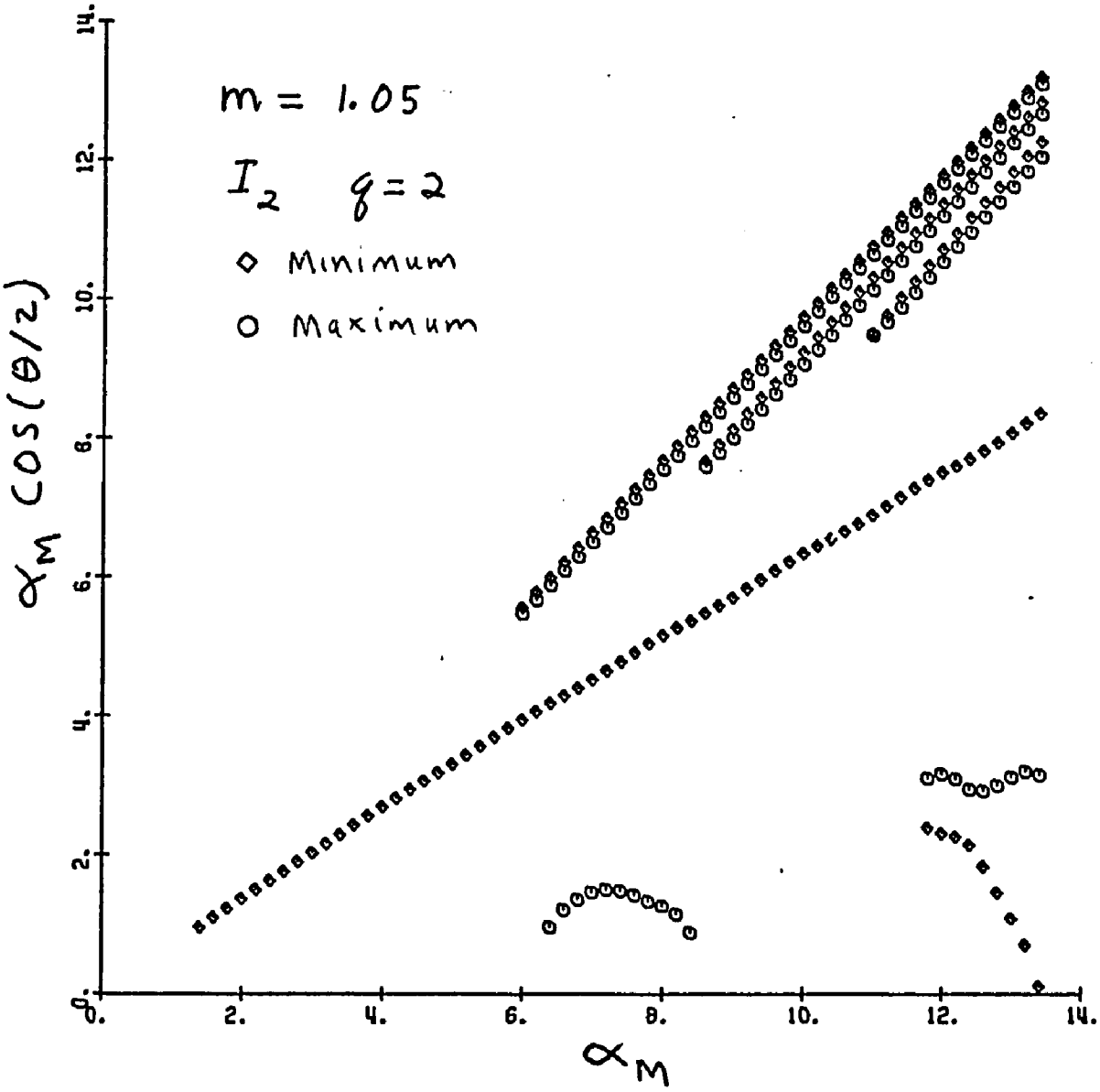

Fig. 93. Angular Location of I_2 Extrema for m=1.05 and q=2 Plotted as $\alpha\cos(\theta/2)$ Versus α

tion crosses the particle surface and is seen as a diffraction pattern in the forward direction. The fraction of radiation that is transmitted is determined by Fresnel's equations. The remaining fraction of the radiation undergoes an internal reflection at the particle surface and consequently moves in the opposite direction. The reflected wave then travels through the particle in the opposite direction of the original wave and is transmitted across the particle surface in accord with Fresnel's equations. This reflected wave is now observed in the scattering diagram at the angle $\pi-\theta$ if the original wave, as obtained from the RGD theory, were moving in the direction θ.

One might naturally ask that if internal reflections are possible then the particle should also exhibit external reflections from the incident radiation. Hodkinson and Greenleaves[49] had indeed shown that external reflections must be taken into account to describe the scattering in the forward direction for particles even as small as $\alpha = 10$. However the angular variation of this external reflection is very smooth and would not change the basic pattern of the reflected extrema as described in this Section. Figure 93 shows the intensity of the external reflection for I_1 and I_2 plotted against the angle of observation. Note that both curves have a very smooth variation of the intensity in both the forward and backward direction and therefore would not introduce any additional extrema into the scattering pattern. The physical interpretation of the angular location of the intensity extrema in the backward direction can therefore neglect the external reflection.

b. Empirical Equations for Reflection Maxima

Empirical equations analogous to equation 18 for the diffraction extrema can also be developed for the reflection extrema. These

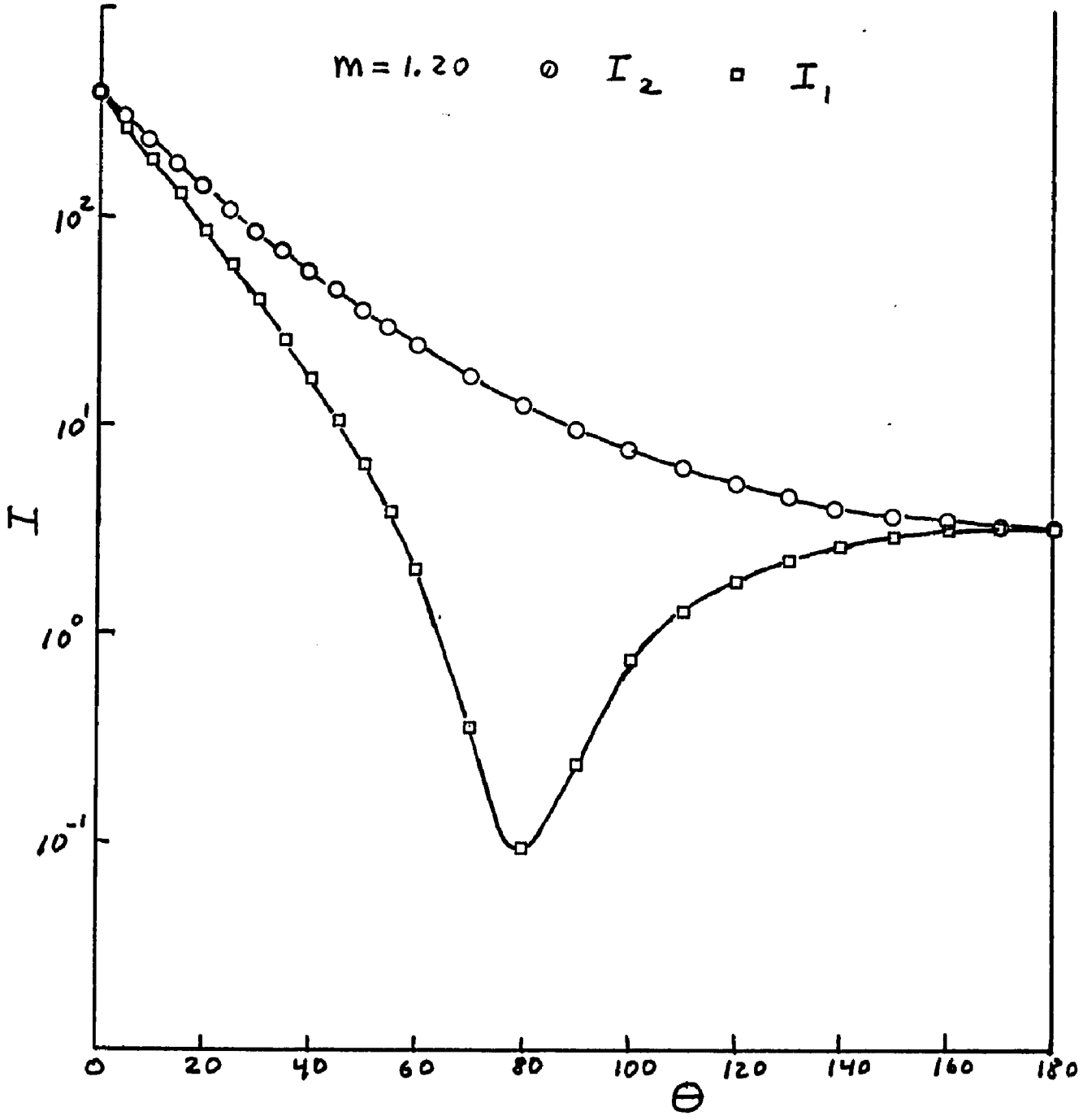

Fig. 94. Intensity of the External Reflection for I_1 and I_2 Plotted Against the Angle of Observation

equations would be described by

$$\alpha \cos (\theta/2) = k_{0i} - k_{1i} \tag{29}$$

where k_{0i} and k_{1i} are empirical constants and i represents the order of the extrema counting from the backward direction. This equation, however, only applies to the reflection maxima because of the large oscillations in the minima. The constants k_{0i} and k_{1i} show very similar behavior to the corresponding constants in equation 18 for the diffraction extrema. The constant k_{0i} increases with increasing extrema order and decreases with increasing m value. Similarly the constant k_{1i} increases with increasing m although the values are much smaller than the corresponding values from the diffraction extrema. This can be seen in the nearly horizontal lines for the maxima in Figures 89 and 91.

V. Methods for Determining Particle Size Distributions Using Angular Intensity Extrema

Chapter IV presented a detailed dicussion of several trends in the relationship between the angular intensity extrema and the particle size distribution for a given m and polarization of the incident light. This chapter will present several methods for using these trends to infer the particle size distribution from the angular intensity extrema. All of the methods require that the relative refractive index of the particle be known so that the proper relationship can be used.

A. Methods Based On Separating The Effect Of The Mode And The Distribution Width

A common feature in most of the methods presented in this chapter is the assumption that the effect of heterodispersion can be separated from the intensity extrema. The complete determination of the unknown size distribution then requires two arguments. One argument determines the mode or an average size of the distribution while the other argument determines the width of the distribution. The error in the resulting size distribution increases as the separation of the mode and the width of the distribution becomes less distinct.

1. Determining the Distribution Mode From The Extrema Locations

The present investigation used the angular location of the intensity minima to determine the mode of the distribution independent of the hetero distribution. Kerker et al[47] had first pointed out this possibility which was later developed by Wallace and Kratohvil[24] into an empirical method for determining particle size distributions. A qualitative explanation for the independence of the location of the

angular extrema from the degree of heterodispersion was given in Chapter IV. The fundamental requirement of removing the effect of the heterodispersion on the extrema locations is to maintain a constant mode or another measure of the distribution average. For heterodispersions, the particles larger than the mode will shift the extrema locations in one direction while the particles smaller than the mode will shift the extrema locations in the other direction. On the average the two shifts will cancel and result in the same extrema locations as the monodisperse distributions.

To test the validity of removing the effect of heterodispersion from the extrema location, a number of calculations were performed on a series of heterodispersions having a constant mode. The results of these calculations are shown in Figures 95-100 where the angular location of the extrema are plotted against the heterodispersion parameter q for m = 1.20. Each figure represents the extrema from heterodispersions having a constant mode. Figures 95, 96, and 97 show the I_1 extrema for α_M = 5, 10 and 15 respectively. The maxima and minima are shown by the dashed and solid lines respectively.

Several trends are seen in these figures that define the region where the extrema locations are independent of q. In general, these regions occur in the angular scattering diagram where the diffraction and reflection extrema are well established. Thus, the extrema will be independent of q in both the forward and backward direction. However, in the forward direction, only the minima remain constant with increasing q while the maxima migrate toward the minima. This migration becomes less pronounced as the modal size increases. The minima also shifts toward the maxima shortly before the extrema pairs wash out.

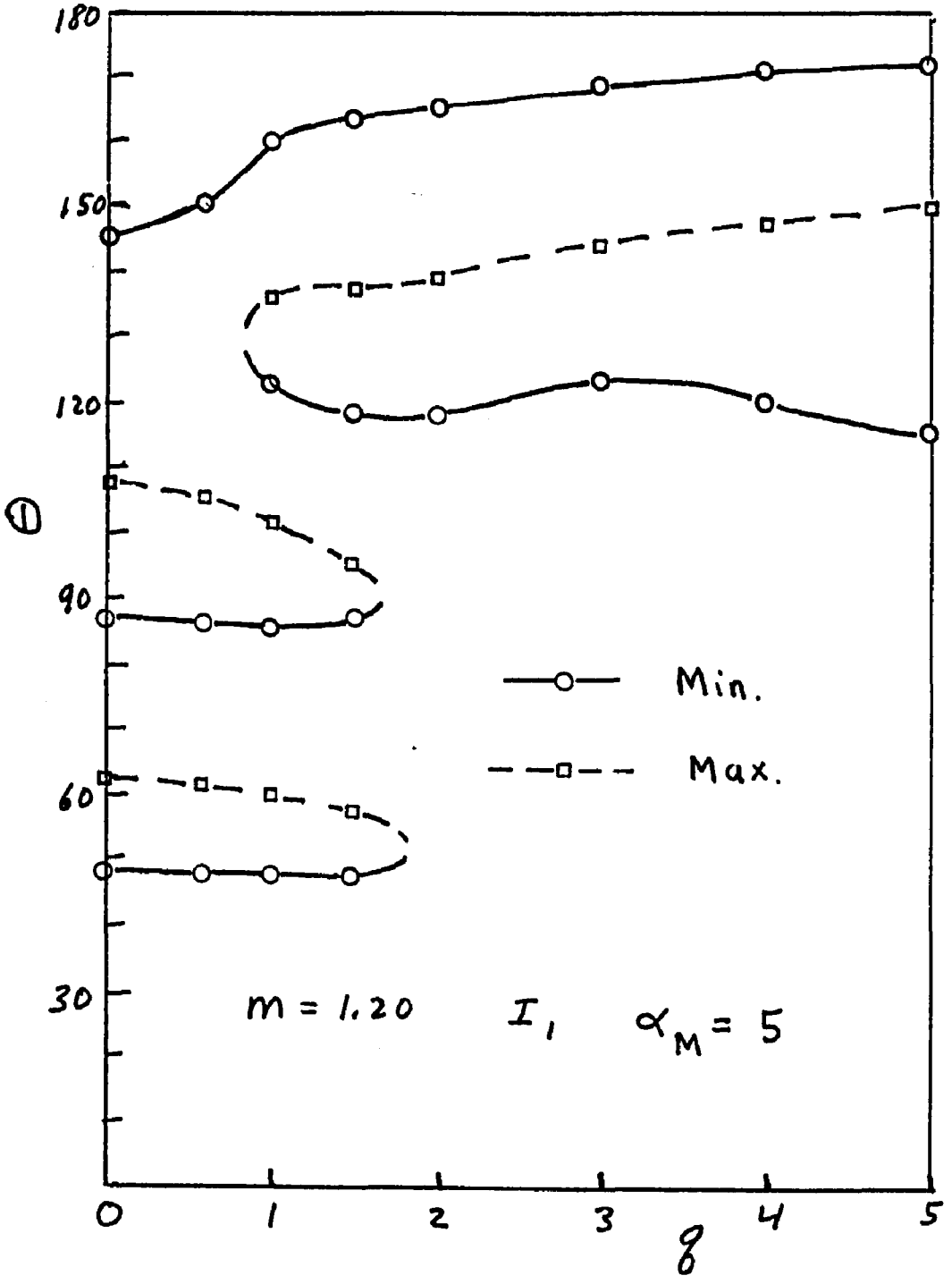

Fig. 95. Angular Location of I_1 Extrema as a Function of q for Distributions with m=1.20 and α_M=5

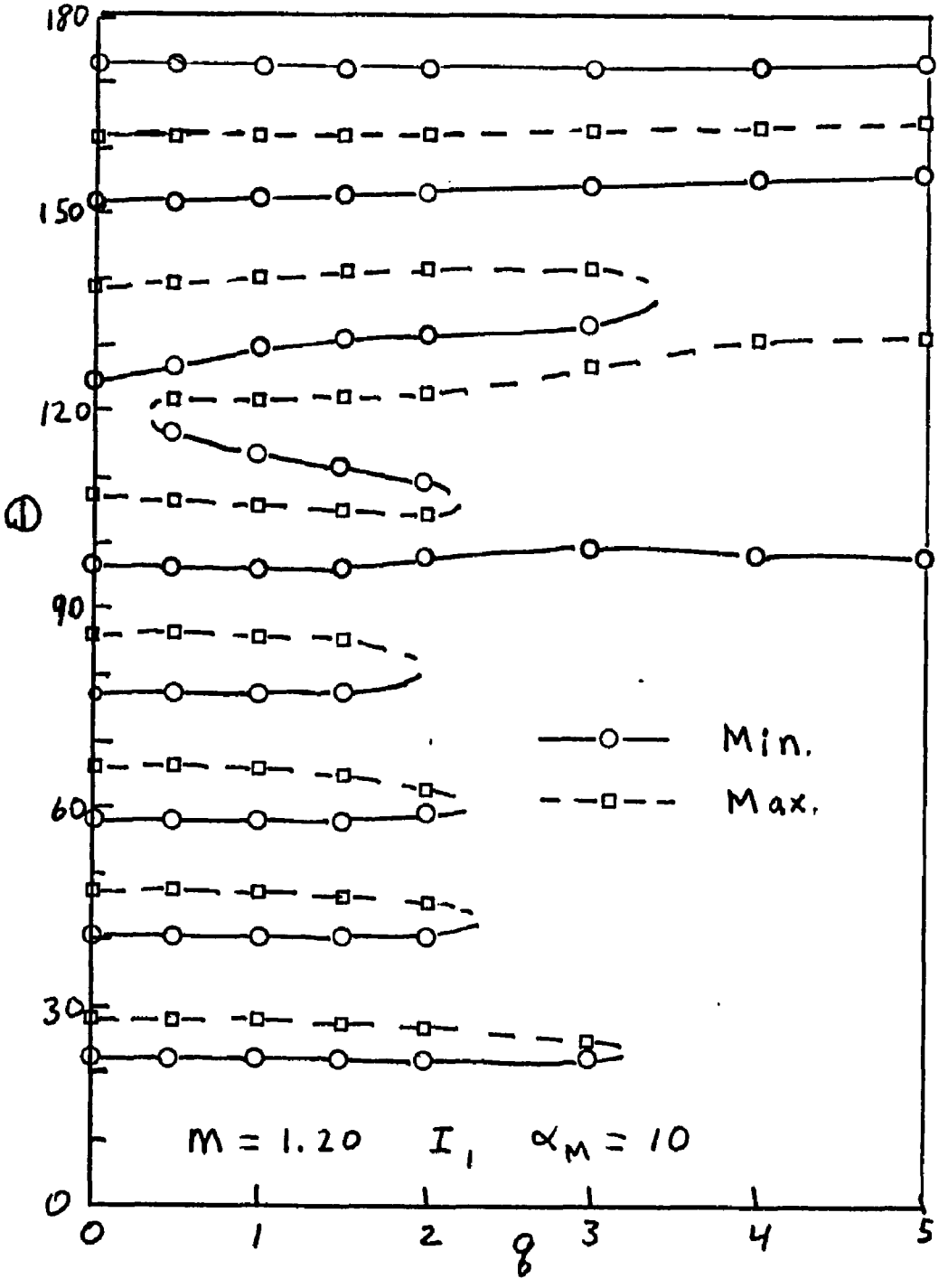

Fig. 96. Angular Location of I_1 Extrema as a Function of q for Distributions with M=1.20 and α_M=10

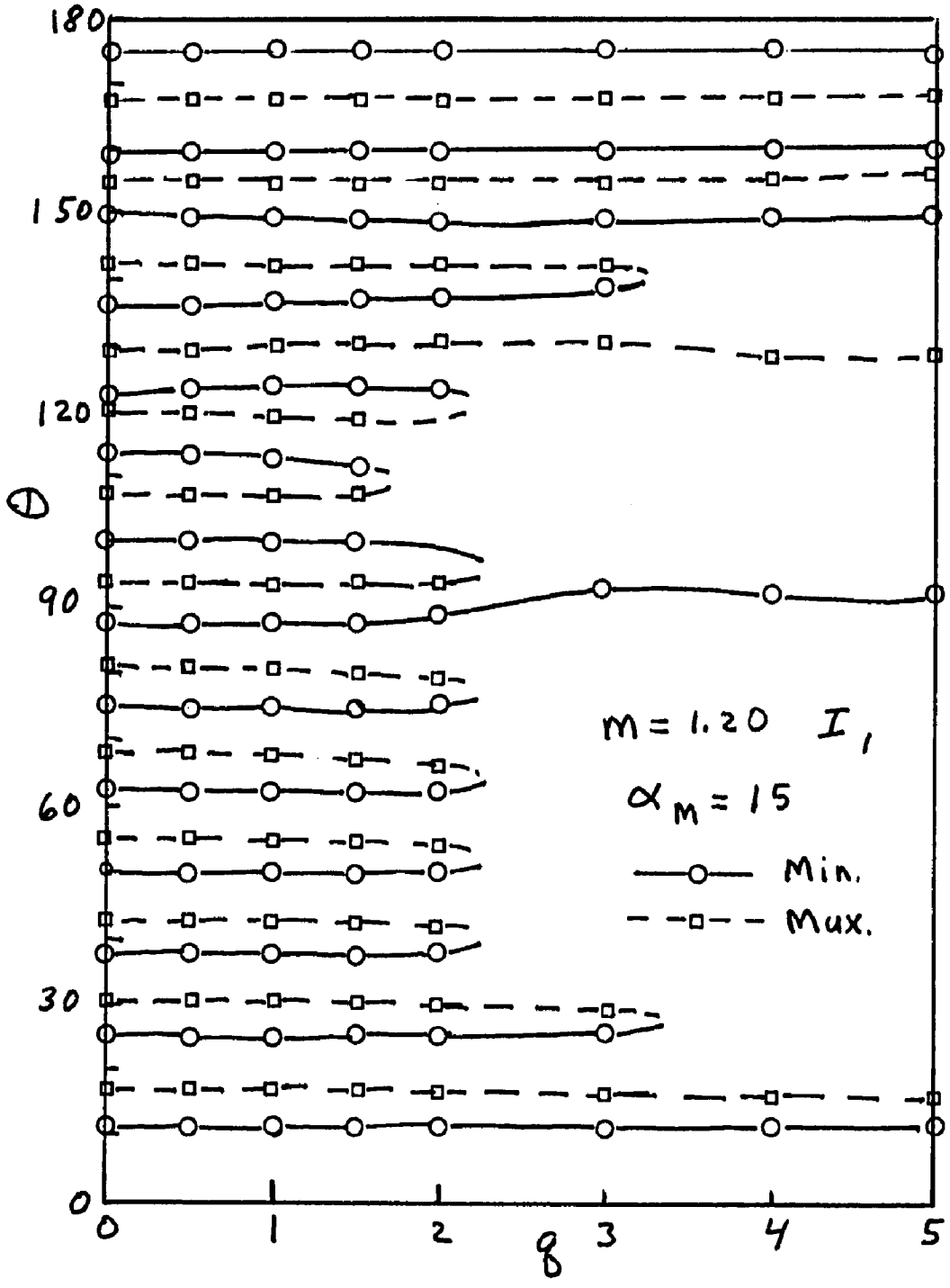

Fig. 97. Angular Location of I_1 Extrema as a Function of q for Distributions with M=1.20 and α_M=15

In the backward direction removing the effect of the heterodispersion from the extrema location is only feasible for the larger particle sizes where the reflection extrema are well established. Figure 95 shows that for $\alpha_M = 5$ the extrema locations are not constant as q increases since the backward direction has not yet developed a pronounced reflection region. In fact, the appearance of a new extrema pair indicates that the region represents the boundary between the reflection and diffraction extrema.

Increasing the particle size to $\alpha_M = 10$ and 15 in Figures 96 and 97 respectively results in a larger and more established reflection region with a resulting greater independence of q. Note that both the maxima and minima in the backward direction are approximately independent of q. A comparison of all the extrema in Figures 95-97 show that the reflection extrema in the backward direction can be used to determine α_M even for large q values where the diffraction extrema have been washed out. These figures also show that the extrema closer to the boundary separating the diffraction and reflection extrema wash out faster than those extrema farther removed.

The I_2 extrema shown in Figures 98-100 have a similar trend as the I_1 extrema except for a greater tendency of the diffraction extrema to wash out at lower q values. This is illustrated in Figure 98 where the first order diffraction extrema wash out before $q = 0.5$ while the second order extrema are not even seen at $q = 0.0$. The diffraction extrema for larger particle sizes do not wash out as rapidly with increasing q values. Figures 99 and 100 also show the pronounced trend whereby the extrema pairs wash out more rapidly with increasing q the closer they are to the boundary separating the reflection and diffrac-

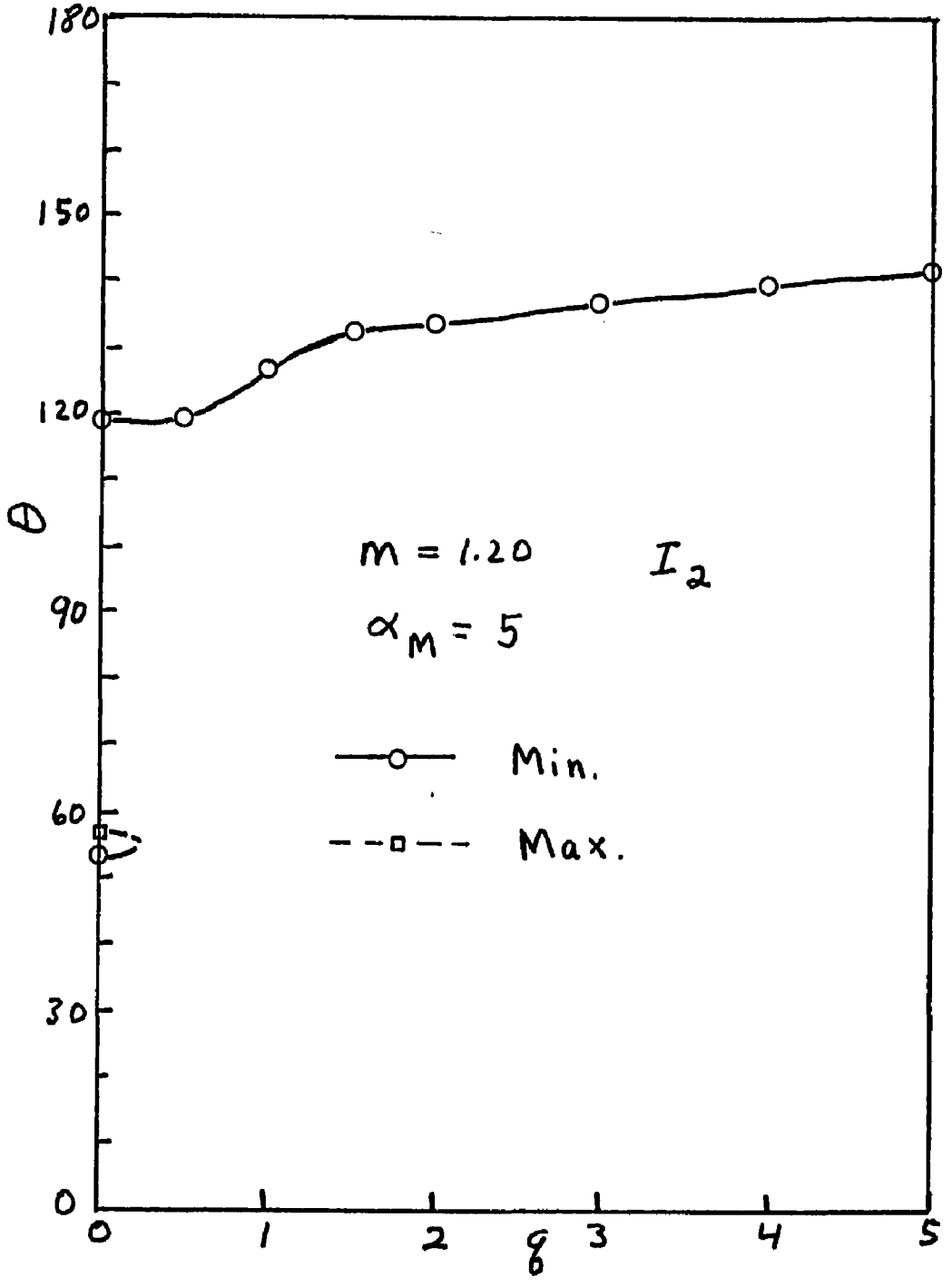

Fig. 98. Angular Location of I_2 Extrema as a Function of q for Distributions with m=1.20 and α_M=5

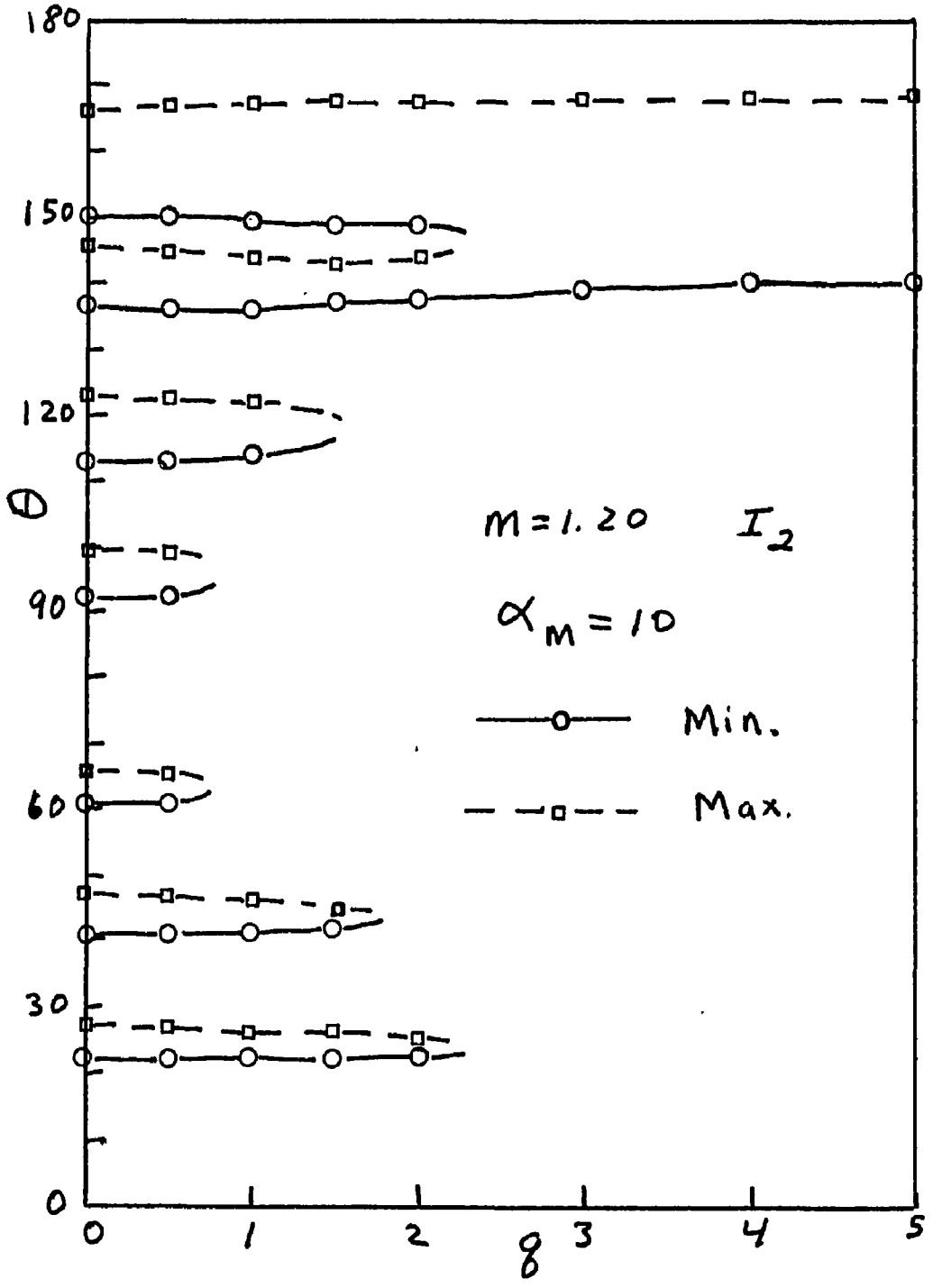

Fig. 99. Angular Location of I_2 Extrema as a Function of q for Distributions with M=1.20 and α_M=10

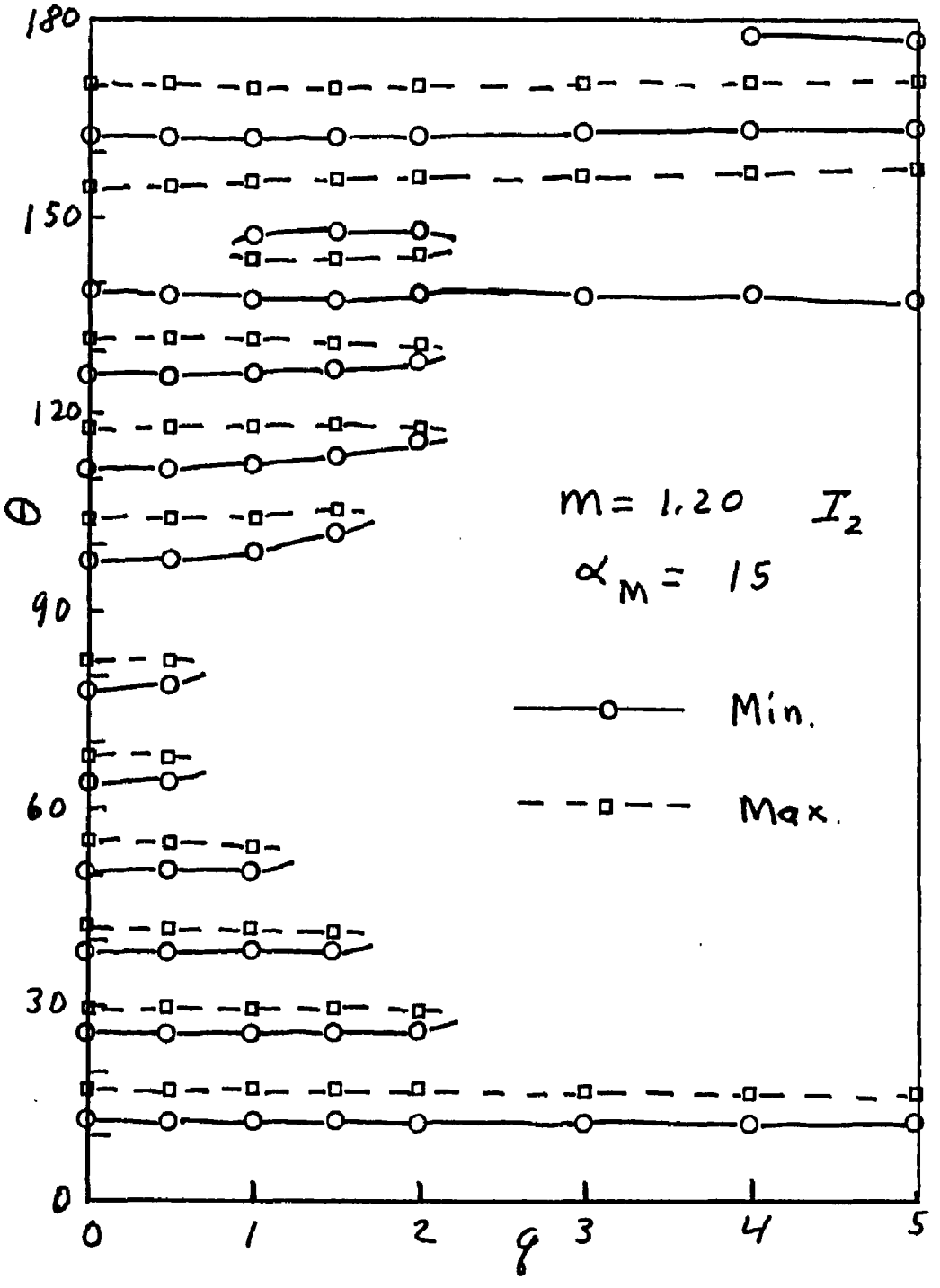

Fig. 100. Angular Location of I_2 Extrema as a Function of q for Distributions with m=1.20 and α_M=15

tion regions.

The mode of the distribution can be determined from the location of the extrema that are independent of the heterodispersion. These extrema occur in the well established regions of diffraction and reflection as seen in Figures 95-100. Wallace and Kratohvil[24] had previously used the minima in the forward direction to determine the mode. They showed that the minima remained approximately constant for a constant mode while the maxima shifted toward the minima as the heterodispersion increased. The present investigation indicates that both the maxima and minima in the backward direction also remain constant for larger particle sizes as the heterodispersion increases if the mode is kept constant.

Wallace and Kratohvil[24] argued that since the minima angles were independent of q the mode α_M of the heterodispersion would be equal to the monodisperse particle size having the same angular location of the minima. The mode could then be rapidly determined by matching the minima locations from the heterodispersion with the extrema contour plots of α versus θ from monodisperse distributions having the same m value. The calculations in the present investigation have verified that the diffraction minima are approximately independent of the heterodispersion and can therefore be used to determine the mode of the distribution. However, the method begins to fail at larger q values where the minima locations shift with increasing q.

2. Determination of the Distribution Width

The next step after finding the mode is to determine the width of the distribution. Several methods have been investigated using

the intensities and angular location of the extrema. These methods relate the width of the distribution to the intensity ratio of the extrema pair, the intensity slope between the extrema pair and the angular difference between the extrema pair.

a. Intensity Ratio of Extrema Pair

Wallace and Kratohvil[24] had previously shown that the width of the distribution could be determined from the ratio of the intensity maximum to the intensity minimum. Although previous investigators[47] had known that the extrema wash out with increasing heterodispersion, they did not attempt to develop a quantitative measure of this behavior. The technique developed by Wallace and Kratohvil[24] was therefore the only way that the complete size distribution could be determined from angular extrema measurements. This technique required that the distribution mode must first be determined as described in the previous section. The heterodispersion is then separately determined by comparing the measured intensity ratio with the theoretical curve corresponding to the same modal size. A different curve is used for each modal size and each extrema order.

Figure 101 shows several curves of I_{max}/I_{min} versus q generated from the angular variation of I_1. The I_{max} corresponds to the maximum intensity of a given extrema pair while I_{min} corresponds to the minimum intensity of the same extrema pair. The upper graph represents the intensity ratio of the first extrema pair from distributions having a constant mode of 5, 7 and 10. One sees that the curves for the smaller modes have a higher intensity ratio for q = 0 and decrease more rapidly with increasing q than the corresponding curves for the larger modes. When the intensity ratio has decreased to the limiting value of 1.0 the

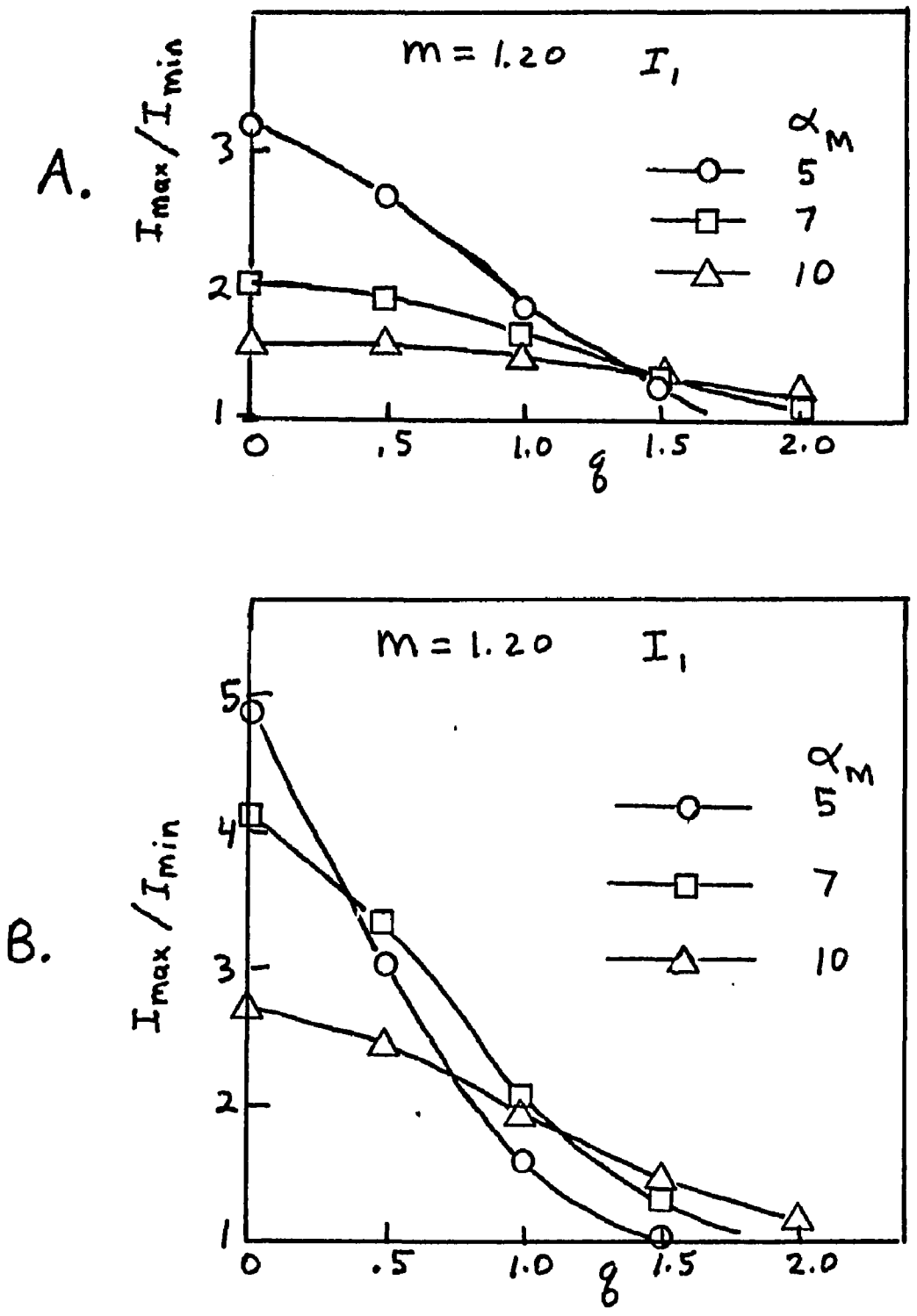

Fig. 101. Intensity Ratio I max/I min Versus q for (A) The First Extrema Order and (B) The Second Extrema Order Generated from the Angular Variation of I_1 for Different Hetero-dispersions with m=1.20

extrema pair disappears. A similar pattern is seen for the intensity ratio from the second extrema pair shown in the lower graph in Figure 101. However, the intensity ratios decrease much faster for the second extrema pair than for the first extrema pair. The explanation for the higher rate at which the intensity ratio decreases (i.e., extrema pairs washing out) with increasing q for the higher extrema pairs and smaller modal values was given earlier in Chapter IV.

The corresponding curves of I_{max}/I_{min} versus q that are generated from the angular variation of I_2 are shown in Figure 102. These curves have ratios that are close to 1.0 even for monodisperse distributions due to the very shallow extrema. Figure 102 shows that, as in the I_1 case, the I_2 intensity ratio decreases with increasing q at a higher rate for the higher extrema pairs and smaller modal values. Note that the first extrema pair for a mode of 5 disappears before q = 0.5, and the second extrema pair for modes of 5 and 7 are not even seen. In addition, the trend of smaller modes having larger intensity ratios no longer holds.

Wallace et al[24-26] had previously computed the intensity ratio for I_1, I_2 and I_u as well as the ratio of the maximum polarization ratio to the minimum polarization ratio ρ_{max}/ρ_{min} for m = 1.17 and m = 1.21 for a number of different modal sizes. In general, they found that for each type of ratio the smaller modal sizes had a larger ratio value than the larger modal sizes and the ratio values for a given modal size decreased at a faster rate with increasing q for the larger orders than for the smaller orders. They also showed that very small ratio values are obtained for the I_2 extrema as seen in Figure 102.

According to the Wallace-Kratohvil method, the width of the distribution is determined from an intensity ratio curve corresponding to

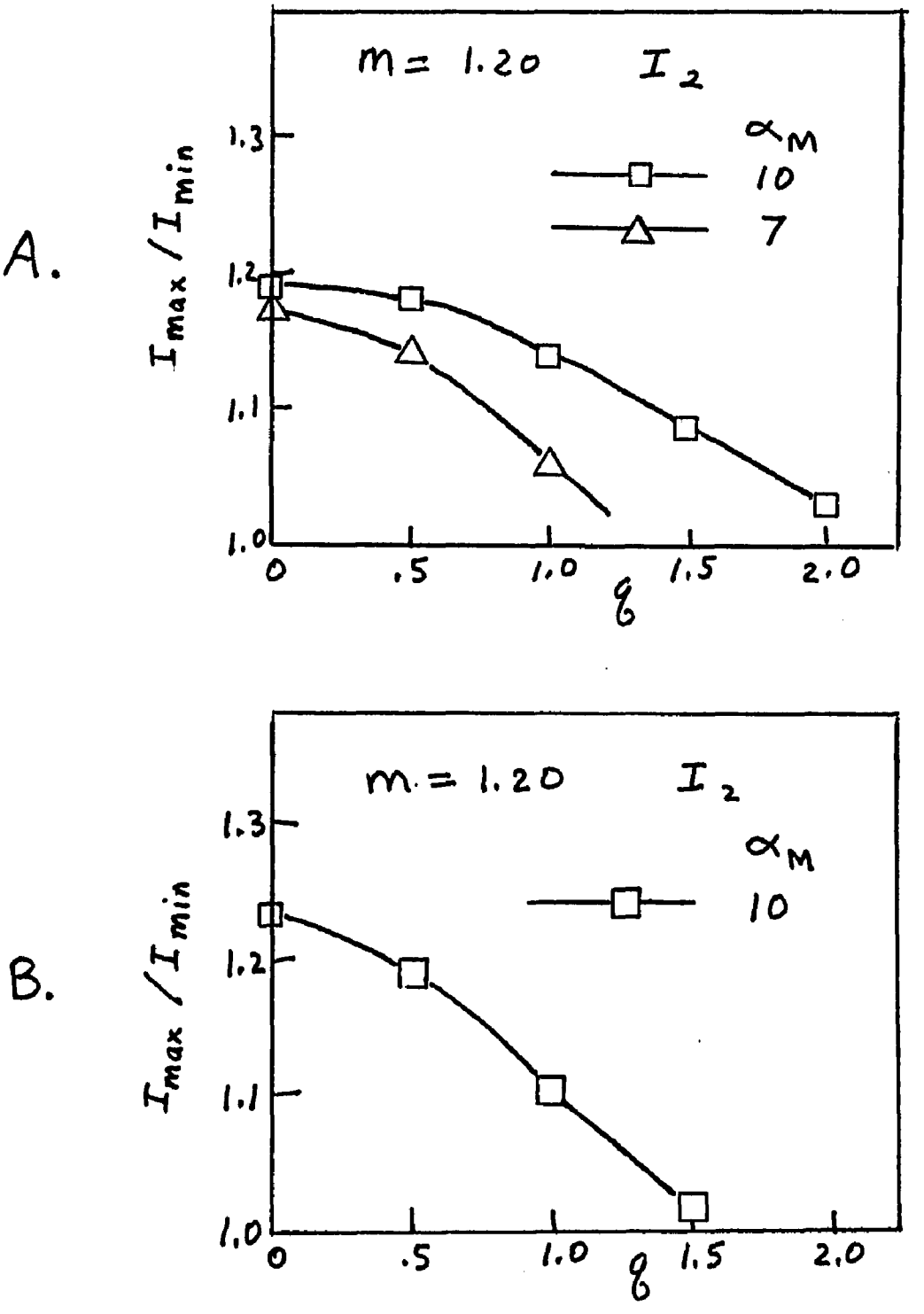

Fig. 102. Intensity Ratio I max/I min Versus q for (A) The First Extrema Order and (B) The Second Extrema Order Generated from the Angular Variation of I_2 for Different Hetero-dispersions with m=1.20

a particular modal size. Particle size distributions having a different mode would then require a different curve for the intensity ratios. Wallace and Kratohvil[24] suggested that a family of curves like the ones shown in Figures 101 and 102 which cover the desired range of modal sizes at sufficiently small size increments would be adequate to determine the width of a distribution. The curves representing intermediate modal values could be determined by interpolation. However, the detailed extrema calculations in the present investigation have revealed that the intensity ratio curves have considerable oscillations as a function of the mode which causes an error in the interpolation and destroys the systematic pattern in the family of intensity ratio curves. Figure 103 shows the oscillations of the intensity ratio curves for the first three extrema orders plotted as a function of modal size. These curves correspond to the I_1 scattering from a monodisperse distribution having $m = 1.20$. Note that the oscillations increase with increasing extrema order at a fixed modal size and decrease with increasing modal size at a fixed extrema order.

The loss of a systematic pattern and the difficulty in the interpolation due to the oscillations seen in Figure 103 can be eliminated by normalizing the intensity ratio. This normalization is accomplished by dividing the intensity ratio from the heterodisperse distribution by the intensity ratio from the monodisperse distribution. However, the mode of the heterodisperse distribution must be equal to the monodisperse particle size. Thus, plots of

$$\left(\frac{I_{max}}{I_{min}}\right)_q \Bigg/ \left(\frac{I_{max}}{I_{min}}\right)_{q=0}$$ versus q will provide

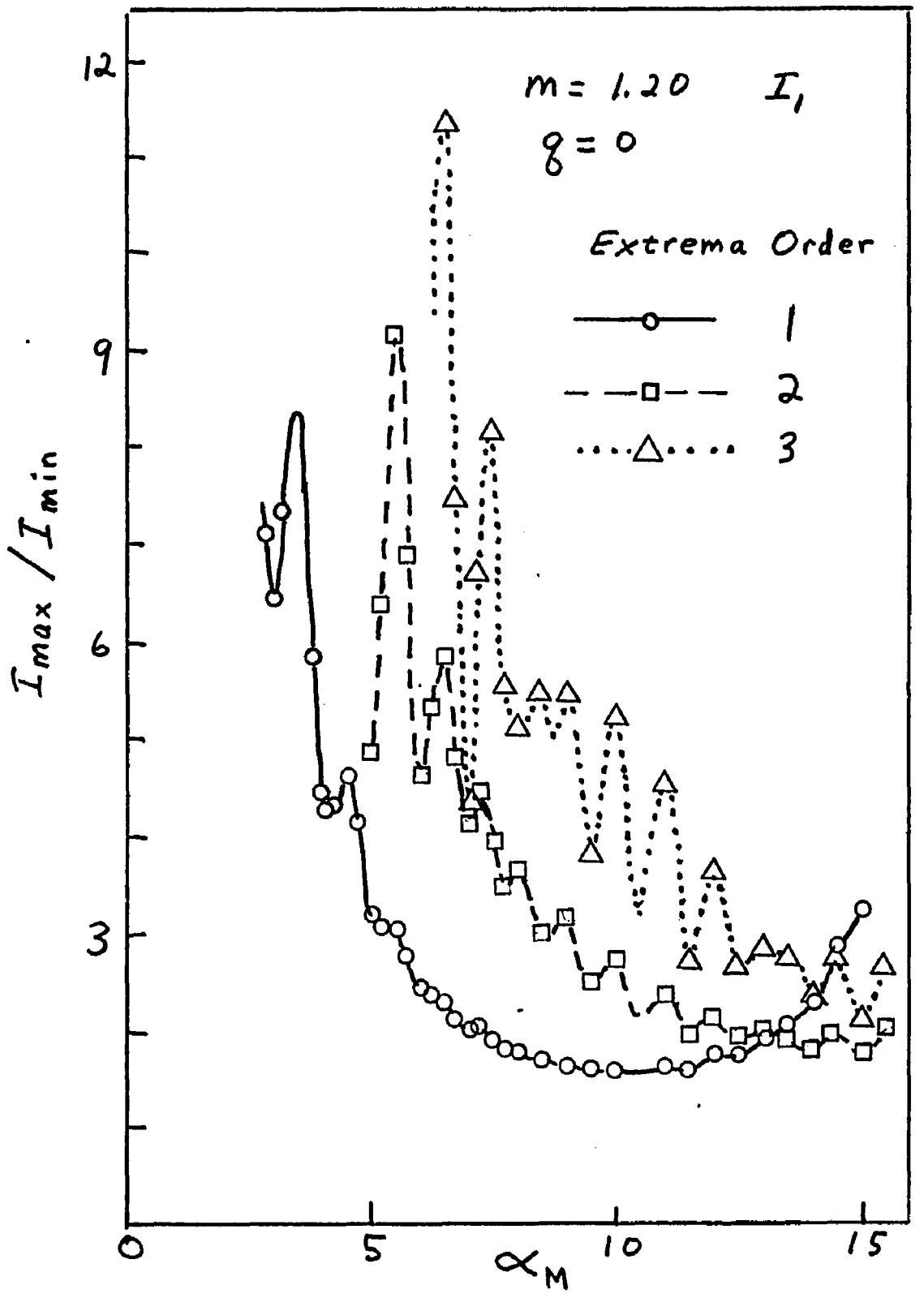

Fig. 103. Intensity Ratio I max/I min Versus Modal Size α_M for Different Extrema Orders Generated from the Angular Variation of I_1 for Monodisperse Distributions with m=1.20

a systematic pattern for determining the heterodispersion and allow interpolations.

The normalized intensity ratio for various heterodispersions having a constant mode ranging from $\alpha_M = 3$ to $\alpha_M = 12$ for the first, second and third extrema pairs are shown in Figures 104, 105 and 106 respectively. These curves were generated from I_1 data for spheres having m = 1.20. Each curve represents a size distribution that maintains a constant modal size as the width of the distribution increases with increasing q. Note that the normalized intensity ratio changes from 1.0 at q = 0 to 0.0 at the q value where the extrema pair disappears. In contrast to the intensity ratios as proposed by Wallace and Kratohvil, the normalized intensity ratios allow quantitative comparisons of different extrema pairs and different modal sizes. Figures 104-106 show that for a given extrema pair the normalized intensity ratio decreases with increasing q at a faster rate for heterodispersions with a smaller mode than for heterodispersions with a larger mode. Note that the heterodispersions with smaller modes do not have higher extrema pairs.

Plots of the normalized intensity ratio for different extrema orders having a constant mode are shown in Figures 107 and 108 for $\alpha_M = 5$ and 10 respectively. One readily sees that the larger modes have more extrema orders than the smaller modes. These figures show that the normalized intensity ratio decreases at a faster rate with increasing q for the higher extrema orders than for the lower extrema orders. The explanation for the relative rates at which the normalized intensity ratio decreases with increasing q for different modal sizes and different extrema orders was given earlier in Chapter IV.

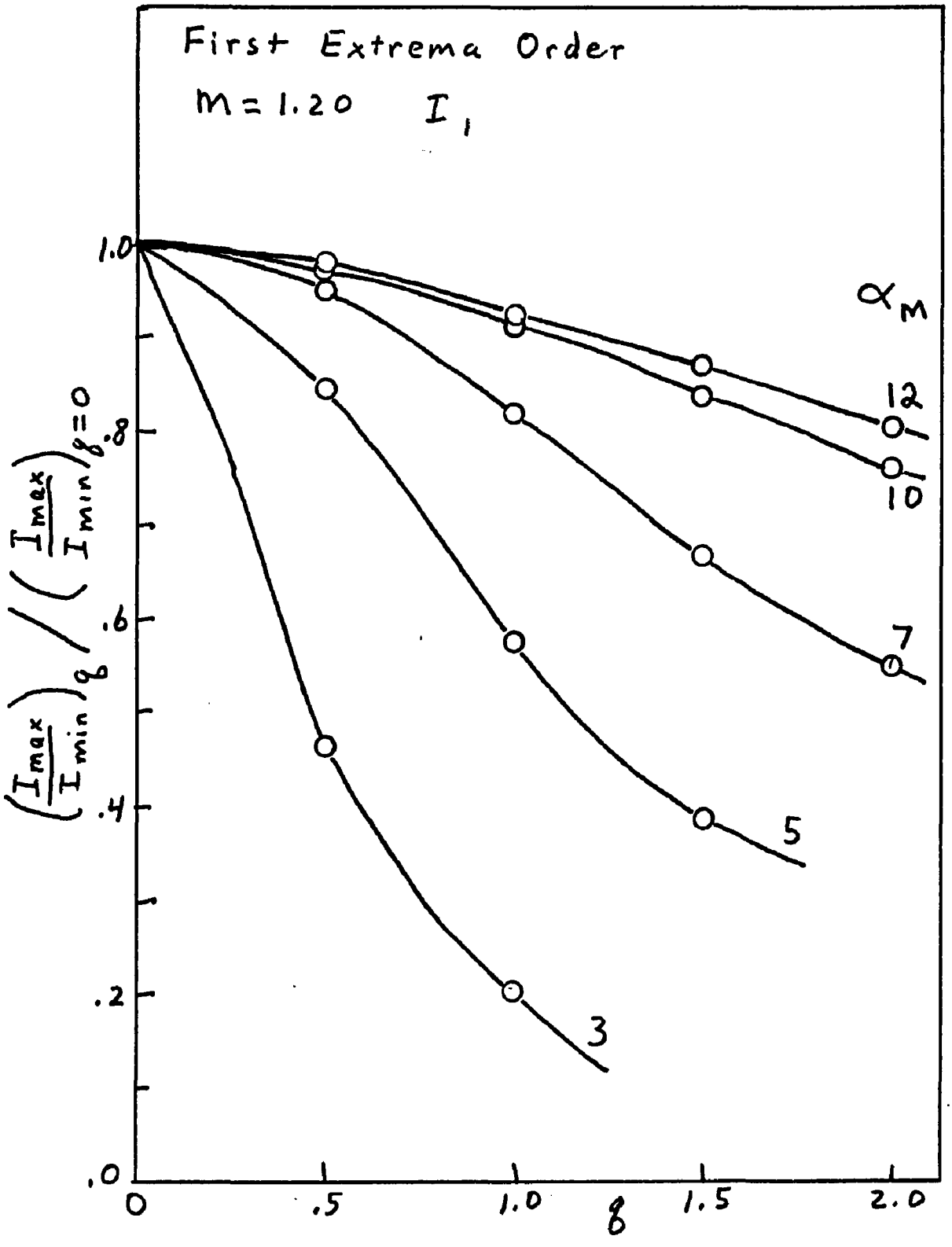

Fig. 104. Normalized Intensity Ratio Versus q for the First Extrema Order Generated from the Angular Variation of I_1 for Heterodispersions Having m=1.20 and Different Modal Sizes

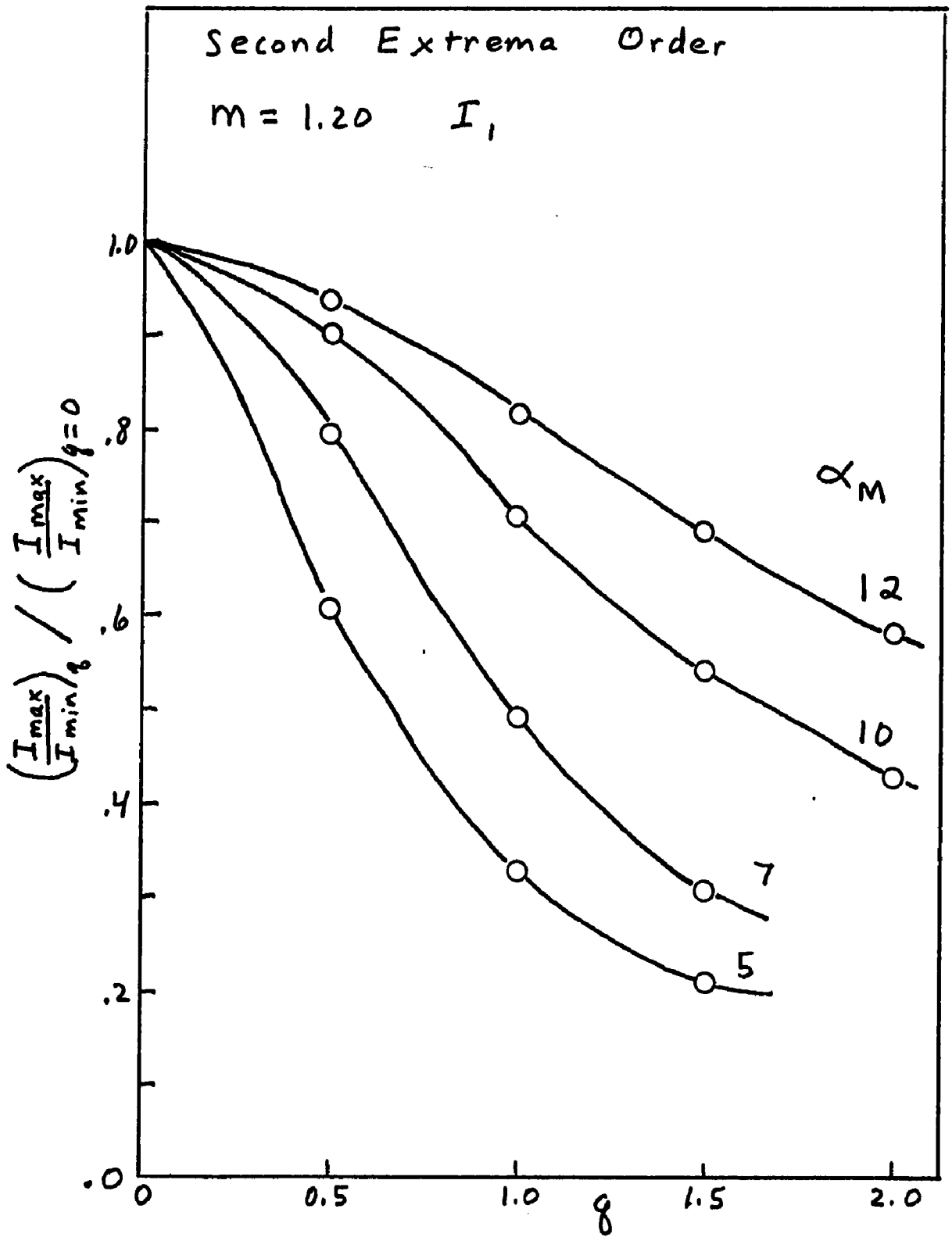

Fig. 105. Normalized Intensity Ratio Versus q for the Second Extrema Order Generated from the Angular Variation of I_1 for Heterodispersions Having m=1.20 and Different Modal Sizes

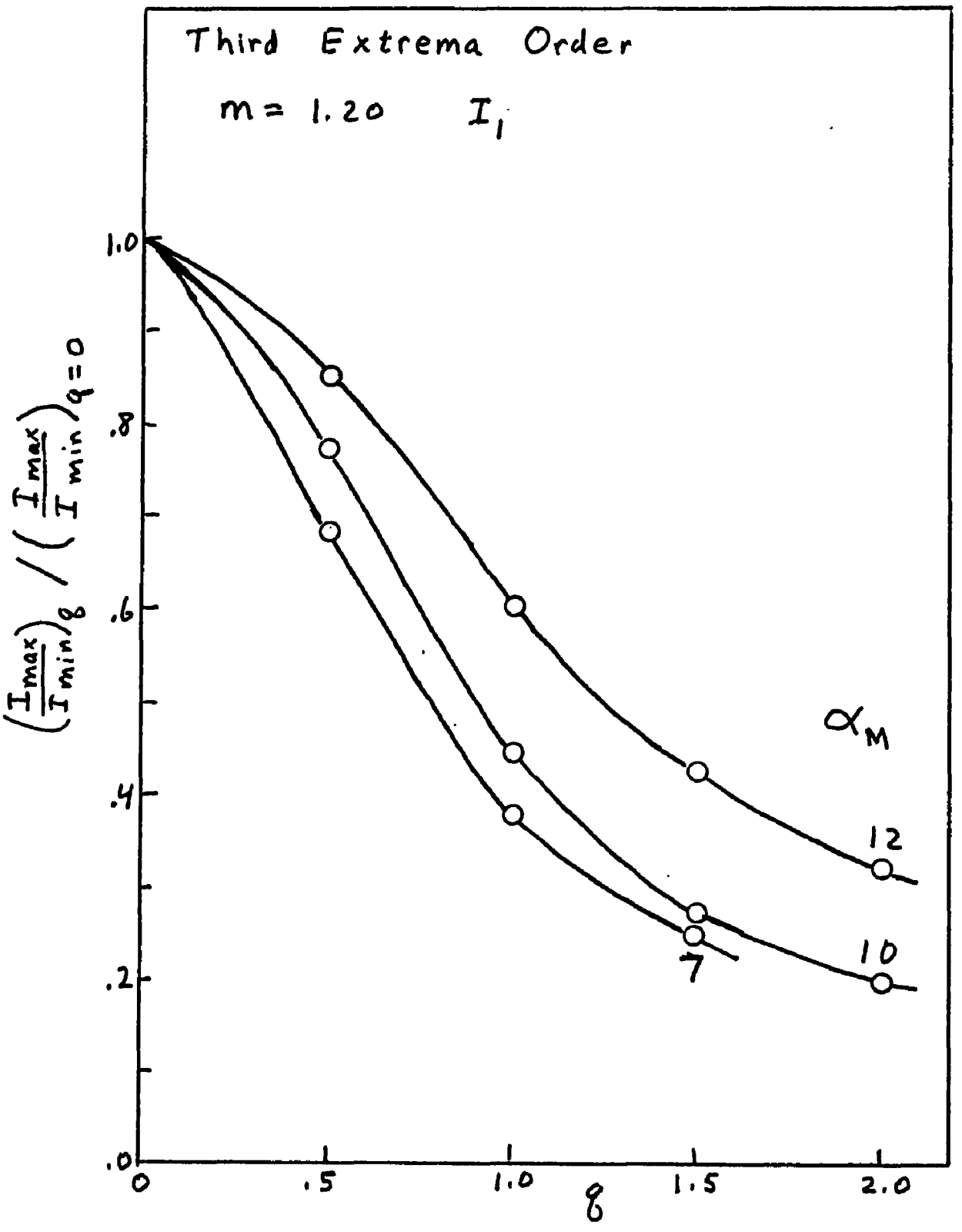

Fig. 106. Normalized Intensity Ratio Versus q for the Third Extrema Order Generated from the Angular Variation of I_1 for Heterodispersions Having m=1.20 and Different Modal Sizes

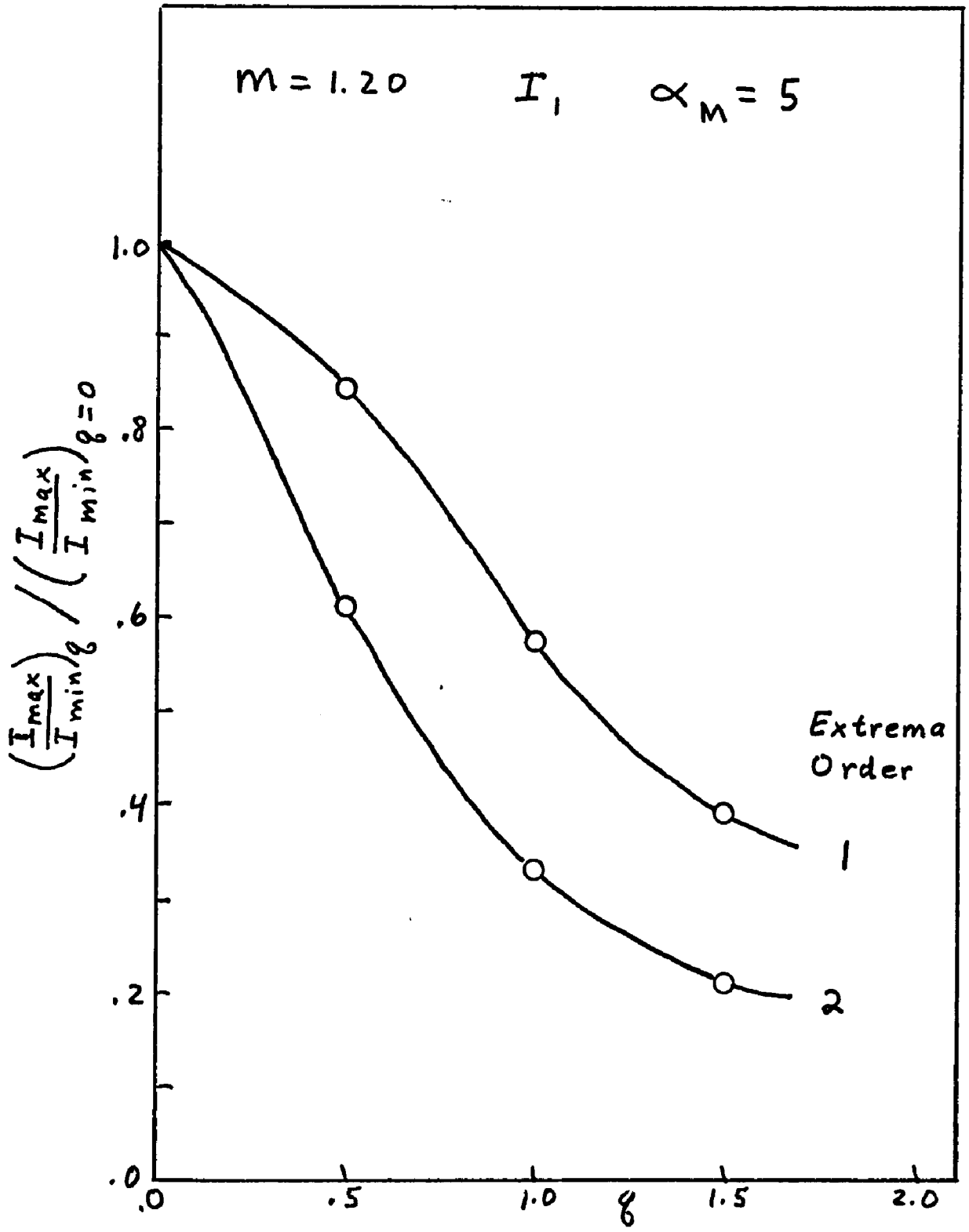

Fig. 107. Normalized Intensity Ratio Versus q for the First and Second Extrema Orders Generated from the Angular Variation of I_1 for Heterodispersions Having m=1.20 and α_M=5

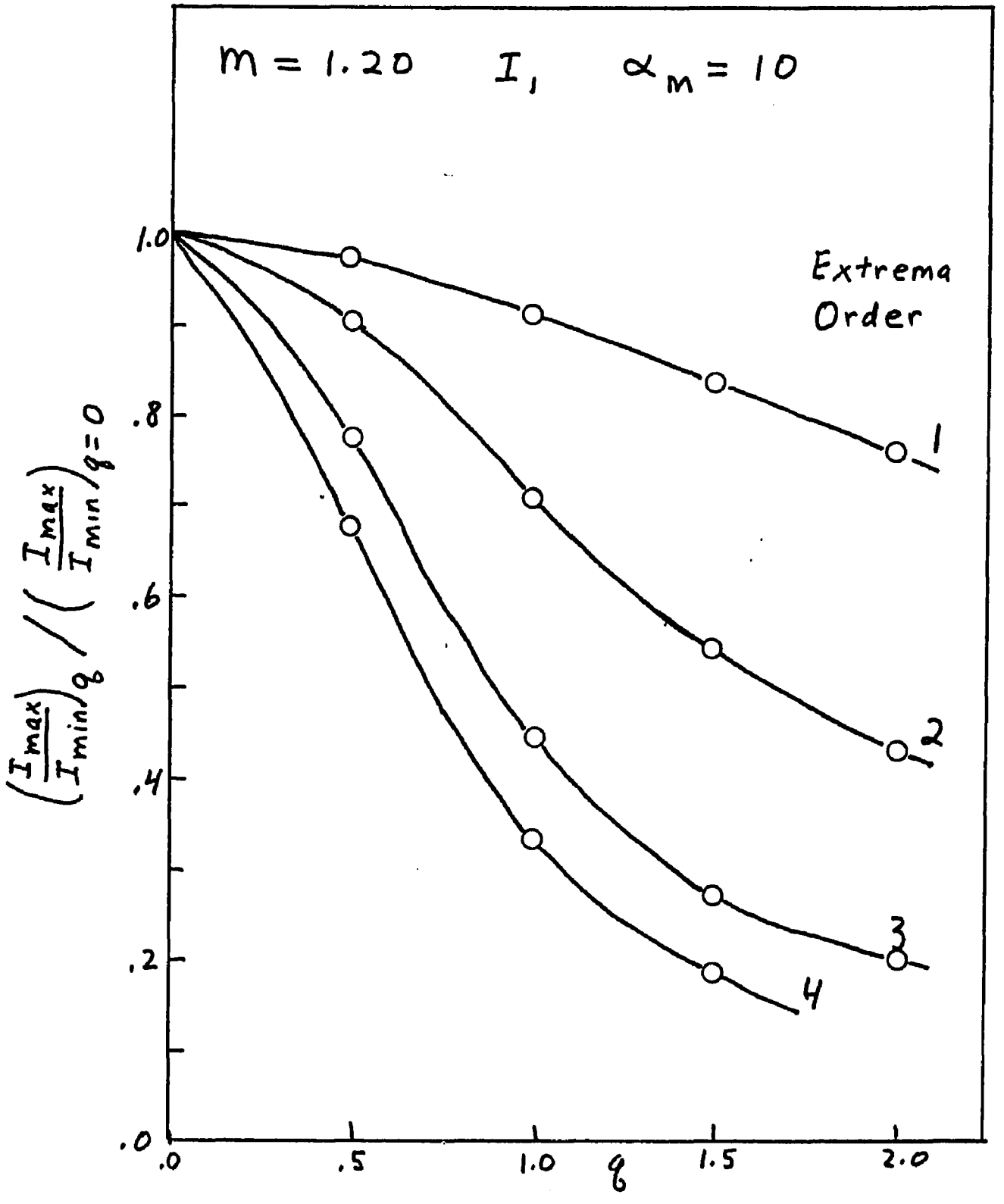

Fig. 108. Normalized Intensity Ratio Versus q for the First Four Extrema Orders Generated from the Angular Variation of I_1 for Heterodispersions Having m=1.20 and α_M=10

Empirical equations can be generated to approximate the curves shown in Figures 104-108. These equations have the following form:

$$\left(\frac{I_{max}}{I_{min}}\right)_q \Big/ \left(\frac{I_{max}}{I_{min}}\right)_{q=0} = 1 - \frac{q^2}{c_1 \alpha_M - c_2} \qquad (30)$$

where c_1 and c_2 are empirical constants that depend on the extrema order, m and the polarization of the incident light.

b. Intensity Slope Methods

1) Finite Difference Slope

In addition to the normalized intensity ratio other techniques were investigated that use the intensity of scattered light to determine the degree of heterodispersion. These techniques were developed from the following variations of the incremental intensity change $\frac{\Delta I}{I}$ applied to the intensity extrema:

$$\frac{I_{max}}{I_{min}} - 1 \quad \text{and} \quad \frac{I_{max} - I_{min}}{(I_{max} + I_{min})/2} .$$

The two cases differ only in the intensity value used for the denominator. In the former case the minimum intensity is used while in the latter case the average of the maximum and minimum intensity is used.

The behavior of $\frac{\Delta I}{I}$ with increasing q at a constant α_M is very similar to that seen for $\frac{I_{max}}{I_{min}}$ and need not be repeated. From the discussions in Chapter IV the major change that occurs in a given extrema pair with increasing q at a constant α_M can be represented by $\frac{\Delta I}{I}$. The

angular separation $\Delta\theta$ of the extrema remains approximately constant until the extrema pair have nearly washed out. Examples of this behavior were seen in Figures 35 and 37. Since $\Delta\theta$ remains approximately constant with increasing q one can normalize the incremental intensity change with respect to the angular separation yielding $\frac{\Delta I}{I\Delta\theta}$. This term represents the slope of the line segment connecting the maximum and minimum intensity of an extrema pair.

The intensity ratio of light scattered at two different angles can be shown to be closely related to the slope of the angular scattering curve. If the angular separation $\Delta\theta$ becomes very small the incremental change can be approximated by a derivative

$$\frac{\Delta I}{I\Delta\theta} \approx \frac{dI}{Id\theta} = \frac{d \ln I}{d\theta} \tag{31}$$

Conversely, if intensity measurements are made over a finite angular range one has

$$\frac{d \ln I}{d\theta} \approx \frac{\ln I}{\Delta\theta} = \frac{1}{\Delta\theta}\left(\ln I_{\theta_2} - \ln I_{\theta_1}\right) = \frac{1}{\Delta\theta} \ln\left(\frac{I_{\theta_2}}{I_{\theta_1}}\right) \tag{32}$$

combining equations 32 and 33,

$$\frac{\Delta I}{I\Delta\theta} \approx \frac{1}{\Delta\theta} \ln\left(\frac{I_{\theta_2}}{I_{\theta_1}}\right) \tag{33}$$

one sees that the logarithm of the intensity ratio divided by the angular separation is equal to the normalized intensity slope.

Hodkinson[50] had previously used the intensity ratio of light scattered at two different angles to measure the particle size. He had shown that the intensity ratio of light scattered at two different angles within the main lobe of the Fraunhoffer diffraction pattern would provide a unique particle size measurement. Gravatt[52] has recently developed an apparatus using Hodkinson's method to measure particle size distributions. Thus, the intensity ratio of light scattered at two different angles provides a measure of the particle size if the angles are in the forward direction (main Fraunhoffer lobe) and a measure of the heterodispersion if the angles represent the location of intensity extrema. These techniques can be considered to be limiting cases of the intensity slope measurement which automatically provides both the size and heterodispersion of a given size distribution as will be seen later.

The intensity slopes were initially used as an alternative to the intensity ratio for finding the breadth of a given size distribution. The mode of the distribution was, as before, determined from the angular location of the intensity minima. As seen previously for the $\frac{I_{max}}{I_{min}}$ curves, the $\frac{\Delta I}{I\Delta\theta}$ curves have considerable oscillations as a function of the mode. These oscillations cause interpolation errors and destroy the systematic pattern of the family of $\frac{\Delta I}{I\Delta\theta}$ versus q curves. Figure 109 shows the oscillations of $\frac{\Delta I}{I\Delta\theta}$ for the first three extrema orders plotted as a function of modal size. These curves correspond to the I_1 scattering from a monodisperse distribution having m = 1.20 and represents the same data seen in Figure 103 where $\frac{I_{max}}{I_{min}}$ was plotted. The oscillations in $\frac{\Delta I}{I\Delta\theta}$ increase with increasing extrema order at a fixed modal size and in-

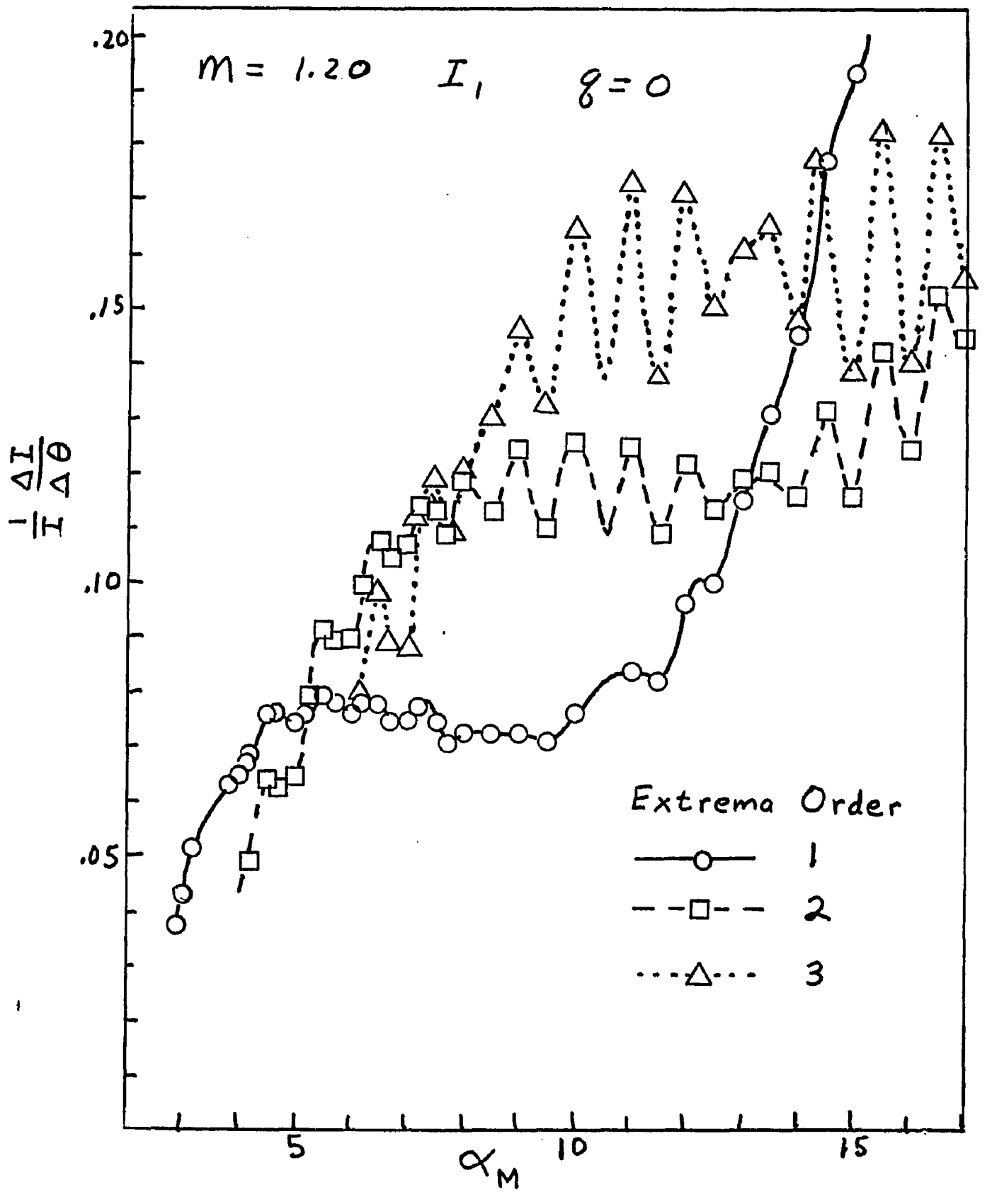

Fig. 109. Intensity Slope $\frac{\Delta I}{I \Delta \theta}$ Versus Modal Size α_M for Different Extrema Orders Generated from the Angular Variation of I_1 for Monodisperse Distributions with m=1.20

crease with increasing modal size at a fixed extrema order. This trend is similar to that seen for $\frac{I_{max}}{I_{min}}$ with respect to increasing extrema order but is opposite to the trend seen for increasing α_M. In addition, the values of $\frac{\Delta I}{I\Delta\theta}$ generally increase with increasing α_M in contrast to $\frac{I_{max}}{I_{min}}$ which generally decreases with increasing α_M.

A similar strategy used previously on the $\frac{I_{max}}{I_{min}}$ curves will provide a systematic pattern in the slope curves and allow interpolation. This strategy involves normalizing the slope $\frac{\Delta I}{I\Delta\theta}$ with its value at q = 0.

A series of graphs of the normalized slope,

$$\left(\frac{\Delta I}{I\Delta\theta}\right)_q \Big/ \left(\frac{\Delta I}{I\Delta\theta}\right)_{q=0}$$

, versus q were then plotted to show the systematic behavior with respect to α_M and the extremum order. The normalized intensity slopes for various heterodispersions having constant modes ranging from $\alpha_M = 3$ to $\alpha_M = 12$ for the first, second and third extrema pairs are shown in Figures 110, 111 and 112 respectively. The same data in these figures was previously plotted as $\frac{I_{max}}{I_{min}}$ in Figures 104-106. Comparing the graphs for the normalized slopes with the graphs for the normalized intensity ratio shows that they have a very similar behavior. Both functions decrease with increasing q at a faster rate for smaller modal sizes at a fixed extrema order and for higher extrema orders at a fixed modal size. Graphs of the normalized slopes for different extrema orders having a constant mode are shown in Figures 113 and 114 for $\alpha_M = 5$ and 10 respectively. Again note the greater number of extrema pairs for the larger mode.

Empirical equations can be developed to approximate the normalized intensity curves shown in Figures 110-114. These equations have

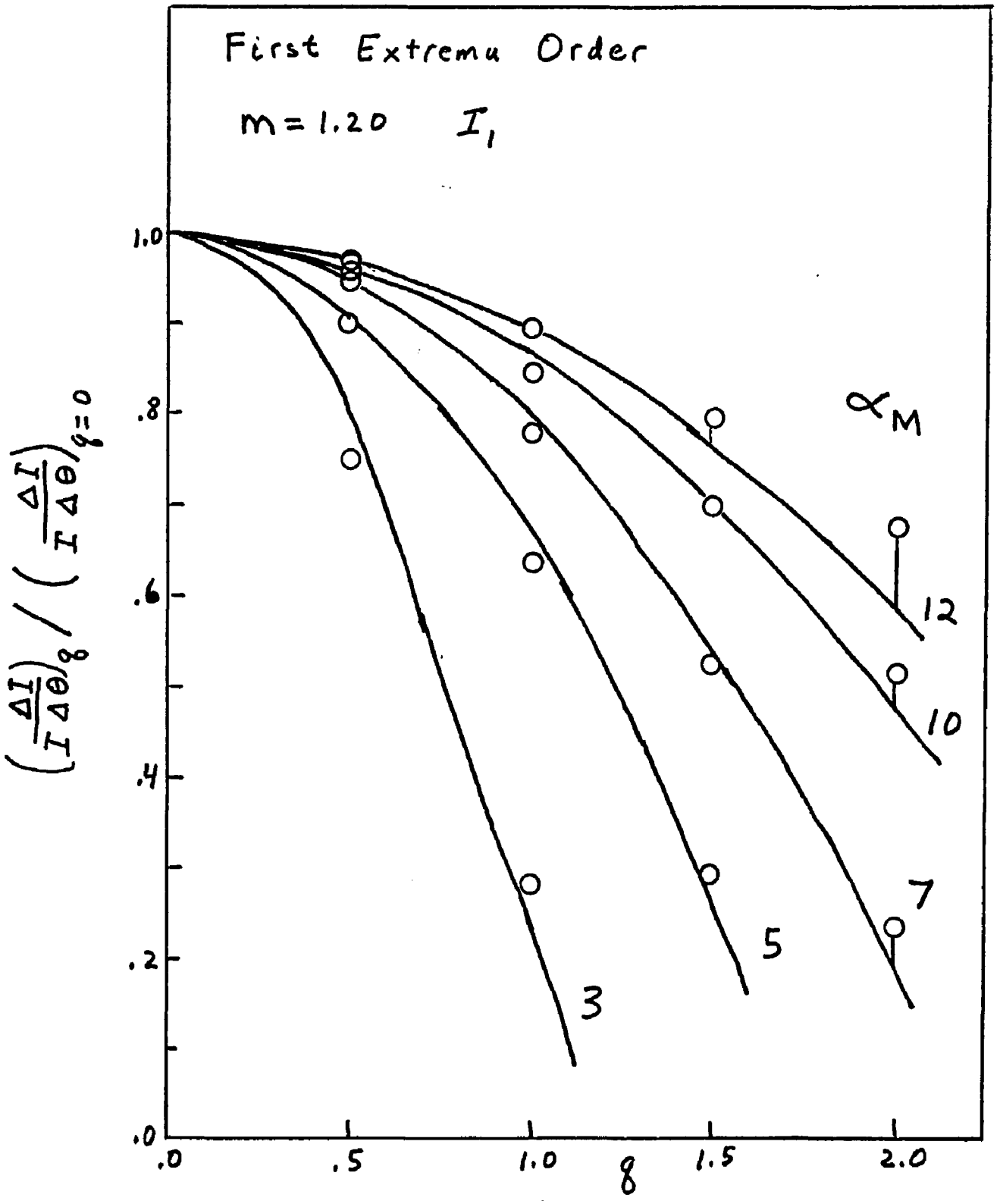

Fig. 110. Normalized Intensity Slope Versus q for the First Extrema Order Generated from the Angular Variation of I_1 for Heterodispersions Having m=1.20 and Different Modal Sizes

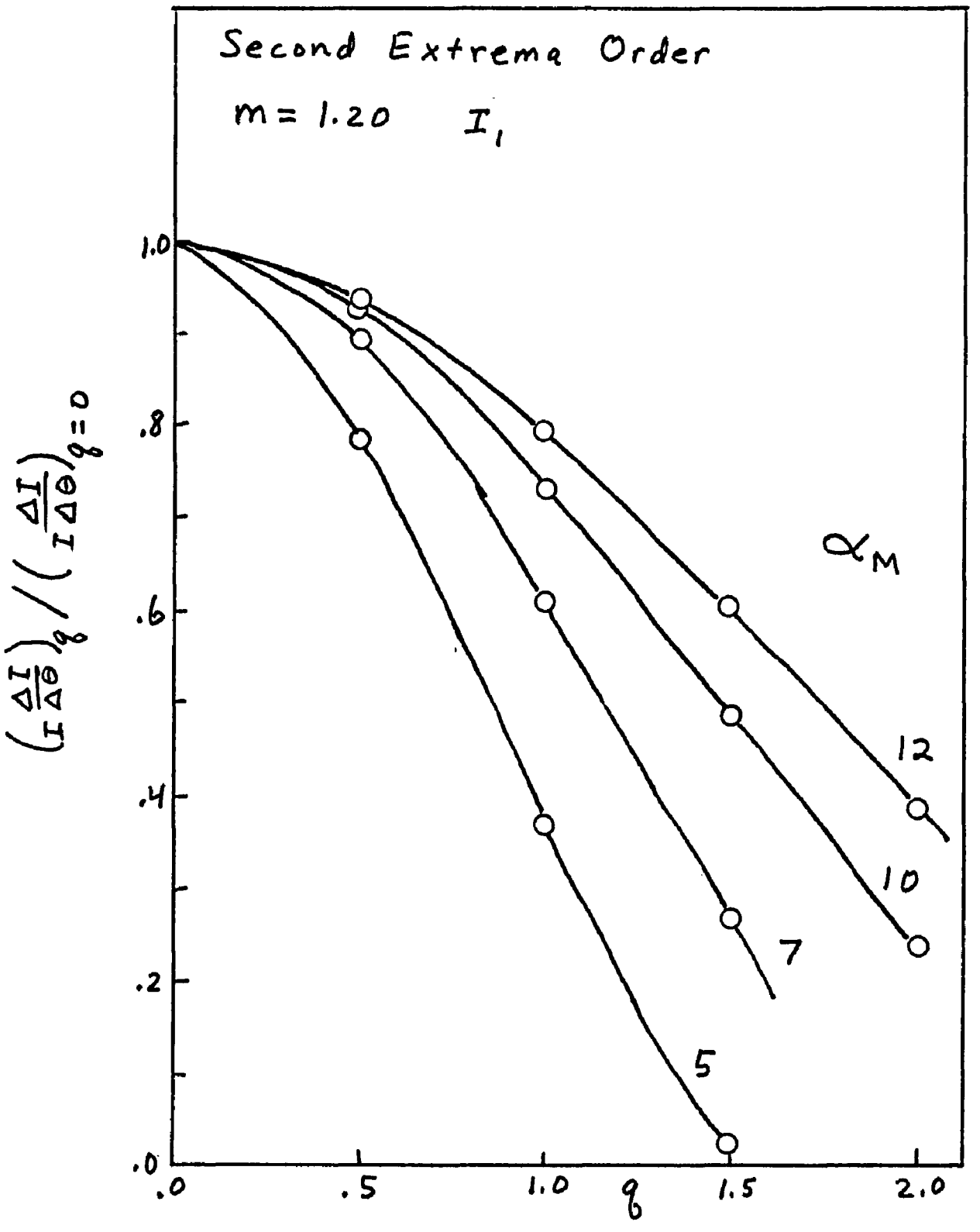

Fig. 111. Normalized Intensity Slope Versus q for the Second Extrema Order Generated from the Angular Variation of I_1 for Heterodispersions Having m=1.20 and Different Modal Sizes

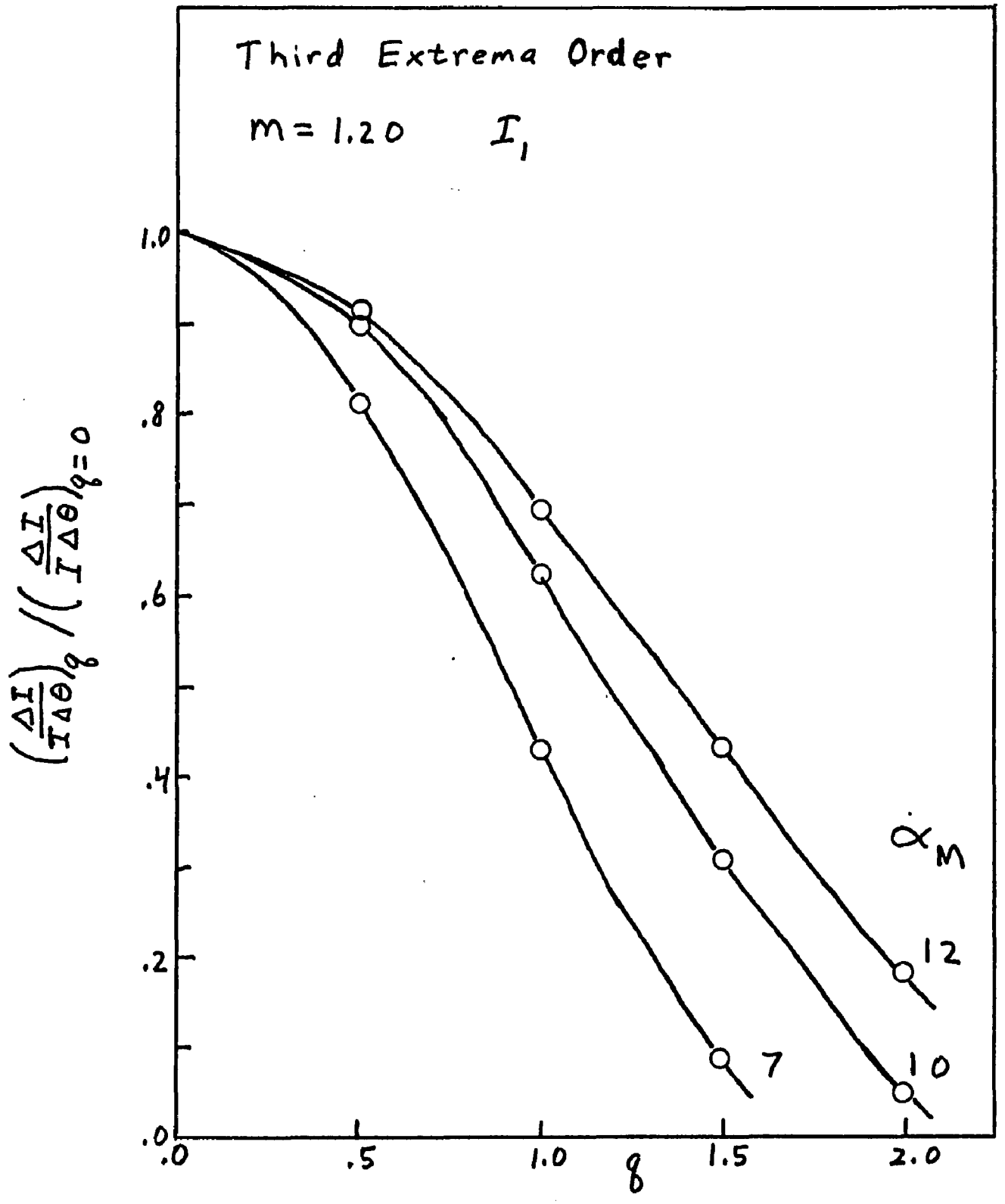

Fig. 112. Normalized Intensity Slope Versus q for the Third Extrema Order Generated from the Angular Variation of I_1 for Heterodispersions Having m=1.20 and Different Modal Sizes

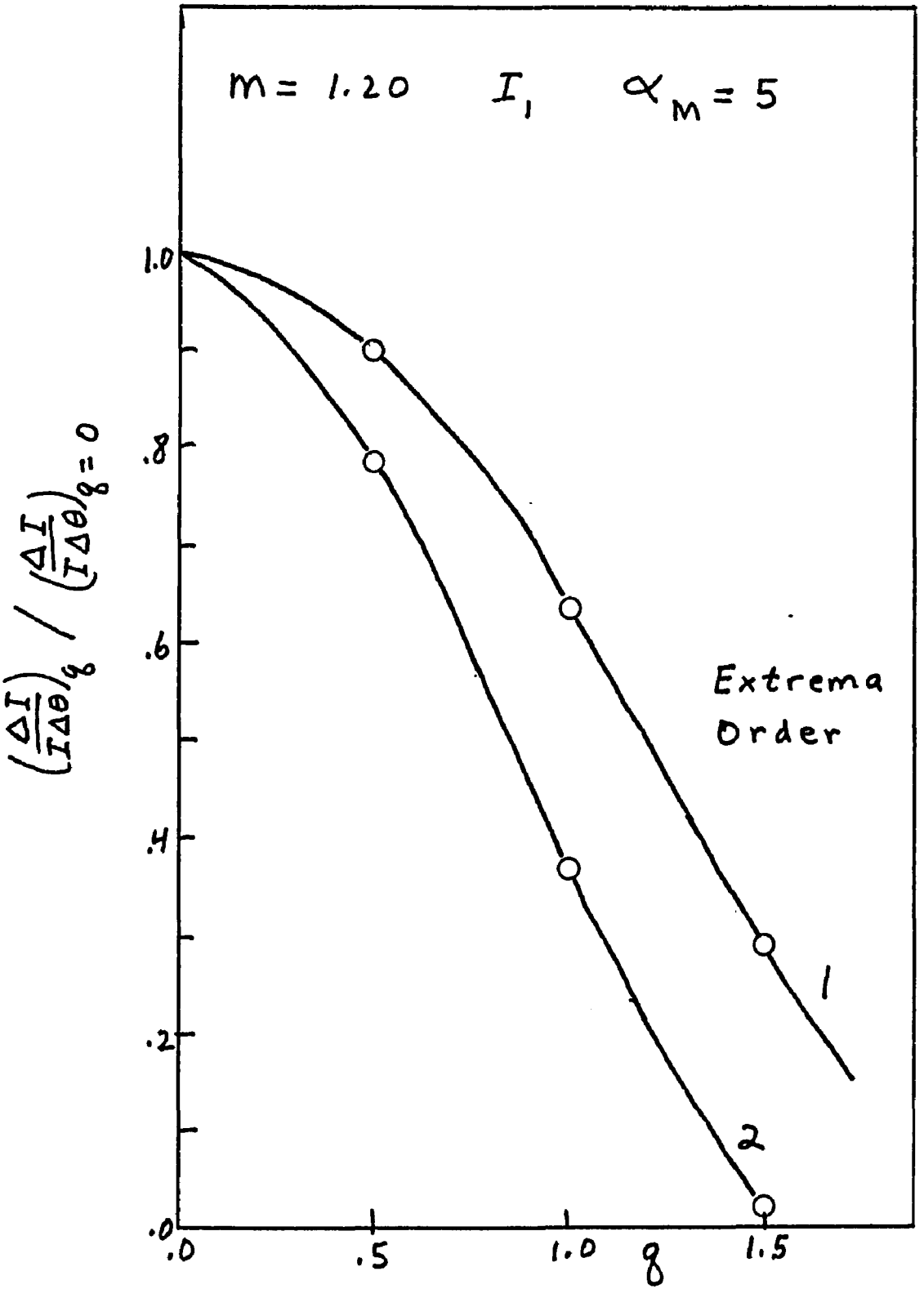

Fig. 113. Normalized Intensity Slope Versus q for the First and Second Extrema Orders Generated from the Angular Variation of I_1 for Heterodispersions Having $m=1.20$ and $\alpha_M=5$

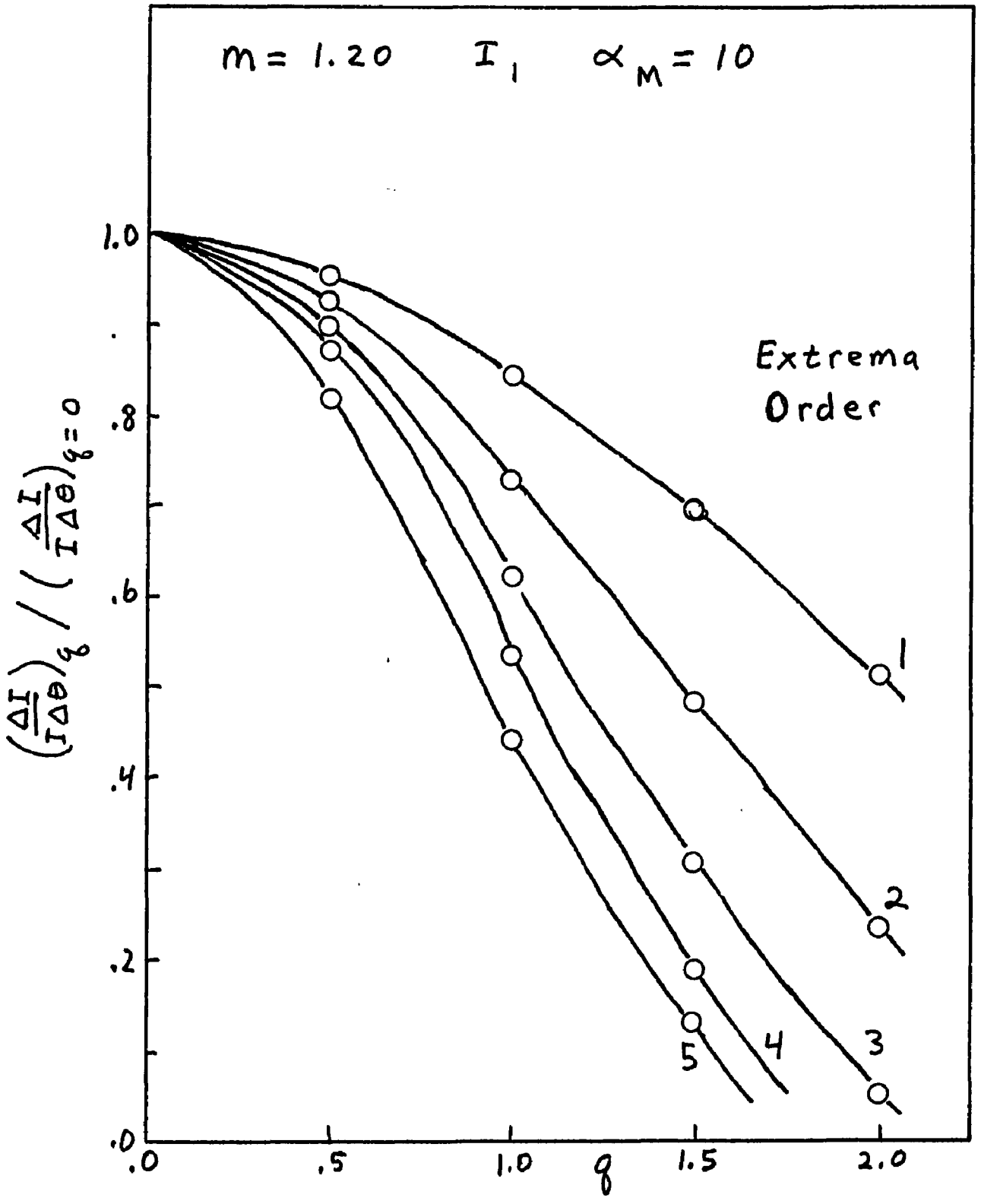

Fig. 114. Normalized Intensity Slope Versus q for the First Five Extrema Orders Generated from the Angular Variation of I_1 for Heterodispersions Having m=1.20 and α_M=10

the following form:

$$\left(\frac{\Delta I}{I\Delta\theta}\right)_q \Big/ \left(\frac{\Delta I}{I\Delta\theta}\right)_{q=0} = 1 - \frac{q^2}{c_1 \alpha_M - c_2} \qquad (34)$$

where c_1 and c_2 are empirical constants that depend on the extrema order, m and the polarization of the incident light. Note that equation 35 for the normalized slope has the same form as equation 30 for the normalized intensity ratio. The equivalence of the two equations is not surprising because of the close relation between intensity ratios at two angles and the intensity slopes. Although equations 30 and 35 are reasonable approximations of the actual data, they can be considerably improved by using a more complicated expression of α_M and q. However, this would make them less attractive because of the additional calculations required. The accuracy of the empirical equation in approximating the data is illustrated in Figure 110 where the solid lines were drawn from equation 35. The constants c_1 and c_2 in this case are 0.9 and 1.4 respectively. Note that a significant deviation between the empirical equation and data points only occurs at the largest modal size and largest heterodispersion.

Using the normalized slopes to determine the breadth of a distribution is equivalent to using the normalized intensity ratio if the slopes are calculated from the intensity extrema. The same experimental measurements and errors of the intensity extrema would be used in both cases. As will be shown in Chapter VI, accurate measurements of the intensity minima are very difficult and will cause a significant error in the determination of the distribution width. One minor advantage of

the normalized slope method over the normalized intensity ratio is the possible elimination of the background scattering from the solvent and optical cell. If the angular variation of the scattered intensity due to the background is much smaller than the angular variation due to the particles, then the background intensity will be eliminated in the slope calculations.

2) Differential Slope

The primary advantage of the normalized slope method results when intensity measurements are made over a very small angular increment instead of the angular separation between the intensity extrema. If the angular increment is sufficiently small the slope then approximates a derivative and intensity slopes can be determined over the entire scattering range. These differential slopes can be experimentally measured while the finite slopes calculated from the extrema do not correspond to a physical measurement. Moreover, the slope calculated from the intensity extrema is significantly smaller than the actual intensity slope between the extrema even if the extrema intensities were measured with no error. However, in practice there is a significant error in the extrema measurements which reduces the calculated slope even further. The major source of this error is due to multiple scattering and a large solid angle in the detector. Both of these sources of error are greatest at the intensity extrema locations. Measuring the differential slope between the extrema instead of the finite slope calculated from the extrema minimizes this error.

A series of calculations were then made to determine the angular derivative of the scattered light from different particle size distributions having a constant mode. These derivatives were obtained from the Stirling's polynomials used to approximate the angular scattering

data. Figures 115-118 show the results of some of these calculations for I_1 and m = 1.20. The same distributions had been previously plotted as the scattered intensity versus the angle of observation in Figures 18-21. Each figure shows the normalized angular derivative $\frac{1}{I} \frac{dI}{d\theta}$ of the scattered intensity plotted against the angle θ for several heterodispersions having the same mode but different distribution widths. Note that the derivatives can have positive, negative or zero values. When the derivative is zero at a given angle the angular intensity curve has an extremum at that position.

Figure 115 shows the angular derivative curves for particle size distributions having a constant mode of $\alpha_M = 3$ and heterodisperse parameters of q = 0.0, 0.5 and 1.0. This figure shows the common features present in all of the derivative curves. As the angle θ increases from 0^o the slope becomes more negative, reaches a minimum and then rapidly increases. This region corresponds to the forward scattering lobe. The slope then crosses 0, reaches a maximum value and then decreases again to a zero slope. The angle at which the slope first crosses through 0 represents the first minimum while the second crossing represents the first maximum. Note that the slope changes very rapidly in the first crossing which represents a deep minimum and gradually in the second crossing which represents a shallow maximum. All three curves have a zero slope value at $\theta = 85^o$ as expected from previous discussions showing that the minima remain constant with increasing heterodispersion. However, the angles at which the slope crosses through zero the second time decreases with increasing heterodispersion. This migration of the angular location of zero slope with increasing q corresponds to the migration of the maximum location toward the minimum as seen in Figure 18.

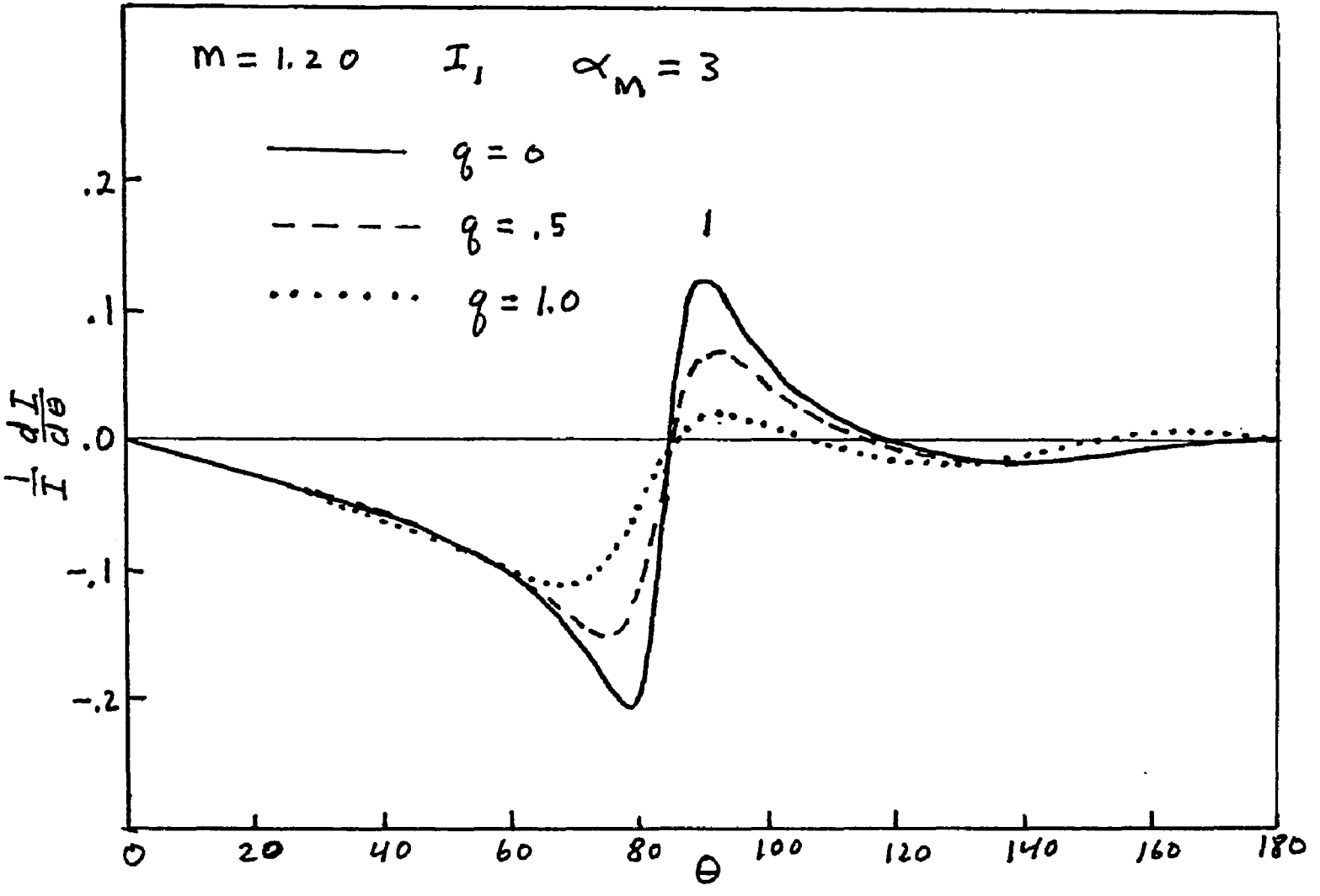

Fig. 115. Normalized Angular Derivative of I_1 for Heterodisperse Distributions Having m=1.20 and α_M=3

The intensity slope has a maximum value between the two angles of zero slope and is shown by the number 1. Note that the angular location of this maximum slope remains approximately constant while the magnitude of the slope decreases with increasing heterodispersion. The angular location of this maximum slope is very close to the intensity minimum. Figure 115 thus illustrates a new method that can be used to determine particle size distributions. The mode is determined from the angular location of the maximum slope while the width of the distribution is determined from the value of the maximum slope. This approach assumes that the angular location of the maximum slope is independent of the distribution width. The previous techniques in this chapter used the intensity minima to find the mode and had assumed that the angular location of the intensity minima was independent of the distribution width. Although the mode of the distribution can also be determined from the location of the intensity minima (zero slope) the maximum slope method is applicable to much wider distributions. This is possible because the maximum slope remains long after the minimum intensity has been washed out.

The differential slope method was developed as an extension of the method discussed previously where the slope of the line segment connecting the intensity extrema was used to determine the width of the distribution. The important differences between the two methods should be pointed out. The differential slope seen in Figure 115 increases from zero at the intensity minimum to a maximum value and then decreases to zero again at the intensity maximum. In contrast, the line segment connecting the maximum and minimum intensity has a constant slope over

the angular range between the extrema. This constant slope value is the average of the differential slope values in Figure 115 taken over the angular range defined by the maximum and minimum intensity. One sees that both the maximum slope value and the average slope value decreases with increasing heterodispersion. However, the average slope method is no longer applicable when the heterodispersion increases to the point where the extrema pair are washed out. The differential slope can still be used to determine both the mode and width of the distribution long after the extrema have washed out.

Very similar patterns are seen for angular derivative curves from particle size distributions with larger modes. Since larger particle sizes have a greater number of intensity extrema than smaller particle sizes the angular derivative curves will also show a greater number of derivative maxima. Figure 116 shows the angular derivative curve for particle size distributions having a constant mode of $\alpha_M = 5$ and various degrees of heterodispersion ranging from q = 0.0 to 2.0. This figure shows that there are now two derivative maxima shown by the numbers 1 and 2, that can be used to determine the mode and width of the distribution. Note that the angular location of the maximum slopes remain constant with increasing heterodispersion while the value of the slopes decrease. As seen previously with the intensity ratio and the normalized slopes, the values of the differential slopes decrease at a faster rate for the higher extrema pairs.

Figure 116 shows that at q = 2.0 the first two extrema pairs have disappeared completely. This size distribution could not be detected by any of the previous techniques discussed. However, the derivative

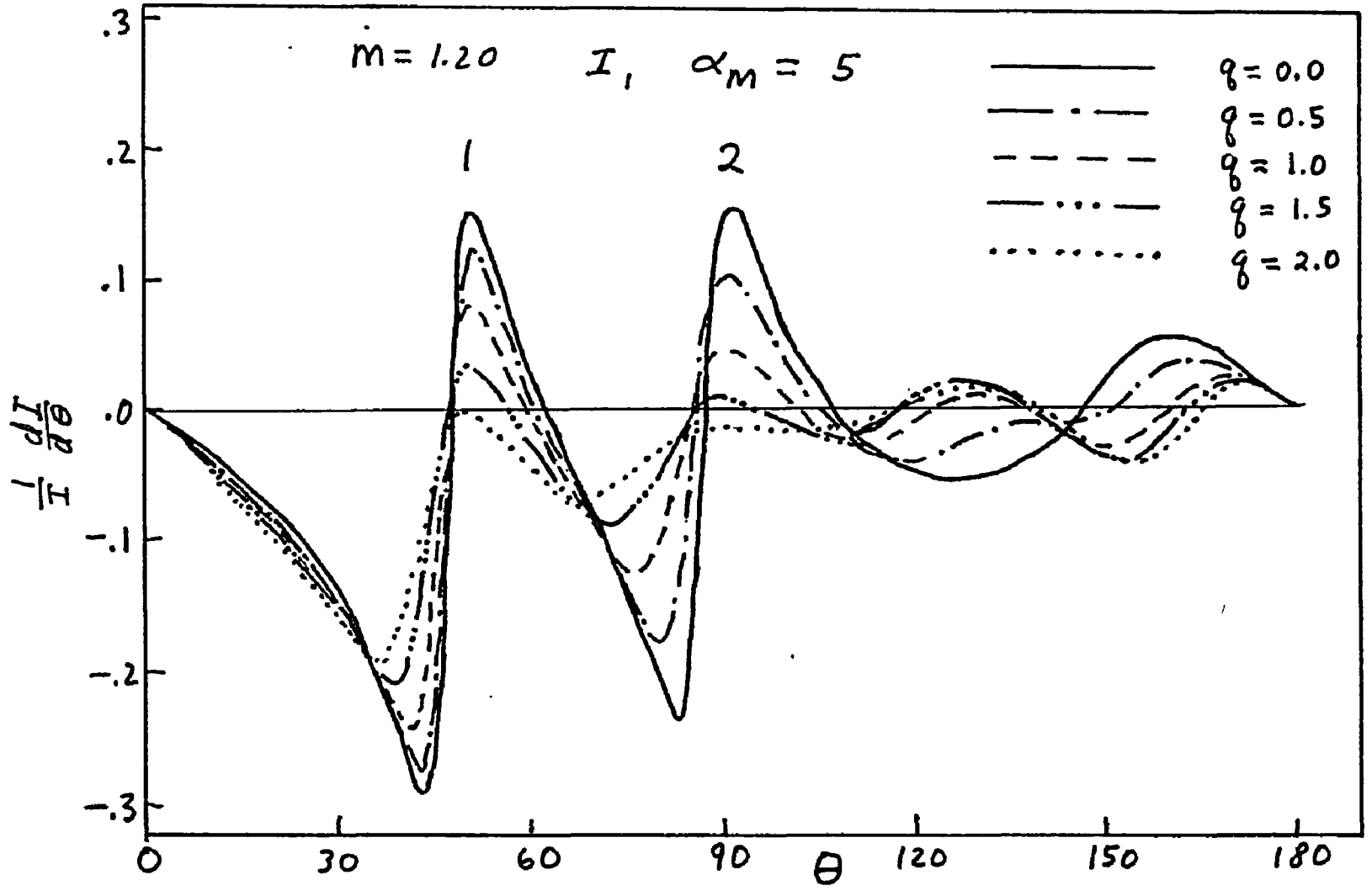

Fig. 116. Normalized Angular Derivative of I_1 for Heterodisperse Distributions Having m=1.20 and α_M=5

curve has a well defined maximum at 1 which allows both the mode and the width of the distribution to be determined. Note that the derivative has a zero value at the maximum for q = 2.0. Distributions with larger q values would have negative values at the maximum slope. With increasing heterodispersion, a limiting negative value of the slope is eventually reached. This limiting value is approximately the average of the maximum and minimum slope values of the curve representing a monodisperse distribution. The second maximum slope in Figure 116 has nearly reached this limiting value.

Increasing the modal size to α_M = 10 results in a greater number of derivative maxima. Figure 117 shows that there are now five derivative maxima designated by the numbers 1-5 that can be used to determine the particle size distributions. The increasing rate at which the value of the derivative maxima decrease with increasing q for the higher orders can be used as a Vernier scale to obtain accurate distribution mode and width measurements. Figure 117 shows that the derivative slopes have reached their limiting value for the derivative maxima designated as 2-5. Note that these limiting values are the average of the maximum and minimum values of the monodisperse curve. The size distribution can still be accurately determined using the first derivative maximum for the q = 5 curve. None of the previously discussed methods will work for the large heterodispersions since the intensity extrema disappear at much lower q values.

Figure 117 also shows the very pronounced derivative in the backward direction. The scattering curves in this region were previously shown to originate from a reflection phenomenon. Note that the

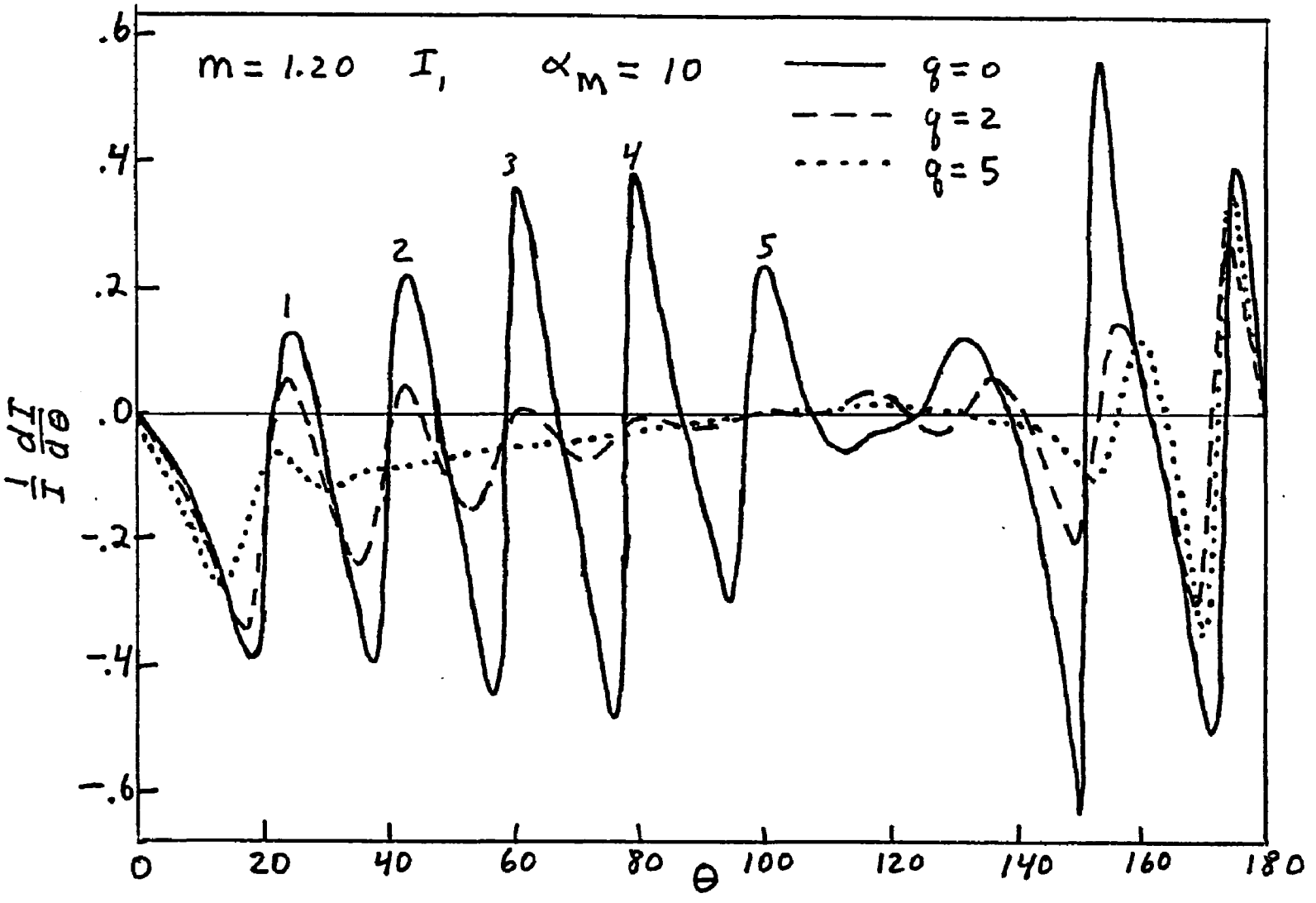

Fig. 117. Normalized Angular Derivative of I_1 for Heterodisperse Distributions Having m=1.20 and α_M=10

differential slopes in the backward direction are much less affected by the increasing heterodispersion than are the corresponding slopes in the forward direction. This behavior was previously pointed out for the angular intensity curves. Figure 117 also shows the boundary between the regions characterized by diffraction in the forward direction and reflection in the backward direction. A similar behavior is seen for α_M =15 in Figure 118. The ordinate scale in this figure is greatly reduced.

The corresponding graphs for the differential slopes from I_2 are very similar to those seen from I_1 except for the modifications resulting from the Rayleigh minimum and the very shallow extrema in the forward direction. The Rayleigh minimum was shown to shift from $\theta = 90^o$ to larger angles as the particle size increased from $\alpha_M = 0$. This shift allows one to use the differential slope method to determine particle size distributins for particle sizes in the Rayleigh region (smaller than $\alpha_M = 0.5$). Figure 119 shows the differential slope of I_2 plotted against the angle θ for different distributions having a constant mode $\alpha_M = 1.06$ and heterodispersions of q = 0.0, 0.5 and 1.0. Since the intensity curve has only one minimum close to 90^o the differential slope crosses through zero only once. As expected, the curves for all of these distributions cross through zero at the same angle. The derivative maximum, designated by 1, is also located at a fixed angular position for all three distributions. Thus, either the location of the derivative zero or the derivative maximum can be used to determine the modal size.

The smallest modal size that can be measured depends on the

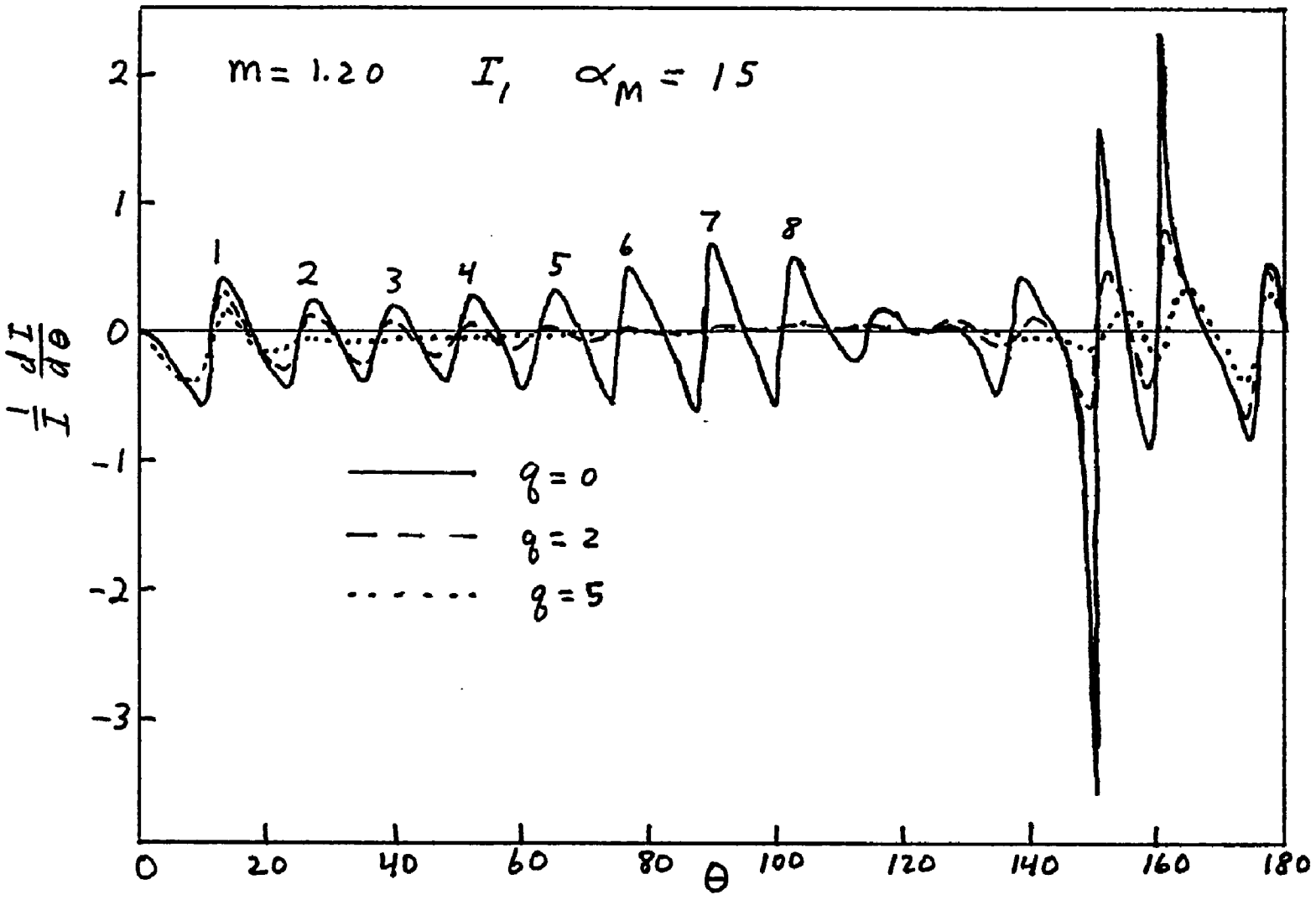

Fig. 118. Normalized Angular Derivative of I_1 for Heterodisperse Distributions Having m=1.20 and α_M=15

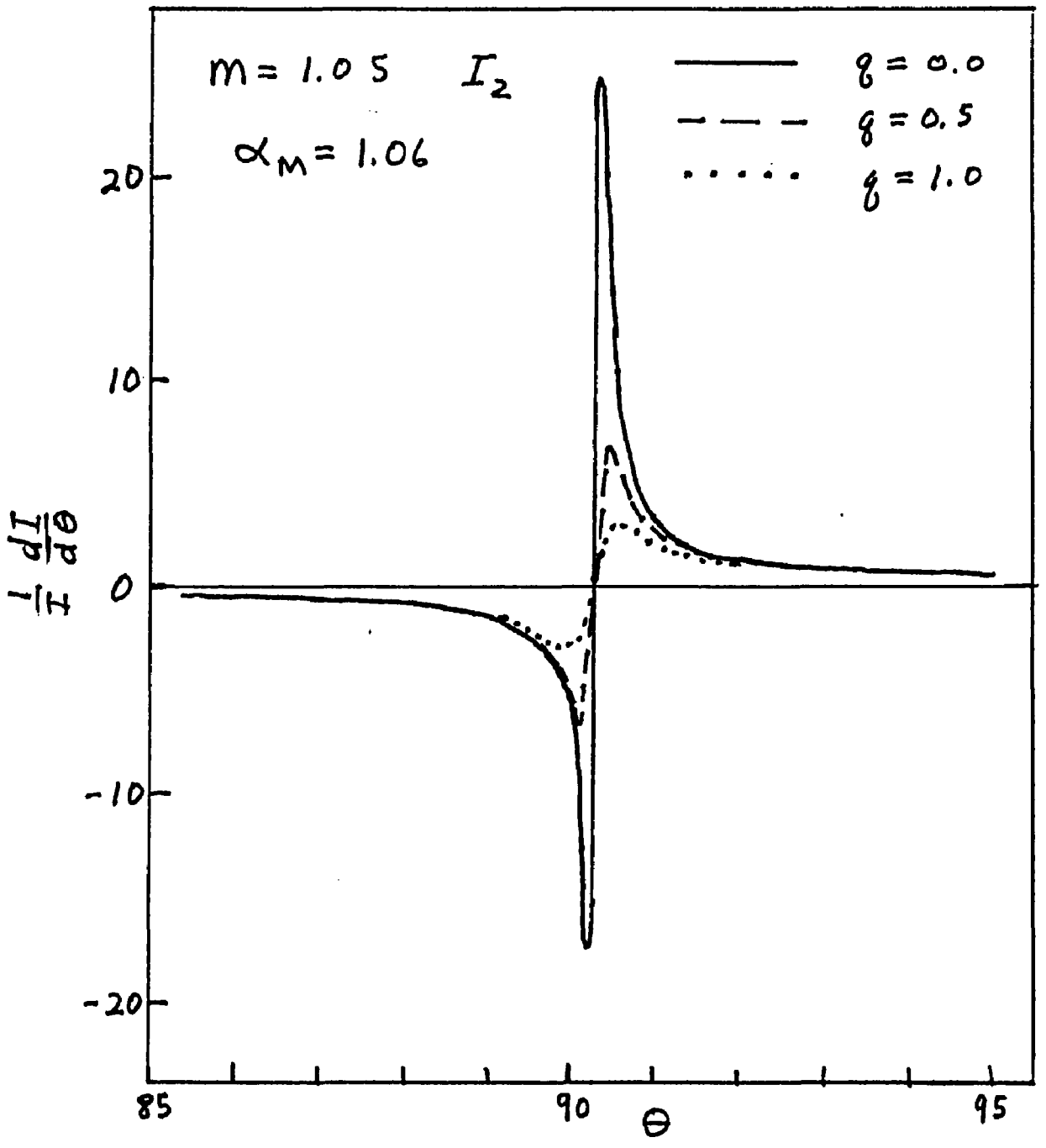

Fig. 119. Normalized Angular Derivative of I_2 for Heterodisperse Distributions Having m=1.05 and α_M=1.06

accuracy of the angular range of the measurement. For example, if one can measure the light scattered at angles within 0.1^{o} then one can determine distribution modes to within $\alpha_M = 0.4$. Smaller angles will allow even smaller modal sizes to be determined. The graphs in Figure 119 also show that the width of the distribution can reliably be determined from the value of the maximum slope. The value of the maximum slope decreases with increasing degree of heterodispersion.

In addition to the Rayleigh minimum, the second dominating feature in the I_2 differential slope is the very shallow extrema in the forward direction. Figure 120 shows the I_2 differential slope for different heterodispersions having a constant mode of $\alpha_M = 5.0$. Note that even for the monodisperse case the maximum derivative designated by 1 barely crosses the zero slope line while the maximum derivative designated by 2 is far removed from the line. This behavior differs considerably from the I_1 curves shown in Figure 116. As pointed out earlier, the differential slope method can still be effectively used to determine particle size distributions even when there are no intensity extrema present. Thus the first maximum derivative in Figure 120 can still be used to determine to mode and width of the distribution. Figure 120 also shows a very pronounced derivative minimum and maximum in the backward direction that quickly washes out with increasing heterodispersion. This pattern is very similar to that seen in Figure 119 and is due to the Rayleigh minimum. The I_2 differential slopes for distributions having $\alpha_M = 10$ and 15 are shown in Figures 121 and 122 respectively. Except for the effect from more shallow extrema in the forward direction, the differential slopes appear very

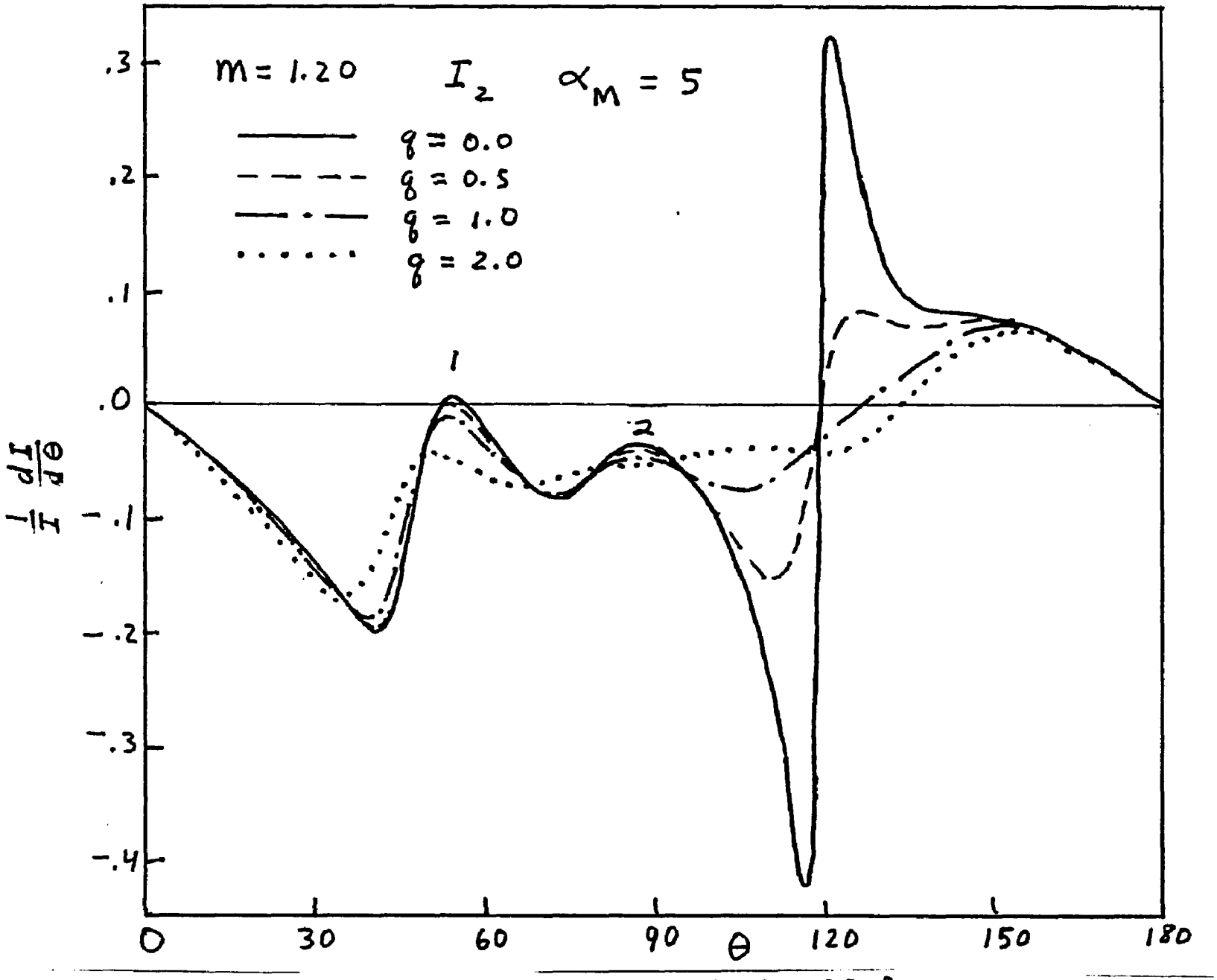

Fig. 120. Normalized Angular Derivative of I_2 for Heterodispersions Having m=1.20 and α_M=5

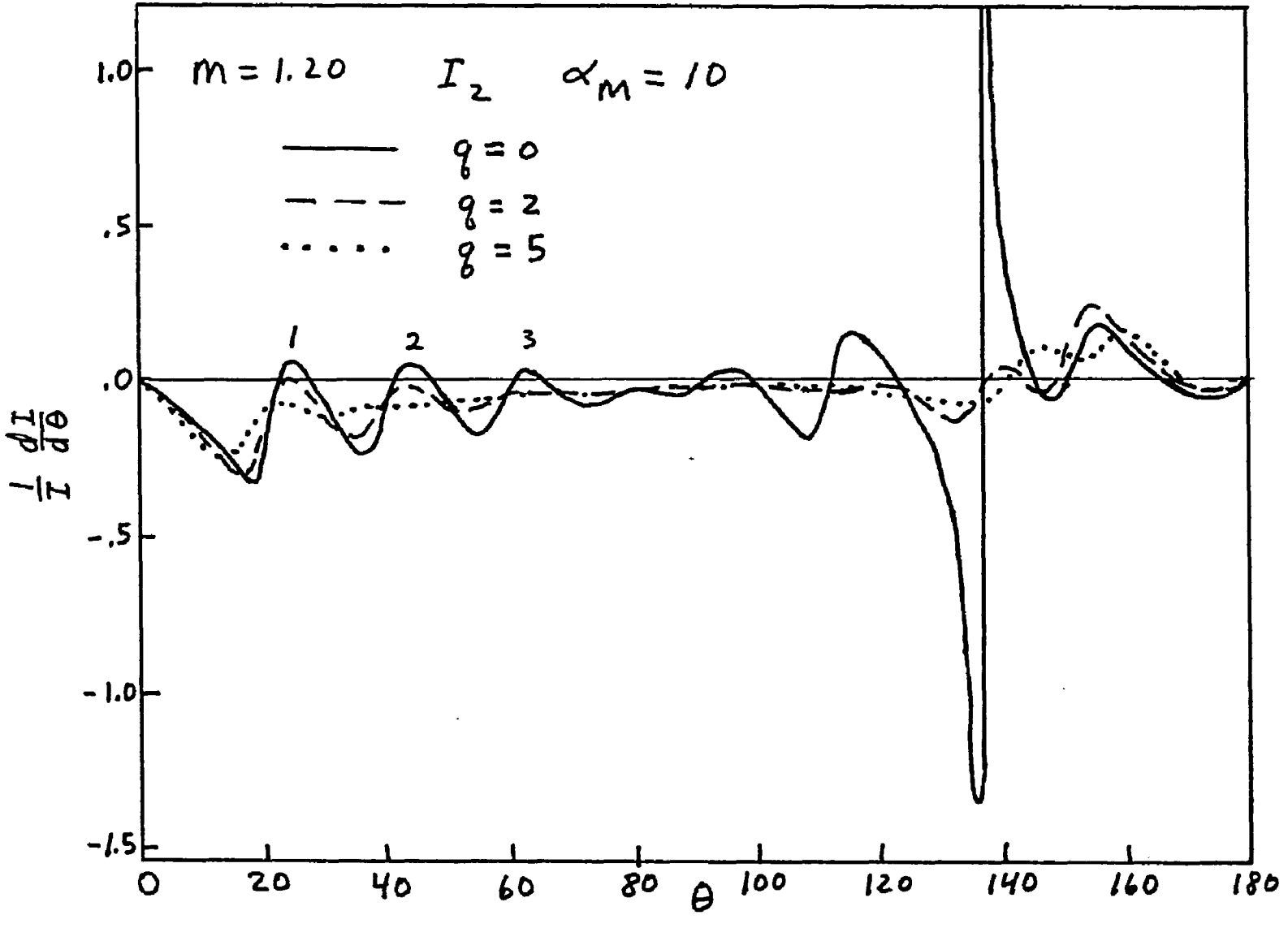

Fig. 121. Normalized Angular Derivative of I_2 for Heterodispersions Having m=1.20 and α_M=10

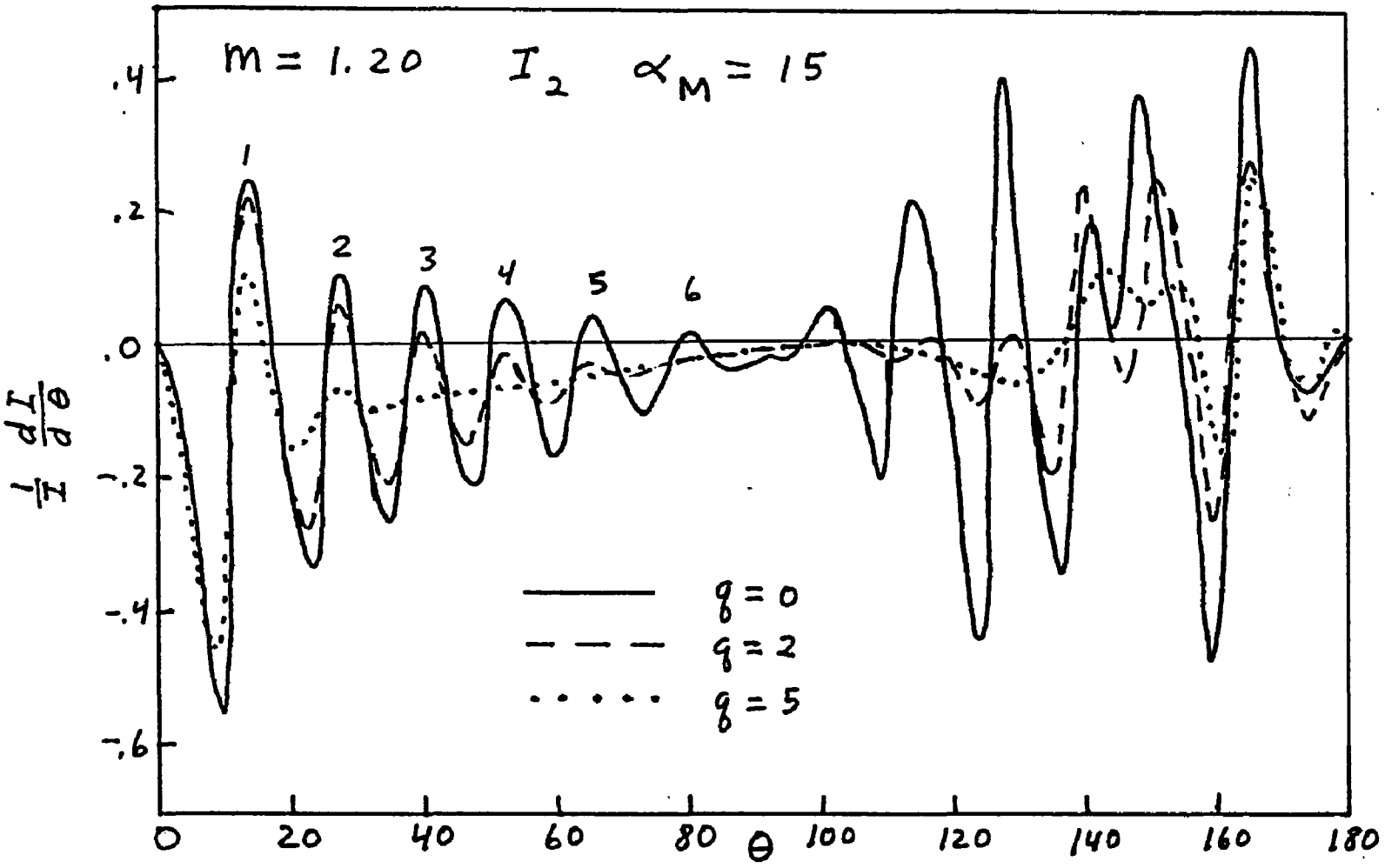

Fig. 122. Normalized Angular Derivative of I_2 for Heterodispersions Having m=1.20 and α_M=15

similar to the corresponding curves seen for I_1.

The differential slope method can therefore be used to determine particle size distributions for much smaller particle sizes and much larger heterodispersions than possible for the other techniques based on the intensity extrema. Very small particle sizes can be determined using the differential slope of I_2. This determination is possible because of of the angular shift of the Rayleight minimum with increasing particle size. For very wide particle size distributions the techniques based on the intensity extrema are useless since the extrema wash out. However, the differential slope method has derivative maxima that allow particle size distributions to be determined for extremely wide distributions where all of the intensity extrema are washed out.

c. Angular Difference Between Extrema Pairs

The previous techniques used to determine the width of a distribution in this section were based on intensity measurements. These techniques were developed from the major effects seen in the angular intensity plots due to increasing heterodispersion. Increasing the heterodispersion for distributions having a constant mode results in a dampening of the intensity extrema which remain at approximately the same angular location.

A more detailed examination of the less prominent effects showed that increasing the heterodispersion results in a shift of the intensity maximum toward a fixed intensity minimum. Wallace and Kratohvil[24] had previously observed that the intensity minima remain relatively constant while the maxima shift toward the minima with increasing heterodispersion at a constant mode. They therefore recommended that the location of the minimum intensity be used for determining the distribution mode. This section of

Chapter V will explore the possibility of using the angular difference between the intensity maximum and minimum of a given extremum pair to determine the distribution width.

The general approach for obtaining the size distribution using this method is, as before, divided into two parts. The first part uses the angular location of the intensity minima to determine the distribution mode. The distribution width is then determined in a second step from the angular difference between the intensity maximum and minimum of a given extremum pair. This method was tested on the light scattered from a series of particle size distributions having a constant mode and different heterodispersions.

Figures 123-125 show the angular difference $\Delta\theta$ between the I_1 extrema plotted against q for different particle size distributions having M = 1.20. The solid curves represent the angular difference $\Delta\theta$ of the extrema locations while the dashed curves represent the relative angular shift in the minima locations. A horizontal dashed line would mean that the minimum location has not shifted. Higher $\Delta\theta$ values for the dashed line implies a shift in the minimum location away from the maximum while lower $\Delta\theta$ values imply a shift toward the maximum.

The curves representing the minima locations were arbitrarily superimposed over the angular difference curves at q = o to show the relative shift of the minima compared to the angular difference of the extrema pair. Subtracting the value of the minimum curve from the angular difference curve will give the relative shift of the maximum extremum. If the minimum curve (dashed curve) is a horizontal line, then the entire change in the angular difference $\Delta\theta$ with increasing q

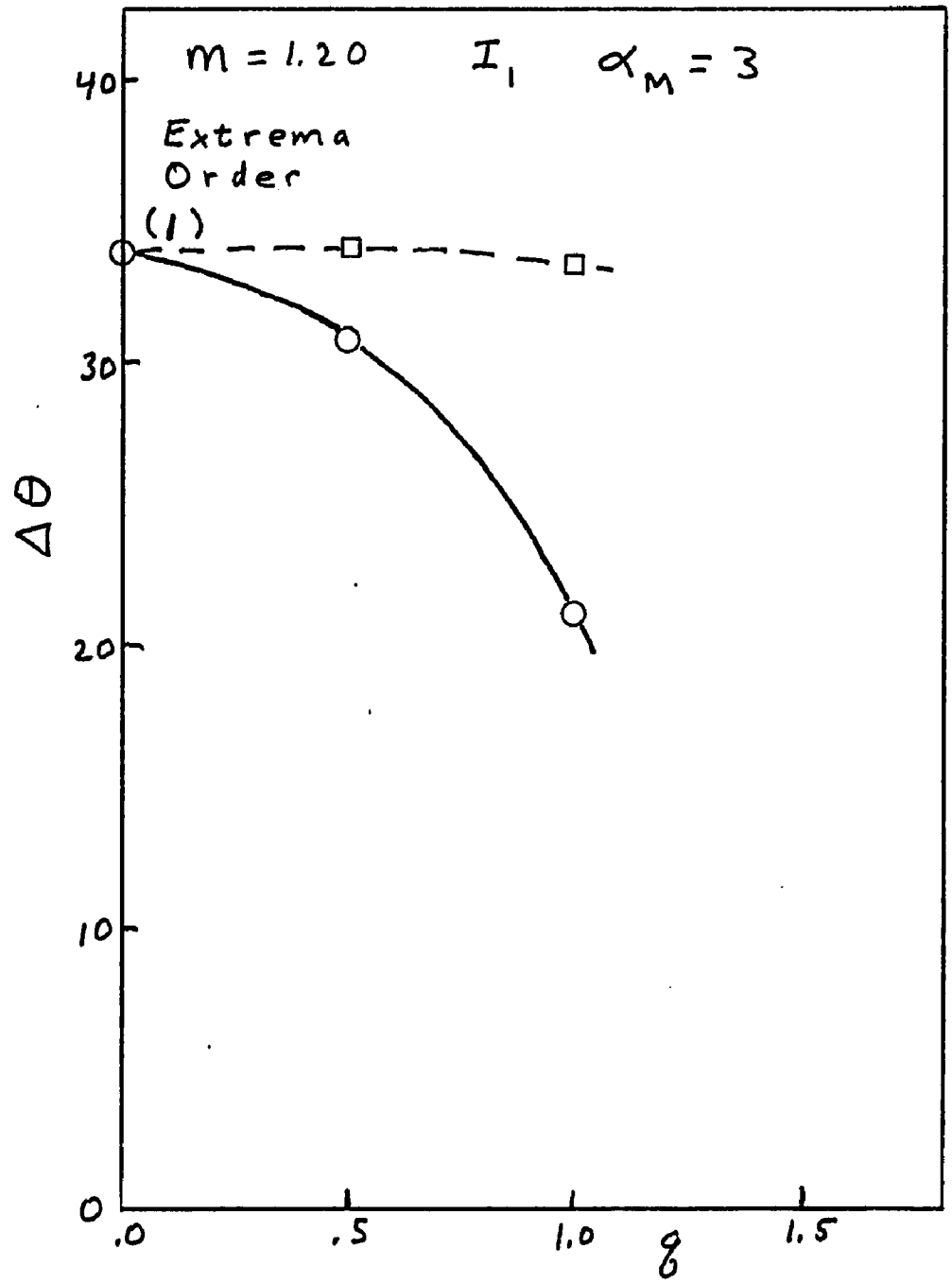

Fig. 123. Angular Difference Between the I_1 Maximum and Minimum of the First Extrema Order as a Function of q for Heterodisperse Distributions Having m=1.20 and α_M=3

is due to the shift of the maximum. However, if the minimum curve shifts with increasing q then only a portion of the total change in $\Delta\theta$ is due to the maximum shift. Figure 123 for $\alpha_M = 3$ shows that almost all of the shift in $\Delta\theta$ with increasing q is due to the shift of the maximum. Thus one can use the minimum position to determine the distribution mode and $\Delta\theta$ to determine the distribution width. Since the extrema pair disappears at q values slightly larger than q = 1, both curves will bend sharply toward zero $\Delta\theta$ values.

Increasing the modal size to $\alpha_M = 5$ in Figure 124 shows two sets of curves that represent the first and second extrema pairs. Note that $\Delta\theta$ for the second extrema pair is much larger than $\Delta\theta$ for the first extrema pair. The second extrema pair also shows a larger shift in both the angular difference $\Delta\theta$ and the minimum location for increasing q than the first extrema pair. This trend, where higher higher extrema orders wash out at a faster rate with increasing q than lower extrema orders, has been seen in all previous techniques.

An optimum approach would use the minimum location of the lowest order minimum to determine the distribution mode and the highest order angular difference to determine the distribution width. This method begins to break down at the high q values since the minimum location also shifts with increasing q thus making the mode determination uncertain. However, at low q values the shift in the angular difference $\Delta\theta$ is very small which makes the determination of the distribution width more difficult. A comparison of Figures 123 and 124 shows that the angular resolution of the extrema location must be much greater for the larger modal sizes.

Larger modal sizes have a greater number of extrema orders

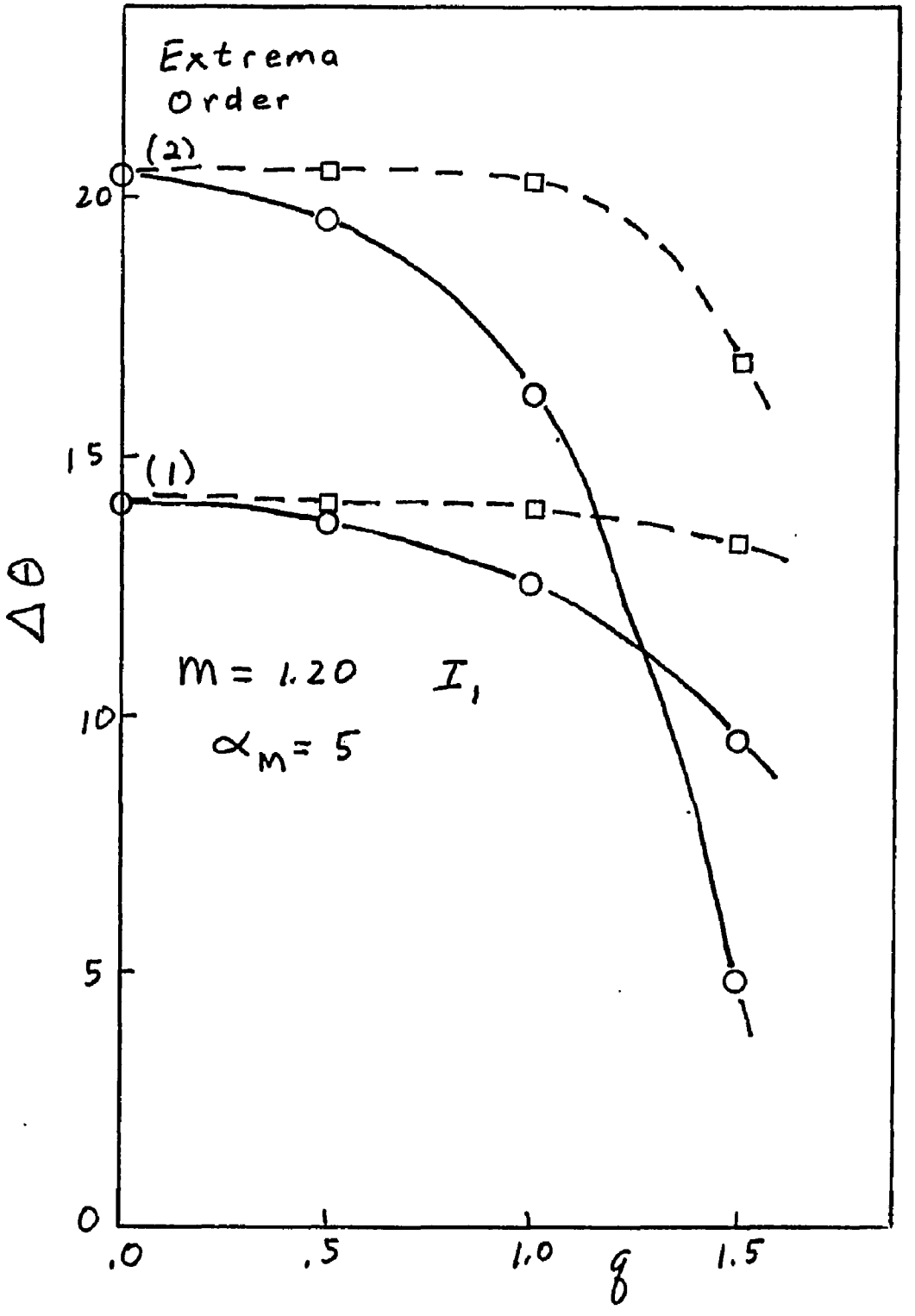

Fig. 124. Angular Difference Between the I_1 Maximum and Minimum of the First and Second Extrema Orders as a Function of q for Heterodisperse Distributions Having m=1.20 and α_M=5

to determine the particle size distributions but require very precise measurements of the extrema locations. Figure 125 shows the angular difference between the extrema and the relative minima locations for the first four extrema orders for distributions having a constant mode of $\alpha_M = 10$. Below q = 0.5 one needs angular extrema measurements with accuracies much better than 0.1° to determine the distribution width. Even the higher extrema orders do not have a sufficient change in the $\Delta\theta$ values to allow accurate q determinations. At higher q values the distribution width can be adequately determined with extrema measurements accurate to 0.1°. When the change in the angular difference of the I_1 extrema is too small to permit accurate measurements of the distribution width one can generally use the I_2 extrema. Figure 126 shows the angular difference of the I_2 extrema for the first four extrema orders having $\alpha_M = 10$. Note that the third and fourth extrema pairs have a sufficiently large $\Delta\theta$ shift to permit accurate measurements of the distribution width. Since the I_2 extrema have the appearance of much more heterodisperse I_1 extrema, one can use this behavior to accurately measure the distribution width.

The angular difference for a given extrema pair and modal size can be normalized with respect to its value at q = o so that different modal sizes and extrema orders can be compared. Figure 127 shows plots of $(\Delta\theta)_q/(\Delta\theta)_{q=o}$ versus q for the first extrema pair in distributions having a constant mode ranging from $\alpha_M = 3$ to $\alpha_M = 12$. One sees that the smaller modal sizes have a larger change in $(\Delta\theta)_q/(\Delta\theta)_{q=o}$ with increasing q than the larger modal sizes. The same trend is seen in Figure 128 for the second extrema pair.

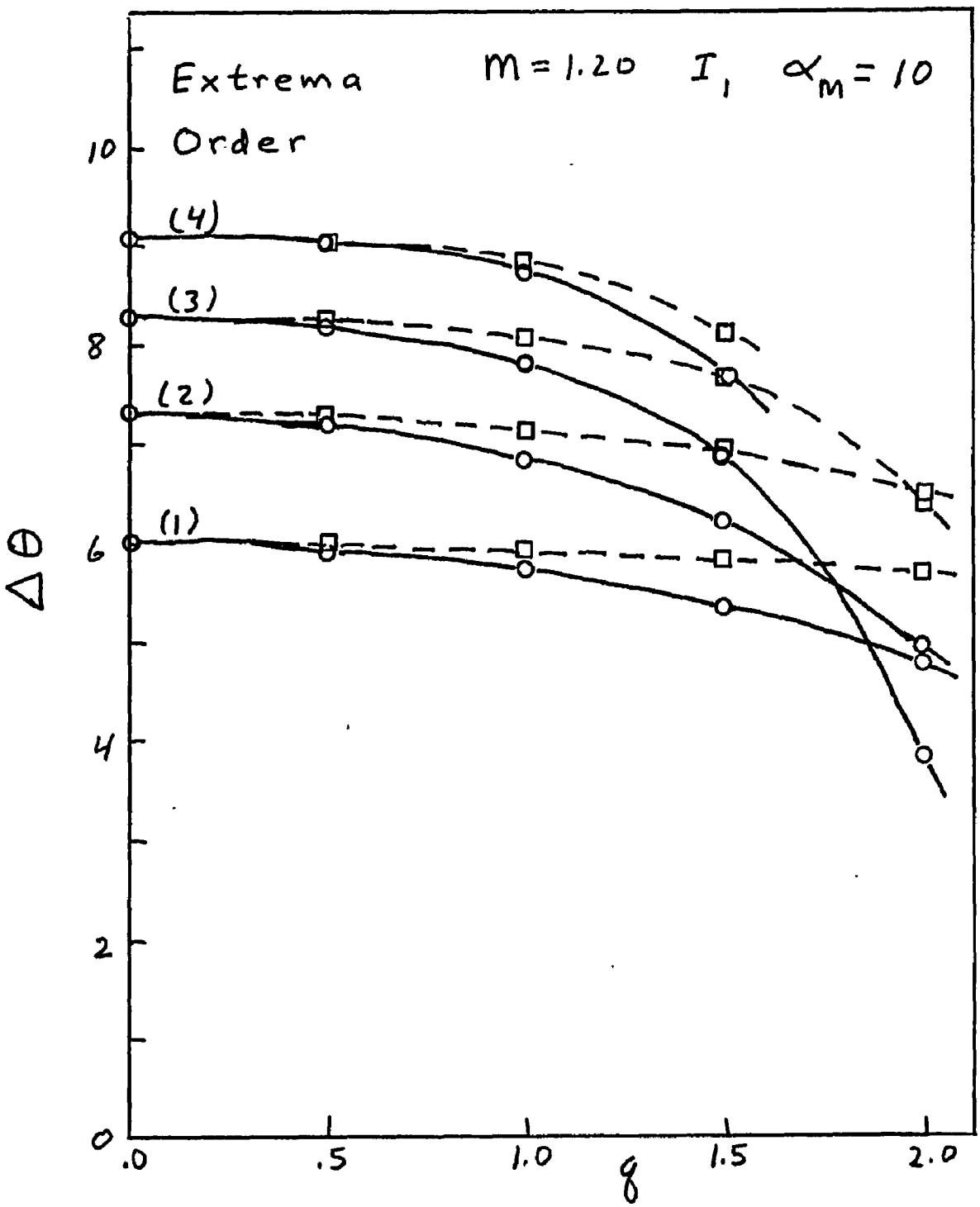

Fig. 125. Angular Difference Between the I_1 Maximum and Minimum of the First Four Extrema Orders as a Function of q for Heterodisperse Distributions Having m=1.20 and α_M=10

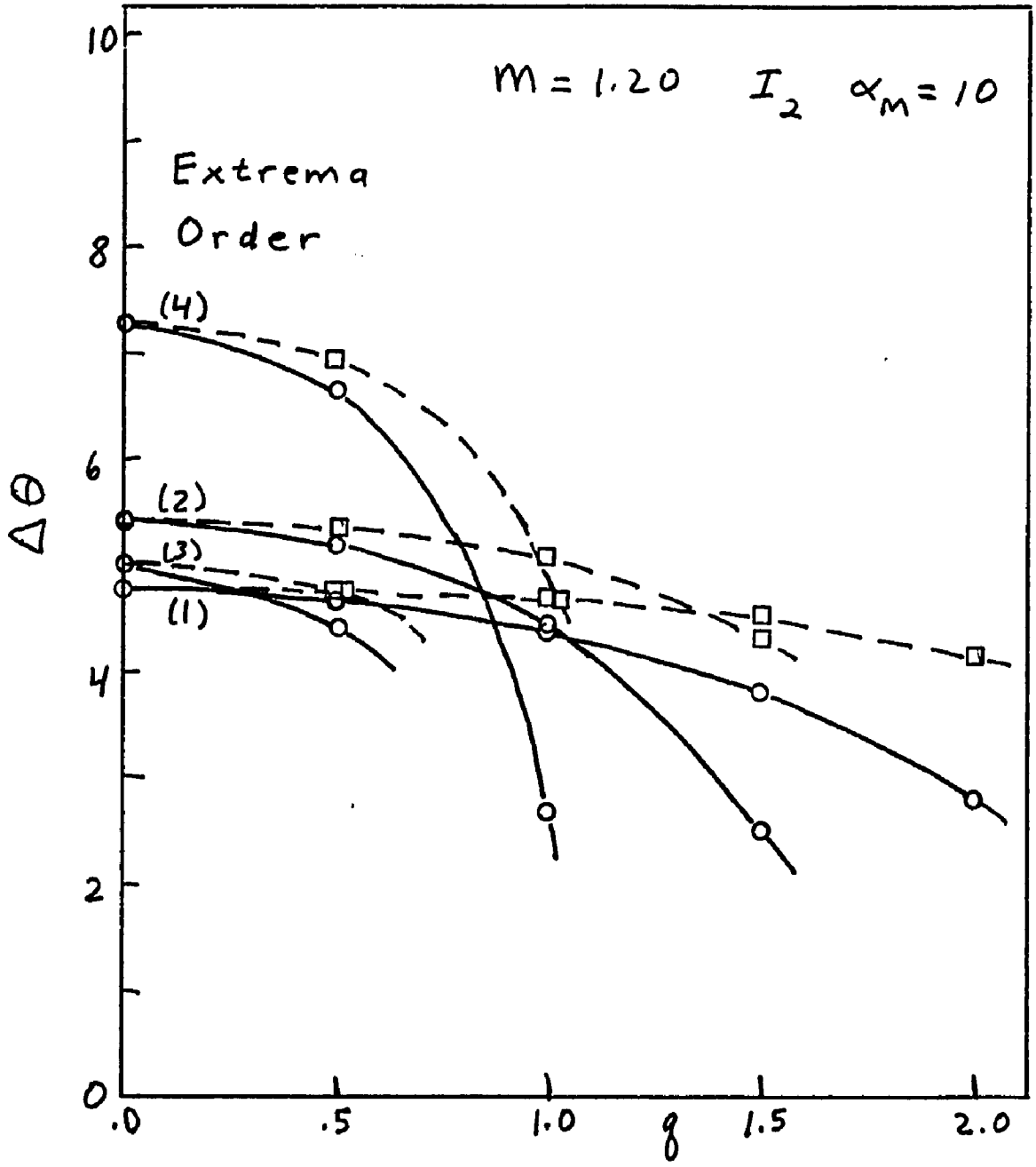

Fig. 126. Angular Difference Between the I_2 Maximum and Minimum of the First Four Extrema Orders as a Function of q for Heterodisperse Distributions Having =1.20 and α_M=10

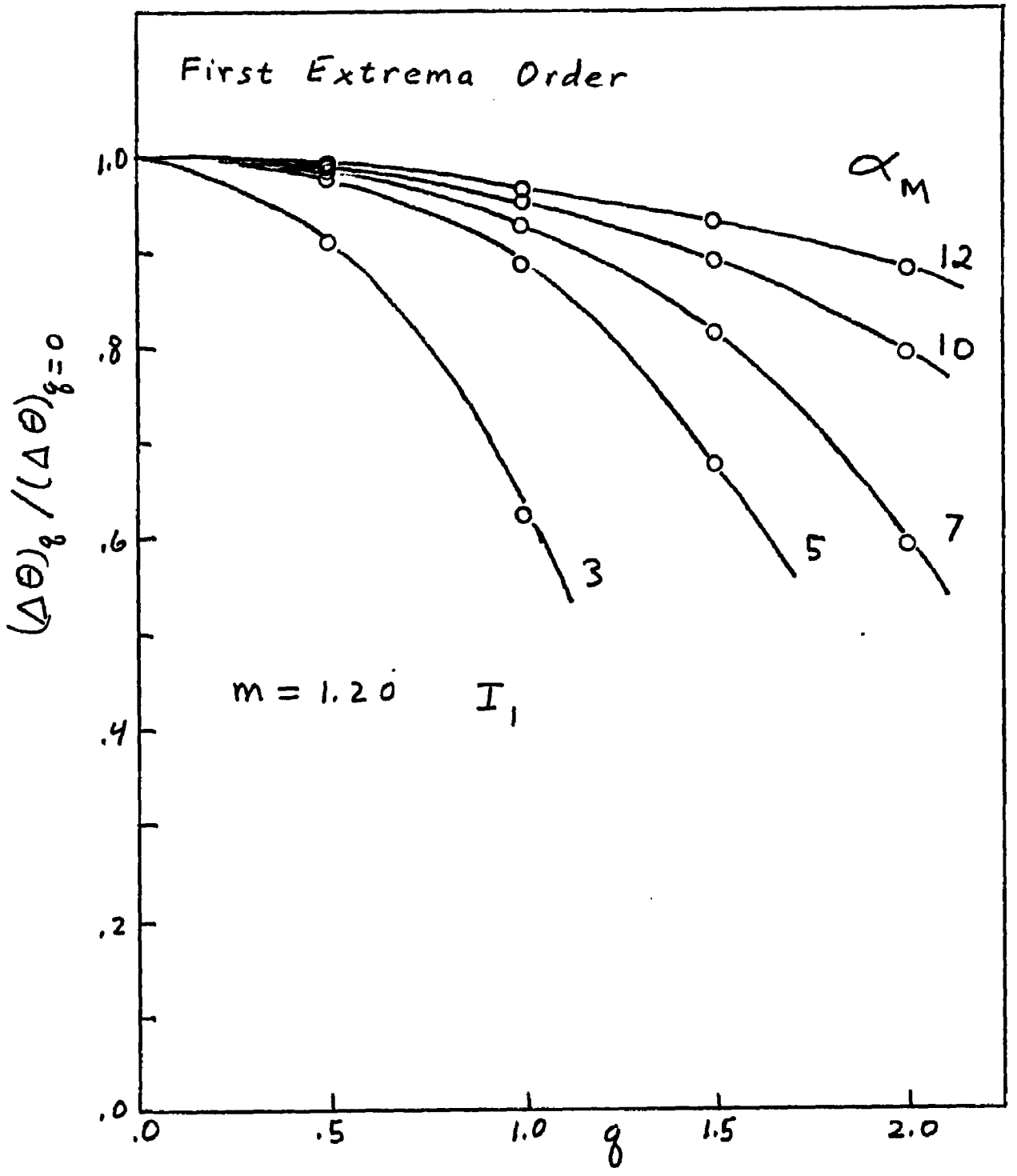

Fig. 127. Normalized Angular Difference Between the I_1 Maximum and Minimum of the First Extrema Order as a Function of q for Heterodispersions Having m=1.20 and Different α_M Values

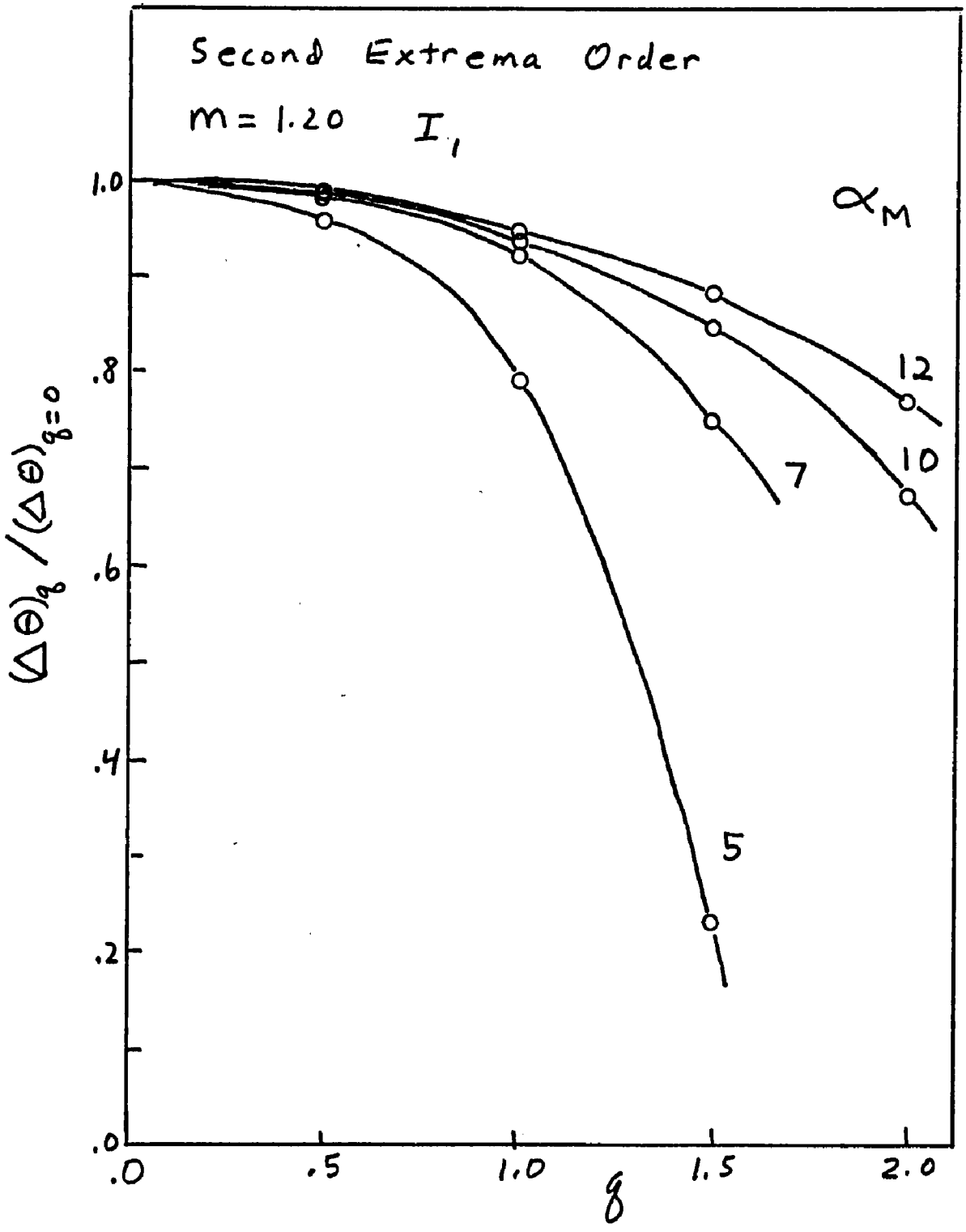

Fig. 128. Normalized Angular Difference Between the I_1 Maximum and Minimum of the Second Extrema Order as a Function of q for Heterodispersions Having m=1.20 and Different α_M Values

Empirical equations can be developed to approximate the curves seen in Figures 127 and 128. These equations have the following form:

$$\frac{(\Delta\theta)_q}{(\Delta\theta)_{q=o}} = 1 - \frac{q^2}{C_1\alpha_M - C_2} \tag{35}$$

where C_1 and C_2 are empirical constants that depend on m and the incident polarization. Higher extrema pairs also show a similar trend but have some irregularities with different curves crossing over each other. At a fixed modal size the higher extrema orders have a larger change in $(\Delta\theta)_q/(\Delta\theta)_{q=o}$ with increasing q than the lower extrema orders. This is seen in Figure 129 where the normalized angular difference for the first three extrema orders are plotted for distributions having a constant mode $\alpha_M = 7$.

The angular difference of the extrema locations is a very attractive approach to measuring the width of a distribution because of the relatively easy task of measuring extrema locations rather than the scattered intensity. However, except for the size distributions having very small modes, this approach requires angular measurements accurate to 0.1^o. This angular resolution necessitates that a laser be used for the incident radiation.

B. General Methods For Determining Particle Size Distribution

The previous methods discussed in this chapter to measure particle size distributions were based on separating the effects of the mode and the distribution width. Except for the differential slope method, the mode of the distribution was determined from the angular location of the intensity minima. The differential slope method used

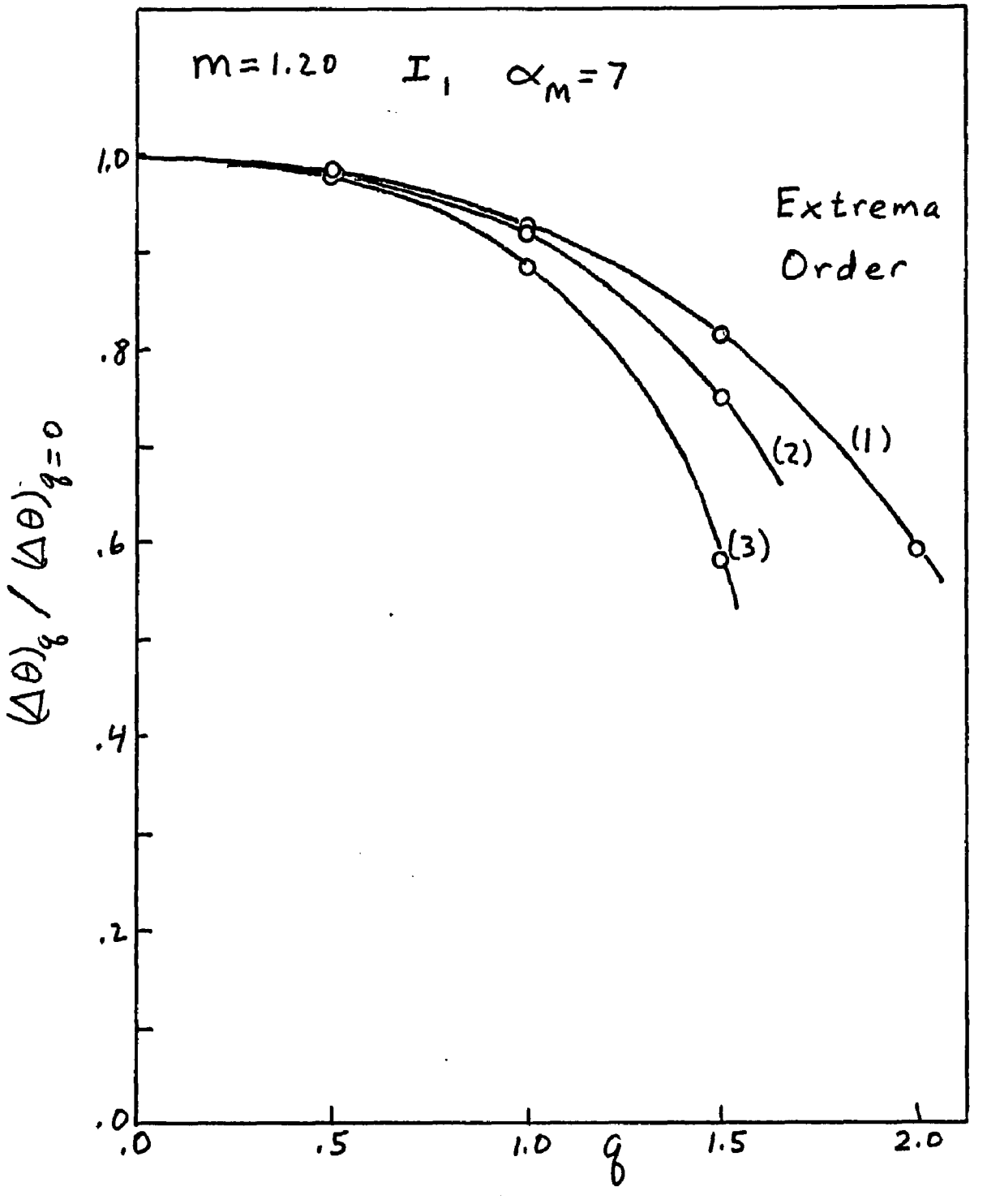

Fig. 129. Normalized Angular Difference Between the I_1 Maximum and Minimum of the First Three Extrema Orders as a Function of q for Heterodispersions Having $m=1.20$ and $\alpha_M=7$

the location of the maximum derivative to determine the distribution mode. However at a large heterodispersion the angular location of the intensity minima and, to a lesser extent, the maximum derivative would shift while maintaining a constant mode. This shift causes an error in the mode determination. Professor Heller[53] has recently developed a technique that allows one to determine the complete size distribution using angular extrema measurements without separating the effect of the distribution mode from the distribution width. He has kindly permitted a summary of this technique to be included here prior to publication.

1. Simultaneous Equation Method

The previous methods for determining particle size distributions in this chapter were based on determining the distribution mode and width in two separate light scattering measurements. Eac' measurement was either a function of the distribution mode or the distribution width, but not both. If a light scattering measurement had a dependence on both the mode and width of the distribution, then errors would occur. It had been previously shown that at high q values, the intensity minimum is both a function of the mode and width and therefore caused an error in the determination of the size distribution.

The technique proposed by Professor Heller also uses two light scattering measurements as arguments for determining particle size distributions. However, in this method each light scattering measurement is allowed to be a function of both the distribution mode and width. The solution is then obtained by solving the set of two simultaneous equations in two unknowns. Since no analytical equations are used for the complicated curves in this method, the simultaneous equations are solved either graphically or numerically by a computer. Among the different light

scattering arguments that one may use are (1) the angular location of an extremum, (2) the angular difference between successive extrema and (3) the mid-value of I_1, i.e., $(I_{max} + I_{min})/2$ which should be almost independent of solid angle and concentration as long as neither exceeds reasonable limits which are easily ascertained for a given system. Any combination of two types of measurements can be used in this method.

An example will illustrate how this simultaneous equation method yields a particle size distribution. The two arguments used in this example are the angular location of the third maximum and $(I_{max2} + I_{min3})/2$ which is half of the sum of intensities at the second maximum and third minimum. All of the data in this example refers to I_1 and $m = 1.20$. A curve is then generated in the α_M versus q plane for each argument. The curve representating the third maximum is generated in the following manner. A family of curves for various q values are plotted in Figure 130 to show how the angular location of the third maximum varies with p. The data for these diagonal curves were taken from tables of light scattering extrema[46]. The vertical line indicates the experimental angle Θ at which the third maximum is observed. The points of intersection of these curves with the vertical line furnish (see equation 14) the various α_M and q values that define the curve for the third maximum. A similar procedure is used to generate a curve for the average intensity of the second maximum and third minimum.

The two curves are then plotted in Figure 131 where curve I represents the third maximum and curve II the average intensity of the second maximum and third minimum. Their point of intersection uniquely defines the quantities α_M and q (and also p using equation 14) which, in turn, defines the size distribution. There are, of course, instances

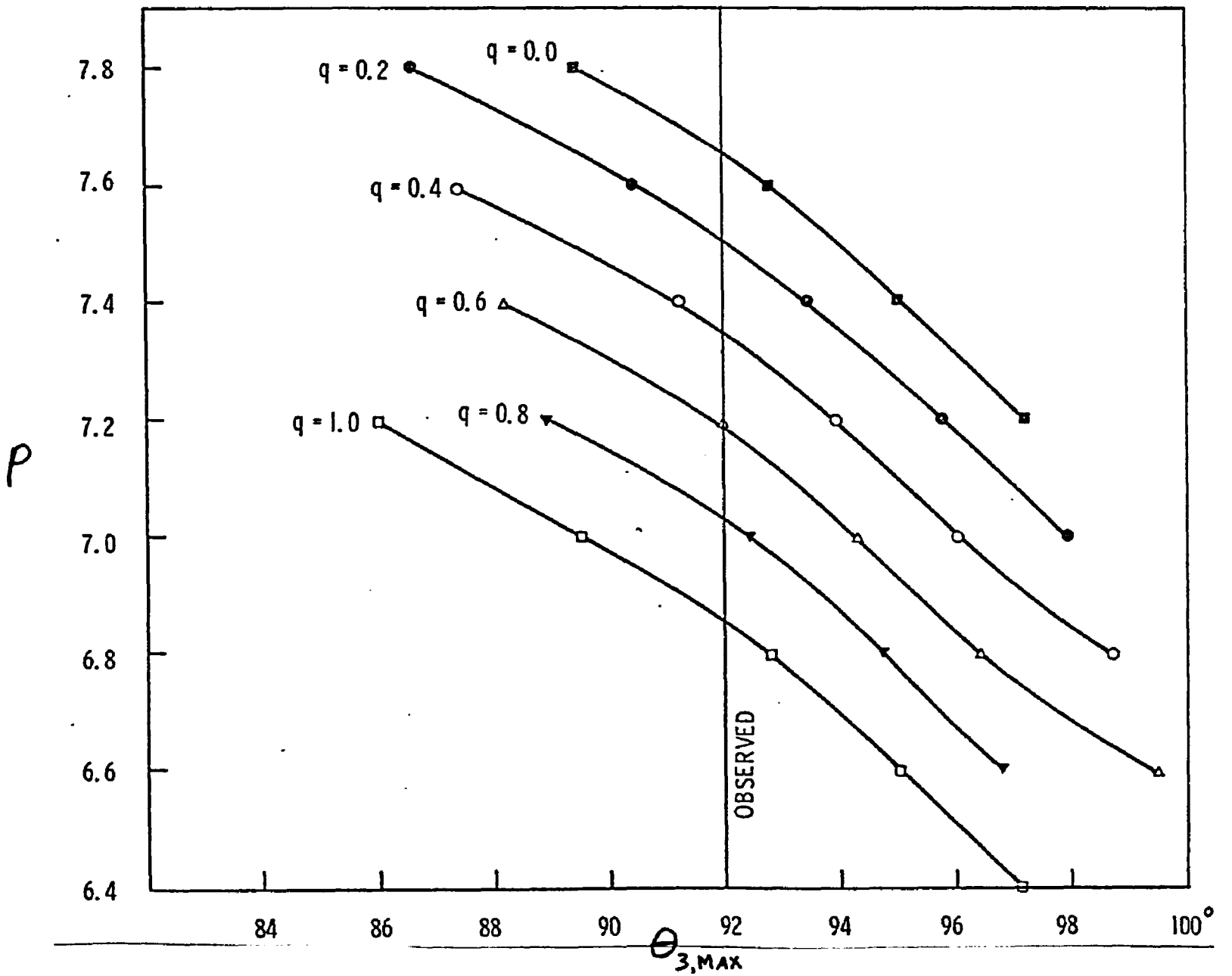

Fig. 130. Generating a Curve Having Variables α_M and q that Represents a Constant Angle for the Intensity Maximum of the Third Order. The Data Points for the Curve are Obtained from the Intersection of the Observed Angle and Theoretical Curves Showing the Angular Location of the Intensity Maximum of the Third Order Versus p for Different q Values

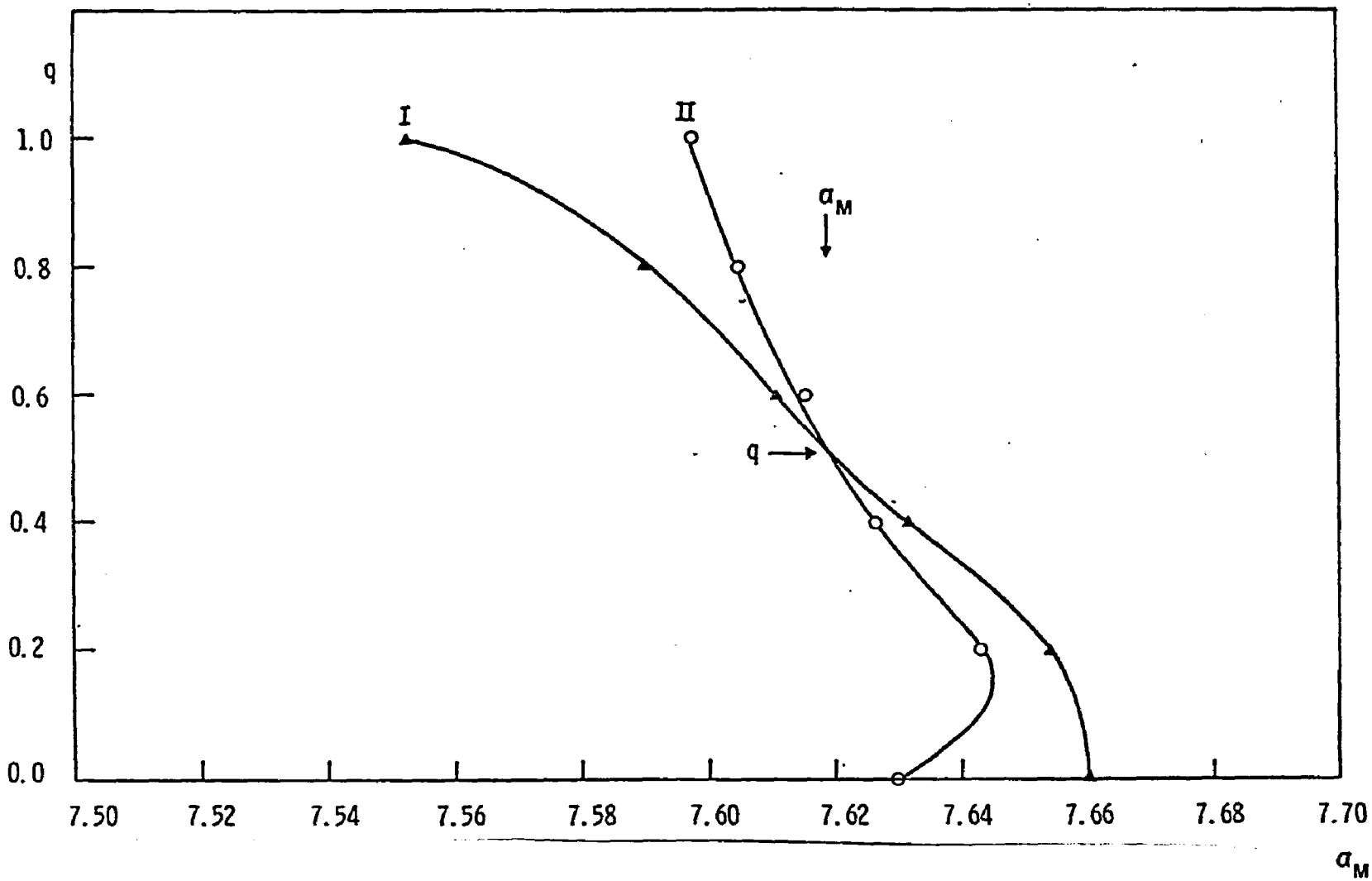

Fig. 131. Determination of the Size Distribution Parameters α_M and q from the Intersection of Curves Having (I) a Constant Value of $\theta_{max,3}$ and (II) a Constant Value of $(I_{max,2} + min,3)/2$

where the assymetry in the variation of the two light scattering quantities with increasing width of the distribution at constant d_M is not sufficiently different to lead to an intersection as shown in Figure 131. In that case consideration of one or two other available experiment criteria will resolve the problem.

2. Inverting The Scattering Matrix

The techniques for measuring particle size distributions discussed in the preceding sections were all based on comparing experimental measurements to theoretical calculations for a number of different size distributions. When a suitable agreement between the experimental measurement and theoretical calculations are found then the size distribution of the experimental system is assumed to be the same as in the theoretical system. The size distribution used in these comparisons is generally a positively skewed unimodal function in which two parameters determine the distribution width and modal size. The present investigation used the distribution shown in equation 5 to perform theoretical scattering calculations. Other distributions used in theoretical calculations are discussed by Kerker.[3] The difficulty in these comparison techniques is that one is limited to a particular distribution type and the increment and range of the parameters defining the distribution. Thus, particle size distributions not covered in the calculations, like multimodal distributions, could not be determined using the various comparison techniques. In addition, these approaches have only a limited number of size distributions that can be reasonably stored and searched within a computer system.

An approach having a much greater potential, at least theoretically, for determining particle size distributions is the inversion of the

scattering integral. This approach is very appealing because any particle size distribution can be theoretically determined since no assumptions are made of the distribution. The inversion of the scattering integral is accomplished by determining the particle size distribution $f(\alpha)$ from measurements of $I(\theta)$ defined by

$$I(\theta) = \int_{\alpha_S}^{\alpha_L} f(\alpha)\ i(\alpha, \theta)\ d\alpha \tag{36}$$

where α_S is the smallest particle present

α_L is the largest particle present

$i(\alpha, \theta)$ is the theoretical scattering intensity from a single particle of size α at angle θ.

Equation 36 shows that the angular variation of the scattered intensity is used to determine the size distribution. One could also use the wavelength or polarization of the incident light as the experimental variable.

If the function describing the scattered intensity from a single particle is sufficiently simple then the inversion can be accomplished by an analytical transformation. Since small angle x-ray scattering from polydisperse systems can be described by the Rayleigh-Gans-Debye (RGD) theory, one can perform an integral transform on the scattered intensity to obtain the particle size distribution. Kerker[3] describes the procedure for performing this transform. The other theoretical scattering function that can be inverted in the scattering integral is the Fraunhoffer diffraction which is applicable for very large particle sizes. Chin, et al.,[54, 55] have developed a technique that performs a Mellin transformation on the angular variation of diffracted light to obtain the desired particle size distribution. A very similar trans-

formation technique was developed by Shifrin[56, 57] to measure particle size distributions using Fraunhoffer diffraction theory. Unfortunately the RGD and Fraunhoffer diffraction theories can be used in only a limited number of practical cases.

The majority of cases involving particle size determinations from light scattering measurements require the complicated Mie theory. The approach most frequently used for this case transforms the integral equation into a vector matrix equation and then numerically inverts the scattering matrix to obtain the particle size distribution. If the integral in equation 36 is approximated as a summation over fixed size intervals $\Delta\alpha$ one has

$$I(\theta_J) = \sum_{k=1}^{k=n} f(\bar{\alpha}_k)\, i(\theta_J, \bar{\alpha}_k) \tag{37}$$

where $\bar{\alpha}_k$ is the average particle size in the k size interval

θ_J is the Jth angle measured.

If the scattering at n different angles is measured then the resulting n equations would allow up to n intervals of the size distribution to be determined. The equations are shown below in the expanded form.

$$\begin{aligned}
I(\theta_1) &= f(\bar{\alpha}_1)\, i(\theta_1, \bar{\alpha}_1) + f(\bar{\alpha}_2)\, i(\theta_1, \bar{\alpha}_2) \text{ — — — } + f(\bar{\alpha}_n)\, i(\theta_1, \bar{\alpha}_n) \\
I(\theta_2) &= f(\bar{\alpha}_1)\, i(\theta_2, \bar{\alpha}_1) + f(\bar{\alpha}_2)\, i(\theta_2, \bar{\alpha}_2) \text{ — — — } + f(\bar{\alpha}_n)\, i(\theta_2, \bar{\alpha}_n) \\
&\vdots \\
I(\theta_n) &= f(\bar{\alpha}_1)\, i(\theta_n, \bar{\alpha}_1) + f(\bar{\alpha}_2)\, i(\theta_n, \bar{\alpha}_2) \text{ — — — } + f(\bar{\alpha}_n)\, i(\theta_n, \bar{\alpha}_n)
\end{aligned} \tag{38}$$

Writing this set of equations in a vector matrix equation and abbreviating the variable identification one has

$$\begin{bmatrix} I_1 \\ I_2 \\ \vdots \\ I_n \end{bmatrix} = \begin{bmatrix} i_{1,1} & i_{1,2} \cdots i_{1,n} \\ i_{2,1} & i_{2,2} \cdots i_{2,n} \\ \vdots & \vdots \\ i_{n,1} & i_{n,2} \cdots i_{n,n} \end{bmatrix} \begin{bmatrix} f_1 \\ f_2 \\ \vdots \\ f_n \end{bmatrix} \tag{39}$$

or $I = SF$

where I is the experimental intensity vector

S is the theoretical scattering matrix

F if the size distribution vector to be determined

The unknown size distribution vector can then be found by inverting the scattering matrix S.

$$F = S^{-1} I \tag{40}$$

A number of different numerical techniques have been used to invert the scattering matrix. Unfortunately, direct inversion techniques using least squares yield wildly oscillating solutions as well as negative number densities in some size intervals [58, 59], Mallove and Hinds[59] have used a non-negative least squares technique that prohibits unrealistic negative solutions of the size distribution with moderate success. The most successful of the inversion techniques[58-61] perform smoothing operations on the derived size distribution, the extent of the smoothing being varied until the desired smoothness is obtained. However, these techniques suffer because (1) there is no criterion for the degree of smoothness necessary and (2) true variations in the particle size distribution will

be washed out. Despite these objections, the methods are vastly superior to the direct inversion of the scattering matrix.

The results of the present investigation on the angular extrema of scattered light have suggested a new solution to the problem of inverting the scattering equation. This solution is based on the fundamental relationship between particle size and the light scattering patterns. Figure 132 shows the angular scattering patterns for three different sized particles. The left half of this figure shows the relative size of the three particles superimposed over the electric component of the electromagnetic wave. The right half of this figure shows the corresponding angular scattering diagrams with the angle θ measured from the forward direction ($\theta = 0^{\circ}$). The scattering diagrams are not to scale since the intensity increases considerably with size.

The intensity of scattered light is proportional to the length of the radius from the center of the particle to the contour of the scattering pattern. Note that as the angle is changed from 0° to θ, the intensity of the scattered light remains constant for the small particle, decreases moderately for the intermediate particle, and decreases considerably for the large particle. For a very small angular change from $\theta = 0^{\circ}$ only the large particle would show any change in intensity. As the angle is further increased the intermediate size particle would also begin to show a change in the intensity.

If the angular derivative of the intensity $\frac{dI}{d\theta}$ were measured instead of the intensity I, then only those particles that show a change in intensity are measured. Thus a scan of the derivative of the angular intensity from $\theta = 0^{\circ}$ will measure initially only the largest particles present and, as the angle θ is increased, will measure progressively smaller particles. Each

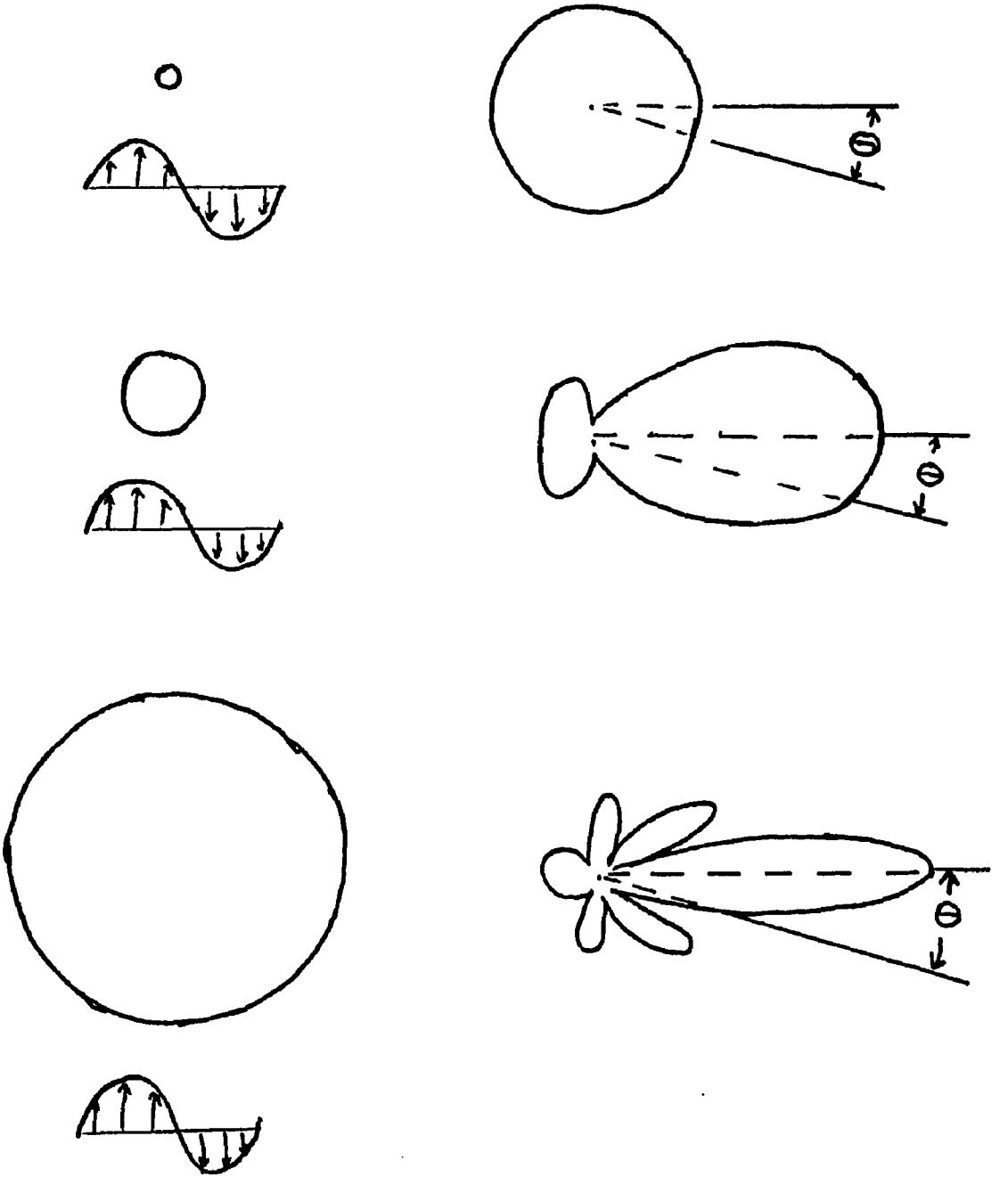

Fig. 132. Angular Scattering Patterns for Three Different Sized Particles

particle size α has a characteristic angle θ_α below which the angular derivative of the scattering pattern is not detectable. As the angular scan is made at increasing the θ intensity derivative measurement will represent the sum of the intensity derivatives from an increasing number of particles.

The necessary equations for obtaining particle size distributions from the derivative of angular intensity measurements will now be developed. The derivative at the first angle away from the forward direction measures only the largest particle present. Since the value of the intensity and derivative vary over many orders of magnitude the derivative is normalized with respect to the intensity yielding.

$$\frac{1}{I}\left(\frac{dI}{d\theta}\right)_{\theta_1} = \frac{1}{I}\,\frac{\partial}{\partial\theta}\left(i(\theta_1, \bar{\alpha}_n)\right)\quad f(\bar{\alpha}_n) \tag{41}$$

The derivative at the next larger angle will include a smaller size particle

$$\frac{1}{I}\left(\frac{dI}{d\theta}\right)_{\theta_2} = \frac{1}{I}\,\frac{\partial}{\partial\theta}\left(i(\theta_2, \bar{\alpha}_{n-1})\right) f(\bar{\alpha}_{n-1}) + \frac{1}{I}\,\frac{\partial}{\partial\theta}\left(i(\theta_2, \bar{\alpha}_n)\right) f(\bar{\alpha}_n) \tag{42}$$

The process is continued until we have reached an angle where all particle sizes are detected.

$$\begin{aligned}\frac{1}{I}\left(\frac{dI}{d\theta}\right)_{\theta_n} = {} & \frac{1}{I}\,\frac{\partial}{\partial\theta}\left(i(\theta_n, \bar{\alpha}_1)\right)\quad f(\bar{\alpha}_1) \quad - - - - - - - \\ & + \frac{1}{I}\,\frac{\partial}{\partial\theta}\left(i(\theta_n, \bar{\alpha}_{n-1})\right) f(\bar{\alpha}_{n-1}) + \frac{1}{I}\,\frac{\partial}{\partial\theta}\left(i(\theta_n, \bar{\alpha}_n)\right) f(\bar{\alpha}_n)\end{aligned} \tag{43}$$

Abbreviating the variable identification one can write the set of n equations as a vector-matrix equation.

$$\begin{bmatrix} I_1^1 \\ I_2^1 \\ I_3^1 \\ \vdots \\ I_n^1 \end{bmatrix} = \begin{bmatrix} 0 & \cdots & 0 & 0 & i_1^1,_n \\ 0 & \cdots & 0 & i_2^1,_{n-1} & i_2^1,_n \\ 0 & \cdots & i_3^1,_{n-2} & i_3^1,_{n-1} & i_3^1,_n \\ \vdots & & \vdots & \vdots & \vdots \\ i_n^1,_1 & \cdots & i_n^1,_{n-2} & i_n^1,_{n-1} & i_n^1,_n \end{bmatrix} \begin{bmatrix} f_1 \\ \vdots \\ f_{n-2} \\ f_{n-1} \\ f_n \end{bmatrix} \quad (44)$$

One sees that the derivative has effectively produced a diagonal matrix which can be easily inverted to yield the size distribution.

The increments of the size distribution and the values of the matrix elements are a function of the angles at which the derivative measurements are made. A resolution of the particle size distribution into small size increments will require many closely spaced angular measurements. In addition the value of the matrix elements must be averaged over the solid angle of the intensity measurement and over the appropriate size increment.

It is important to emphasize that the complete theoretical and experimental evaluation of the angular derivative method must still be performed. Tests must be conducted to determine the performance of the angular derivative method under a variety of different size distributions using angular intensity measurements having various degrees of error. Such tests can be readily performed on the angular derivative method as were done on various other methods[58-61] for obtaining particle size distributions from angular intensity measurements.

VI. Experimental Determination of Particle Size Distributions

This chapter will illustrate how different techniques presented in Chapter V are used to determine particle size distributions in experimental systems of polystyrene latex spheres. The experimental data used in this chapter was kindly furnished by Jack P. Witeczek[62]. He had previously used this data to calculate scattering ratios that were published in his Ph.D. thesis

A. Experimental Procedure

Angular light scattering measurements from several colloidal suspensions of polystyrene latex in water were carried out on a Brice-Phoenix light scattering photometer (Phoenix Precision Instrument Co., Philadelphia, Pennsylvania). This instrument used a high pressure mercury vapor lamp coupled with appropriate filters and a Glan-Thompson prism to provide monochromatic incident light that was plane polarized with vacuum wavelengths of λ_o = 546.1 nm and 435.8 nm. The incident light beam passed through the center of a scattering cell specially designed by Heller and Witeczek[64] to eliminate reflections. Scattered light from the cell was then measured by a photomultiplier tube that was mounted on a rotating arm calibrated to provide the scattering angle θ.

The experiment consisted of measuring the photomultiplier output from the scattered light at 5° intervals from θ = 35° to 145°. Four measurements of the photomultiplier output were made at each scattering angle corresponding to incident radiation polarized parallel and perpendicular to the plane of observation and having a vacuum wavelength

of λ_o = 546.1 nm and 435.8 nm. Since these measurements were originally intended to be used for measuring the scattering ratio (i.e. I_2/I_1) at a given angle, no attempt was made to obtain absolute intensities.

The experimental scattering data obtained from Witeczek[62] therefore represents a quantity that is proportional to the scattered intensity in which the proportionality constant is unknown. Moreover, this proportionality constant differs from sample to sample because of different light intensities and photomultiplier sensitivities. These changes in the proportionality constant were not important for measuring the scattering ratio since they affected I_1 and I_2 equally and would cancel in the scattering ratio I_2/I_1, This cancellation of instrumental variations is one of the attractive features of using the scattering ratio[64]. However, for angular intensity measurements one must correct for these changes.

The background scattering from the stabilizer solution* and stray light was also measured so that it could be subtracted from the scattering measurements of the colloidal suspension. If the instrument constants are not the same for the background scattering and the scattering from the colloidal suspensions then experimental errors will result if the appropriate corrections are not made. Since the instrument constants were not known for Witerzek's data, a small error is present in both the scattering ratios and the intensities. Kratohvil and Smart[65] have shown how absolute angular intensity measurements can be obtained using instrument calibration factors.

*A soap solution was added to the suspension of latex spheres to prevent coagulation.

Two systems of polystyrene latex spheres were used having different distribution widths and approximately the same model diameter. One system, referred to here as Latex-11, represented a monodisperse size distribution. The manufacturer (Dow Chemical Co.) specified that the system had an average diameter of 0.894μm and a standard deviation of 0.0044μm. The scattering data from this system was obtained in experiments using a double horn cell[64] that did not require any reflection corrections.

The other system, referred to as Blend A, represented a heterodisperse size distribution. This system was made by blending known quantities of different monodisperse latexes to yield the desired heterodispersion. The angular scattering data for this sytem was obtained in experiments using a wide angle horn cell[64] that required a reflection correction. Experimental details of the apparatus and procedure can be found in Witeczek's thesis[63].

B. Data Reduction

A number of numerical corrections had to be applied to the photomultiplier output data before it could be used in the present investigation. These corrections were necessary to allow comparisons of the experimental and theoretical intensity data. Heller[66] has introduced a convenient way of presenting angular scattering data so that it can be directly compared to theory. He showed that the experimental specific intensity $\left(\frac{I_o}{I_o C}\right)^{exp}$ when extrapolated to zero concentration, is related to the theoretical intensity I^{theo} by equation 45

$$\left(\frac{I_o}{I_o C}\right)^{exp}_{C=0} = \frac{3}{2\lambda\alpha^3}\frac{d_{12}}{d_2}\left(I^{theo}\right) \qquad (45)$$

where

C is the concentration of the latex spheres

λ is the wavelength of the incident beam

d_2 and d_{12} are the densities of the latex particle and solution, respectively.

The experimental data from the photomultiplier output therefore had to be converted into the specific intensity. This conversion required several corrections to the experimental data.

The first correction involved subtracting the background scattering from the scattering of the heterodisperse system of latex spheres. Ideally, the relative photomultiplier output $\frac{P_\theta^1}{P_o^1}$ woud be determined from equation 46

$$\frac{P_\theta^1}{P_o^1} = \left(\frac{F_o P_\theta}{F_\theta P_o}\right)_{\text{Solution}} - \left(\frac{F_o P_\theta}{F_\theta P_o}\right)_{\text{Solvent}} \tag{46}$$

where

F represents the transmission of the neutral density filters inserted to attenuate the incident beam

P represents the photomultiplier output and the subscripts represent the angles θ and 0°

Since the P_o measurements were not available for either the solution or solvent, they were assumed to be equal and combined with the instrument constants.

The data from the Blend A system required an additional correction because of the reflection of the incident light in the wide-angle horn cell. Part of the incident light passing through the cell is reflected back from the exit window and acts as a secondary incident beam. This

secondary beam gives rise to scattering at the complimentary angle $180^{o} - \theta$ and must be subtracted from the calculated intensity in equation 46. The correction for the reflection is given by equation 47.

$$\frac{P_{\Theta}''}{P_{o}''} = \frac{\left(\frac{P_{\Theta}'}{P_{o}'}\right) - 2A\left(\frac{P_{180-\Theta}'}{P_{o}'}\right)}{B(1 - 4A^{2})} \qquad (47)$$

where A and B are the Fresnel coefficients.

This correction was not required for Latex 11 because the cell used to obtain the data had two Rayleigh horns to trap the reflected light.

$\frac{P_{\Theta}'}{P_{o}'}$ for Latex 11 is therefore equal to $\frac{P_{\Theta}''}{P_{o}''}$.

The experimental data was also corrected for variations in the scattering volume with angle θ. Since the optically effective volume in the experimental apparatus is inversely proportional to $\sin\Theta$, the photomultiplier measurements will also vary as $1/\sin\theta$. The solvent and reflection corrected data from equation 47 was therefore multiplied by $\sin\theta$ to correct for changes in the optically effective volume. This product was then divided by the concentration C to yield a quantity proportional to the specific intensity.

The proportionality constant K relating experimental measurements to specific intensities depends on a number of instrumental variables and can be determined using a procedure described by Kratohvil and Smart[65]. Since the data used in the present investigation was intended for scattering ratios and not for intensities, the constant K was not determined. Not having a value for K did not pose a serious problem in the present investigation because an arbitrary scale could be used to bring the theoretical and experimental

intensities into coincidence at a particular angle. This is a common practice and has been used by a number of investigators[67,68]. However the lack of the incident intensity I_o was very serious and prevented the intensity data from being used to determine the width of the distribution.

C. Minimizing Effects of Multiple Scattering

Experimental light scattering measurements are complicated by the multiple scattering* that occurs for finite partcle concentrations. Heller and Witeczek[64] have shown that the experimental complications due to multiple scattering can be eliminated by measuring the scattering at several different particle concentrations and extrapolating the measurements to zero concentration. However, the experimental measurements must a finite value at zero concentration for the extrapolation to be meaningful. Thus, the scattering ratio I_2/I_1 and intensity ratio I max/ I min can be extrapolated to zero concentration while the intensity I cannot. Since the scattered intensity approaches zero at zero particle concentration, one has to extrapolate the specific intensity $\frac{I_\Theta}{I_o C}$ to obtain experimental intensities free from multiple scattering. Unfortunately, this extrapolation was not possible since the incident intensity I_o was not determined in the experiments by Witeczek.

In contrast to the intensity extrapolation, the lack of the incident intensity was not important for the extrapolation involving intensity ratios. This follows because the incident intensity occurs both in the numerator and denominator of the ratio and will cancel. For example, the ratio of the maximum intensity to the minimum intensity equals the

*Multiple scattering refers to a particle rescattering the light previously scattered by another particle.

desired ratio of the specific intensities.

$$\frac{I_{max}}{I_{min}} = \left(\frac{I_{max}}{I_o C}\right) \Big/ \left(\frac{I_{min}}{I_o C}\right) \tag{48}$$

Similar cancelations occur for $\frac{\Delta I}{I\Delta\theta}$, $\frac{dI}{Id\theta}$ and the scattering ratio I_2/I_1.* These ratios of intensities at different angles, polarizations and wavelengths have the additional advantage of not requiring any instrumental constants to relate the experiments to theory.

1. Angular Derivative Curves at Different Particle Concentrations

The extrapolation of the angular derivative $\frac{dI}{Id\theta}$ were the most useful in the present investigation because they provide information on the distribution mode and width without requiring intensity extrema. The other two functions I_{max}/I_{min} and $\frac{\Delta I}{I\Delta\theta}$ only provide the distribution width once the mode is determined from the location of the intensity minima. In addition, these two functions are only useful in the presnce of intensity extrema. All three functions were used whenever possible to determine the particle size distribution for the two suspensions of PSL spheres.

Figure 133 shows several curves of $\frac{dI}{Id\theta}$** versus θ for Latex 11 using incident light having a wavelength of 546 nm. The derivatives $\frac{dI}{Id\theta}$ were obtained from the derivatives of the Stirling's polynomial used to fit the experimental intensity data. Each curve represents a different particle concentration and has an increasing amplitude of oscillation as the concentration decreases. The first four curves, in order of

*Witeczek[63] used extrapolations of the scattering ratio to remove effects due to multiple scattering.

**Since all of the experimental data presented in this chapter used incident light polarized perpendicular to the plane of observation, the subscripts denoting the polarization were dropped for clarity.

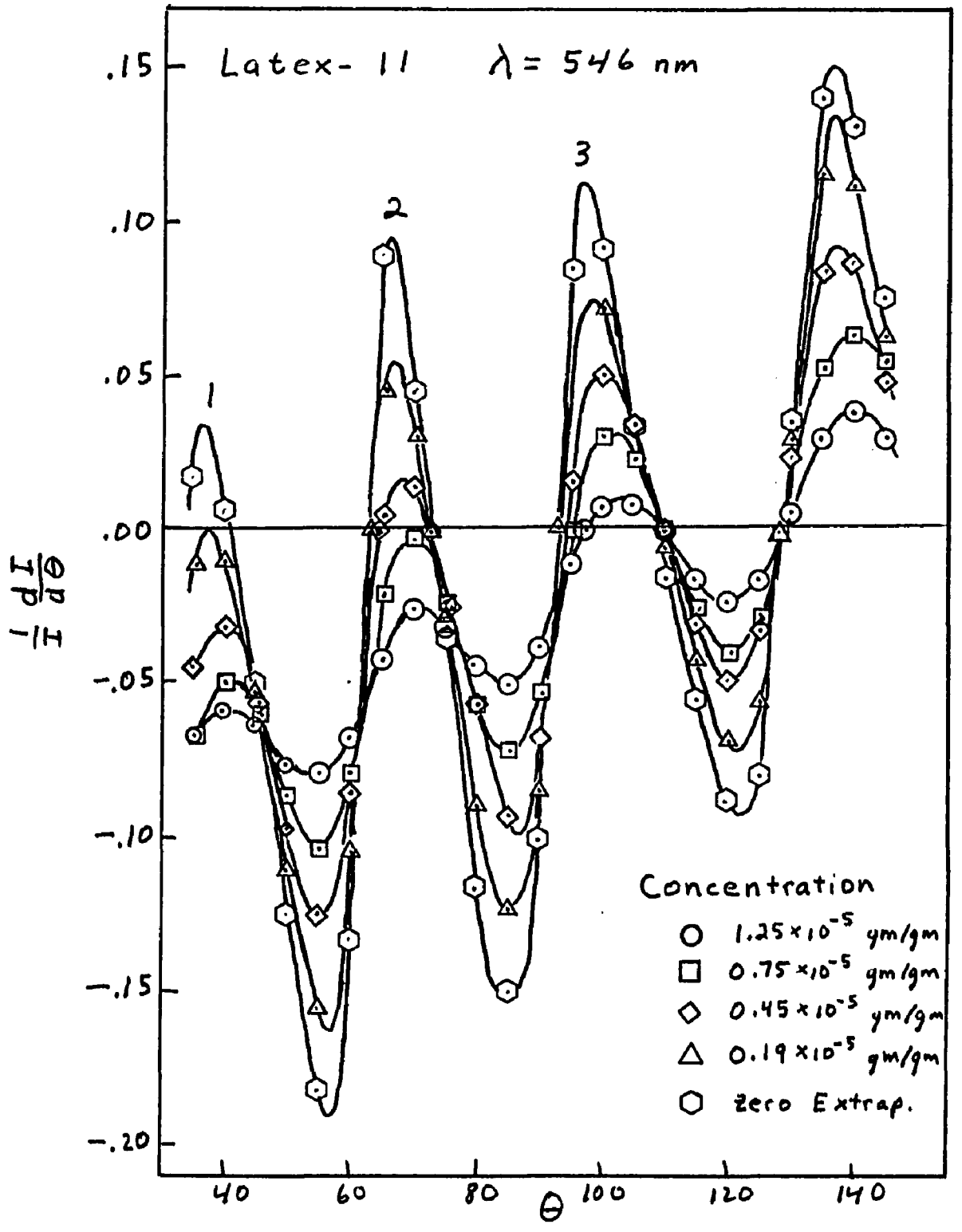

Fig. 133. Normalized Angular Derivative of I_1 from Latex-11 at Different Particle Concentrations Using Incident Light Having a Wavelength of 546nm

increasing amplitude of oscillation, represent concentrations of 1.25×10^{-5} gm/gm, 0.75×10^{-5} gm/gm, 0.45×10^{-5} gm/gm and 0.19×10^{-5} gm/gm respectively. The final curve, which has the greatest amplitude of oscillation, represents the extrapolation to zero concentration. Figure 133 also shows the extrema pairs counting from the forward direction as numbers above the derivative maxima. The intensity extrema occur at the zeros of the derivatives with the minimum of a given extrema pair at the smaller angle and the maximum at the larger angle. Note that if the derivative curves do not cross through zero then there will be no intensity extrema. However the derivative curves still show significant oscillation patterns which allow particle size determinations long after the extrema have been washed out.

Extrapolating light scattering measurements to zero concentration is very important to obtain accurate particle size distributions. A comparison of Figures 133 with Figures 116 and 117 shows that increasing particle concentration has a very similar appearance to increasing heterodispersion. If multiple scattering is not successfully removed by extrapolating light scattering measurements to zero concentration, then the calculated size distibution will have an erroneously high degree of heterodispersion. However a more detailed comparison reveals a significant difference in the trend of increasing multiple scattering seen in Figure 133 and the trend of increasing heterodispersion seen in Figures 116 and 117. Increasing the degree of heterodispersion at a constant mode results in the higher extrema pairs (counting from the forward direction) washing out faster than the lower extrema pairs. However increasing the particle concentration at a fixed size distribution

washes out the lower extrema pairs faster than the higher extrema pairs. One should therefore use experimental light scattering data furthest from the forward direction to obtain accurate particle size distributions.

The stronger effect of multiple scattering in the forward direction compared to other directions can be explained on a qualitative basis. This explanation is based on the increasing intensity of the primary scattered light toward the forward direction. The primary scattered light then acts as a source of incident light to produce secondary scattered light. It follows that since the primary scattered light is strongest in the forward direction, the secondary scattering will also be greatest in the forward direction. A detailed analysis of secondary and higher order scattering in the multiple scattering problem is very complicated and beyond the scope of this investigation.

Experimental tests on the same concentrations of Latex 11 using incident light with a wavelength of 436 nm produced similar results seen previously in Figure 133. The curves representing the four concentrations and the extrapolation to zero concentration are shown in Figure 134 where $dI/Id0$ is plotted against θ. However, there are now a greater number of oscillations in the curves since the smaller wavelength increases the relative particle size α. The numbers above the derivative maxima identify the extrema pairs counting from the forward direction. Figure 134 also shows the greater effect of increasing multiple scattering (i.e. increasing concentration) in the forward direction compared to the backward direction.

A similar analysis was performed on Latex-A using incident light having wavelengths of 546 nm and 436 nm shown in Figures 135 and 136

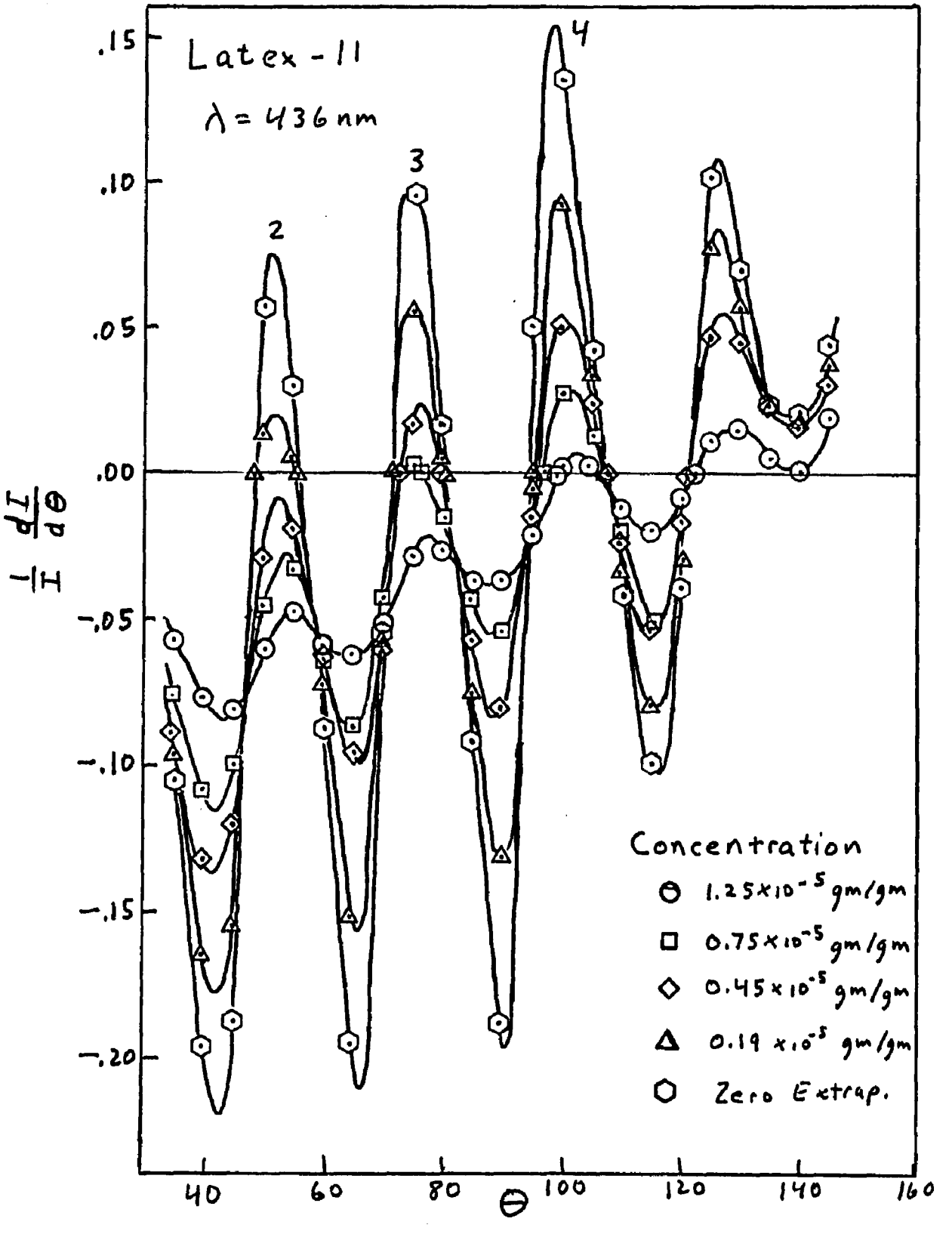

Fig. 134. Normalized Angular Derivative of I_1 from Latex-11 at Different Particle Concentrations Using Incident Light Having a Wavelength of 436nm

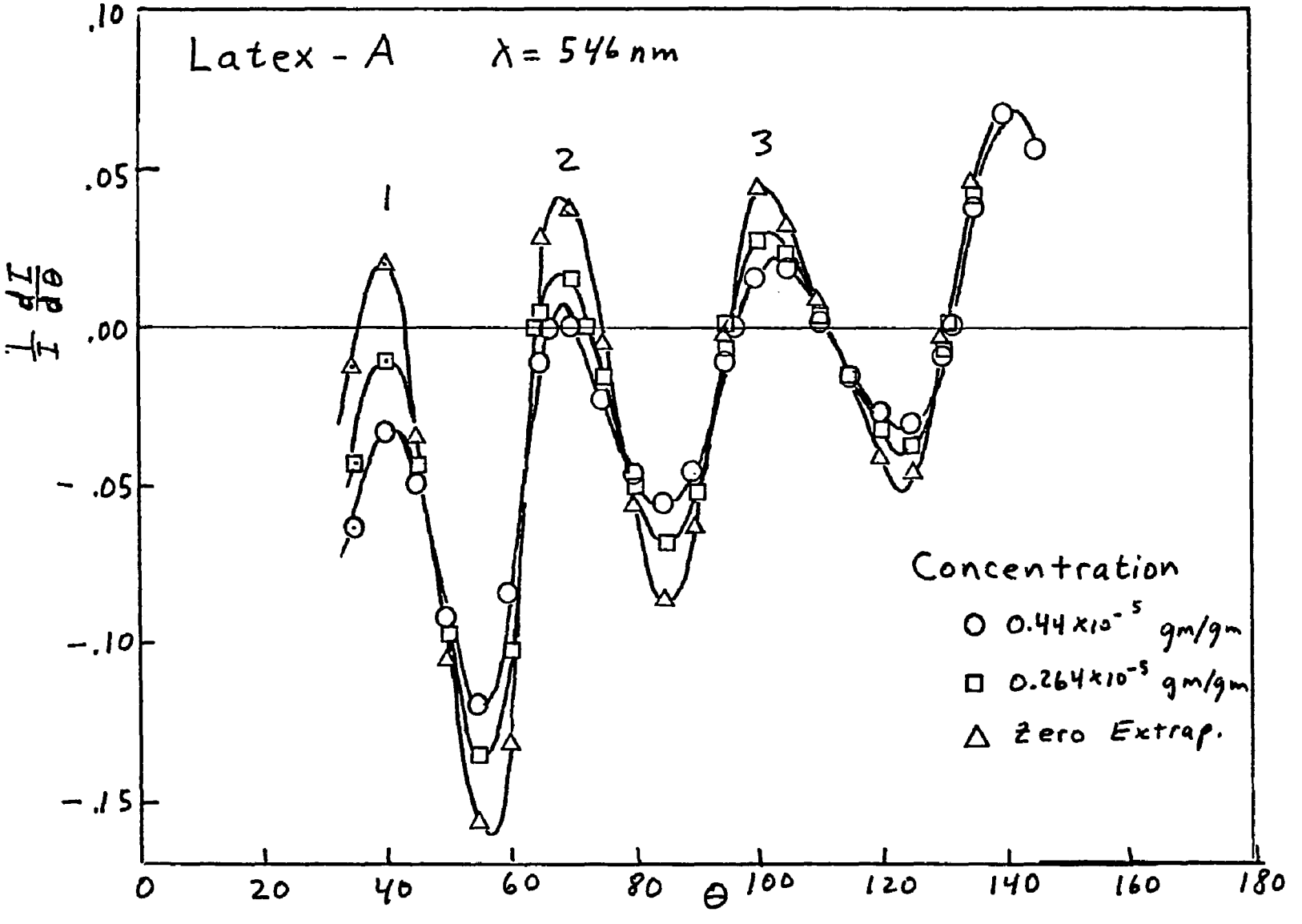

Fig. 135. Normalized Angular Derivative of I_1 from Latex-A at Different Particle Concentrations Using Incident Light Having a Wavelength of 546nm

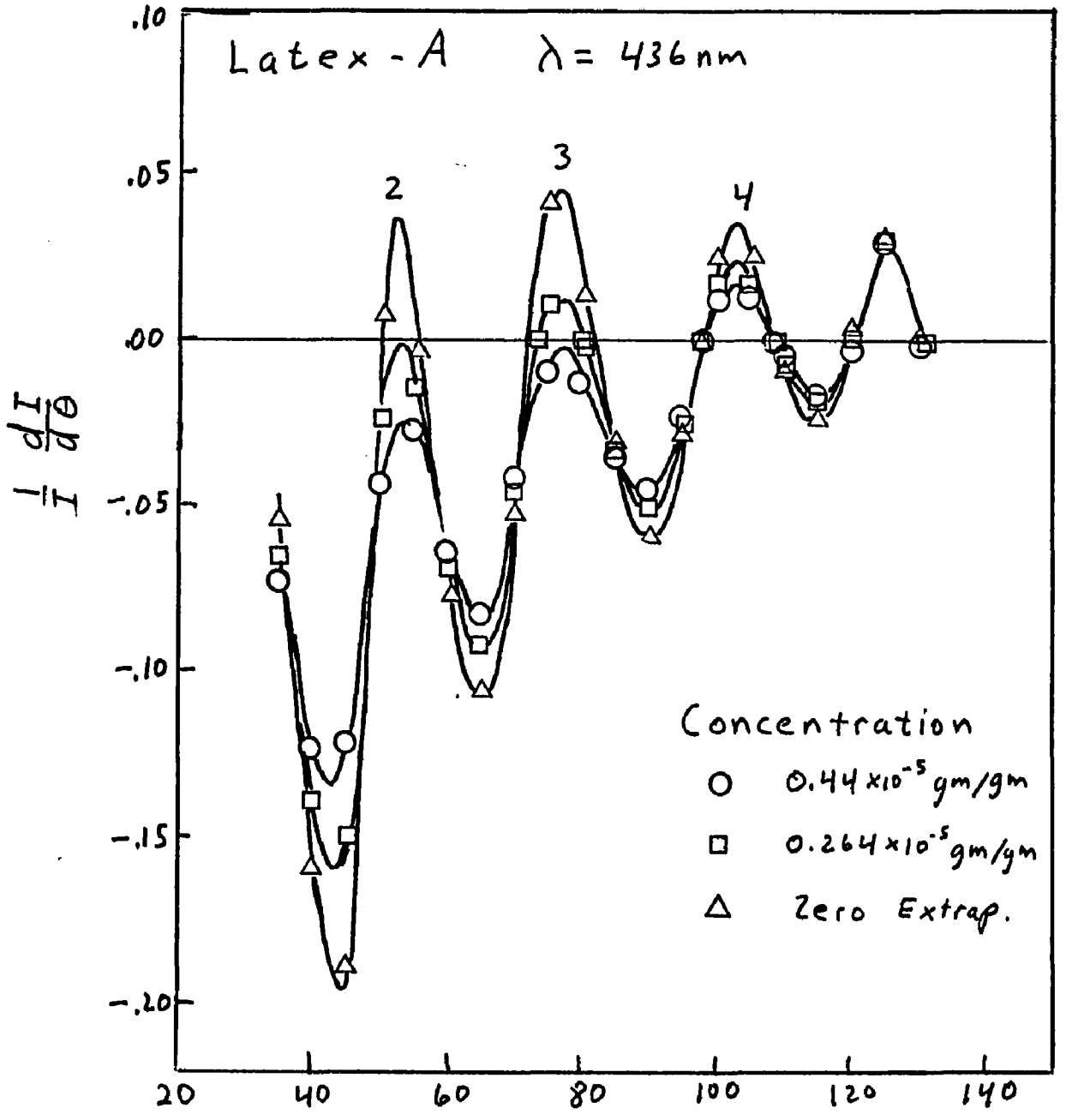

Fig. 136. Normalized Angular Derivative of I_1 from Latex-A at Different Particle Concentrations Using Incident Light Having a Wavelength of 546nm

respectively. These figures show three curves of increasing amplitude of oscillation and represent particle concentrations of 0.44×10^{-5} gm/gm, 0.264×10^{-5} gm/gm and the extrapolation to zero concentration. Since only two concentrations were available to extrapolate the scattering to zero concentration, the extrapolations have a lower value (and hence a higher degree of heterodispersion) than would occur with more concentrations.* The behavior of the curves in Figures 135 and 136 for Latex-A is the same as described earlier for Latex-11 and need not be repeated. However, the derivative curves for Latex-A show a much smaller amplitude of oscillation than the corresponding curves for Latex-11. This smaller amplitude of oscillation indicates that Latex-A is more heterodisperse than Latex-11.

2. Extrapolation of Light Scattering Measurement to Zero Concentration

One of the most critical steps in determining particle size distributions is to obtain accurate extrapolations of light scattering measurements. These extrapolations are very difficult in regions of local maxima or minima for the measurement used. However the regions of local maxima or minima are precisely the regions that vary the most with particle size distribution and must be accurately determined. Figure 137 illustrates a typical extrapolation of $dI/Id\theta$ to zero concentration. The data in this figure represents values of $\frac{1}{I}\frac{dI}{d\theta}$ at $\theta = 100^{o}$ and the stated concentrations for Latex-11 using incident light with a wavelength 436 nm. The extrapolated curves in Figures 133-136 were obtained from curves similar to that in Figure 137. Note that the extrapolation to zero concentration

*Witeczek[63] used four concentrations of Latex-A to extrapolate scattering ratios to zero concentration. Unfortunately he was only able to find the two lowest concentrations for use in this investigation.

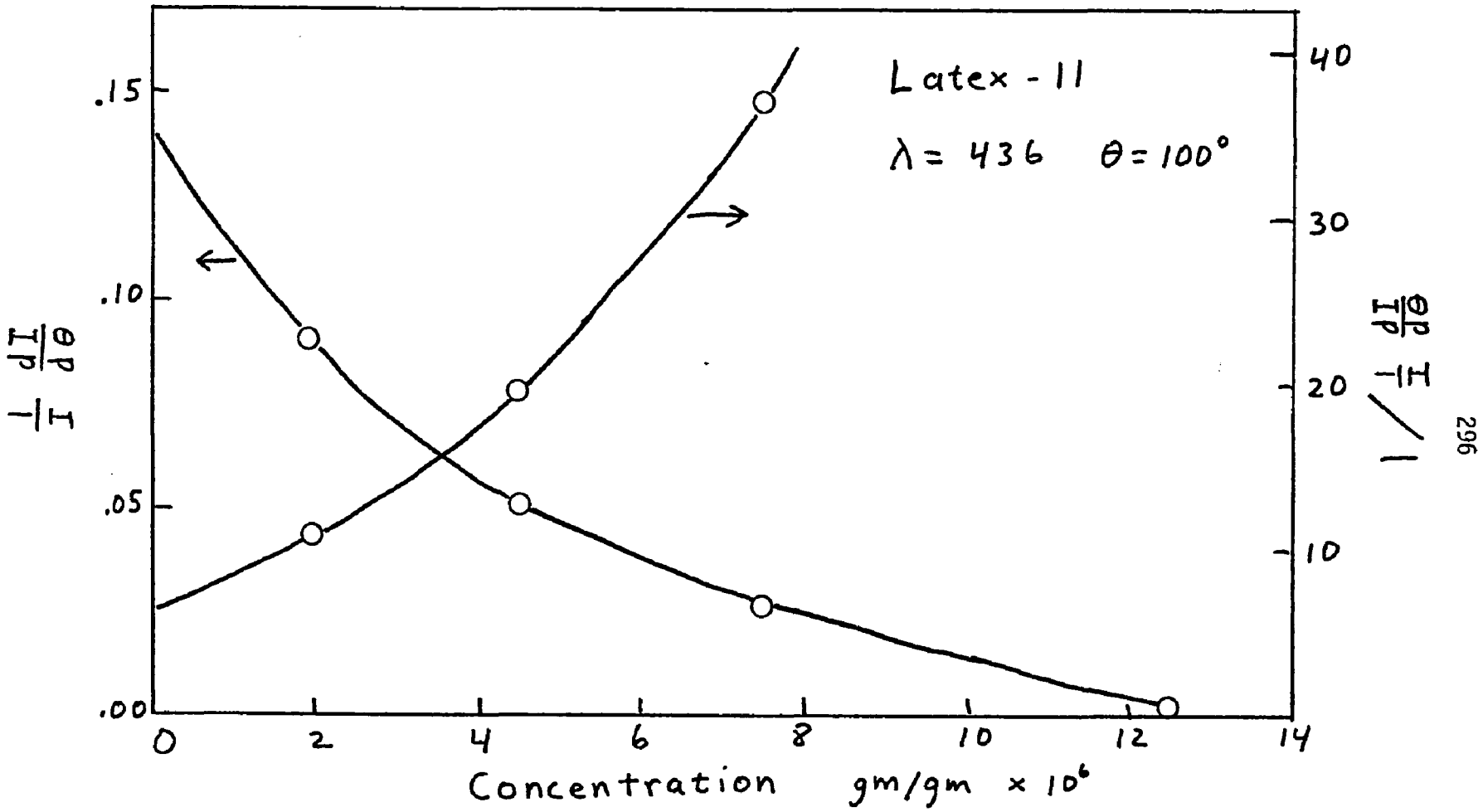

Fig. 137. Extrapolating the Normalized Angular Derivative of I_1 to Zero Particle Concentration

is not definite and may differ considerably from the curve drawn. The universe of this function was also extrapolated to zero concentration as recommended by Heller and Witeczek[64] for those cases where the normal extrapolations are uncertain.

All of the other experimental light scattering quantities used in this investigation were also extrapolated to zero concentration. Figure 138 shows a curve extrapolating I_{max}/I_{min} to zero concentration for the third extrema pair of Latex-11 with incident light of wavelength 546 nm. Note that the extrema pair disappears when the ratio equals 1.0. The inverse of this ratio was also extrapolated to zero concentration. Figure 139 shows the same extrema pair from Figure 138 replotted as $\frac{\Delta I}{I \Delta \theta}$.

The angular separation between the maximum and minimum of an extrema pair must also be extrapolated to zero concentration. Figure 140 shows the angular separation $\Delta\theta$ for the third and fourth extrema pairs from Latex-11 using incident light with a wavelength of 436 nm. Note that the third extrema pair has a much larger change in the angular separation with a change in concentration than the fourth extrema pair. This behavior is consistant with the previous observation that multiple scattering has an increasing effect on the scattering measurements in the forward direction. In addition, most of the change in $\Delta\theta$ is due to a shift in the position of the minimum location. This shift presents a serious problem since many of the techniques discussed in this investigation use the minimum location to identify the distribution mode.

The angular separation of the extrema was not used in this investigation to determine particle size distributions since the initial scattering data was obtained at 5^{o} intervals and the extrapolation of the extrema

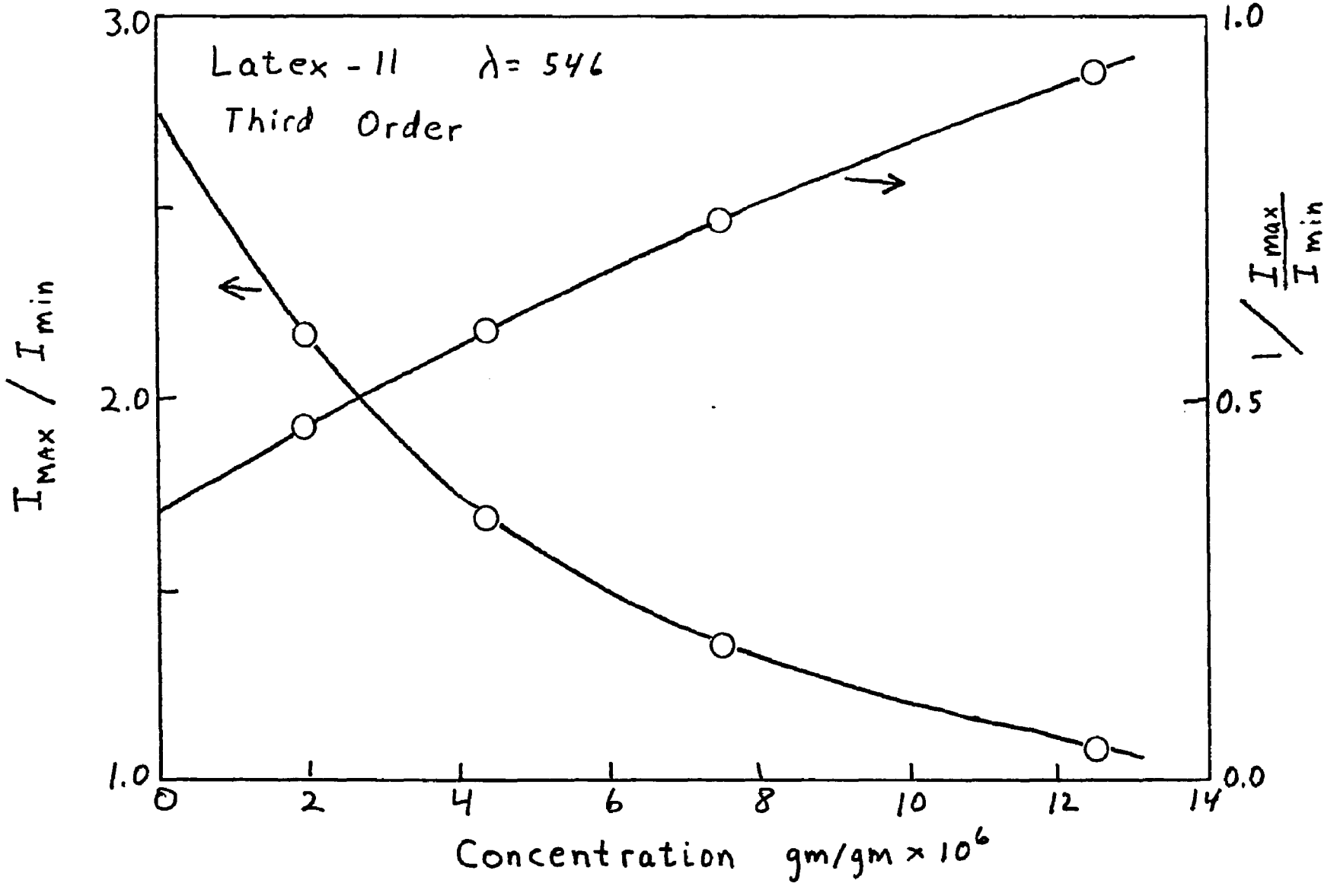

Fig. 138. Extrapolating the Intensity Ratio I max/I min to Zero Particle Concentration

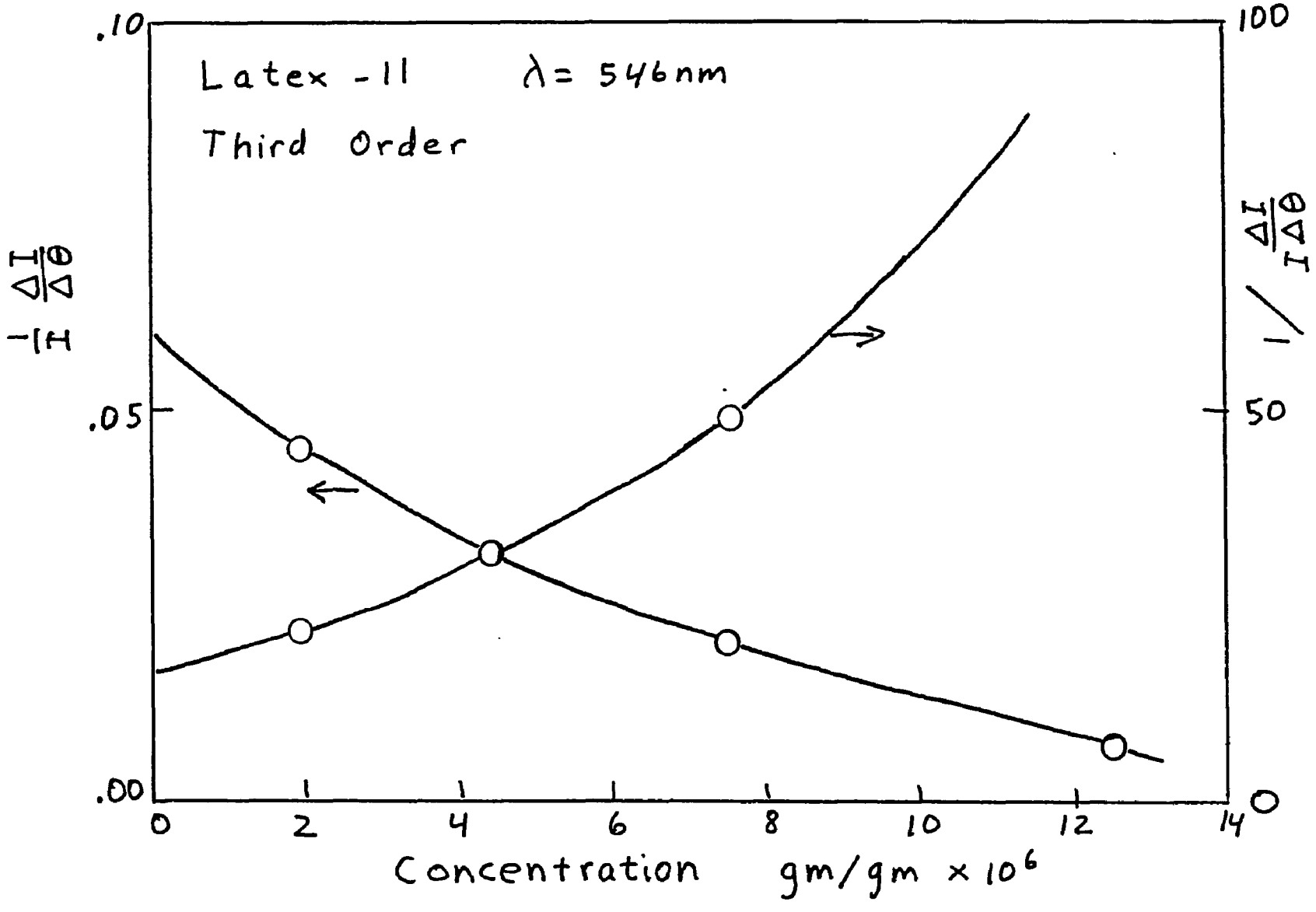

Fig. 139. Extrapolating the Intensity Slope $\frac{\Delta I}{I \Delta \theta}$ to Zero Particle Concentration

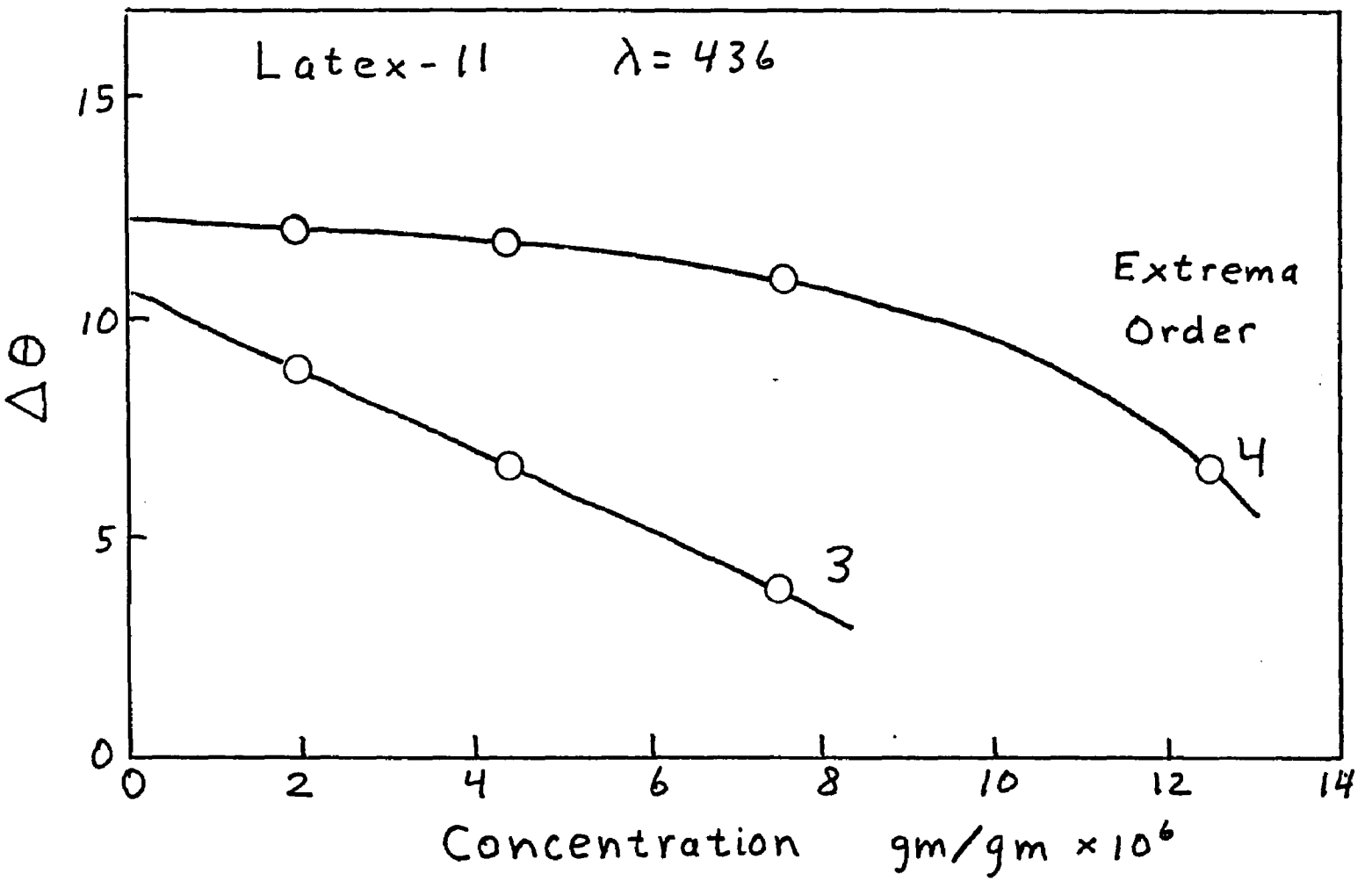

Fig. 140. Extrapolating the Angular Difference Between the I_1 Maximum and Minimum of the Third and Fourth Extrema Orders to Zero Particle Concentration

locations were only accurate to approximately $\pm$ 1°. To be useful in determining particle size distributions, the angular separation of the extrema should be determined to within $\pm$ 0.1°.

Once again a quantity (the angular location of the minimum) that is the least sensitive to variations in the degree of heterodispersion is the most sensitive to multiple scattering. The intensity ratios $\frac{I_{max}}{I_{min}}$, $\frac{\Delta I}{I\Delta\Theta}$ and $\frac{dI}{Id\Theta}$ were previously shown to be relatively insensitive to heterodispersion in the forward direction but very sensitive to multiple scattering. In contrast to the minimum location, the location of the maximum intensity is relatively insensitive to multiple scattering but sensitive to changes in heterodispersion.

D. Experimental Error Due to the Finite Solid Angle of the Detector

The other experimental parameter that should be extrapolated to a zero value is the solid angle of the detection system. Unfortunately this was not done for Witeczek's data. A large solid angle will measure the scattered light averaged over a range of angles and yield an apparent distribution that is more heterodisperse than actually exists. The extent to which the heterodispersion is overestimated depends on the variation of the angular intensity as well as the solid angle of the detector. Thus large variations in the scattered light over a small angular range, as occur for monodisperse distributions of large particles, will appear to be heterodisperse unless a very small solid angle is used. However, heterodisperse distributions in which the intensity varies gradually with angle can be accurately measured with relatively large solid angles.

The solid angle used in Witeczek's experimental data was 5.5×10^{-3} steradians which corresponds to a projected planer angle of $\pm$ 2.4°. Since the scattering measurements at each angle were averaged over a 4.8° range

the data representing the monodisperse Latex-11 will have an erroneously high heterodispersion. Latex-A, however, should not be affected by the large solid angle because the intensity varies slowly with angle.

Since multiple scattering from high particle concentrations and intensity averaging from large solid angles combine to give erroneously large heterodispersions, both variables must be extrapolated to zero values. Extrapolation of only one variable to its zero value will still yield a high estimate of the heterodispersion if the scattered intensity varies rapidly with angle. This difficulty is illustrated using data on Latex-11 published previously by Heller and Witeczek[64]. Figure 7 of reference 67 shows that extrapolating the solid angle of the detector to zero for a number of angles does not change the scattering ratio. However, the concentration used to perform the solid angle extrapolation was 5.45×10^{-6} gm/gm and has a considerable amount of multiple scattering that washes out the large angular intensity variation. Figure 5 of reference 64 shows the large change in the scattering ratios at several angles when the concentration is extrapolated to zero concentration compared to 5.45×10^{-6} gm/gm. Thus the independence of the scattering ratio to the solid angle was misleading because of the large particle concentration used. Heller and Witeczek[64] were aware of this problem and stated "that the effect of changes in the solid angle is apt to be masked by multiple scattering if the concentration is not sufficiently small."

The desired extrapolations to zero concentration and zero solid angle were not possible with the Brice-Phoenix photometer used to perform the experiments. This instrument, which used a mercury arc lamp and a IP21 photomultiplier tube for the light source and detector respectively, was

not capable of accurately measuring the scattered light at low particle concentrations and small solid angles. Future experiments should be conducted with a larger incident intensity using a laser and a more sensitive photomultiplier tube. However, when using a laser for the source, precautions must be taken to remove the coherence of the beam. The resulting speckel pattern would otherwise introduce an intolerable noise in the scattering measurements[69].

E. Results and Discussion

After extrapolating the functions $\frac{dI}{Id\theta}$, $\frac{\Delta I}{I\Delta\theta}$ and $\frac{I_{max}}{I_{min}}$ to zero concentration, they were used to determine the particle size distribution. The size distributions were obtained using the methods based on finding the distribution mode and the distribution width in separate steps. The experimental data was not suitable for testing the more general methods presented in this investigation. Inverting the scattering matrix would require scattering measurements over the angular range from 0^{o} to 180^{o} instead of the smaller range of the present data. Heller's simultaneous equation method would require precise locations of the extrema rather than interpolating between 5^{o} intervals.

1. Determination of the Distribution Mode

The first step in obtaining the particle size distribution is the determination of the distribution mode. This is accomplished by matching the experimental locations of the intensity minima with theoretical curves that show the variation of extrema location with particle size. The location of the minimum intensities was previously shown to be insensitive to changes in heterodispersion if a constant mode is maintained. Thus one figure showing the extrema locations versus relative particle size for monodisperse systems would be sufficient for each polarization and m value to determine the modal

diameter for any heterodispersion. Since all of the experimental data presented in this investigation pertains to I_1 scattering with m = 1.20* the corresponding extrema curves for monodisperse systems are shown in Figure 31.

The angular locations of the intensity extrema were obtained from the derivative curves extrapolated to zero concentration shown in Figures 133-136. The zeros of the derivative curves determined the angular location of the intensity extrema which are tabulated in Table V. Figure 31 was then used to find the correspoding α values which are also shown in Table V. In general, the α values corresponding to the intensity minima are constant while those corresponding to the intensity maxima are larger and tend to vary. If the four data sets in Table V represented true monodisperse systems then all of the angular extrema would have the same α value. The difference between the α value corresponding to the angular minima and maxima results from the shift in the angular location of the maxima intensities with increasing heterodispersion. Note that the difference between the α values for the maxima and minima is significantly larger for Latex-A than for Latex-11 and suggests that Latex-A is more heterodisperse than Latex-11. Table V also shows the modal diameter α_M averaged from the α values corresponding to the intensity minima.

2. Determination of the Distribution Width

Once the modal diameters were obtained for the four data sets, the associated distribution widths could be determined. This was accomplished

*The small change in the relative refractive index due to dispersion at two different wavelengths is ignored.

TABLE V

Determination of Modal Diameter From Extrema Locations

Latex - 11				Latex - A			
546nm		436nm		546nm		436nm	
θ	α	θ	α	θ	α	θ	α
41.0*	7.10	48.7	8.40	36.0	6.50	50.0	8.20
63.0	6.63	56.2*	8.60	43.0*	6.85	55.0*	8.75
72.8*	6.85	71.2	8.40	64.0	6.50	73.0	8.10
92.6	6.70	80.8*	8.50	74.8*	6.70	81.5*	8.40
108.3*	6.78	94.7	8.40	95.0	6.50	97.5	8.15
128.4	6.70	107.8*	8.35	111.5*	6.60	109.0*	8.20
		121.0	8.15	130.5	6.50	120.0	8.50
						131.0*	9.00
α_M =	6.70		8.40		6.50		8.20

*Locations of maximum intensity

by using the procedure discussed in detail in Chapter V, where an experimental light scattering quantity was compared to the corresponding theoretical curve plotted against increasing heterodispersion at a constant mode. For example, if the experimental quantity were $\frac{\Delta I}{I\Delta\theta}$ for the second extrema pair from a distribution having a mode $\alpha_M = 10$, one could find the heterodispersion q directly from the curve for $\alpha_M = 10$ in Figure 111. Although it is possible to interpolate between the α_M values used in Chapter V, new theoretical curves were generated for the four modal values shown in Table V. The experimental quantities $\frac{I_{max}}{I_{min}}$, $\frac{\Delta I}{I\Delta\theta}$ and $\frac{dI}{Id\theta}$ were then compared to the appropriate theoretical curves and the heterodispersion determined.

Table VI shows the resulting q values determined from each of the three experimental quantities for Latex-11 with $\lambda = 546$ nm. The experimental data for $\frac{I_{max}}{I_{min}}$, $\frac{\Delta I}{I\Delta\theta}$ and $\frac{dI}{Id\theta}$ and the corresponding inverses were extrapolated to zero concentration as shown in Figures 138, 139 and 137 respectively. In general the q value obtained from the extapolation of the light scattering function and its inverse agree very well. Table VI also shows that the q values obtained from $\frac{I_{max}}{I_{min}}$ and $\frac{\Delta I}{I\Delta\theta}$ for the lower extrema orders are larger than those obtained for the higher extrema orders. Similarly the q values obtained for $\frac{dI}{Id\theta}$ at smaller θ angles are also higher than at larger angles. This apparent increase in the heterodispersion toward the forward direction had been discussed earlier in terms of the increased effect of multiple scattering.

To reduce the effect of the multiple scattering, the distribution width was determined by only using the functions that were furthest from the forward direction. These values are indicated by an asterisk (*) in

TABLE VI

Determination of the Heterodispersion for Latex-11 with λ = 546nm and α_M = 6.70

$\frac{I\ max}{I\ min}$			$\frac{\Delta I}{I\Delta\theta}$			$\frac{dI}{Id\theta}$		
Extrema Order	q Extrapolation Normal	Inverse	Extrema Order	q Extrapolation Normal	Inverse	θ	q Extrapolation Normal	Inverse
2	1.08	1.10	2	1.01	---	65	1.09	1.07
3*	0.72	0.70	3*	0.65	0.65	95*	0.73	0.65
						100*	0.67	0.67
						135	0.52	0.57

*Data used to determine the average q (q = 0.68)

Table VI. The q values derived from both the normal and inverse extrapolations were averaged for each of the three functions tabulated. Note that the q values derived from $\frac{dI}{Id\Theta}$ extrapolations at two different angles were used in computing the average q. These two angles were used because they are the closest to the derivative maximum at 97° in Figure 133. Ideally, the extrapolations of $\frac{dI}{Id\Theta}$ should be made at the angular location of the derivative maxima to obtain the most accurate q values. The q values at 135° were not used because the angle falls within the reflection region of the scattering diagram rather than the diffraction region.

After an average q value is obtained for each of the three tabulated functions, a total average is obtained giving equal weights to each of the three functions. The average q for the data in Table VI is 0.68. A similar procedure is used to determine the average q value for Latex-11 with λ = 436 nm and Latex-A with λ = 546 nm and 436 nm. The data used in these determinations are shown in Tables VII, VIII and IX. Note that in Table IX the q values from the fourth extrema order of $\frac{I_{max}}{I_{min}}$ and $\frac{\Delta I}{I\Delta\Theta}$ were used instead of the fifth extrema order. This was done because the fourth extrema order is the last order in the diffraction region and all higher orders fall in the reflection region.

Theoretical curves of $\frac{dI}{Id\Theta}$ were then generated for the particle size distributions obtained from Tables V-IX and compared to the experimental data extrapolated to zero concentration. Figure 141 shows the theoretical curve of $\frac{dI}{Id\Theta}$ versus Θ for a distribution with α_M = 6.7 and q = 0.68. The circles represent the extrapolations to zero concentration in Figure 133. One sees that the best fit occurs at the third derivative maximum, as expected, since the experimental measurements near the third derivative

TABLE VII

Determination of the Heterodispersion for Latex-11 with λ = 436nm and α_M = 8.40

$\frac{I\ max}{I\ min}$			$\frac{\Delta I}{I\Delta\theta}$			$\frac{dI}{Id\theta}$		
Extrema Order	q Extrapolation Normal	Inverse	Extrema Order	q Extrapolation Normal	Inverse	θ	q Extrapolation Normal	Inverse
3	1.05	1.08	3	1.30	0.90			
4*	0.79	0.88	4*	0.79	0.74	75	1.13	1.10
						100*	0.85	0.77
						125	1.04	0.81

*Data used to determine the average q (q = 0.81)

TABLE VIII

Determination of the Heterodispersion for Latex-A with λ = 546nm and α_M = 6.50

$\frac{I\ max}{I\ min}$			$\frac{\Delta I}{I\Delta\theta}$			$\frac{dI}{Id\theta}$		
Extrema Order	q Extrapolation Normal	Inverse	Extrema Order	q Extrapolation Normal	Inverse	θ	q Extrapolation Normal	Inverse
2	1.40	1.39	2	1.39	---	70	1.42	---
3*	1.26	1.22	3*	1.23	0.96	100*	1.21	---

*Data used to determine the average q (q = 1.18)

TABLE IX

Determination of the Heterodispersion for Latex-A with λ = 436nm and α_M = 8.20

	$\frac{I\ max}{I\ min}$		$\frac{\Delta I}{I\Delta\theta}$			$\frac{dI}{Id\theta}$		
Extrema Order	q Extrapolation Normal	Inverse	Extrema Order	q Extrapolation Normal	Inverse	θ	q Extrapolation Normal	Inverse
4*	1.49	1.48	4*	1.51	1.41	50	1.62	---
5	2.50	2.49	5	1.96	2.00	75	1.46	---
						80	1.50	---
						100*	1.56	1.41

*Data used to determine the average q (q = 1.49)

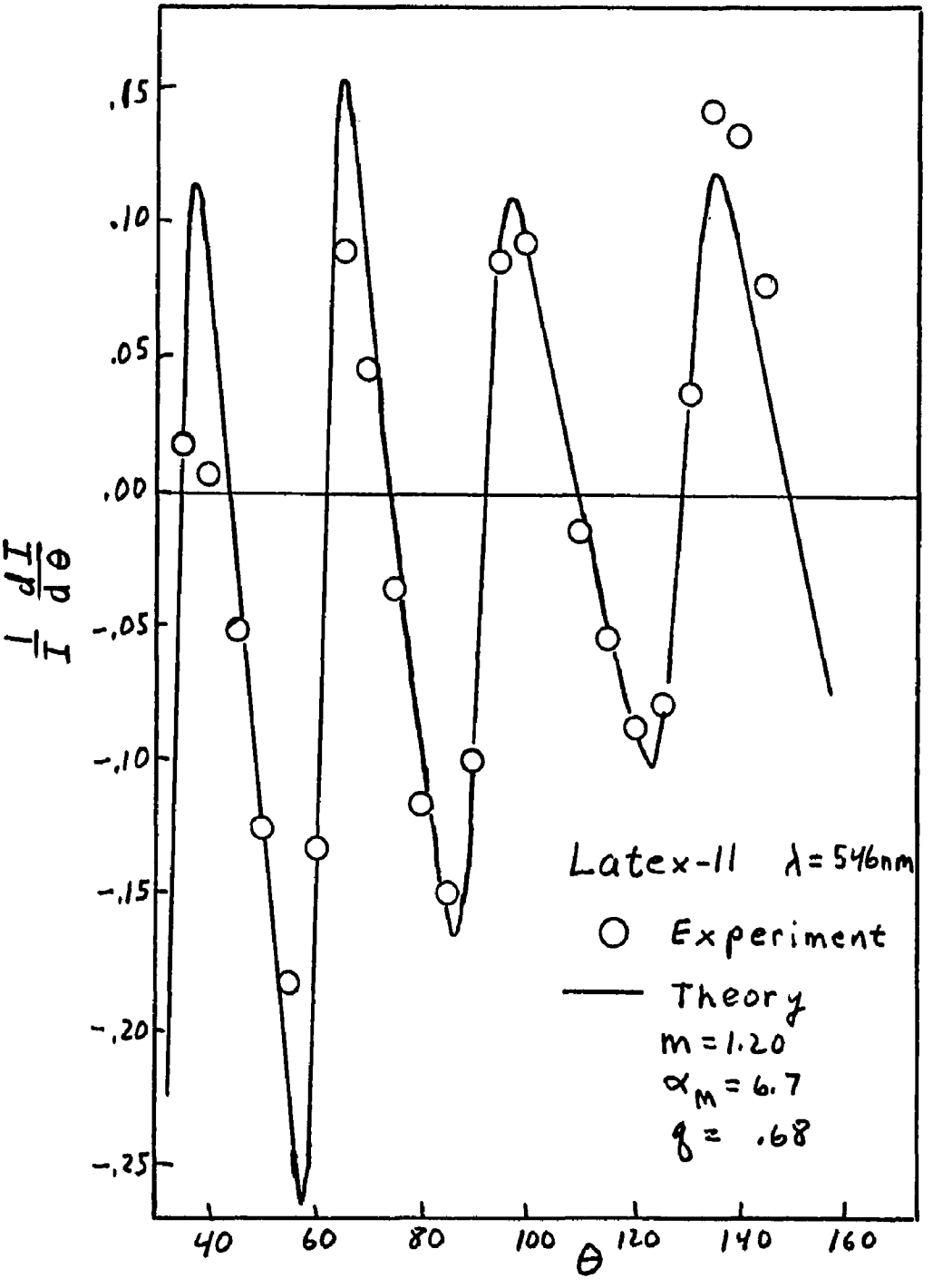

Fig. 141. Comparison of $\frac{dI}{I\,d\theta}$ Theoretical and Experimental Data for Latex-11 Using Incident Light Having a Wavelength of 546nm

maximum were used to determine the heterodispersion q. Note that the deviation between the theoretical curve and experimental curve increases toward the forward direction. The apparent increase in the heterodispersion for the experimental data, which is seen by a dampening of the amplitude of oscillation, was attributed to the increasing multiple scattering. Similar comparisons of the theoretical curve with experimental data for Latex-11 at λ = 436 nm and Latex A at λ = 546nm and 436 nm are shown in Figures 142, 143 and 144 respectively.

A good fit between experimental and theoretical light scattering curves do not necessarily imply that the particle size distribution of the experimental system is the same as that of the theoretical system. Complications in the experimental measurements such as multiple scattering or a large solid angle of detection would give an appearance of a much wider distribution than actually exists. These complications are especially difficult because they affect the light scattering pattern in a very similar fashion as increasing heterodispersion. The only satisfactory method of evaluating the performance of a light scattering technique for measuring particle size distributions is to verify the experimental distribution using an independent measurement technique such as electron microscopy. Such a comparison was performed for the two latex systems studied.

3. Comparison of Particle Size Distributions Obtained from Light Scattering and Electron Microscope Measurements

Figure 145 shows the comparison of the particle size distribution for Latex-11 obtained from electron microscopy, shown as the histogram, and light scattering measurements, shown as the smooth curves. The major features of this comparison indicate that the light scattering measurements

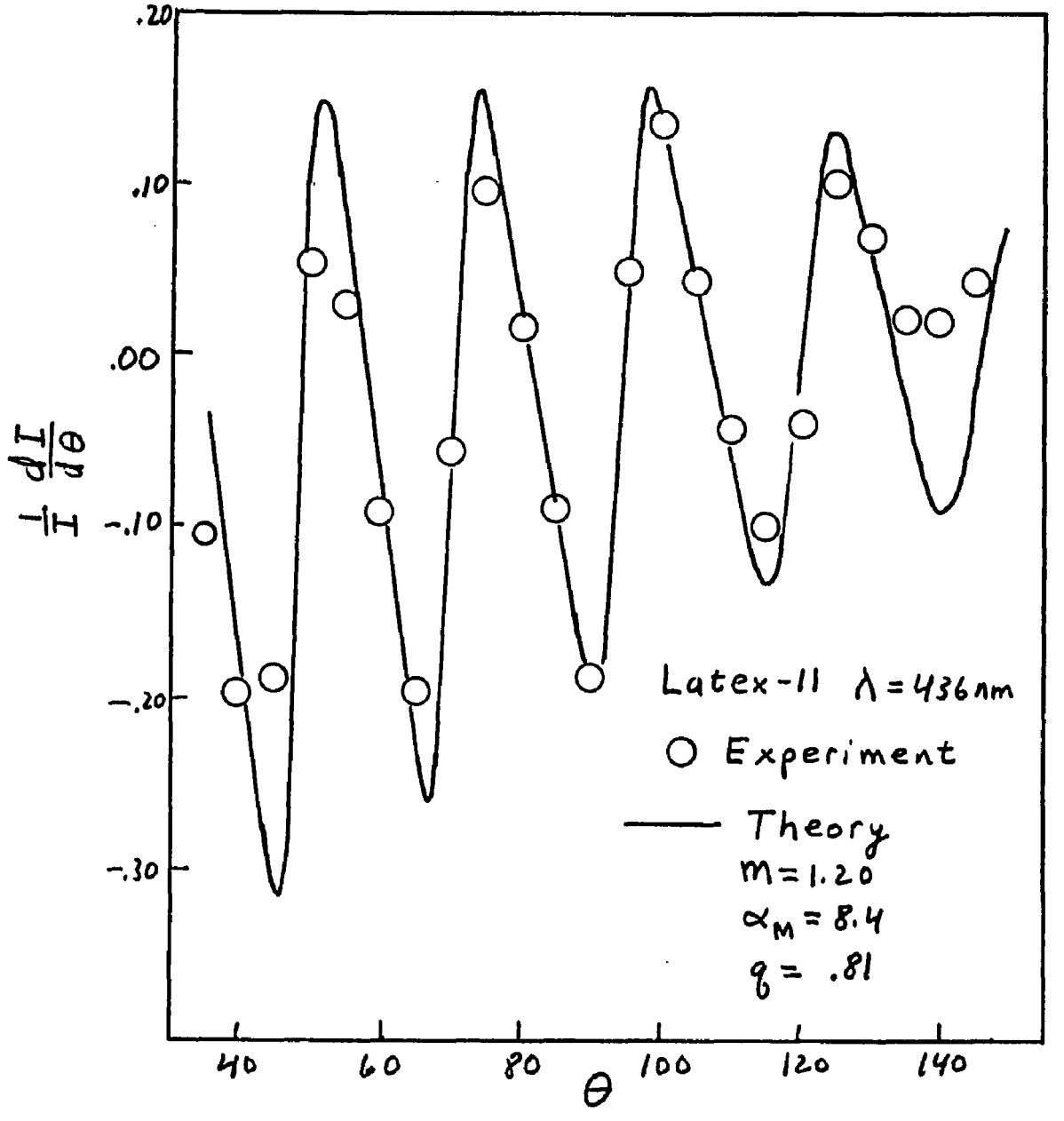

Fig. 142. Comparison of $\frac{1}{I}\frac{dI}{d\theta}$ Theoretical and Experimental Data for Latex-11 Using Incident Light Having a Wavelength of 436nm

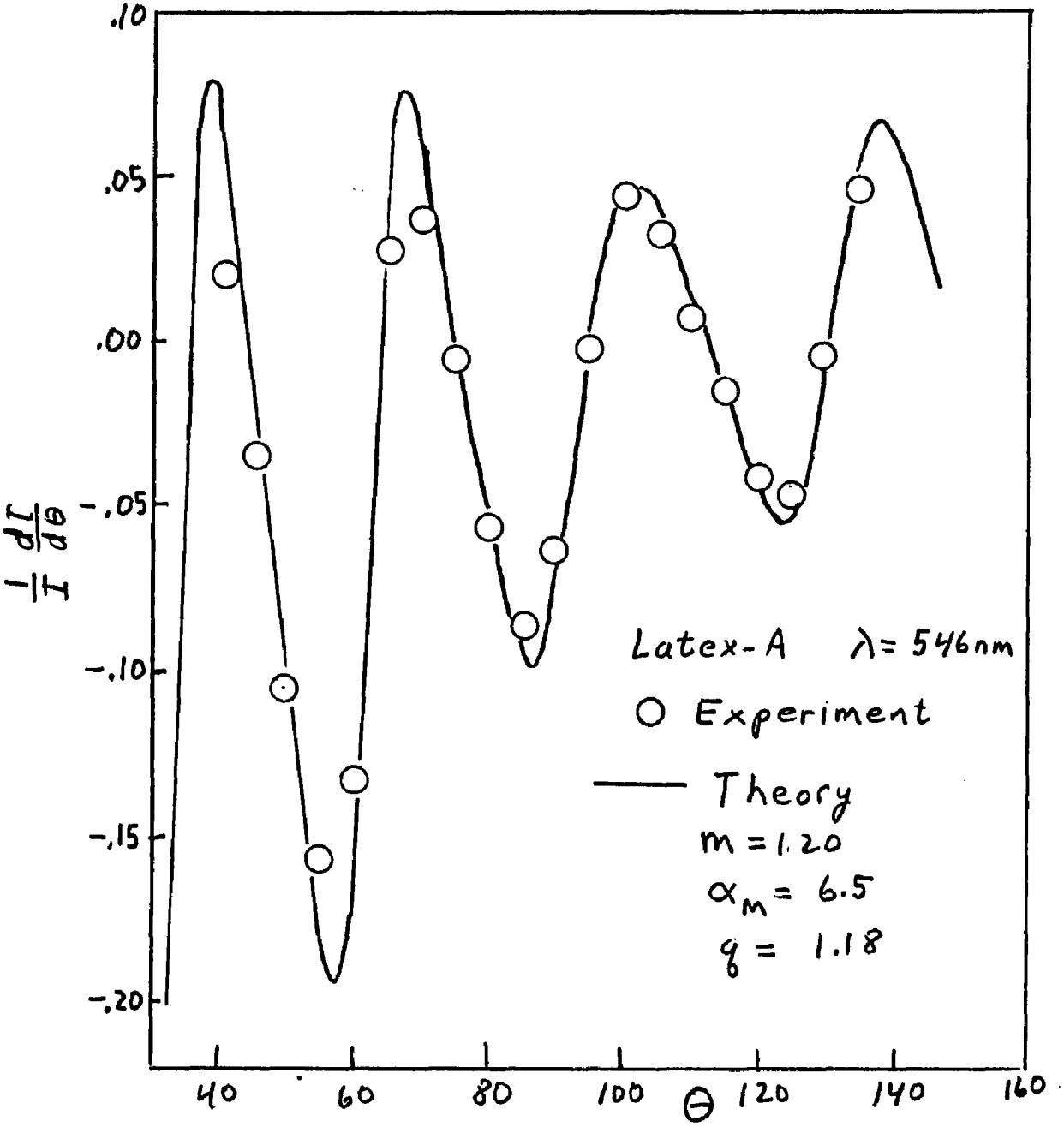

Fig. 143. Comparison of $\frac{1}{I}\frac{dI}{d\theta}$ Theoretical and Experimental Data for Latex-A Using Incident Light Having a Wavelength of 546nm

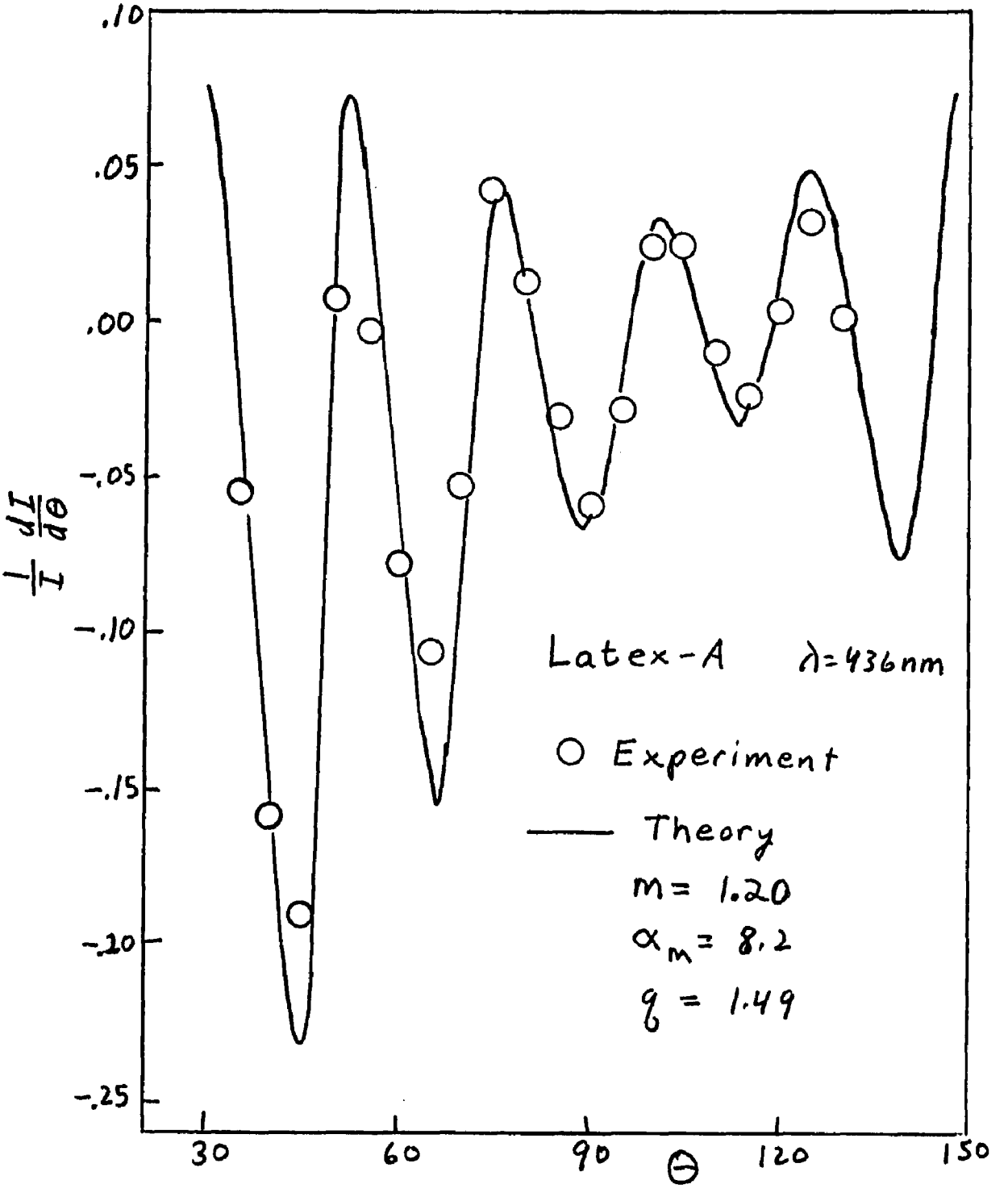

Fig. 144. Comparison of $\frac{dI}{I\,d\theta}$ Theoretical and Experimental Data for Latex-A Using Incident Light Having a Wavelength of 436nm

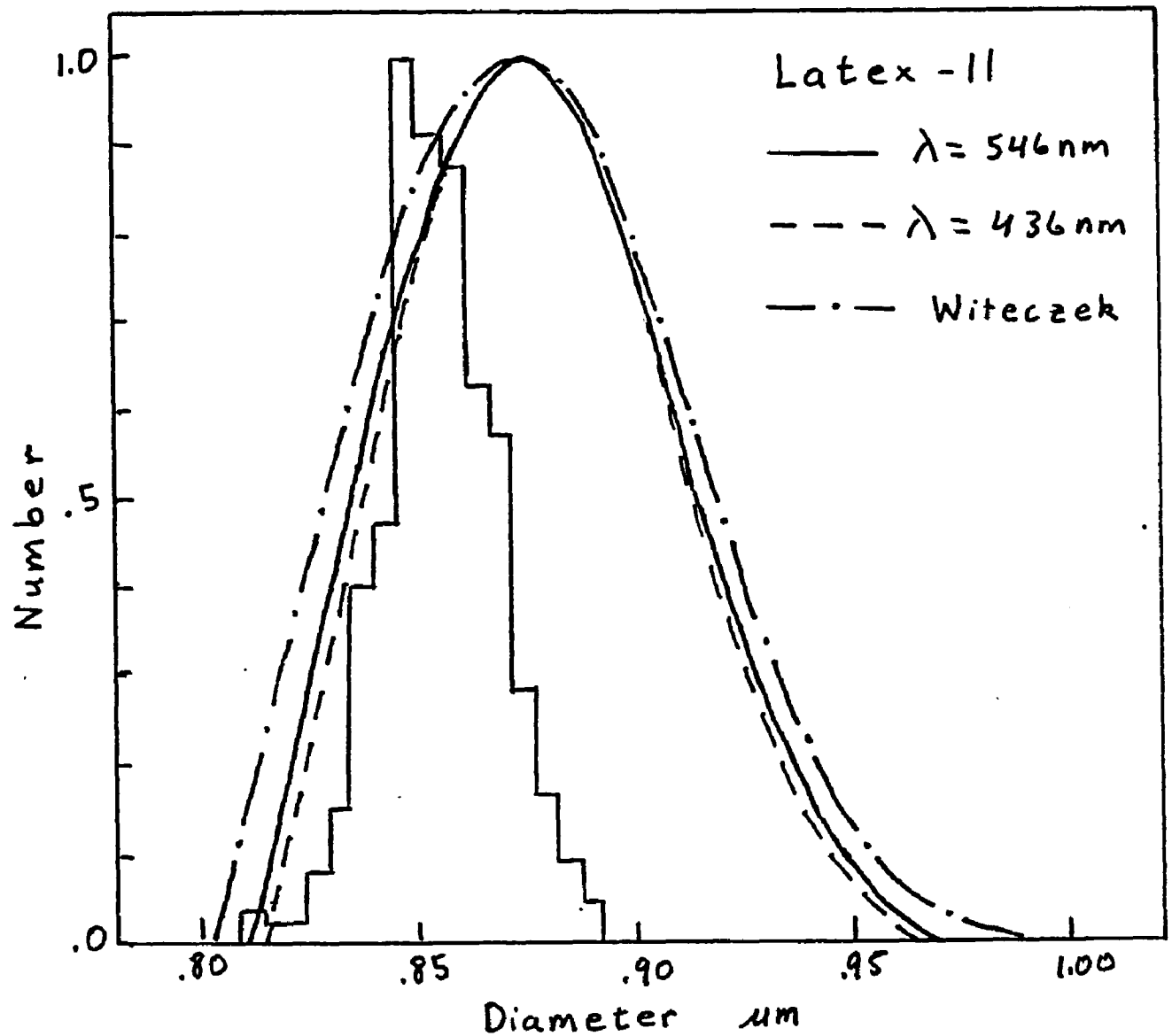

Fig. 145. Comparison of the Particle Size Distribution for Latex-11 Obtained from Electron Microscopy, Shown by the Histogram, and Light Scattering Measurements, Shown by the Smooth Curves

have a slightly larger mode and a much larger heterodispersion than the the electron microscopy measurements. The mode of the electron microscope measurements is about 3% smaller than the mode for the light scattering measurements (0.85 μm instead of 0.87 μm). However, electron microscope measurements from the manufacturer, Dow Chemical Co., specified an average diameter of 0.89 m for the sample, which is 3% larger than the light scattering measurements. This small variation in electron microscope measurements suggest that the mode obtained from light scattering represents the actual mode better than the electron microscope measurements.

The second and more serious discrepancy between the light scattering and electron microscope results is the determination of distribution widths. Here the light scattering measurements predict erroneously large distribution widths compared to electron microscopy*. The source of this error is believed to be primarily due to the large solid angle of the detector which integrates the scattering measurements over 4.8°.

Large detector solid angles are especially serious for angular scattering curves that have large intensity changes over small angular ranges. Such scattering curves are typical of particle size distributions having narrow widths and large model diameters like Latex-11. The averaging effect of the large solid angle produces an apparent angular scattering pattern that varies slowly with a change in angle and hence an apparent greater heterodispersion.

*Even if the electron microscope had a small error in the absolute size measurement, the relative size of one particle to another, and hence the distribution width, is extremely accurate.

Multiple scattering may also make a small contribution to the erroneously large distribution width. The attempt to eliminate multiple scattering by extrapolating the light scattering function to zero concentration, as shown in Figures 137-139, is very uncertain and may have a small contribution from multiple scattering. This is possible even though the heterodispersion was determined from the appropriate scattering measurements farthest from the forward direction.

The three distribution curves in Figure 145, derived from light scattering measurements, illustrate the good agreement between a number of different techniques on Latex-11. This is not surprising considering that the same experimental data was used for the different techniques. The two curves designated by the wavelength of the incident light were determined by first finding the distribution mode and then the distribution width in two separate steps discussed previously. Note that the two experiments at λ = 546 nm and λ = 436 nm have nearly identical distributions despite large differences in the angular scattering pattern (compare Figures 133 and 134). The other curve was obtained by Witeczek[63] using the angular variation of the scattering ratio, I_2/I_1. This curve represents the average results for the two wavelengths 546 nm and 436 nm.

The procedure for determining particle size distributions from the angular variation of the scattering ratio is similar to that presented in this investigation for $\frac{1}{I}\frac{dI}{d\theta}$. Angular measurements of I_1 and I_2 are made for a number of different concentrations and the ratios I_2/I_1 extrapolated to zero concentration. An extensive computer search was then made through a library of theoretical I_2/I_1 versus θ curves that correspond

to many different size distributions. Each theoretical curve was compared to the experimental data using least squares to evaluate the fit. The size distribution corresponding to the theoretical curve having the best fit was then chosen to represent the experimental system. Figure 146 shows the comparison of the experimental I_2/I_1 data for Latex-11 at 546 nm extrapolated to zero concentration and the theoretical curve representing the least square deviation.

The comparison of the size distribution curves in Figure 147 obtained from light scattering and electron microscopy measurements on Latex-A indicate fairly good agreement for both the distribution mode and width. The two curves designated by the wavelength of the incident light were obtained from the techniques presented in this investigation and show good agreement. However, these distribution curves are shifted slightly toward a smaller particle size compared to the distribution curve obtained by Witeczek using I_2/I_1. This shift is believe to be due to the difference in the extrapolation of the light scattering data to zero concentration. Witeczek extrapolated his I_2/I_1 data to zero concentration using four different concentrations. However, only the lowest two concentrations were available for this investigation and consequently required a linear extrapolation.

The distribution width determined from electron microscopy and light scattering measurements agree very well for Latex-A. Since the scattered intensity for this system varies slowly with angle, the large solid angle of the detector does not have the effect of increasing the apparent distribution width seen for Latex-11 in Figure 145. The electron microscope measurements in Figure 147 also indicates a bimodal distribution.

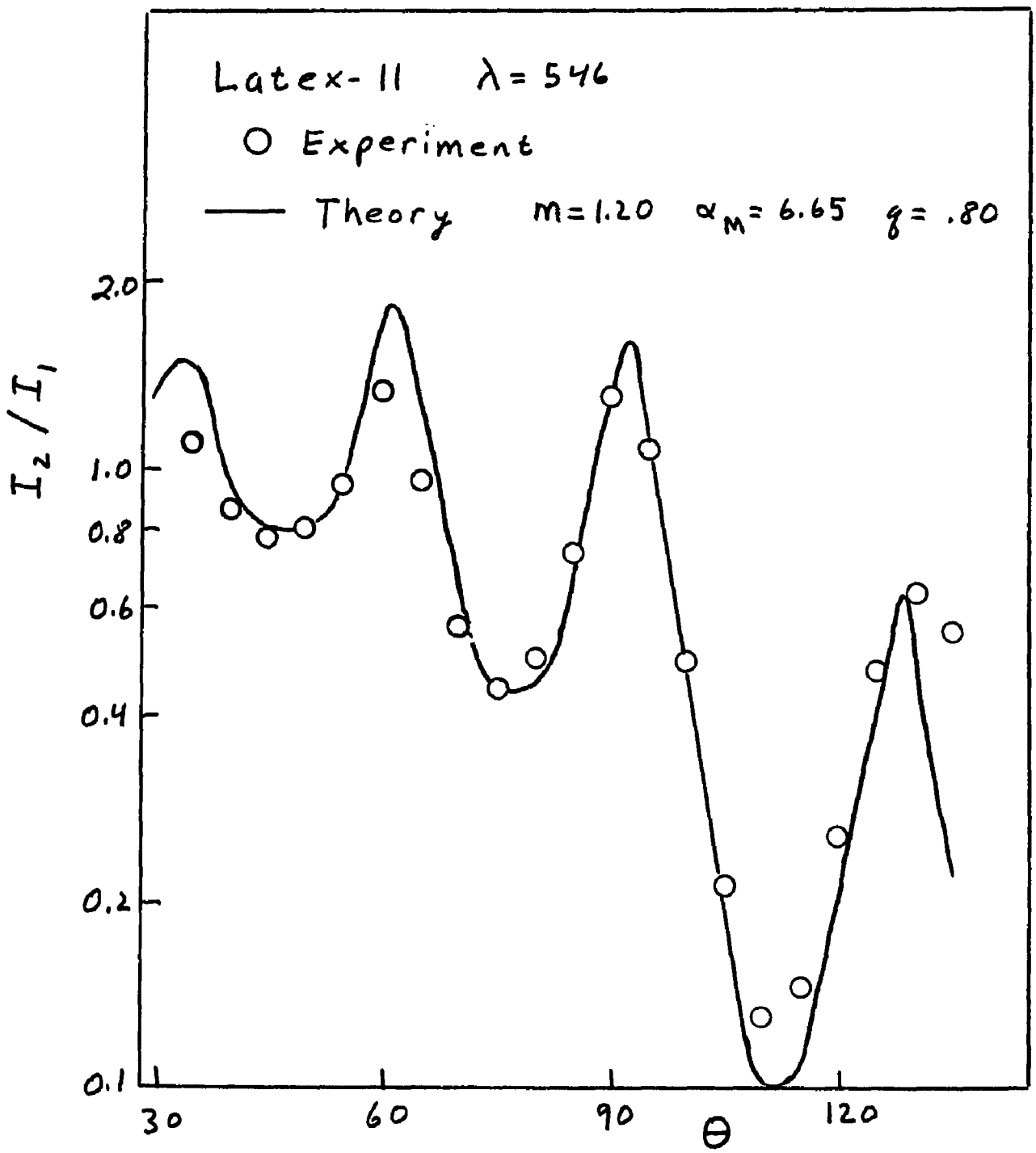

Fig. 146. Comparison of I_2/I_1 Theoretical and Experimental Data for Latex-11 Using Incident Light Having a Wavelength of 546nm

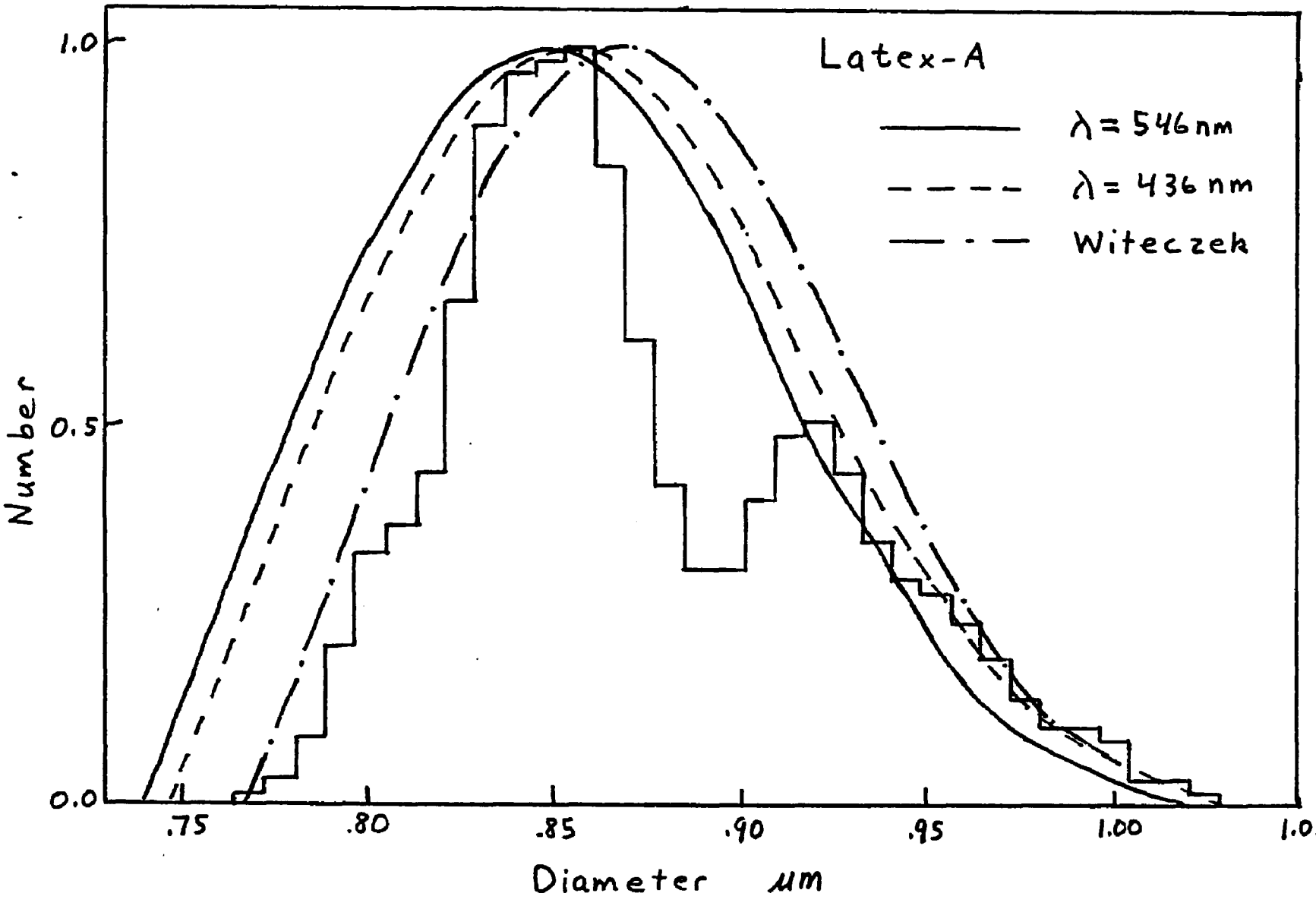

Fig. 147. Comparison of the Particle Size Distribution for Latex-A Obtained from Electron Microscopy, Shown by the Histogram, and Light Scattering Measurements, Shown by the Smooth Curves

Unfortunately, the uncertainty of the experimental data (caused primarily from the extrapolation to zero concentration and the large solid angle of the detector) was too large to attempt to match with bimodal theoretical data.

A survey of the size distributions for Latex-11 and Latex-A as determined from the various experimental techniques are shown in Table X. The mode α_M and heterodispersion q for wavelengths of 436 nm were normalized to their equivalent values at 546 nm for easier comparison. One sees that the size distribution parameters for all of the techniques give nearly identical results except for a slightly lower value of α_M discussed previously for Latex-A.

The difference between the various techniques thus reduces to the amount of work required to obtain the size distribution parameters from the same experimental measurements. In principle all of the techniques require matching an experimental measurement of unknown size distribution with a corresponding theoretical quantity of known size distribution. However, in pratctice, the techniques based on determining the distribution mode and width in two separate steps provide a systematic approach to the matching of experimental data which is not available in the standard library search methods. It should be noted that the I_2/I_1 function can also be used in the two step apprach as shown by Wallace[25]. Of the different techniques listed in Table X, the most versatile method is the one based on $\frac{dI}{Id\theta}$ since the technique is still able to provide size distribution information even when all of the intensity extrema have disappeared.

TABLE X

Comparison of Techniques for Determining Particle Size Distributions

Sample	Technique	α_M 546nm	α_M 436nm*	q 546nm	q 436nm*
Latex-11	$\frac{Imax}{Imin}, \frac{\Delta I}{I\Delta\theta}, \frac{dI}{Id\theta}$	6.70	6.71	0.68	0.65
	$\frac{I_2}{I_1}$	6.65	6.72	0.80	0.72
Latex-A	$\frac{Imax}{Imin}, \frac{\Delta I}{I\Delta\theta}, \frac{dI}{Id\theta}$	6.50	6.55	1.18	1.19
	$\frac{I_2}{I_1}$	6.66	6.68	1.10	1.12

*The α_M and q values were normalized to 546nm

Bibliography

1. G. J. Sem, J. A. Borgos, J. G. Olin, J. P. Pilney, B. Y. H. Liu, N. Barsic, K. T. Whitby and F. D. Dorman, National Technical Information Service Publication PB-202-665 (1971).

2. "Fine Particles, Aerosol Generation, Measurement, Sampling and Analysis", B. Y. H. Liu, ed., Academic Press, Inc. New York (1976.

3. M. Kerker, "The Scattering of Light and Other Electromagnetic Radiation", Academic Press, New York, 1969.

4. I. Johnson and V. K. LaMer, J. Am. Chem. Soc., 60, 1184 (1947).

5. D. Sinclair and V. K. LaMer, Chem Revs., 44, 245 (1949).

6. A. S. Kenyon and V. K. LaMer, J. Colloid Sci. 4, 163 (1949).

7. M. Kerker, W. Farone and W. Espenscheid, J. Colloid & Interface Sci., 21, 459 (1966).

8. J. M. Greenberg and T. P. Roark, Astrophys, J., 147, 917 (1967).

9. W. B. Dandliker, J. Am. Chem. Soc. 72, 5110 (1950).

10. M. Nakagaki and W. Heller, J. Chem. Phys., 32, 835 (1960).

11. W. Heller and M. Nakagaki, J. Chem. Phys., 64, 4912 (1976).

12. G. Dezelic and J. P. Kratohvil, J. Colloid. Sci., 16, 561 (1961).

13. S. H. Maron, P. E. Pierce and M. E. Elder, J. Colloid Sci., 18, 391 (1963).

14. S. H. Maron and M. E. Elder, J. Colloid. Sci., 18, 107 (1963).

15. S. H. Maron, P. E. Pierce and M. E. Elder, J. Colloid. Sci., 19, 591 (1964).

16. P. E. Pierce and S. H. Maron, J. Colloid. Sci., 19, 658 (1964).

17. M. Kerker, W. A. Farone, L. B. Smith and E. Matijevic, J. Colloid. Sci., 19, 193 (1964).

18. W. J. Pangonis and W. Heller, "Angular Scattering Functions for Spherical Particles", Wayne State Univ. Press, Detroit, Michigan (1960).

19. A. N. Lowan, "Tables of Scattering Functions for Spherical Particles" (Natl. Bur. of Std. Appl. Math. Ser. 4). U.S. Govt. Printing Office, Washington, D.C. (1948).

Bibliography

20. A. J. Patitsas, IEEE Trans. on Antennas and Propagation, 21, 243 (1973).

21. A. J. Patitsas, J. Colloid & Interface Sci. 43, 359 (1973).

22. A. J. Patitsas, J. Colloid & Interface Sci., 46, 266 (1974).

23. A. J. Patitsas, J. Colloid & Interface Sci., 46, 276 (1974).

24. T. P. Wallace and J. P. Kratohvil, J. Polymer Sci., A2, 8, 1425 (1970).

25. T. P. Wallace, J. Polymer Sci., A2, 9, 595 (1971).

26. T. P. Wallace and W. B. Scott, J. Polymer Sci., A2, 10, 527 (1972).

27. H. C. Van DeHulst, Thesis Utrecht, Rech. Aston. Obs. d'Utrecht 11, Pt. 1. (1946).

28. H. C. Van DeHulst, "Light Scattering by Small Particles" Wiley, New York (1957).

29. R. Penndorf in "Electromagnetic Scattering", M. Kerker, ed., Pergamon Press, Oxford (1963).

30. R. B. Penndorf, Tech. Report RAD-TR-61-32 Air Force Cambridge Res. Lab., Bedford, Mass. (1961).

31. R. B. Penndorf, Tech. Report RAD-TR-63-9 Air Force Cambridge Res. Lab, Bedford, Mass. (1962).

32. R. L. Rowell, Report No. 1, Goessmann Lab., Univ. of Massachusetts, Amherst, Mass. (1962).

33. R. B. Penndorf, Tech. Report RAD-TR-63-26 Air Force Cambridge Res. Lab., Bedford, Mass. (1963).

34. D. D. McCracken and W. S. Dorn, "Numerical Methods and Fortran Programming", Wiley New York (1964).

35. M. Yajnik, J. Witeczek and W. Heller, J. Polymer Sci., Part C, 25, 99 (1968).

36. M. Yajnik, W. Heller and J. Witeczek, "Tables of Angular Scattering Functions for Heterodisperse Systems of Spheres', Wayne State Univ. Press, Detroit, 1969.

37. J. L. Kuester and J. H. Mize, "Optimization Techniques with Fortran", McGraw-Hill New York, 1973.

Bibliography

38. H. H. Denman, W. Heller and W. J. Pangonis "Angular Scattering Functions for Spheres", Wayne State University Press, Detroit, 1966.

39. A. F. Stevenson, W. Heller and M. Wallach, J. Chem. Phys., 34, 1789 (1961).

40. B. Carnahan, H. A. Luther and J. O. Wilkes, "Applied Numerical Methods", Wiley, New York, 1969.

41. W. Heller and M. Nakagaki, J. Chem. Phys., 31, 1188 (1959).

42. J. V. Dave, Applied Optics, 8, 1161 (1969).

43. Computer Science Department, Ford Motor Company, P.O. Box 2053, Dearborn, Michigan.

44. W. Murray in, "Numerical Methods for Unconcstrained Optimization", W. Murray, ed., Academic Press, New York, 1972.

45. F. Scheid, "Theory and Problems of Numerical Analysis", McGraw-Hill, New York 1968.

46. W. Bergman and W. Heller, "Mie Scattering Maxima and Minima in Heterodisperse Systems", Wayne State University Press, Detroit, Mich. 1977.

47. M. Kerker, E. Matijevic, W. Espenscheid, W. Farone and S. Kitani, J. Colloid Sci., 19, 213 (1964).

48. W. Heller, W. Pangonis and N. Economou, J. Chem. Phys. 34, 971 (1961)1

49. J. R. Hodkinson and I. Greenleaves, J. Optical Society of America, 53, 577 (1963).

50. J. R. Hodkinson, Applied Optics, 5, 839 (1966).

51. R. Penndorf, J. Phys. Chem. 62, 1537 (1958).

52. G. C. Gravatt, Jr., J. Air Pollution Control Assoc., 23, 1035 (1973).

53. W. Heller, Private Communication.

54. J. H. Chin, C. M. Sliepcevich and M. Tribus, J. Phys. Chem. 59, 841 (1955).

55. J. H. Chin, C. M. Sliepcevich and M. Tribus, J. Phys. Chem. 59. 845 (1955).

Bibliography

56. K. S. Shifrin, "Studies of Clouds, Precipitation and Storm Electricity", Inst. of Appl. Geophys. of USSR, Acad. of Sci., Moscow (1957).

57. K. S. Shifrin and A. Y. Perelman in "Electromagnetic Scattering", R. L. Rowell and Stein, eds., Gordon and Breach Science Publishers, New York, 1967.

58. J. V. Dave, Applied Optics, 10, 2035 (1971).

59. E. F. Mallove and W. C. Hinds, J. Aerosol Science, 7, 409 (1976).

60. L. C. Chow and C. L. Tien, Applied Optics 15, 378 (1976).

61. M. J. Post, J. Opt. Soc. Am. 66, 483 (1976).

62. J. P. Witeczek, Clairol, Stamford, Conn., Private Communication. (1976).

63. J. P. Witeczek, Ph.D. Thesis, "Determination of Particle Size Distributions in Colloidal Systems by Light Scattering", Wayne State University, Detroit, Mich. 1969.

64. W. Heller and J. Witeczek, J. Physical Chem., 74, 4241 (1970).

65. J. P. Kratohvil and C. Smart, J. of Colloid Chem. 20, 875 (1965).

66. W. Heller, in "Electromagnetic Scattering", p. 110, M. Kerker, ed., Pergamon Press, London 1963.

67. F. T. Gucker and R. L. Rowell, Discussion Faraday Soc. 30, 185 (1960).

68. D. H. Napper and R. H. Ottewill, Trans. Faraday Soc. 60, 1466 (1964).

69. M. E. Myers and A. M. Wims, Applied Optics 11, 947 (1972).

AUTOBIOGRAPHICAL STATEMENT

Name:	Werner Bergman
Birth:	June 24, 1945; Göppingen, Germany
Education:	Bentley High School, Livonia, Michigan High School Diploma 1963
	Wayne State University, Detroit, Michigan BS in Chemistry 1969
	Wayne State University, Detroit, Michigan PhD in Chemistry 1977
Positions:	Research Engineer, Ford Motor Company Dearborn, Michigan June 1969 - January 1974
	Chemist, Lawrence Livermore Laboratory Livermore, California September 1976 - present
Membership:	American Chemical Society Air Pollution Control Association Society of Sigma Xi
Publications:	J.S. Ninomiya, W. Bergman and B.H. Simpson, "Automotive Particulate Emissions", in Proc. Second International Clean Air Congress, Academic Press, New York, 1971.
	W. Bergman and W. Heller, "Mie Scattering Maxima and Minima in Heterodisperse Systems", Wayne State University Press, Detroit, Michigan, 1977.